THE HONG KONG POLYTECHNIC UNIVERSITY

DEPARTMENT OF CIVIL AND ENVIRONMENTAL ENGINEERING

SECOND-ORDER DESIGN AND ADVANCED ANALYSIS OF HYBRID STEEL AND CONCRETE FRAMED STRUCTURES

By

LIU Siwei

A Thesis Submitted in

Partial Fulfillment of the Requirements for

the Degree of Doctor of Philosophy

August 2013

CERTIFICATE OF ORIGINALITY

I hereby declare that this thesis is my own work and that, to the best of my knowledge and belief, it reproduces no material previously published or written nor material which has been accepted for the award of any other degree or diploma, except where due acknowledgement has been made in the text.

_____ (Signed)

LIU Siwei (Name of student)

To my wife & parents

for their love and encouragements

ABSTRACT

Hybrid steel and concrete framed structures, which consist of bare steel (BS), reinforced concrete (RC) and steel-concrete composite (SCC) members, are more increasingly and extensively used in modern buildings. The structural benefit of this system is to combine the advantages of two construction materials with concrete having high compression strength, large damping ratio and good corrosion resistance and steel possessing of high tension strength, good ductility and efficiency in constructability. This structural form is superior to traditional BS and RC framed systems, and therefore, it becomes a popular selection in modern high-rise buildings.

It is noted that the current design practice for this structural form is both inconvenient and inconsistent to apply. Design guidance and principles in most codes are mainly derived for first-order analysis, and the tedious and cumbersome hand calculations used in conjunction with complicated formulas are necessarily required, such as the assumptions of K-factors or the effective length for members in sway or non-sway frames. In addition, the related clauses for stability check vary in BS, RC and SCC design codes and these lead to the design procedure being inconsistent and inefficient. In this research, a unified second-order design method is proposed and it only requires section capacity check at critical locations of a member by failure surfaces without needs of using the prescriptive formulae in various codes.

The philosophy of advanced analysis method is to consider the various effects inherent to real structures, namely as initial imperfections, geometric and material nonlinearities and so on. Due to the differences in material characteristics between concrete and steel, BS members are slender usually with critical stability problems, while RC members always show significant plasticity and both of these nonlinear behaviors are observed in SCC members. Moreover, frame global and member local imperfections are initially existed, which influence deflections as well as force distributions and need to be properly modeled. To these ends, a practical and efficient advanced analysis approach is proposed for designing of hybrid steel and concrete framed structure with considerations of all these vital effects.

In this thesis, a beam-column finite element with an arbitrarily-located plastic hinge (ALH element) is firstly proposed for both second-order elastic and advanced plastic analysis. This element is initially curved such that member local imperfections can be directly modeled. Due to existence of the internal degree of freedoms, only one element is sufficient to simulate large deflections in members. Two plastic hinges are further incorporated into the element ends that inelastic behaviour of the element can be more accurately presented. Furthermore, the additional degrees of freedom in the proposed element are condensed and this dramatically improves numerical efficiency and brings much convenience to computer programming. Apart from the conventional formulation requiring two and more elements to model imperfections or capture the locations of plastic-hinges, one element per member is adequate in the proposed analytical model. It is believed that this numerical procedure is efficient and the saving in computer time and data manipulation efforts is considerable.

In order to evaluate a section under axial force and biaxial bending, three types of sectional yield surfaces are generated namely as initial yield, failure and concrete fracture surfaces. The initial yield and failure surface defines the elastic-limit and ultimate-limit states, respectively, while the concrete fracture surface is constructed with the use of the Branson's model for simulating concrete cracking effects. In addition, a refined plastic hinge model integrated with these sectional yield surfaces for various material types of members is also proposed in this thesis.

In generating of the sectional yield surfaces, an analysis technique for arbitrary sections is proposed. The quasi-Newton iterative scheme is adopted for determining the location of neutral axis of a section. Two types of stress-resultant approaches for concrete components are provided as the equivalent stress block and elaborated layer-integration methods. The former is limited to the ultimate limit states, whereas the latter can be utilized for any specified conditions. A structural steel component is automatically meshed into small fibers and each rebar is lumped into a point that occupies a certain area. The openings and voids occupied by other components are excluded by the negative area approach.

The recently published codes, such as Eurocode 3 (2005) and Eurocode 4 (2004), recommend the use of second-order analysis method for different types of structural members. The corresponding second-order design perspectives in Eurocodes for RC, BS and SCC members are investigated. Furthermore, several design examples are also analysed and presented to demonstrate the feasibility of using the proposed second-order design method in modern practice.

In the proposed advanced analysis approach, the material constitutive models are required and they are critical to the accuracy. Therefore, the material models from Eurocodes and available literatures are selected and discussed. Since the Eurocode 4 (2004) only permits the use of normal strength concrete in concrete-filled composite construction, an experimental investigation on the material properties of high-strength concrete (HSC) in circular and octagonal steel tubes is demonstrated.

A series of benchmark examples in literatures and experiments are selected for verifying the accuracy and feasibility of the proposed analysis approach for cross sections, individual members and framed structures to elaborate the efficiency and validity of the proposed method.

The distinct feature of this research includes development of an efficient curved beam-column finite element and integration with an accurate cross section analysis technique, which only requires material constitutive relations. Based on the proposed formulations, unified and practical second-order design and advanced analysis method for hybrid steel and concrete members and framed structures are developed.

PUBLICATIONS

Journal Papers:

1) Si-Wei Liu, Yao-Peng Liu, and Siu-Lai Chan (2009), Pushover analysis by one element per member for performance-based seismic design, *International Journal of Structural Stability and Dynamics*, 10, 111-126.

2) Si-Wei Liu, Yao-Peng Liu, and Siu-Lai Chan (2012), Advanced analysis of hybrid steel and concrete frames: Part 1: Cross-section analysis technique and second-order analysis, *Journal of Constructional Steel Research*, 70, 326-36.

3) Si-Wei Liu, Yao-Peng Liu, and Siu-Lai Chan (2012), Advanced analysis of hybrid steel and concrete frames: Part 2: Refined plastic hinge and advanced analysis, *Journal of Constructional Steel Researc*h, 70, 337-49.

4) Si-Wei Liu, Yao-Peng Liu, and Siu-Lai Chan (2013), Direct analysis by a new beam-column element with an arbitrarily-located plastic hinge: Part 1: Planar analysis (Submitted).

5) Si-Wei Liu, Yao-Peng Liu, and Siu-Lai Chan (2013), Direct analysis by a new beam-column element with an arbitrarily-located plastic hinge: Part 2: Spatial analysis (Submitted).

Conference Papers:

1) Si-Wei Liu, Yao-Peng Liu, and Siu-Lai Chan, *Second-order plastic analysis of steel frames by a single element per member allowing for arbitrarily located plastic hinge*, The Pacific Structural Steel Conference (PSSC 2013), Singapore, 8 - 11 October 2013.

2) Siu-Lai Chan, Si-Wei Liu and Yao-Peng Liu, *Unified design of steel, concrete and composite structures by direct analysis*, 10th International Conference on Advances in Steel Concrete Composite and Hybrid Structures, Singapore, 2 - 4 July 2012.

3) Yao-Peng Liu, Si-Wei Liu, Zhi-Hua Zhou and Siu-Lai Chan, *Second-order analysis for long span steel structure protecting a heritage building*, IJSSD Symposium 2012 on Progress in Structural Stability and Dynamic, Nanjing, China, 14 - 16 April 2012.

4) Siu-Lai Chan, Yao-Peng Liu and Si-Wei Liu, *Structural Design in the Post-Effective Length Era*, The Proceedings of the Twelfth East Asia-Pacific Conference on Structural Engineering and Construction EASEC12.

5) Siu-Lai Chan, Si-Wei Liu and Yao-Peng Liu, *Advanced analysis of hybrid frame structures by refined plastic-hinge approach*, 4th International Conference on Steel & Composite Structures, Sydney, Australia, 21 - 23 July 2010.

6) Si-Wei Liu, Yao-Peng Liu, Bo Li, Huan-Jian Mo, Man Fong and Siu-Lai Chan, *Recent development of computational design by software NIDA*, International Conference ICASS '09 / IJSSD / IStructE Asia-Pacific Forum Sixth International Conference on Advances in Steel Structures in conjunction with IJSSD symposium on Progress in Structural Stability and Dynamics & IStructE Asia-Pacific Forum, Hong Kong, China, 16 - 18 December 2009.

7) Siu-Lai Chan, Yao-Peng Liu and Si-Wei Liu, *Second-order analysis and design of wall-framed structures*, Academic Conference of China Steel Code published 35 years, Xi An, China, April 2009.

8) Siu-Lai Chan, Man. Fong and Si-Wei Liu, *Design of angle trusses - Linear and Second-Order Analysis*, Academic Conference of the 9th Modern Structural engineering Workshop, Ji-Nan, China, July 2009.

ACKNOWLEDGEMENTS

I would like to express the sincerely gratitude to my supervisor, Professor S. L. Chan, for his enlightening guidance, constant encouragement, invaluable suggestions and continued inspiration. I would like to thank him for giving me this precious opportunity to carry out this research project and providing me many unique chances to study the nonlinear analysis theory and design philosophy. His deep insights and wide knowledge in various scientific and engineering disciplines, research enthusiasm and sincere attitude will keep encouraging me throughout my life.

I would like to give my sincere and special thanks to Dr. Y. P. Liu for his warmest helps and valuable guidance in the past years, and deeply appreciate his reviews and comments for my research and this thesis. His attitude to scientific research and engineering works has inspired me to strive for excellence in future.

I acknowledge the fully financial support of the research project "Advanced Analysis & Design of Mixed Steel-concrete Structures" funded by the Research Grant Council grant from the Hong Kong SAR Government, and appreciate the Hong Kong Polytechnic University for providing the supports during the project period.

I am deeply indebted to my wife, Mei Yang, for her love, support and encouragement during these years, and to my parents, Guoxin Liu and Haihua Zeng,

for their loves and dedications that provides the emotional and mental supports for this work.

Finally, I would like to further thank the NIDA team members, including Dr. Z. H. Zhou, Mr B. Li, Mr. H. J, Mo, Dr. M. Fong, Dr. S. H. Cho, Mr. Sam Chan, Mr. Y. Q. Tang, Miss H. Yu, Miss L. Jiang, Mr. W. F. Chen, Mr. Geoffery Chu, Mr. T. J. Li, Mr Z. L. Du, Mr R. Bai, Miss W.Q. Tan, Mr J.W. He, Dr W. Q. Jiang, Mr. J. Y. Li and Mr. P. S. Zheng for their constructive discussions and assistances. And I also thank Dr. Y. M. Hu, Dr. S. Weng, Dr. Nancy Sheng, Mr. K. L. Lu, Mr. E. F. Du, Mr. J. R. Zhou, Miss Miya Lau, Miss Emmy Ko, Mr. M. T. Ho, Mr. W. K. Tung, Mr. M. C. Ng and Y. H. Yiu for their great helps during the past research life.

CONTENTS

CERTIFICATE OF ORIGINALITY ..... **I**

ABSTRACT ..... **III**

PUBLICATIONS ..... **VII**

ACKNOWLEDGEMENTS ..... **X**

CONTENTS ..... **XII**

LIST OF FIGURES ..... **XVIII**

LIST OF TABLES ..... **XXIV**

LIST OF SYMBOLS ..... **XXV**

CHAPTER 1 INTRODUCTION **1**

1.1. Background 2

1.2. Research objectives 6

1.3. Layout of the thesis 9

CHAPTER 2 LITERATURE REVIEW **15**

2.1. Beam-column finite element methods for nonlinear analysis 15

2.1.1 Cubic Hermite element 16

2.1.2 Curved Pointwise Equilibrating Polynomial (PEP) element 18

2.1.3 Stability function element 20

2.1.4 Beam element with mid-span and end springs 22

2.1.5 Other elements 25

2.1.6 Discussions 25

2.2. Inelastic analysis methods for beam-column element 27

2.2.1 Plastic hinge approaches 28

2.2.2 Plastic zone approaches 30

2.2.3 Discussions 31
2.3. Cross section analysis methods 32
2.4. Second-order design approach 38
2.4.1 Consideration of initial imperfections 39
2.4.2 Current codes for second-order design 40
2.5. Advanced analysis method 42
2.6. Concluding Remarks 45

CHAPTER 3 ANALYTICAL MODEL FOR ADVANCED ANALYSIS BY ONE ELEMENT PER MEMBER 49

3.1. Introduction 50
3.2. Assumptions 53
3.3. Curved beam-column element with an arbitrarily located hinge 54
3.3.1 Background 54
3.3.2 Formulation of displacement function 55
3.3.3 Bowing effects 57
3.3.4 Secant relations 58
3.3.5 Tangent stiffness matrix 61
3.3.6 Condensed stiffness matrix and generalized nodal forces 65
3.3.7 Equivalent nodal forces 66
3.3.8 Transformation matrix [A] from member basic force displacement to member intermediate force / displacement 67
3.3.9 Transformation matrix [T] from member intermediate force/ displacement to nodal global force/displacement 70
3.4. Formulation of the three hinges element 71
3.4.1 Background 71
3.4.2 Element stiffness formulation 72
3.4.3 Refined plastic hinge model 74
3.4.4 Correction of force point movement after full plastic yielding 75
3.5. Numerical solution strategies for nonlinear analysis 75
3.5.1 General 75
3.5.2 Newton-Raphson strategy 77

3.5.3 Basic formulation and constraint equations 78
3.5.4 Interaction scheme by minimum residual displacement method 79
3.5.5 Interaction scheme by displacement control method 81
3.5.6 Interaction scheme by arc-length control method 82
3.5.7 Convergence criteria 84
3.5.8 Summaries 84
3.6. Verification examples 85
3.6.1 Closed-form solutions of single initially curved members 85
3.6.2 Advanced analysis of a simply supported column 88
3.6.3 Second-order and advanced analysis of a cantilever column 89
3.6.4 Advanced plastic analysis of a portal frame 91
3.6.5 Advanced analysis of Vogel's six story frame 92
3.7. Concluding remarks 93
3.8. Appendix I -the derivation of matrix [D] 94

CHAPTER 4 ADVANCED ANALYSIS AND DESIGN OF THREE-DIMENSIONAL FRAMED STRUCTURES 114

4.1. Introduction 115
4.2. Three-dimensional curved element with arbitrarily located hinge 118
4.2.1 Basic force vs. displacement relations 118
4.2.2 Total potential energy function 120
4.2.3 Bowing effects 121
4.2.4 Secant relations 122
4.2.5 Tangent stiffness matrix 125
4.2.6 Condensed stiffness matrix and generalized nodal forces 137
4.2.7 Incorporation of two end plastic hinges 138
4.3. Kinematic descriptions of motion 140
4.3.1 The incremental secant stiffness method 141
4.3.2 Transformation matrix [T] from member basic force/displacements to member local axes 144
4.3.3 Matrix [N] for the rigid body movement 144
4.3.4 Transformation matrix [L] from member local to global axes 145

4.3.5 Relations between member local axes and global axes 147
4.4. Verification examples 148
4.4.1 Biaxially-loaded cantilever column 148
4.4.2 Two story space steel frame with I sections 149
4.4.3 Harrison's space frame 150
4.4.4 Two story space steel frame with rectangular sections 151
4.4.5 Six story space steel frame 152
4.4.6 Twenty story space steel frame 153
4.5. Concluding remarks 154

CHAPTER 5 SECTIONAL YIELD SURFACES FOR SECOND-ORDER DESIGN AND ADVANCED ANALYSIS 172

5.1. Introduction 173
5.2. Assumptions 175
5.3. Cross-section analysis technique 176
5.3.1 Referenced loading axes 177
5.3.2 Coordinate systems 178
5.3.3 Stress resultants in concrete by equivalent stress block method 179
5.3.4 Stress resultants in concrete by elaborated integration method 180
5.3.5 Stress resultants in steel 181
5.3.6 Opening area 182
5.3.7 Total force and moments 182
5.3.8 Iteration scheme 183
5.4. Sectional yield surfaces 183
5.4.1 Failure surface 184
5.4.2 Initial yield surface 184
5.4.3 Concrete fracture surface 185
5.4.4 Index of surfaces 186
5.5. Verifications of the cross-section analysis technique 187
5.5.1 Bi-axially loaded and doubly symmetric steel sections 188
5.5.2 Bi-axial analysis of an irregular composite cross-section 189
5.5.3 Rectangular reinforced concrete section analyzed by Eurocode 2 190

5.5.4 Extensive testing of six typical RC sections 191
5.5.5 Typical composite sections analyzed by Eurocode 4 192
5.6. Concluding remarks 193

CHAPTER 6 SECOND-ORDER DESIGN OF HYBRID STEEL AND CONCRETE FRAMES 229

6.1 Introduction 230
6.2 Unified second-order design method 233
6.2.1 P-Δ and P-δ effects 233
6.2.2 Initial member imperfection 234
6.2.3 Initial frame imperfection 236
6.2.4 Member strength check 237
6.2.5 Summary 239
6.3 Effective flexural stiffness modeling 239
6.4 Verification examples 241
6.4.1 Buckling strength of steel columns vs. codified buckling curves 241
6.4.2 Design of an RC portal frame 242
6.4.3 Design of a SCC portal frame 243
6.5 Concluding remarks 244

CHAPTER 7 ADVANCED ANALYSIS OF HYRBID STEEL AND CONCRETE FRAMES 261

7.1 Introduction 262
7.2 Assumptions 266
7.3 Flexural stiffness modeling 267
7.4 Plastic hinge formulations 268
7.5 Material constitutive models 269
7.5.1 Constitutive model for structural steel and rebar 270
7.5.2 Constitutive model for the compression of unconfined concrete 270
7.5.3 Constitutive model for the tension of concrete 271
7.5.4 Constitutive model for the compression of confined concrete 271

7.6 Experiment on high-strength concrete (HSC) in steel tubes 272
7.6.1 Introduction 272
7.6.2 Dimensions of specimens 273
7.6.3 Material properties of high strength concrete 274
7.6.4 Material properties of steel 274
7.6.5 Experimental design 275
7.6.6 Experimental results 276
7.6.7 Discussions 277
7.7 Verification examples 277
7.7.1 Foure's RC column 278
7.7.2 Concrete-filled steel tubular columns 279
7.7.3 Concrete-filled circular hollow steel columns 280
7.7.4 Cranston's portal frame 281
7.8 Concluding remarks 282

CHAPTER 8 CONCLUSIONS AND RECOMMENDATIONS 306

8.1. Conclusions 306
8.2. Recommendations for future work 310

REFERENCES 312

LIST OF FIGURES

Figure 1.1 Illustrations of hybrid steel and concrete frames 13

Figure 1.2 Common sections in a hybrid steel and concrete framed structure 14

Figure 2.1 Forces vs. deformation in a beam-column element 46

Figure 2.2 Forces vs. deformation of the curved PEP element 46

Figure 2.3 Beam element with mid-span and ended springs..... 46

Figure 2.4 Illustration of plastic hinge approach..... 47

Figure 2.5 Behaviors of plastic hinge and refined plastic hinge 47

Figure 2.6 Illustration of plastic zone approach 48

Figure 3.1 A typical hybrid steel and concrete framed structure..... 97

Figure 3.2 The forces vs. displacements relations of the ALH element 98

Figure 3.3 Member deformations and associated forces..... 100

Figure 3.4 Equivalent nodal forces..... 101

Figure 3.5 Rotational relationships in a plastic hinge at end-zone..... 102

Figure 3.6 Two types of Newton-Raphson strategies..... 103

Figure 3.7 The Minimum Residual Displacement (MRD) Method 104

Figure 3.8 The displacement control method..... 104

Figure 3.9 The Arc-length control method..... 105

Figure 3.10 Comparison results of the pinned-pinned column 105

Figure 3.11 Comparison results of the fixed-pinned column..... 106

Figure 3.12 Comparison results of the fixed- fixed column 106

Figure 3.13 Modeling of initial member imperfection 107

Figure 3.14 Advanced analysis of an axial-loaded simply supported column 108

Figure 3.15 Advanced analysis of a simply supported column under UDL 108

Figure 3.16 Second-order elastic analysis results of a cantilever column 109

Figure 3.17 Advanced plastic analysis results of a cantilever column 109

Figure 3.18 Geometry and loading pattern of the portal frame 110

Figure 3.19 Horizontal displacement of the portal frame 111

Figure 3.20 Vertical displacement of the portal frame 111

Figure 3.21 Geometry and loading pattern of the Vogel's six story frame 112

Figure 3.22 Horizontal displacement of the Vogel's six story frame 113

Figure 4.1 Non-vectorial property of large rotations in three-dimensional space ... 155

Figure 4.2 The element local coordinate system 156

Figure 4.3 The inclination of principle axes 156

Figure 4.4 Relative member basic forces and deformations 157

Figure 4.5 Incremental kinematics of an element in three-dimensional space 158

Figure 4.6 Member deformations and associated forces in local axes 159

Figure 4.7 Member deformations and associated forces in global axes 160

Figure 4.8 Geometry and loadings of the cantilever column 161

Figure 4.9 Vertical displacement at the top node 161

Figure 4.10 Geometry and loadings of two story space frame with I section 162

Figure 4.11 Displacement along X-direction at the roof level 163

Figure 4.12 Displacement along X-direction at the 2nd floor level 163

Figure 4.13 Geometry and loadings of the Harrison's space frame 164

Figure 4.14 Horizontal sway of the Harrison's space frame 164

Figure 4.15 Geometry and loadings of two story frame with rectangular section .. 165

Figure 4.16 Horizontal displacement of the two story frame 166

Figure 4.17 Geometry of the six story space frame 167

Figure 4.18 Load vs. displacement along Y-axis of the six story space frame 168

Figure 4.19 Load vs. displacement along X-axis of the six story space frame 168

Figure 4.20 Geometry of the twenty story space frame 169

Figure 4.21 Roof displacement of the twenty story space frame 170

Figure 5.1 Illustration of failure, initial yield, concrete fracture surfaces 194

Figure 5.2 Illustration of concrete fracture surface 195

Figure 5.3 Arbitrarily shaped composite cross-section..... 196

Figure 5.4 Stress resultants by the equivalent stress block method..... 197

Figure 5.5 Stress resultants by the elaborated layer-integration method 198

Figure 5.6 Flowchart of generating the yield surfaces under given axial load 199

Figure 5.7 Indexed interaction strength suface..... 200

Figure 5.8 Screenshots of RCD 2013 201

Figure 5.9 Comparison results for a wide flange steel section..... 202

Figure 5.10 Comparison results for a double web steel section 203

Figure 5.11 Comparison results for a circular hollow steel section 204

Figure 5.12 Irregular composite cross-section 205

Figure 5.13 My vs. Mz interaction curve under axial load Nx=4120kN 206

Figure 5.14 Three dimensional yield surface of the irregular composite section ... 206

Figure 5.15 Typical rectangular reinforced concrete section 207

Figure 5.16 Results of the RC section by equivalent stress block method 208

Figure 5.17 Results of the RC section by elaborated layer-integration method..... 208

Figure 5.18 Comparison results of Rosati's RC Section - Rectangular..... 211

Figure 5.19 Comparison results of Rosati's RC Section – T Shaped Section 214

Figure 5.20 Comparison results of Rosati's RC Section – L Shaped Section 217

Figure 5.21 Comparison results of Rosati's RC Section – C Shaped Section 220

Figure 5.22 Comparison results of Rosati's RC Section – G Shaped Section 223

Figure 5.23 Comparison results of Rosati's RC Section – Multicell Section..... 226

Figure 5.24 Typical encased composite section 227

Figure 5.25 Comparison results of typical encased composite section 227

Figure 5.26 Typical concrete filled rectangular hollow section 228

Figure 5.27 Comparison results of concrete filled rectangular hollow section..... 228

Figure 6.1 The conventional second-order design method 246

Figure 6.2 The proposed second-order design approach 246

Figure 6.3 The P-Δ and P-δ Effects 247

Figure 6.4 Modeling initial member imperfections 248

Figure 6.5 Modeling initial frame imperfections..... 248

Figure 6.6 Behaviour of concrete component in flexure 249

Figure 6.7 Comparison results of buckling curve for Group 1 250

Figure 6.8 Comparison results of buckling curve for Group 2 250

Figure 6.9 Comparison results of buckling curve for Group 3 251

Figure 6.10 Comparison results of buckling curve for Group 4..... 251

Figure 6.11 Comparison results of buckling curve for Group 5..... 252

Figure 6.12 Comparison results of buckling curve for Group 6..... 252

Figure 6.13 Properties of the RC portal frame 253

Figure 6.14 Properties of the SCC portal frame 254

Figure 7.1 Constitutive relations of steel and concrete 283
Figure 7.2 Initial and failure yield surfaces under praticular axial force 284
Figure 7.3 Typical stress vs. strain curves for normal and high strength concrete . 285
Figure 7.4 Tests for the cube and cylinder specimens 285
Figure 7.5 Confined specimens with same d/t ratio 286
Figure 7.6 Unconfined specimens with the same size of concrete core 286
Figure 7.7 Schematic of specimen setup 287
Figure 7.8 Strain gages setup for confined specimens 287
Figure 7.9 Experimental setup for confined specimens 288
Figure 7.10 Stress vs. strain curves of confined specimens 289
Figure 7.11 Results between the circular confined and unconfined specimens 290
Figure 7.12 Results between the octagonal confined and unconfined specimens ... 290
Figure 7.13 Foure's column 291
Figure 7.14 Load vs. deflection curve of the Foure's column 292
Figure 7.15 Cross section properties and eccentricity of loading 293
Figure 7.16 Comparison results of SHC -1 294
Figure 7.17 Comparison results of SHC -2 294
Figure 7.18 Comparison results of SHC -3 295
Figure 7.19 Comparison results of SHC -4 295
Figure 7.20 Comparison results of SHC -5 296
Figure 7.21 Comparison results of SHC -6 296
Figure 7.22 Comparison results of SHC -7 297
Figure 7.23 Comparison results of SHC -8 297
Figure 7.24 Comparison between experiment and present study (M5) 298

Figure 7.25 Load vs. deflection curves for specimens of M1 to M3 298

Figure 7.26 Load vs. deflection curves for specimens of M4, M6 and M7 299

Figure 7.27 Load vs. deflection curves for specimens of M8 to M10 299

Figure 7.28 Cranston's portal frame 300

Figure 7.29 Horizontal deflection of Cranston's portal frame 300

LIST OF TABLES

Table 4.1 Out-of-plumpness imperfection of two story space frame 171

Table 6. 1 Member imperfections for steel members in Eurocode 3 (2005) 255

Table 6. 2 Member imperfections for composite members in Eurocode 4 (2004).. 256

Table 6. 3 Design value of initial imperfection e_0/L for members 256

Table 6. 4 Selected groups of the columns to be analyzed 257

Table 6. 5 Linear design of the RC portal frame 259

Table 6. 6 Design results of the RC portal frame 259

Table 6. 7 Linear design of the SCC portal frame 260

Table 6. 8 Design results of the SCC portal frame 260

Table 7.1. Dimensions of confined specimens in CHS 194 group 301

Table 7.2. Dimensions of confined specimens in OHS 194 group..... 301

Table 7.3. Compressive strength of concrete obtained from cube and cylinder test 301

Table 7.4. Concrete properties obtained from cylinder test 302

Table 7.5. Steel properties obtained from coupon test 302

Table 7.6. Summarized experimental results 302

Table 7.7. Geometrical dimension 303

Table 7.8. Material Properties 303

Table 7.9. Summary of comparisons 304

Table 7.10. Geometrical layout and material properties 304

Table 7.11. Comparisons between the experiment and proposed approach 305

LIST OF SYMBOLS

$\mathbf{a_i}$	Coefficients for the polynomial shape function in the lateral direction of an element
$\mathbf{A_c, A_r, A_s, A_o}$	Total area of concrete, reinforcing bars, structural steel and openings, respectively
$\mathbf{b_i}$	Coefficients for the polynomial shape function in the axially shortening direction of an element
$\mathbf{c_1, c_2}$	Parameters for the stability functions
$\mathbf{d_n}$	Depth of neutral axis of a cross section
D	Overall width of a cross section
e	Axial deformation of an element
$\mathbf{E_c, E_{c,c}}$	Young's modulus of unconfined concrete and confined concrete, respectively
$\mathbf{E_t}$	Yong's modulus of concrete in tension
$\mathbf{E_s}$	Young's modulus of steel
EA	Axial rigidity
EI	Flexural rigidity
f	Vector of the generalized force
$\mathbf{f_c, f_{c,c}}$	Compressive stress of the unconfined and confined concrete, respectively
$\mathbf{f_r}$	Characteristic strength of reinforcing bars; or the confining stress

$\mathbf{f_s}$	Characteristic strength of structural steel
$\mathbf{f_v}$	Vertical stress induced by the friction between the steel and concrete interface
$\mathbf{f_y}$	Design strength of steel
$\mathbf{F}$	Vector of the external forces
$\mathbf{F^{EQV}}$	Vector of the equivalent nodal forces
$\mathbf{\bar{F}}$	Force vector at the member local axes
$\mathbf{G}$	Shear modulus of elasticity
$\mathbf{GJ}$	Torsional rigidity
$\mathbf{i}$	Iteration number
$\mathbf{I_{cr}}$	Second moments of area for the cracked section
$\mathbf{I_e}$	Effective second moments of area as adopted in analysis
$\mathbf{I_{un}}$	Second moments of area for the uncracked section
$\mathbf{k^*}$	Condensed tangent stiffness matrix
$\mathbf{k_e}$	Element stiffness matrix
$\mathbf{k_L}$	Linear stiffness matrix
$\mathbf{k_G}$	Geometric stiffness matrix
$\mathbf{k_S}$	Spring stiffness matrix for considering the material yielding at the internal plastic hinge location
$\mathbf{K_e}$	Element stiffness matrix in the global coordinate system
$\mathbf{L}$	Length of the element
$\mathbf{L_0}$	Original length of the element
$\mathbf{L_i}$	Updated member length at the last known configuration
$\mathbf{R}$	Vector of the resisting forces

$\mathbf{M_1}$, $\mathbf{M_2}$	Bending moments at the left and right ends of the element, respectively
$\mathbf{M_1^*}$, $\mathbf{M_2^*}$	Condensed member resisting moments at two ends
$\mathbf{M_{cr}}$	Cracking moment of a section composing of concrete
$\mathbf{M_t}$	Torsional moment
$\mathbf{M_u}$, $\mathbf{M_v}$	Bending moments about two major axes by referring to the uov axes
$\mathbf{M_y}$, $\mathbf{M_z}$	Bending moments about two major axes by referring to the yoz axes
$\mathbf{M_{py}}$, $\mathbf{M_{pz}}$	Bending moments by referring to the local axes yoz with the origin of the plastic centroid
$\boldsymbol{M_e^\zeta}$, $\boldsymbol{M_p^\zeta}$	Initial yield and failure moment capacities under current axial load
n	An exponent in the concrete constitutive model in Eurocode 2
$\mathbf{n_c}$	Number of vertices of the compression zone
$\mathbf{n_L}$	Number of the sectional layers
$\mathbf{n_v(i)}$	Number of intersection points in the corresponding layers
$\mathbf{N_x}$	Axial force by referring to uov axes
$\mathbf{N_{xd}}$	Current design axial loading
$\mathbf{N(x)}$	Shape function for the proposed element
$\mathbf{N_1}$ **and** $\mathbf{N_2}$	Vector of the shape function parameters
$\mathbf{N_{11}}$, $\mathbf{N_{12}}$, $\mathbf{N_{13}}$, $\mathbf{N_{21}}$, $\mathbf{N_{22}}$, $\mathbf{N_{23}}$	Parameters for shape functions
NELE	Total number of the element

$\mathbf{P}$	Axial force
$\mathbf{P}^*$	Condensed member axial force
$\mathbf{P_{cr}}$	Euler's buckling load as $\pi^2 EI/L$
$\mathbf{q(x)}$	An arbitrary lateral distribution forces
$\mathbf{R}$	Internal resisting loads which can be calculated by the function of the nodal displacement u; or spring stiffness at the mid-span and connects the two sub-elements; or plasticity parameter related to the loading state
$\mathbf{R_g}$	External resisting forces at global axes
$\mathbf{R_i}$	Local resisting forces at member local axes
$\mathbf{R_m}$	Plasticity parameter related to the loading state at the internal plastic hinge
$\mathbf{S}$	Initial arc-length distance
$\mathbf{S_k}$	Current stiffness parameter
$\mathbf{S_m}$	Spring stiffness at the middle hinge
$\mathbf{S_L}$, $\mathbf{S_R}$	Spring stiffness at the left and right hinges respectively
TOL	A value for the acceptable accuracy and usually assumed to be 0.1% in conventional practice
$\mathbf{u}$	Degree of freedoms in an element; or the coordinates in uov axes
$\mathbf{u_e}$, $\mathbf{u_i}$	External and internal degree of freedoms in an element respectively
$\mathbf{u_g}$	Total displacement at the external nodes in global directions
$\mathbf{U}$	Strain energy

$\mathbf{v}$	Lateral displacement function of an element; or the coordinates in uov axes
$\mathbf{v_0}$	Lateral displacement function of the initial member curvature
$\mathbf{v_{m0}}$	Amplitude of initial imperfection at the mid-span
$\mathbf{V}$	Work done due to the external loads
$\mathbf{x, y, z}$	Coordinates in the element local axes
$\mathbf{X1_0, X2_0}$	Coordinates of the element in the original position
$\mathbf{Y1_0, Y2_0}$	
$\mathbf{Z1_0, Z2_0}$	
$\mathbf{Y_{gc}, Z_{gc}}$	Coordinates of geometric centroid of the whole section
$\mathbf{Y_{pc}, Z_{pc}}$	Coordinates of plastic centroid of the whole section
$\gamma_c, \gamma_r, \gamma_s$	Partial safety factors for concrete, reinforcement and steel respectively
$\boldsymbol{\delta}$	Lateral deflection along element length
$\boldsymbol{\delta_0}$	Pre-defined displacement increment at the steering DOF; or the magnitude of the initial curvature at mid-span
$\boldsymbol{\Delta f}$	Vector of the incremental condensed nodal forces
$\mathbf{\Delta F}$	Vector of the unbalanced force; or the incremental shear force at the mid-span
$\mathbf{\Delta F_i, \Delta F_e}$	Vectors of the internal and external unbalanced forces respectively
$\mathbf{\Delta \bar{F}}$	An arbitrary force vector parallel to the applied load
$\boldsymbol{\Delta_m \bar{u}_1}$	Displacement vector associated with an arbitrary load parallel to

	the applied loads
$\boldsymbol{\Delta_m u_i}$	Load increment due to the unbalanced force at the iterations
$\boldsymbol{\Delta u}$	Vector of the unbalanced displacement
$\boldsymbol{\Delta u_g}$, $\boldsymbol{\Delta u_i}$	Vectors of the incremental displacements at external and internal nodes respectively
$\boldsymbol{\Delta \bar{u}}$	Corresponding displacement vector conjugate to $\Delta\bar{F}$
$\boldsymbol{\Delta v}$	Incremental lateral displacement at the mid-span
$\boldsymbol{\Delta v_{1i}}$, $\boldsymbol{\Delta v_{2i}}$	Incremental displacement at member local axes along y-axis
$\boldsymbol{\Delta w_{1i}}$, $\boldsymbol{\Delta w_{2i}}$	Incremental displacement at member local axes along z-axis
$\boldsymbol{\Delta X1_i}$, $\boldsymbol{\Delta X2_i}$	Incremental displacements in global axes
$\boldsymbol{\Delta Y1_i}$, $\boldsymbol{\Delta Y2_i}$	
$\boldsymbol{\Delta Z1_i}$, $\boldsymbol{\Delta Z2_i}$	
$\boldsymbol{\Delta\alpha_{y1i}}$, $\boldsymbol{\Delta\alpha_{y2i}}$	Incremental rotations about the last known configuration
$\boldsymbol{\Delta\alpha_{z1i}}$, $\boldsymbol{\Delta\alpha_{z2i}}$	
$\boldsymbol{\Delta\beta_{yi}}$, $\boldsymbol{\Delta\beta_{zi}}$	Incremental rigid body rotations
$\boldsymbol{\Delta\theta_b}$, $\boldsymbol{\Delta\theta_s}$	Incremental rotations at the element and the section spring respectively
$\boldsymbol{\Delta_1\theta_1}$, $\boldsymbol{\Delta_1\theta_2}$	Incremental element rotations at the left and right sub-elements,
$\boldsymbol{\Delta_2\theta_1}$, $\boldsymbol{\Delta_2\theta_2}$	respectively
$\boldsymbol{\Delta\lambda}$	Load correction factor for imposing the constrain condition
$\boldsymbol{\theta_m}$	Rotation at the middle hinge
$\boldsymbol{\theta_t}$	Twist angle along with torsional moment
$\boldsymbol{\theta_{11}}$, $\boldsymbol{\theta_{22}}$	Rotations at two external ends
$\boldsymbol{\theta_{12}}$, $\boldsymbol{\theta_{21}}$	Rotations at the left and right sides of the internal hinge

	respectively
$\boldsymbol{\varepsilon, \sigma}$	Strain and stress
$\boldsymbol{\varepsilon_0, \varepsilon_{0,c}}$	Strain at reaching the maximum strength for the plain and confined concrete respectively
$\boldsymbol{\varepsilon_{ce}, \varepsilon_{ce,c}}$	Elastic limit strain at reaching the maximum strength for the plain and confined concrete respectively
$\boldsymbol{\varepsilon_{cu}, \varepsilon_{cu,c}}$	Compressive fracture strain for the plain and confined concrete respectively
$\boldsymbol{\varepsilon_{t0}}$	Concrete strain at the peak tensile strength
$\boldsymbol{\varepsilon_{tu}}$	Concrete strains at the peak tensile fracture
$\boldsymbol{\xi}$	Location of the internal plastic hinge; or the dimensionless coordinate along the element
$\boldsymbol{\Pi}$	Total potential energy function
$\boldsymbol{\sigma_2}$	Effective lateral compression due to confinement
$\boldsymbol{\Omega}$	Indexed strength interaction surface

CHAPTER 1

INTRODUCTION

Steel-concrete structures take the best characteristics of steel and concrete materials for production of a more efficient structural form and many structural benefits can be found in a hybrid steel and concrete framed structure, which is usually superior to the traditional steel and reinforced concrete constructions in regard to the cost-effectiveness, constructional efficiency, seismic performance and so on. However, the current design and analysis practice for this structural form is complicated, inconvenient and inconsistent. Moreover, the initial imperfections including the global frame imperfection and the local member imperfection, which are important factors affecting structural stability and force-distributions, cannot be properly presented and modeled in the conventional analysis approach. To alleviate the drawbacks, a new and superior design and analysis methods for the hybrid steel and concrete members and frames are explored in the present research.

This thesis proposes a unified second-order design and an efficient advanced analysis method for hybrid steel and concrete framed structures. Herein, a curved beam-column finite element with arbitrarily located plastic hinge (ALH) is firstly derived for simulating large deflections and inelastic behaviors of planar and spatial frames. Further, a robust cross section analysis technique based on the quasi-Newton numerical scheme is developed for arbitrary sections. Sequentially, three types of sectional yield surfaces are generated for evaluating the sectional strength and a

refined plastic hinge model combined with these surfaces are given for various types of members. With these formulations, the unified design and analysis approach requiring only the fundamental material constitutive models is developed. In addition, an experimental investigation on the use of high-strength concrete (HSC) in the concrete-filled composite construction is carried out. Extensive numerical examples have been employed from the available literatures and experiments for verification of the accuracy, reliability and practicality of the proposed analytical methods, and several design cases are also adopted to demonstrate the application of the proposed approach.

In this chapter, a review on the background of the relevant research is presented and the objectives of the research are also detailed. Finally, the layout of this thesis is briefly illustrated.

1.1. Background

Hybrid steel and concrete framed systems have been increasingly adopted in the past decades, where different material types of structural members are simultaneously used in a building system. The common types of hybrid steel and concrete framed structures are illustrated in Figure 1.1, which may consist of bare steel (BS), reinforced concrete (RC) and steel-concrete composite (SCC) members.

Many structural benefits can be found in a hybrid steel and concrete framed structure including the structural efficiencies in terms of strength, stiffness and

ductility and cost-effectiveness with the optimal use of materials according to their mechanical characteristics. For example, concrete has high compressive strength, large damping ratio and good corrosion resistance, while steel possesses high-tensile strength, excellent ductility and efficient constructability. Griffis (1986) studied the hybrid constructions and found that, besides time-efficient construction process could be achieved, the concrete components usually offered considerable damping properties to the whole structural system, while the steel components with lighter self-weight could reduce the foundation cost.

Besides the member strength checks, the flexural buckling of axially-compressive members and the overall stability of framed structures are always concerned in both analysis and design. The initial imperfections and the P-δ effects are vital for the individual column buckling and further affect the overall-system stability. In the past, due to the limitation of the computer technology, the design practice is mainly based on the hand calculation associated with the linear elastic assumptions. In order to consider the buckling effects, Euler (1759) firstly derived a buckling equation for a theoretically isolated and perfectly straight column under different boundary conditions. Since then, a stability design method by assuming the column effective length determined by the related K-factors had been proposed and still widely adopted until now. Later, the Perry-Robertson formula was derived by Ayrton and Perry (1886) and Robertson (1925) based on the Euler's buckling equation (1759) with consideration of the initial member imperfections; and a series of buckling curves for different values of imperfections were obtained and adopted in most of the design codes and guidance since then.

With rapid development of computer technology, the traditional first-order linear design approach is gradually recommended to be replaced by the second-order nonlinear design method. Second-order design method, which is also called direct analysis method in the AISC (2010) code, is a numerical and simulation-based approach. In this design method, the P-Δ and P-δ effects and the initial imperfections for individual members and the complete frame are directly considered in analysis. Member-local and frame-global stabilities can be accurately reflected in the analysis process, and as a result the assumption for the effective length by K-factors is eliminated. The successful applications of the second-order design approach have been demonstrated by Liew *et al*. (1993a, 1993b), Chan and Zhou (1994, 1995), Chen *et al*. (1995) and so on in the last decades.

In the current design practice, separated codes for design of members made of different materials are referred to. For example, Eurocode-2 (2004) is employed for RC members, Eurocode-3 (2005) for BS members and Eurocode-4 (2004) for SCC members. This brings much inconvenience and sometimes confusions to the structural engineers. Although the descriptions for stability design in the steel, concrete and composite codes may be different, the requirements for consideration of second-order effects, such as P-Δ and P-δ effects and the initial imperfections, are conceptually the same. It is noted that the P-δ effect is commonly ignored in most previous research and therefore the tedious member buckling strength check by codes is still needed. To this, a unified design approach for the hybrid steel and concrete systems is needed to be investigated for both design efficiency and analysis accuracy.

In second-order analysis design approach, as the P-Δ and P-δ effects and the initial imperfections have been directly reflected in analysis, the member strength can be simply evaluated by the cross section check at its critical locations. However, different types of sections can be found in a hybrid steel and concrete frame, such as reinforced concrete, single or built-up steel and encased or in-filled concrete composite sections shown in Figure 1.2. In order to calculate the sectional capacities of these sections, the complicated and tedious formulations in codes for various types of sections are still required. Therefore, a robust and generalized cross section analysis technique for arbitrary sections is necessary to be explored.

The philosophy of the advanced analysis approach is to accurately reflect the structural behaviour inherent to a real structure, and therefore, various effects are needed to be considered such as initial imperfections, concrete cracking, geometrical and material nonlinearities. Moreover, advanced analysis approach is a fundamental tool for performance-based seismic design, progressive collapse simulation and the failure limit state analysis, and it is useful for investigating the system performance under other extreme event or rare cases. Due to the mechanical properties are significantly varied between the steel and concrete, an efficient and practical advanced analysis approach is required to be investigated.

The use of concrete-filled steel tube (CFT) columns are increasingly popular in the modern structures, especially for the high-rise buildings. However, their applications are commonly limited to typical sectional shapes such as the rectangular or the circular. When one needs to design the uncommonly shaped tubular sections, the existing codes such as Eurocode 4 (2004) do not provide adequate design

formulae and provisions. Furthermore, the specified concrete grades as in Eurocode 4 (2004) are ranged from C25 to C60 for the composite construction, and therefore, the utilization of high strength concrete (HSC) in steel tubular columns is needed to be experimental studied.

In summary, unified second-order design and practical advanced analysis methods for hybrid steel and concrete framed structures are explored in this thesis. In addition to this novel design and analysis approaches, an initially curved beam-column element with capacity of simulating large deflections and high inelastic behavior is needed to be derived. As to avoid the tedious formulae for various types of section capacity checks, a robust cross section analysis technique is to be developed for arbitrary sections composed of concrete, steel reinforcement and steel components. Moreover, a generalized plastic hinge model for the hybrid steel and concrete members is also needed to formulate. The distinct feature of the present study is that an efficient curved beam-column element is derived in conjunction with an accurate cross section analysis technique, where only the basic material constitutive relations are required in both design and analysis.

1.2. Research objectives

The objectives of this thesis are to propose a unified second-order design approach and a practical advanced analysis method for the hybrid steel and concrete composite structures. Due to the mechanical characteristics being significantly different among the various material types of the structural members, a new beam-column element is needed to be formulated for simulation of all these vital factors.

Similarly, a robust cross section analysis technique is needed to be developed for arbitrary sections. The constitutive models are crucial for both the analysis and design and a proper input of the related material properties is a prerequisite for a reliable analysis and design.

Hence, the research objectives are summarized as follows,

1) To propose a new beam-column element with the allowance for initial member curvature and capability for simulating large deflections and inelastic behavior. Under some circumstances, the plastic hinge is likely to form along the member length rather than its ends, especially for a beam under uniformly distributed loads. Therefore, an arbitrarily located plastic hinge within a member needs to be allowed in the proposed element.

2) To develop an analytical model for advanced analysis by one element per member and this can significantly improve the numerical efficiency as well as the reduction on modeling efforts. In order to achieve an efficient nonlinear analysis, the numerical solution methods are explored and studied.

3) To investigate an accurate and robust cross section analysis technique for arbitrary sections in a hybrid steel and concrete framed structure. Various material constitutive models are capable to be considered in analysis. Moreover, different sectional states such as concrete fracture, initial yield and ultimate failure limits need to be evaluated accurately in the proposed method.

4) To extend the refined plastic hinge model for various material types of structural members in a hybrid steel and concrete frame. Since the conventional plastic hinge model is mainly developed for analysis of BS members, the extension of this model to other types of members are needed to be explored.

5) To introduce a unified and practical second-order design approach. The recently published codes, such as Eurocode 3 (2005) and Eurocode 4 (2004), have recommended the direct use of second-order analysis in design practice. A study on the use of these codes is required. Several examples are selected and analyzed by the proposed method and the conventional linear approach for comparisons.

6) To study the proper inputs of the material constitutive models. Since the material properties play an important role on the accuracy in analysis, and therefore, a study on these constitutive models mainly based on Eurocodes is carried out. As the Eurocode 4 (2004) only permits the use of normal strength concrete in concrete-filled composite construction, the material behavior of high-strength concrete (HSC) in steel tubes is needed to be experimentally studied.

7) To propose a practical and efficient advanced analysis approach for the hybrid steel and concrete frames. A series of benchmarking examples from

literatures and experiments are selected for verification of the proposed method.

1.3. Layout of the thesis

This thesis contains eight chapters and the layout is presented as follows,

Chapter 1 reviews the background of this research project, where the characteristics of the hybrid steel and concrete framed structure and its design and analysis methods are summarized. The research objectives of this project are also detailed and the content of this thesis is discussed.

Chapter 2 gives literature reviews covering the major topics in this research project. The second-order analysis methods based on the beam-column finite element as well as their features are discussed. Furthermore, inelastic analysis methods associated with the refined plastic hinge and the plastic zone methods are also discussed. Additionally, the cross section analysis methods for determining the sectional capacities are summarized. Finally, the developments of the second-order design approach and the applications of the advanced analysis method are reviewed.

Chapter 3 proposes an efficient and accurate numerical solution for advanced analysis of beam-column members by one element per member allowing for various effects such as initial member imperfection and geometrical and material nonlinearities. A new curved beam-columns element with arbitrarily-located plastic

hinge (ALH) is proposed. The additional degree of freedoms in the element will be condensed so that it can be easily incorporated into the existing software for nonlinear structural frame analysis. In order to consider large deflections, the formulations of the equilibrium through an updated Lagrangian description are established. In addition, numerical solution strategies for the nonlinear analysis are reviewed. Finally, several examples are presented and the accuracy of the results is investigated by comparing with the benchmark examples.

Chapter 4 extends the element formulations and the applications of the curved ALH element proposed in Chapter 3 to three-dimensional space for large deflections and inelastic analysis of spatial framed structures. A simplified approach, which assumes the space frame with finite but small rotations, is adopted for extending the planar element formulations to the counterpart in three-dimensional space. The updated Lagrangian description and the incremental secant stiffness method are introduced for efficient consideration of large deflections in analysis. The element formulations and the kinematic descriptions of motion are also described. At last, verification examples are given for the validation of the accuracy of the proposed numerical method.

Chapter 5 proposes a cross section analysis technique for arbitrary sections in a hybrid steel and concrete frame. In order to calculate the sectional capacities, a quasi-Newton iterative scheme is adopted for determining the neutral axis of a section. Three types of sectional yield surfaces, namely the initial yield, failure and concrete fracture surfaces, are proposed for the uses in the second-order design and advanced analysis. Finally, the validations for the cross section analysis technique

will be conducted and compared with published works in literatures and design codes.

Chapter 6 gives a unified design approach for hybrid steel and concrete members and frames. By adopting the curved ALH element as proposed previously, the P-Δ and P-δ effects and initial imperfections can be explicitly reflected in analysis and the member design can then be checked simply by the failure surface at the critical locations. In order to clarify the design philosophy, its design principles will be discussed. Further, the codified provisions for the second-order analysis and design of RC, BS and SCC members from Eurocode 2 (2004), Eurocode 3 (2005) and Eurocode 4 (2004), respectively, are discussed. Finally, a series of individual columns and several portal frames are selected for analysis and design.

Chapter 7 proposes an advanced analysis approach for the hybrid steel and concrete members and frames. The curved ALH element, which has maximum three plastic hinges along its length, is adopted allowing for various effects such as initial imperfections, geometric and material nonlinearities. A refined plastic hinge model combined with use of the sectional yield surfaces is proposed for simulating the inelastic behavior of a member. Cracking in concrete component is considered by the flexural stiffness modeling approach based on Branson's model combining with the concrete fracture surface. Consequentially, only the basic material properties are required for analysis and design. To obtain an accurate result, the constitutive models form codes and literatures are discussed. In order to use high strength concrete (HSC) in concrete-filled composite columns, which is still not covered in codes, an

experimental study was established. Finally, several calibrated examples are presented for illustrating the accuracy and validity of the proposed method.

Chapter 8 is the final chapter which concludes the study of this thesis and presents the significance of this research project. Furthermore, the recommendations for future works are also given.

Figures

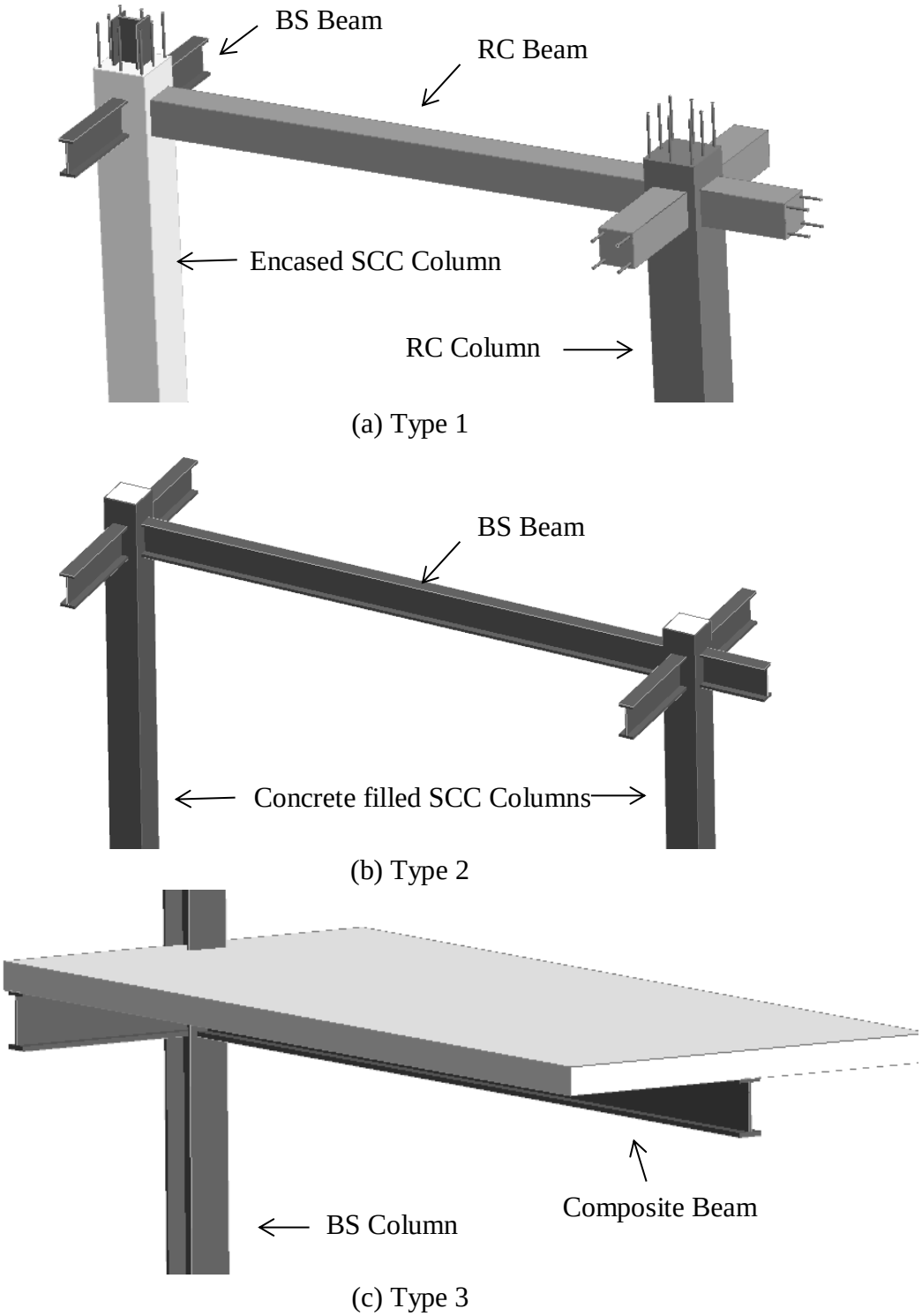

Figure 1.1 Illustrations of hybrid steel and concrete frames

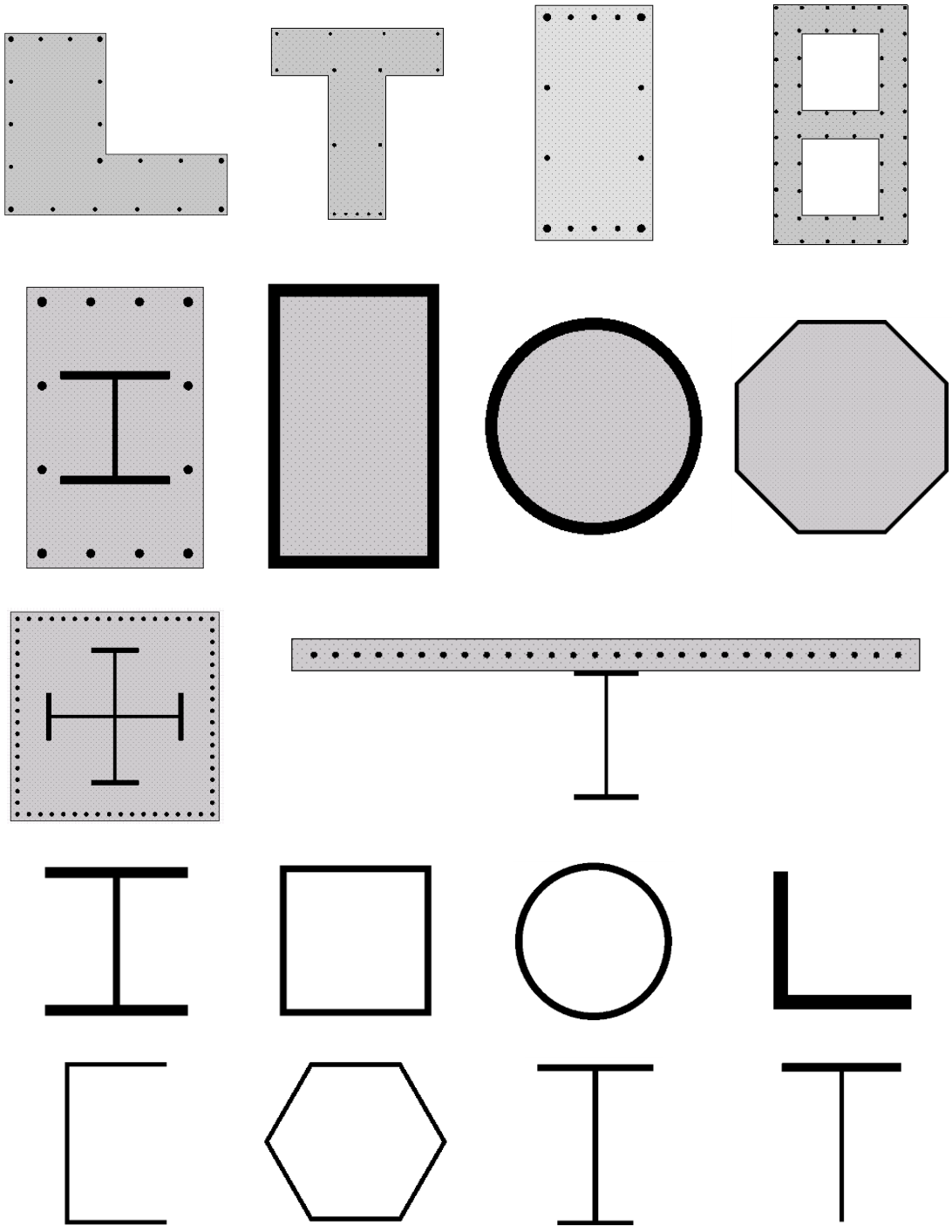

Figure 1.2 Common sections in a hybrid steel and concrete framed structure

CHAPTER 2

LITERATURE REVIEW

This chapter presents a review on the beam-column finite element methods for nonlinear analysis and the features of several available elements are discussed. To consider material nonlinearity, two popular inelastic analysis methods, namely as the plastic hinge and the plastic zone approaches, are concluded. Since the capacities of a cross section under different limit states are the essential parameters in this research, the related analysis techniques are summarized and discussed. In addition, the second-order design and advanced analysis methods are reviewed and elaborated.

2.1. Beam-column finite element methods for nonlinear analysis

The beam-column element analysis method is generally regarded to be considerably efficient and effective in design of practical framed structures and the research has been extensive conducted since 1970s. Along with the rapid development of computer technology with higher speed and larger memory, this beam-column finite element approach has been extended to the structural nonlinear problems. Consequently, extensive efforts had been made by many researchers, including Meek and Tan (1984), Chan and Kitipornchai (1987), Chan (1988), Bridge *et al.* (1990), Chan and Zhou (1994), Chen and Chan (1995), Izzudin and Smith (1996), Spacone *et al.* (1996), Izzuddin (1996), Liew *et al.* (1997), Neuenhofer and Filippou (1998), Pi *et al.* (2006a, 2006b) and so on, who have used various

numerical techniques for solving nonlinear engineering problems. To this end, several reliable and numerically stable beam-column elements have been derived and developed for various types of nonlinear analysis.

In this research project, several beam-column elements have been studied. For clarity, the element formulations of these elements are briefly reviewed in this section.

2.1.1 Cubic Hermite element

The cubic Hermite element is one of the most simple and popular elements used in engineering analysis, which was adopted by many researchers as Connor *et al.* (1967), Bathe and Bolourchi (1979), Meek and Tan (1984), Chan and Kitipornchai (1987), Kassimali and Abbasnia (1991), Teh (2001) and so on. The shape function of the element can be expressed as,

$$v = \sum_{i=0}^{3} a_i x^i = N_1 L\theta_1 + N_2 L\theta_2 \tag{2.1}$$

where, v denotes the lateral displacement along element length; L is the element length; a_i is the coefficients in the shape functions; ξ is the dimensionless coordinate; θ_1 and θ_2 are the rotations at two ends; and N_1 and N_2 are the shape function parameters expressed as,

$$\xi = 2x / L \tag{2.2}$$

$$N_1 = \frac{1}{8}(1-\xi)(1-\xi^2) \tag{2.3}$$

$$N_2 = -\frac{1}{8}(1+\xi)(1-\xi^2) \tag{2.4}$$

Moreover, the axial lengthening due to bowing can be written as,

$$u_b = \int_0^L \left(\frac{dv}{dx}\right)^2 dx = \frac{L}{30}\left(2\theta_1^2 - \theta_1\theta_2 + 2\theta_2^2\right) \tag{2.5}$$

in which, u_b is the axial shortening due to element bowing.

Therefore, the secant relations can be obtained by the first derivation of the total potential energy equation as,

$$P = EA\left[\frac{e}{L} + \frac{1}{30}\left(2\theta_1^2 - \theta_1\theta_2 + 2\theta_2^2\right)\right] \tag{2.6}$$

$$M_1 = \left(\frac{4EI}{L} + \frac{4PL}{30}\right)\theta_1 + \left(\frac{2EI}{L} - \frac{PL}{30}\right)\theta_2 \tag{2.7}$$

$$M_2 = \left(\frac{2EI}{L} - \frac{PL}{30}\right)\theta_1 + \left(\frac{4EI}{L} + \frac{4PL}{30}\right)\theta_2 \tag{2.8}$$

in which, EA is the axial rigidity; EI is the flexural rigidity; e is the total axial shortening; P is the axial forces; and M_1 and M_2 are the bending moments at two ends.

From the element formulations, it is observed that the element deflection cannot be too large otherwise the analysis results could be inaccurate because the deflection function is cubic and under constant shear. Therefore, two and more elements are usually required for modeling a single member in order to minimize the errors. So and Chan (1991) reported that, the buckling load of a simple supported strut was over-estimated by 21.6% if the member was modeling by one cubic element.

Moreover, the initial member curvature and the corresponding P-δ effect are unable to be simulated and therefore this element formulation might be outdated and not suitable for the direct use in second-order nonlinear analysis.

2.1.2 Curved Pointwise Equilibrating Polynomial (PEP) element

The initially curved Pointwise Equilibrating Polynomial (PEP) element as proposed by Chan and Zhou (1995) has been extensively adopted for various types of second-order nonlinear analysis in the past decade. This element is especially suitable for second-order nonlinear analysis and also fulfilled the codified requirements where only one element per member is adequate for most nonlinear analyses. The element is initially curved and the member imperfection can be expressed as,

$$v_0 = v_{mo}(1 - t^2) \qquad t = 2x/L \text{ and } -L/2 \le x \le L/2 \tag{2.9}$$

in which, v_0 is the lateral initial imperfection along the member; t is the non-dimensional distance along the element; and v_{m0} is the amplitude of initial imperfection at the mid-span.

In PEP element, there are totally four and two boundary conditions for compatibility and equilibrium respectively and given as,

$$\text{At } x = \pm\frac{L}{2};\ v = 0 \tag{2.10}$$

$$\text{At } x = \pm\frac{L}{2};\ \dot{v} = 0 \tag{2.11}$$

$$EI\,\ddot{v} = N_x(v + v_0) + \frac{M_1 + M_2}{L}\left(\frac{L}{2} + x\right) - M_1 \tag{2.12}$$

$$EI\ \ddot{v} = N_x \dot{v} + \frac{M_1 + M_2}{L} \tag{2.13}$$

Therefore, a fifth-order polynomial function is assumed as,

$$v = a_0 + a_1 x + a_2 x^2 + a_3 x^3 + a_4 x^4 + a_5 x^5 \tag{2.14}$$

By solving the boundary conditions and the shape function can be written as,

$$v = N_1 \left(L\theta_1 \right) + N_2 (L\theta_2) + N_0 v_{m0} \tag{2.15}$$

where, the N_1, N_2 and N_0 are given by,

$$N_1 = \frac{A}{H_1} + \frac{B}{H_2} \tag{2.16}$$

$$N_2 = \frac{A}{H_1} - \frac{B}{H_2} \tag{2.17}$$

$$N_0 = -q\left(1 - t^2\right)^2 / H_2 \tag{2.18}$$

and,

$$A = -20\frac{x}{L} + (80 - q)\left(\frac{x}{L}\right)^3 + 4q\left(\frac{x}{L}\right)^5 \tag{2.19}$$

$$B = 6 - \frac{1}{2}(48 - q)\left(\frac{x}{L}\right)^2 - 2q\left(\frac{x}{L}\right)^4 \tag{2.20}$$

$$H_1 = 80 + q \tag{2.21}$$

$$H_2 = 48 + q \tag{2.22}$$

$$q = \frac{PL^2}{EI} \tag{2.23}$$

The distinctive advantages of this element lie on the accurate consideration of member initial imperfection and the capacity for simulating large deflections by only one element per member. Zhou and Chan (2004) extended the PEP element for the elasto-plastic and large deflection analysis of steel frames, where an arbitrarily

located elastic-perfectly-plastic hinge can be formed along the element length. Chan and Cho (2008), Cho and Chan (2008) and Fong *et al.* (2009) used the PEP element for second-order analysis of single angle trusses and verified the analysis results by experiments. Fong *et al*. (2010; 2011) studied the application of the PEP element for nonlinear analysis of composite steel and concrete members and frames, and conducted a series of experimental investigations for verifications. Liu *et al*. (2010) utilized this element for performance-based seismic design by the pushover analysis approach.

2.1.3 Stability function element

The stability function element was originally proposed by Livesley and Chandler (1956) and adopted for the analysis of structural steel frames. The stability function was obtained by directly solving the differential equilibrium conditions between the element forces and deformations. Based on the stability function approach, Oran (1973a, 1973b) adopted the co-rotational description and proposed the tangent stiffness matrix for planar and spatial analysis respectively, and the equilibrium equation of his stability function element can be expressed as,

$$M_1 = \frac{EI}{L}\left[c_1\theta_1 + c_2\theta_2\right] \tag{2.24}$$

$$M_2 = \frac{EI}{L}\left[c_2\theta_1 + c_1\theta_2\right] \tag{2.25}$$

$$P = EA\left[\frac{u}{L} - b_1\left(\theta_1 + \theta_2\right)^2 - b_2\left(\theta_1 - \theta_2\right)^2\right] \tag{2.26}$$

where, the b_1 and b_2 are the curvature functions due to axial loads; c_1 and c_2 are the stability function. However, these parameters are different for the compression and tension conditions. For the compression condition, they can be expressed as,

$$c_1 = \frac{\phi(\sin\phi - \phi\cos\phi)}{2(1-\cos\phi) - \phi\sin\phi} \tag{2.27}$$

$$c_2 = \frac{\phi(\phi - \sin\phi)}{2(1-\cos\phi) - \phi\sin\phi} \tag{2.28}$$

$$b_1 = \frac{(c_1 + c_2)(c_2 - 2)}{8\pi^2 q} \tag{2.29}$$

$$b_2 = \frac{c_2}{8(c_1 + c_2)} \tag{2.30}$$

in which

$$\phi^2 = \frac{PL^2}{EI} = \pi^2 q \tag{2.31}$$

$$q = \frac{PL^2}{\pi^2 EI} \tag{2.32}$$

While, for the tension condition, the parameters can be written as,

$$c_1 = \frac{\psi(\sinh\psi - \psi\cosh\psi)}{2(\cosh\psi - 1) - \psi\sinh\psi} \tag{2.33}$$

$$c_2 = \frac{\psi(\psi - \sinh\psi)}{2(\cosh\psi - 1) - \psi\sinh\psi} \tag{2.34}$$

and

$$\psi^2 = -\frac{PL^2}{EI} = -\pi^2 q \tag{2.35}$$

For the special condition that the no axial load exists, the parameters are given as,

$$c_1 = 4 \tag{2.36}$$

$$c_2 = 2 \tag{2.37}$$

According to these sets of parameters, it can be noticed that there may be numerical instability during the analysis when the axial load is very small and numerical divergence may occur.

Later, the stability function approach has been studied and developed by many researchers. Chen and Lui (1987) further refined by a power series and the truncations were eliminated. And Goto and Chen (1987) formulated this power series and proposed a complete set of tangent stiffness matrix for the nonlinear analysis. Ekhande *et al*. (1989) derived a new complete set of stability function for the three-dimensional frames. Chan and Gu (2000) incorporated the initial member imperfection to the stability function and developed a second-order analysis approach using one element per member. Kim *et al*. (2006) proposed a stability function element allowing for the consideration of lateral-torsional buckling.

2.1.4 Beam element with mid-span and end springs

In the conventional plastic hinge approach, the plastic hinges are only allowed to form at the element ends, and many researchers have successfully adopted this method for inelastic analysis of steel frames, such as Al-Mashary and Chen (1991), White (1993), Kim and Chen (1996), Chan and Chui (1997), Chiorean and Barsan (2005), Gong (2006) and so on. Usually, two and more elements are required to model a member since the location of a plastic hinge may occur along the member length due to distributed loads. In order to improve numerical efficiency and reduce the modeling efforts, Chen and Chan (1995) firstly proposed a beam element with one mid-span and two end springs for elasto-plastic analysis of steel beams by single element per member as illustrated in Figure 2.3.This is a super element containing two sub-elements, which are connected by a degradable spring placed at the mid-span. The incremental equilibrium equations can be written as,

$$4EI\begin{bmatrix} \frac{2}{L} & \frac{1}{L} & -\frac{6}{L^2} & 0 & 0 \\ & \frac{2}{L}+\frac{R}{L} & -\frac{6}{L^2} & -\frac{R}{4} & 0 \\ & & \frac{24}{L^3}+\frac{24}{L^3} & \frac{6}{L^2} & \frac{6}{L^2} \\ & \textit{symm.} & & \frac{2}{L}+\frac{R}{L} & \frac{1}{L} \\ & & & & \frac{2}{L} \end{bmatrix}\begin{bmatrix} \Delta_1\theta_1 \\ \Delta_1\theta_2 \\ \Delta v \\ \Delta_2\theta_1 \\ \Delta_2\theta_2 \end{bmatrix}=\begin{bmatrix} \Delta_1 M_1 \\ \Delta_1 M_2 \\ \Delta F \\ \Delta_2 M_1 \\ \Delta_2 M_2 \end{bmatrix} \tag{2.38}$$

where, $\Delta_1\theta_1$ and $\Delta_1\theta_2$ are the element rotations at the left sub-element and the corresponding moments are $\Delta_1 M_1$ and $\Delta_1 M_2$; $\Delta_2\theta_1$ and $\Delta_2\theta_2$ are the element rotations at the right sub-element with the associated moments as $\Delta_2 M_1$ and $\Delta_2 M_2$; Δv and ΔF are respectively the lateral displacement and shear force at the mid-span; and R is the spring stiffness at the mid-span and connects the two sub-elements.

The above equation can be rewritten as,

$$4EI\begin{bmatrix} k_{ii} & k_{ie} \\ k_{ie}^T & k_{ee} \end{bmatrix}\begin{bmatrix} \Delta u_i \\ \Delta u_e \end{bmatrix}=\begin{bmatrix} \Delta M_i \\ \Delta M_e \end{bmatrix} \tag{2.39}$$

in which,

$$\Delta u_i = \{\Delta_1\theta_2 \quad \Delta v \quad \Delta_2\theta_1\}^T \tag{2.40}$$

$$\Delta u_e = \{\Delta_1\theta_1 \quad \Delta_2\theta_2\}^T \tag{2.41}$$

and

$$k_{ii} = 4EI\begin{bmatrix} \frac{2}{L}+\frac{R}{L} & -\frac{6}{L^2} & -\frac{R}{4} \\ & \frac{24}{L^3}+\frac{24}{L^3} & \frac{6}{L^2} \\ \textit{symm.} & & \frac{2}{L}+\frac{R}{L} \end{bmatrix} \tag{2.42}$$

$$k_{ii} = 4EI\begin{bmatrix} \frac{1}{L} & 0 \\ -\frac{6}{L^2} & \frac{6}{L^2} \\ 0 & \frac{1}{L} \end{bmatrix} \tag{2.43}$$

$$k_{ii} = 4EI\begin{bmatrix} \frac{2}{L} & 0 \\ 0 & \frac{2}{L} \end{bmatrix} \tag{2.44}$$

In order to enhance numerical efficiency, the internal degrees of freedoms are condensed and the equilibrium equations are rewritten as,

$$4EI\begin{bmatrix} k_{ii} & k_{ie} \\ k_{ie}^T & k_{ee} \end{bmatrix}\begin{bmatrix} \Delta u_i \\ \Delta u_e \end{bmatrix} = \begin{bmatrix} \Delta M_i \\ \Delta M_e \end{bmatrix} \tag{2.45}$$

and the tangent stiffness and the external loads are condensed as,

$$k^*[\Delta u_e] = \Delta M^* \tag{2.46}$$

where,

$$k^* = k_{ee} - k_{ie}^T k_{ii}^{-1} k_{ie} = EI\begin{bmatrix} \frac{4LR+3}{\beta} & \frac{2LR+3}{\beta} \\ \frac{2LR+3}{\beta} & \frac{4LR+3}{\beta} \end{bmatrix} \tag{2.47}$$

$$\beta = L\left(LR+1\right) \tag{2.48}$$

$$\Delta M^* = \Delta M_e - \frac{L}{4\beta}\begin{bmatrix} LR-1 & -\frac{L^2R}{2}-L & LR+3 \\ LR+3 & \frac{L^2R}{2}+L & LR-1 \end{bmatrix} \cdot \Delta M_i \tag{2.49}$$

However, this element formulation is only suitable for inelastic analysis of beams and the location of the internal plastic hinge is also fixed at the mid-span. Therefore, a new beam-column element is needed to be derived, where the internal

plastic hinge can be arbitrarily located and the second-order effects associated with the initial member imperfection can be reflected.

2.1.5 Other elements

Some elegant elements have been derived by other researchers ,such as King *et al.* (1992), Pi and Trahair (1994a, 1994b), Neuenhofer and Filippou (1998), Barsan and Chiorean (1999), El-Tawil and Deierlein (2001a, 2001b), Nukala and White (2004) and so on, these elements perform well in many frame analysis. However, they are mostly based on straight geometry that initial member imperfections present in practical members and required in codes are not modeled efficiently. On the other hand, curved beam-column elements have been developed, but they are limited to linear analysis so reliable elements allowing for initially curved geometry and large deflection is not available for nonlinear analysis. To this, one objective of this project is to develop such an element for the purpose of efficient advanced analysis of framed structures undergoing large deflection and material yielding with plastic hinges formed along the element length or at its ends.

2.1.6 Discussions

In this section, several types of available beam-column elements have been discussed and the corresponding formulations are briefly presented. Since the material characteristics are different among the members in a hybrid steel and concrete framed structure, the element for the present study should be capable of simulating large-deflection and inelastic-behavior simultaneously. Moreover, the

initial imperfection exists in practical members and needs to be modeled in the nonlinear analysis. Therefore, the element should possess initial imperfection and it should be capable of modeling and locating the critical position for plastic hinge along member length or at its ends.

The cubic Hermite element as illustrated by Meek and Tan (1984) is the most popular beam-column element and widely-adopted in engineering practice. Due to its limited deformation capacity, two and more elements are required for a structural member, which not only causes difficulties in modeling of initial imperfections, but also dramatically increases the computational expenses for the nonlinear analysis.

The curved PEP element proposed by Chan and Zhou (1995) is a high-order and stable element for nonlinear analysis and capable for simulating very large-deflection by only one element per member. The initial member curvature is also modeled in the element formulation. This element is especially suitable for the second-order elastic analysis and design for the slender and irregular framed structures. However, as to reflect the inelastic behavior along member length in an advanced plastic analysis, two elements are still required, which causes difficulties in locating the hinge position and additional modeling efforts. Although it has a version of plastic hinge along a member, it needs to be predominantly under axial load and moment due to loads along member is only assumed at ends.

The stability function element is derived from the differential equilibrium equation based on the Timoshenko's beam-column theory (1935) and is a closed-formed solution. Chan and Gu (2000) developed the classical element and

incorporated the initial member imperfection to element formulations, which is proven to be highly accurate. However, the element formulations are complicated and three sets of tangent stiffness matrix are needed for the analysis, namely as compression, tension and zero axial load cases respectively. Furthermore, the numerical instability might occur when the axial load is very small. Similarly, the plastic hinge cannot form along element length and two more elements are still required for an advanced inelastic analysis.

The beam element with mid-span and end springs proposed by Chen and Chan (1995) is suitable for the inelastic analysis of a beam under uniform distributed loads. However, the second-order effect due to axial load cannot be considered in this element, and the location of the middle hinge is fixed. Moreover, the element formulation is derived for the analysis of the two-dimensional frame, and its extension to spatial frames needs to be explored. The concept of this element is attractive, where two simple elements can be integrated into a super-element for advanced nonlinear problems.

In summary, these available elements are not entirely suitable for the present study, and therefore, a new curved beam-column element is needed to be derived in this thesis.

2.2. Inelastic analysis methods for beam-column element

Material yielding is another major factor controlling the ultimate load and overall stability of a framed structure, which are necessarily considered in the

Advanced Analysis. Conventionally, two methods are widely adapted namely as the plastic hinge and the plastic zone approaches. The plastic hinge analysis method, also named as lumped plasticity approach, is to concentrate the element inelastic behavior at a section along a member with stiffness modeled by the degradable springs. While, the plastic zone analysis method, also referred as the distributed plasticity method, is to simulate the spreading of plasticity within a volume of the member. Both methods have been extensively studied and applied in solving various types of material nonlinear problems. In order to select a practical and efficient inelastic analysis approach for the present study, the plastic hinge and the plastic zone approaches are reviewed in this section.

2.2.1 Plastic hinge approaches

The basic concept of plastic hinge approach assumes plasticity is only lumped at the two ends of an element, while the other portion within the element remains elastic throughout the analysis. Therefore, two zero-length springs are inserted to the ends of the conventional beam-column element shown in Figure 2.4. Two types of plastic hinge models have been widely adopted as the traditional plastic hinge and the refined plastic hinge approaches, as illustrated in Figure 2.5.

In the traditional plastic hinge approach, it assumes that the hinge stiffness is infinitely large before section fails at the hinge location, while it will degrade to a frictionless hinge as its ultimate capacity. Therefore, an abrupt change of the load vs. deflection behavior would occur during the analysis. This method is simple and only the failure criterion for a section is needed. Many researchers have utilized this

method for inelastic analysis of individual members or frames. Harstead *et al*. (1968) used the plastic hinge approach for inelastic analysis of the H-columns under biaxial bending. Alvarez and Birnstiel (1969) proposed an inelastic analysis method for multi-story steel frames. Kassimali (1983) presented a numerical procedure for large deformation and inelastic analysis of steel frames. Wong and Tin-Loi (1990) produced an incremental analysis approach for steel frames accounting for the effects of both geometrical and material nonlinearities. Freitas, and Ribeiro (1992) presented an numerical method for the nonlinear analysis of imperfect space trusses. Guralnick and He (1992) conducted an analysis of the elastic-perfectly plastic framed structures. More recently, Liu *et al*. (2010) adopted this method for performance-based seismic design based on the pushover analysis and reported that the traditional plastic hinge is efficient and suitable for the use in engineering practice.

In contrary to the traditional plastic hinge approach, a smooth transition from ideally elastic to fully plastic stages can be achieved in the refined plastic hinge method, as demonstrated in Figure 2.5. The section springs will be gradually softened according to the loadings that the partial yielding effects can be simulated, where two sectional conditions are needed to be defined as elastic-limit and failure states respectively. The refined plastic hinge method has been studied extensively in the past. Chan and Chui (1997) proposed a generalized design-based elas-to-plastic analysis method for steel framed by section assemblage concept. Kim and Chen (1998) suggested a sensitivity study on the required number of elements in refined plastic-hinge analysis. Liew *et al*. (2000a) developed an improved plastic hinge approach for three-dimensional nonlinear analysis of steel framed structures. Kim *et*

al. (2002, 2003) explored the refined plastic hinge and incorporated the considerations of the local and lateral torsional buckling.

2.2.2 Plastic zone approaches

In the plastic zone analysis, all members and their sections are needed to be discretized into a certain number of sub-elements and fibers as illustrated in Figure 2.6. Each fiber in a section will be monitored, and the overall member deformation is obtained through a numerical integration process across the discretized section at the integrations points along the element length. Herein, the spread of plasticity in the whole volume of the member can be explicitly reflected. The accuracy of the analysis by the plastic zone approach depends on the number of the integration points along the element and the fiber length of the section. Usually, the plastic zone approach is considered to be an exact and elaborated method, and many researchers selected this method for study the inelastic structural behaviors of individual members and simple frames.

The results from the plastic zone approach are usually treated as the benchmark examples for verifying the inelastic analysis approaches as well as the computer programs. Chu and Pabarcius (1964) studied the elastic and inelastic buckling of portal frames. El-Zanaty (1980) evaluated the inelastic behavior of multistory planar steel frames. Yang and Saigal (1984) proposed an analytical model involving geometrical and material nonlinearities for the static and dynamic responses of beams. White (1985) developed a plastic-zone approach for the elastic analysis of planar steel frames. Meek and Lin (1990) used the updated Lagrangian formulation

and the plastic-zone analysis for the thin wall members, and the yielding of the steel plates was considered. Toma and Chen (1992) carefully studied three steel frames and also recommended these examples as benchmark problems for calibrating the inelastic analysis approaches. Fang *et al*. (1999, 2000) developed an approach based on the plastic zone method for inelastic analysis of composite beams with the semi-rigid connections. Teh and Clarke (1999) extended the plastic zone approach for three-dimensional analysis of steel frames.

2.2.3 Discussions

In this section, the two popular inelastic analysis methods are reviewed and discussed. Generally speaking, the plastic hinge method is simple and efficient, but local plasticity cannot be accurately reflected. While, the spread-of-plasticity can be reflected in the plastic zone approach, however, the required computer time is much more extensive. In order to select a practical and accurate inelastic method for the present study, these two methods are compared.

In terms of accuracy, King *et al*. (1992) compared the plastic hinge and plastic zone approaches and summarized that: (a) the plastic hinge method can be satisfactorily performed in most of the common cases; (b) the ultimate strength and the overall load-deflection results by the two approaches are closed; and (c) the local region of a large frame where the columns are under high axial loads, the predicted results by the plastic hinge method might be less accurate than the predictions of the system behavior. Generally, in most engineering applications, the analysis accuracy

of the plastic hinge method is comparable to the plastic zone analysis by adopting the proper plastic hinge models.

When referred to the numerical efficiency, Ziemian (1993) studied the two approaches and indicated that, the required calculation time for the plastic zone analysis method could reach to a hundred times greater than that for the plastic hinge analysis approach. Thus, as a result of the huge computational expense, Kim and Chen (1996) reported that the plastic-zone solution cannot be adopted efficiently in engineering practice and therefore limited to the utilizations in research.

In summary, in order to formulate a practical inelastic analysis method for the moderate and large-scale framed structures, the plastic hinge approach is undoubtedly preferred. However, since the plastic hinge model crucially affects the accuracy of the analysis, its formulation also needs to be studied and investigated in this thesis.

2.3. Cross section analysis methods

The cross section analysis technique for various sections in a framed structure has been extensively studied since the 1960s. However, due to the limited capacities of computers during that time, many hand-calculated equations and design diagrams were proposed for the specified type and shape of a section. Moreover, member subjected to axial load and biaxial bending is very common in practical structures, such as the corner columns, and these equations, including the simplified iterative relations between the two bending axes, may result in an uneconomical design.

Santathadaporn and Chen (1968) studied biaxial bending capacities of two types of steel sections, namely as rectangular and wide-flange I shapes, and proposed the design equations for calculating their lower and upper bound moment capacities. Their formulations are based on an equilibrium approach, and the stress resultant is achieved by mathematical integration. Further, the neutral axis still needs to be pre-determined, and possible locations for a wide-flange I section are evaluated. Several standard sections are analyzed with their whole yield surfaces presented.

The biaxial interaction diagrams of reinforced concrete (RC) sections were widely studied. Bresler (1960) investigated the design criteria for a RC section under pure axial load and biaxial bending and the concept of failure surfaces was introduced. Furlong (1961) investigated the biaxially loaded ultimate strength of square columns, and several design diagrams were given. A simplified ultimate strength method of design for columns subjected to bending about both principal axes was presented by Fleming *et al.* (1965), where a series of non-dimensional design curves were derived. Moreadith (1978) studied the rectangular RC sections under tension and uniaxial bending and proposed the corresponding interaction curve. Later, several irregularly shaped sections, such as T-shaped, L-shaped, channel-shaped and others, had been studied by Hsu and his co-workers (1987, 1988, 1989; 1985) .

With the rapid development of technology in personal computers, the analysis technique for cross sectional capacity of complex shapes and composed of different materials has been extensively developed in the past decades. The tedious and less

accurate hand calculation formulations and design diagrams can be avoided and complex and irregular sections can be designed and analyzed in practice. Several numerical algorithms have been recently proposed for sections of arbitrary shape. In order to distinguish the differences between these methodologies, the following key characteristics are reviewed.

- Whether the composite sections can be analyzed, or the solution is limited to bare steel or reinforced concrete sections;
- Whether arbitrary functions of material constitutive models can be inputted, or the simplified bi-linear material curves are assumed;
- Whether the section is divided into fibers or pieces for the stress integration, or the closed-form integral formulations are adopted; and,
- Whether the location of the neutral axis can be efficiently and accurately determined.

A method of calculating the ultimate flexural capacity of a polygonal concrete cross section with arbitrary reinforcement was proposed by Brondum-Nielsen (1985). The method can be adopted for both the symmetrical and unsymmetrical sections with or without openings and is also suitable for computer programming. However, the position of the neutral axis is needed to be pre-assumed in this approach and this leads to inaccuracy and inconvenience.

Rotter (1985) presented a numerical technique to provide an exact solution for solid polygonal sections without openings. The method is based on the Green's theorem (Sokolnikoff, Redheffer, & Avents, 1958). The stress resultant and the

tangent stiffness are exactly derived. Nonlinear stress versus stain relations can be inputted. The numerical procedure is fast because only several points at the section boundaries are to be evaluated for the stress integrals. However, this method is only limited to analyze of simple and polygonal sections.

Later, an efficient quasi-Newton iterative method for the analysis and design of reinforced concrete sections under uniaxial or biaxial loads was proposed by Yen (1991) which was also suitable for the computer application. In his approach, the stress distribution of concrete is idealized to be a rectangular block and the stress versus strain relation for the reinforcing bears is assumed to be bi-linear. Convergence and numerical stability are not guaranteed for unusual and complex shapes.

Around a similar period, Yau *et al* (1993) presented a numerical procedure for the exact design and analysis of arbitrarily shaped reinforced concrete sections against a combination of axial force and biaxial bending moments. An iterative scheme is proposed for determining the position of the sectional neutral axis, and equivalent stress block method is adopted for calculating the stress resultant of concrete. Their approach can be used for oddly shaped concrete sections and minimum steel area can be calculated.

Vivo and Rosati (1998) proposed two algorithms for evaluating the ultimate strength capacity of reinforced concrete sections of arbitrary shape. A secant strategy is introduced for solving the nonlinear equilibrium equations. The stress resultants of the components are calculated by an accurate integration formula. However, the

concrete constitutive law is needed to be idealized to a fifth-order polynomial interpolation function and the mathematical formulations are complicated. The solutions are noticed to be effective for both regular and irregular sections.

Rodriguez and Aristizabal-Ochoa (1999) introduced a general method for calculating the RC cross section of any orientation of the neutral axis under biaxial bending moments. The closed-form expressions for the stress resultant are proposed, where the nonlinear stress versus strain relation for the concrete is adopted. The creep and confinement effects of the concrete can be considered in the method. The concrete component is required to be divided into several parallel layers and the corresponding stress resultant formulations are derived and given.

Chen *et al.* (2001) further improved the iterative quasi-Newton procedure by selecting the plastic centroid for the reference origins and extended the analysis approach to the steel and concrete composite sections. The convergence, numerical stability and speed are dramatically improved and the complex and irregular sections can be analyzed. The exact integral expressions of the stress resultants for both the polygonal and circular subsections are derived. Various types of material constitutive models can be inputted, while the tensile part of the concrete is neglected. This method is proven to be efficient and effective for ultimate limit state analysis. The sectional states under other specified conditions, such as elastic-limit or cracked-limit states, cannot be calculated by this method.

Sfakianakis (2002) proposed a novel computer technique for analysis of reinforced, composite and repaired concrete sections of arbitrary shape by fiber

model associated with the numerical computer graphics. In his approach, the computer graphics are employed as a computational tool for the integration of normal stress and therefore the whole section is described by a computer image with a certain amount of pixels. There is no iterative procedure in the solution procedure and divergence problem will not occur within each step. However, the required storage space and computational expense are enormous. In order to clearly present a cross section without distortion, the pixel should be tiny enough and the matrix for a cross section is extremely large. Moreover, since each pixel in the computer system is a rectangular block, when the boundary shape of the section is curved or circular, the sizes of each pixel are required to be extremely small in order to maintain a high level of accuracy for the analysis.

Charalampakis and Koumousis (2008) introduced a fiber model algorithm for the analysis of arbitrary composite sections under biaxial bending. The stress resultant is achieved by the analytical method. The complex composite sections containing openings can be analyzed by their method. The moment vs. curvature diagrams, bending moment interactions and failure surfaces can be obtained. In their approach, the structural steel section is divided into curvilinear trapezoids.

Chiorean (2010) proposed an incremental-iterative procedure based on the arc-length constraint equation for the analysis of composite steel and concrete cross sections. The tangent stiffness strategy was adopted for solving the nonlinear equilibrium equations. His approach was capable of dealing with design of arbitrary sections with various material properties. However, divergence is noticed in the given examples under the extreme conditions closed to pure compression or tension.

Papanikolaou (2012) presented a numerical methodology for the analysis of arbitrary composite sections under biaxial bending and axial load. Various types of material constitutive models can be considered as well as the geometry being complex. The stress integration is achieved by using the Green path integral, and an adaptive strain-mapped Gaussian sampling is introduced. An incremental solution strategy is adopted for calculating the ultimate responses. The strength interaction curves, three-dimensional failure surfaces and moment-curvature curves can be outputted by his approach. However, the calculation time might be huge due to the load step needs to be small for minimizing the errors in the incremental procedure.

2.4. Second-order design approach

Second-order method of analysis, which is also called as direct analysis method in AISC (2010), is a nonlinear and simulation-based approach allowing for various types of nonlinear effects for structural strength and stability, such as initial member and global frame imperfections, material residual stresses and so on. Therefore, the forces distribution and the deformations from the analysis are closed to the actual situation that a safe and reliable result can be obtained. Since the P-Δ and P-δ effects as well as the initial imperfections have been directly considered in analysis, the member strength check can be simply conducted by a cross section capacity check at the critical locations of a member. Unlike the conventional linear design method, which requires assumptions of column effective lengths associated with the tedious calculation of the K-factors, this design approach is efficient and the cumbersome assumptions are eliminated.

2.4.1 Consideration of initial imperfections

Imperfections unavoidably exist in all the members and frames caused during fabrication, construction, transportation and other activities like welding and therefore the perfectly straight assumption in the analytical model is unavailable in practice. In the second-order analysis method of design, the considerations of these effects are essential as reported by Chan and Zhou (1998). Two types of imperfections are usually taken into account namely as the initial member curvature and the frame out-of-plumpness. In a correct second-order design method, both these imperfections are needed to be considered in order to ensure the design results will be adequately safe.

The research on modeling of geometric initial imperfections was started in 1980s. Wen and Lange (1981) proposed a curved beam element for buckling analysis of arc members. Later, an investigation on the buckling and post-buckling behaviors due to the initial imperfections were carried out by Chajes (1983). Kam and Lee (1986) proposed a member tangent stiffness matrix for consideration of geometrical imperfections and it also introduced an incremental-interactive procedure to trace the load-displacement path of the frames. Srpčič and Saje (1986) developed an element with initial curvature for large deflection analysis of the thin and curved planar beam. However, the P-δ effect due to the member imperfections was not properly considered in their element formulations and the common types of frames had not been investigated in detail in their research.

Several sophisticated elements with the direct incorporation of the initial member imperfection have been derived and proposed in 1990s. Chan and Zhou (1995) derived a curved PEP (Pointwise Equilibrating Polynomial) element for second-order analysis of steel frames which was based on the finite element method with the high-order shape function. Chan and Gu (2000) further developed the stability function element allowing initial member curvature for practical design of framed structures. These elements are stable and widely accepted in many contemporary engineering practices. In the present research, a new initially-curved element with an internal arbitrarily located hinge is proposed and discussed in Chapters 3 and 4.

The major distinction of a correct second-order analysis method of design is to check whether geometric imperfections have been directly simulated in the analytical model. In this thesis, a unified design approach with considerations of both the initial member curvature and the global frame imperfection is proposed.

2.4.2 Current codes for second-order design

Research on the second-order design method for steel frames has been extensively studied in the past few decades and this method has been well-documented in most modern design codes such as AS4100 (1998), AISC (2010), Eurocode 3 (2005), Hong Kong Steel Code (2011). Further, AS4100 (1998) was the first national design code allows the use of nonlinear analysis approach for the design of steel frames and it was termed as “Advanced analysis”. This approach is also called as the “direct analysis method (DAM)” in AISC (2010) which

recommends its use in place of the traditional linear design method. Numerous steel frames have been designed by the second-order analysis method of design in the last ten years which was proven to be efficient, economical and adequately safe in engineering practice.

Several national codes, including AS5100 (2004), Eurocode 4 (2004), BS5400 (2005) and Hong Kong Steel Code (2011) can be utilized in the design of steel and concrete composite structures. The current approaches for the stability design of compression members are still based on the linear analysis method associated with the assumptions of the effective length or the moment amplification factors. However, the recently published Eurocode 4 (2004) accepts the second-order analysis method and the initial imperfections for various types of sections were also given. This method has been successfully adopted in design of composite members and portal frames as reported by Fong *et al*. (2010).

The second-order effects of slender reinforced concrete (RC) columns are required to be considered in the design codes, such as Eurocode 2 (2004), ACI 318 (2008), Hong Kong Concrete Code (2013) and so on. Nevertheless, these design methods are still based on the linear assumption and the considerations of these nonlinear and buckling effects are done indirectly by the indirect methods, such as the nominal stiffness and the nominal curvature methods in Eurocode 2 (2004). However, the concept and theoretical consideration of these P-Δ and P-δ effects as well as the initial imperfections are the theoretically same regardless of the members in different materials but the values of these imperfections may vary with respect to the types of materials and forming processes. Therefore, the second-order analysis

method of design for RC columns and frames is needed to be investigated and developed.

In order to carry out a second-order analysis for various types of members in a hybrid steel and concrete framed structure, different codes for these materials such as steel code for steel members and reinforced concrete code for RC members are unavoidably needed in design. This causes inconvenience and inconsistence of designing these members and therefore a unified second-order design approach is investigated in this thesis.

2.5. Advanced analysis method

Advanced analysis method is considered as an accurate simulation-based technique for investigating the ultimate behaviors of a structure under some extreme events, such as seismic attacks, progressive collapse and accidental occasions and so on. In order to obtain reliable analysis results, various types of important effects inherent to a real structure should be considered and they include initial imperfections, geometric and material nonlinearities, residual stress and concrete cracking. In the past decades, this method has been extensively studied and many researchers have proposed their analytical models for advanced analysis of framed structures.

White (1993) developed plastic hinge methods for advanced analysis of steel frames. He defined the term “advanced” as a method that sufficiently captures the limit states such that checking of the specification equations was not needed. Two

plastic hinge methods had been discussed and the consideration of geometric imperfection effects was also studied.

Kim and Chen (1996) proposed an advanced analysis method for planar un-braced steel frames. In order to consider the initial frame imperfection, three types of methods were discussed as (a) an explicitly modeling method by offsetting the nodes; (b) an equivalent notional force method and (c) a tangent modulus reduction method. According to their studies, all these methods could produce accurate analysis results by comparing to the plastic-zone analysis approach for the simple planar portal frames. However, these methods were only suitable for the regular planar frames and the P-δ effects induced by the member initial imperfection is modeled by using several elements that the modeling is complicated and inconvenient.

Liew *et al*. (1997) developed an advanced analysis technique for the large-displacement inelastic analysis of spatial structures. An imperfect strut model with one elastic-perfectly-plastic hinge placed at mid-span was proposed for simulating both the geometric and material nonlinearities. The structural instability due to initial imperfections can also be checked in their analytical model. They observed that the method predicts not only the limit load of the structure, but also assists to study the load sharing and force distributions of the framed system and to identify the critical members that their failure leads to progressive collapse.

Liew *et al*. (2000b) summarized the recent development of advanced analysis of spatial structures, where the modeling of inelasticity in beam-column members had been investigated. Further, the inelastic analysis methods for composite beams and

the modeling of semi-rigid connections were also reviewed. They claimed that the use of the advanced design philosophy could help the understanding about the system behavior so that a more rational and cost effective design could be achieved.

Kim and Choi (2001) proposed an advanced analysis method by accounting for the semi-rigid connections between beams and columns. The stability function element was introduced to capture the P-δ effect and the gradual material yielding was considered by the stiffness degradation model. The shear deformation was also included in their analytical model and the effects of the semi-rigid connections based on the Kishi-Chen (1990) power model was studied. From the comparisons with the plastic zone analysis, it showed a more accurate result could be obtained by their method.

Trahair and Chan (2003) reviewed methods for studying the out-of-plane behaviors of two-dimensional frames under in-plane loading, where the inelastic lateral buckling effects involving the residual stresses, initial member imperfections , twists and so on. The difficulties in the method were discussed and the suggestions had also been made for testing the accuracy of an analytical model.

Chan *et al.* (2005) reported a robust advanced analysis method based on a finite-element procedure for the large deflections and inelastic analysis of the imperfect frames with semi-rigid base connections. They introduced the refined plastic hinge approach for modeling of section yielding. The simulations of the framed global imperfections are specially considered and studied by two methods as the notional horizontal force method and the Eigen-buckling mode method. They found that, the

Eigen-buckling mode method was more suitable for engineering practice since the assumption of most adverse directions of imperfections was skipped. Moreover, they further reported that the semi-rigid base connection significantly affected the overall behavior of a structure.

2.6. Concluding Remarks

In this chapter, several beam-column finite elements for nonlinear analysis are reviewed where the four typical elements are presented along with their corresponding formulations. The inelastic analysis methods based on the plastic hinge and plastic zone approaches are summarized and discussed. Further, in order to evaluate various material types of cross sections in a hybrid steel and concrete framed structure, the analysis techniques are discussed. Finally, the development of second-order analysis and advanced analysis methods for design are discussed.

Figures

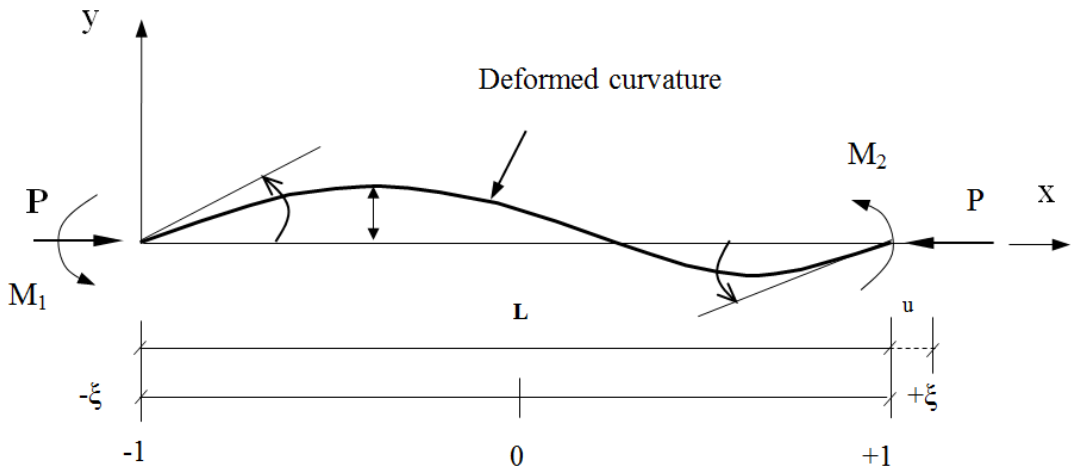

Figure 2.1 Forces vs. deformation in a beam-column element

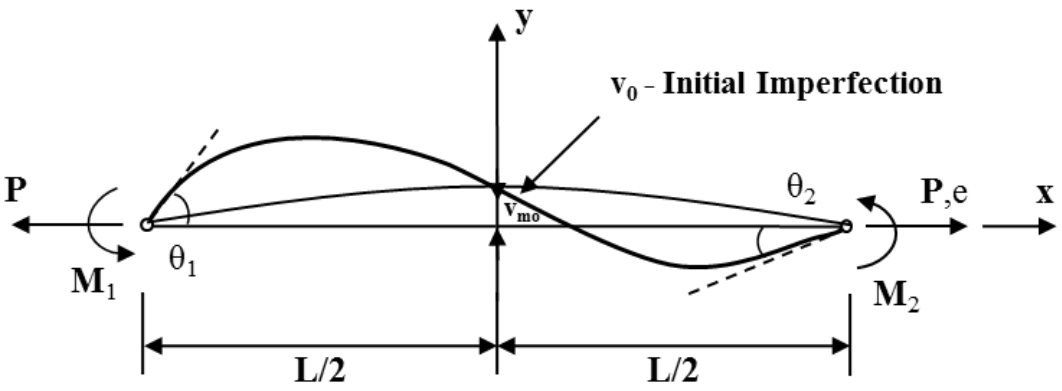

Figure 2.2 Forces vs. deformation of the curved PEP element

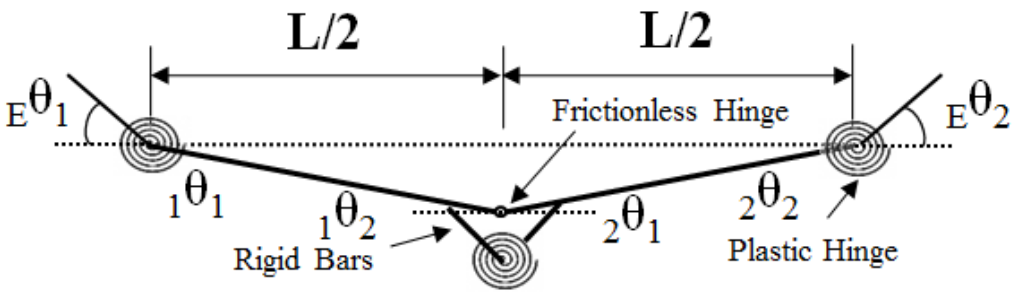

Figure 2.3 Beam element with mid-span and ended springs

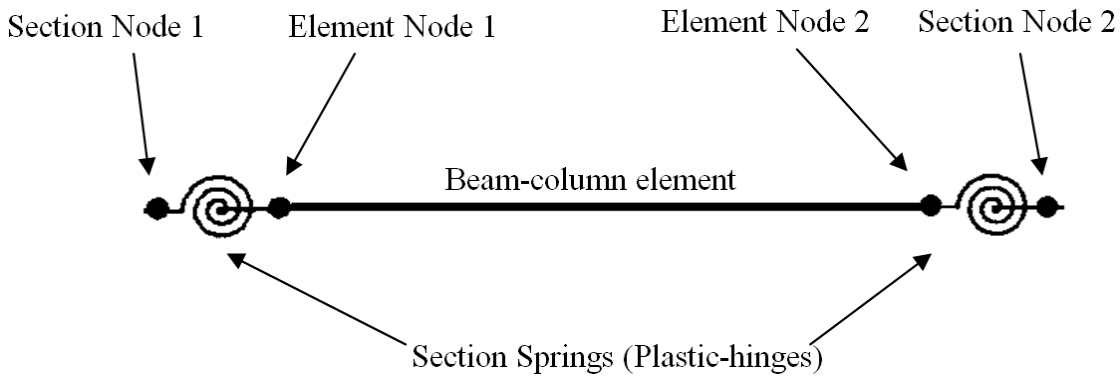

Figure 2.4 Illustration of plastic hinge approach

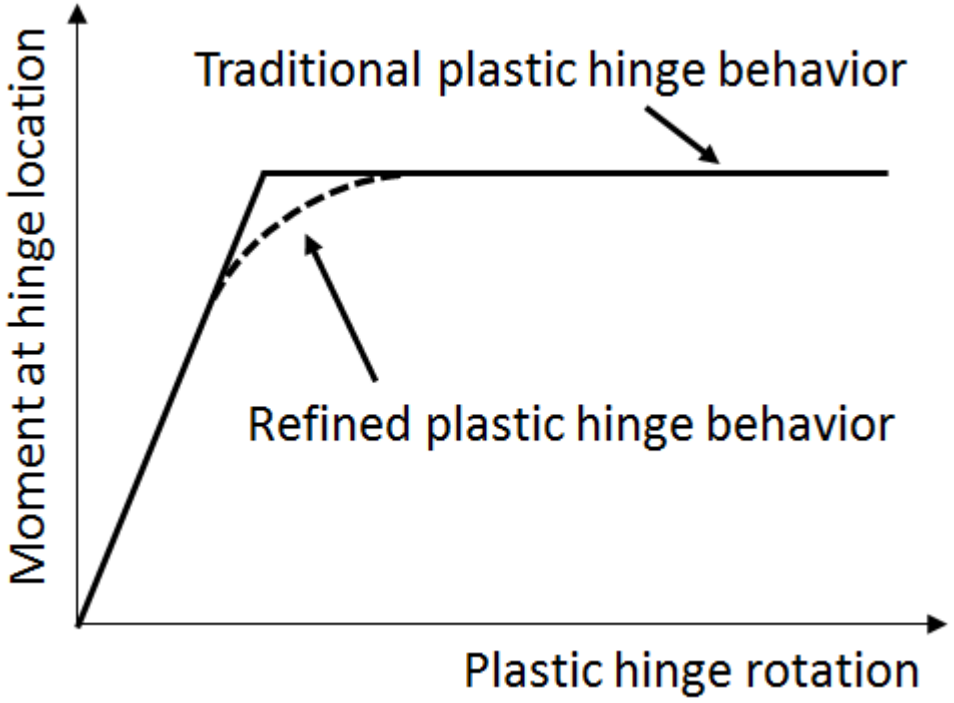

Figure 2.5 Behaviors of plastic hinge and refined plastic hinge

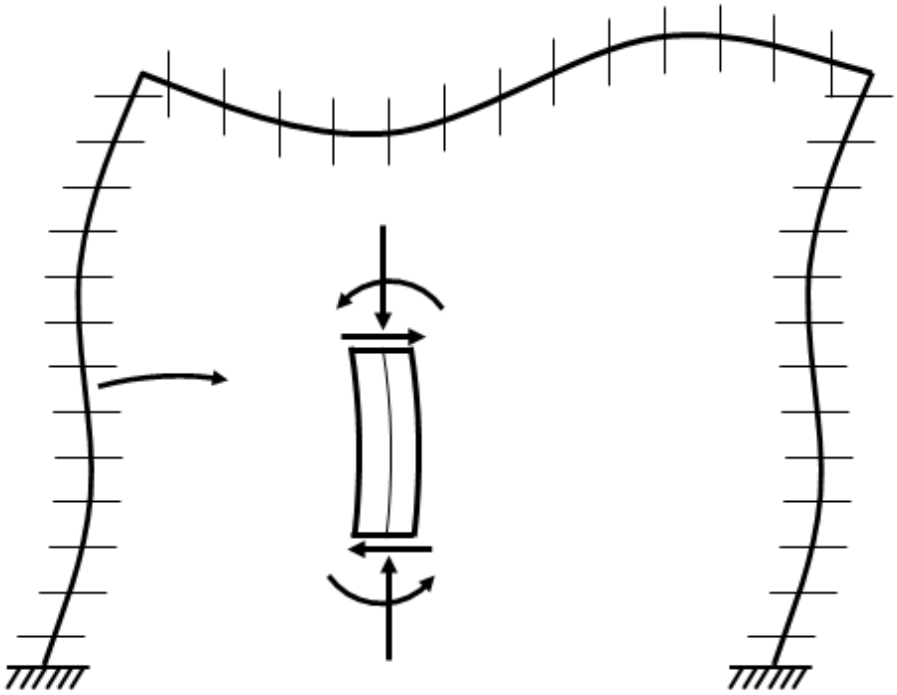

(a) Discrete framed structure

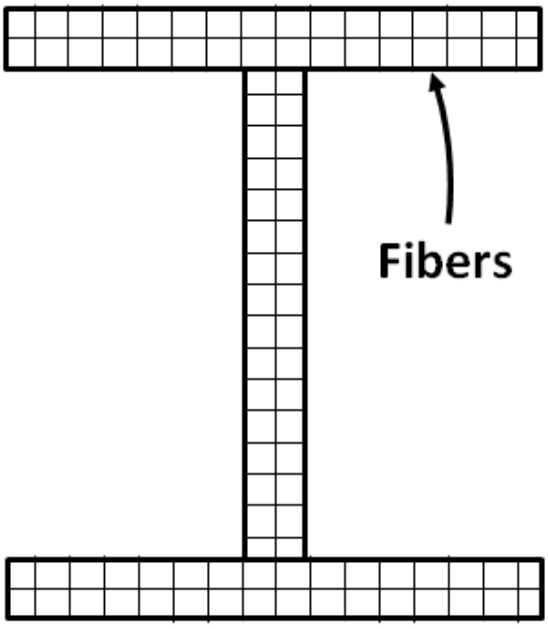

(b) Meshed section with monitored fibers

Figure 2.6 Illustration of plastic zone approach

CHAPTER 3

ANALYTICAL MODEL FOR ADVANCED ANALYSIS BY ONE ELEMENT PER MEMBER

This chapter presents an efficient and accurate numerical solution for advanced analysis of beam-column members by one element per member allowing for various effects such as initial member imperfection, geometrical and material nonlinearities. A new curved beam-column element with an arbitrarily-located plastic hinge is derived in this thesis, which is extended from the three springs beam element proposed by Chen and Chan (1995). The additional degree of freedoms in the element will be condensed that it can be easily incorporated into the existing software. Since structure could exhibit large deformations in an advanced analysis under the ultimate limit state, especially for the inelastic or elastic post-buckling simulation, formulations of the equilibrium through an updated Lagrangian description is established. In addition, numerical solution strategies for the nonlinear analysis will be briefly reviewed. Finally, several examples are presented and the results are found to be in good agreement with the benchmark examples.

3.1. Introduction

The analytical model using one element per member for advanced and second-order design of steel frames has been extensively studied by Chan *et al.* (2000; 2010). This technique not only brings convenience and efficiency in the analysis procedure, but also eases the difficulties of modeling the initial member imperfections, which is essential and crucial for both second-order elastic and advanced plastic analysis.

Due to the significant differences in material properties and characteristics between concrete and steel, the overall mechanical behavior of bare steel (BS), reinforced concrete (RC) and steel-concrete composite (SCC) members is diverse. For example, concrete is brittle and anisotropy with high compressive strength but negligible tensile capacity, while steel is isotropy and possesses high strength and stiffness. Unfortunately, BS members are usually slender and their stability problem is prominent, and the inelastic behavior is always concerned in design of RC members. In general, both the stability and inelastic behavior are required to be taken into account in design of SCC members.

The philosophy of advanced analysis method is to consider the various effects inherent to a real structure, such as initial imperfects, geometric and material nonlinearities and so on. A typical sub-frame of the hybrid steel and concrete frame is shown in Figure 3.1, which consists of different material types of structural members. In order to carry out an analysis for this type of hybrid steel-concrete frame by only one element per member, the element should be capable of capturing all the vital effects.

Initial imperfections exist in all structural members as well as the whole structure, which significantly influence both the stability and strength checks. The importance of proper modeling of initial imperfections has been extensively studied by Chan *et al*. (1995, 1998). The analytical model based on one element per member is critical for accurate presentation of initial imperfection effects. The directions of the initial member imperfections need to be revised according to the loading conditions and usually determined by the first Eigen-buckling mode. Therefore, the approach to model one member by several elements, which not only significantly increases the computational time, but also brings much effort to update the model in each load combination. In this thesis, the formulations for directly modeling the initial member imperfection by one element are introduced.

Conventionally, the plastic hinge approach assumes the plasticity only occurred at a certain length near the ends, thus two lumped hinges are inserted at both ends and deteriorates the rotational stiffness for simulation of the gradual cross-section yielding. However, in some circumstances, the plastic hinge is most likely formed at middle zone of the member rather than at the two ends, or formed at two end-zones and middle zone simultaneously. Therefore, two more elements are usually required for modeling each member, which causes the inconvenience in modeling the member initial imperfections. Against this background, a three hinges beam-column element, which allows plastic hinges to form in middle and two end zones respectively, is firstly proposed.

The kinetic motion of the element can be achieved by the total Lagrangian or updated Lagrangian descriptions. In the total Lagrangian description, the equilibrium is established by referring the original position in the whole analysis procedure and usually limited by the magnitude of the member deflections because of numerical efficiency and accuracy. However, members and frames usually exhibit large deformations under ultimate limit states or some extreme scenarios, such as the post-buckling analysis, studies of progressive collapse, pushover analysis and so on. Therefore, to overcome this problem of large member deflections, an updated Lagrangian approach is conventionally adopted, where the equilibrium is conducted by referring to the last configuration. In order to simplify the derivation, the Co-rotational method (Oran, 1973a, 1973b) is adopted where the effects of pure member deformations are separate from the joint displacements. Therefore, the updated Lagrangian description can be achieved by continuously updating the transformation relations between the local reference system and the global coordinates with the latest configuration, which will be presented in this chapter.

In this chapter, a beam-column element formulation with one arbitrarily located hinge will be presented, and furthermore, the formulations for the plastic hinge at two ends will be studied and the analytical model for the refined plastic hinge will be given. In order to incorporate the proposed element into the existing computer program, the condensation approach for the element stiffness matrix and the generalized external nodal forces are introduced. Since the equilibrium is established by an updated Lagrangian description, the derivation for the transformation matrix is presented. Besides, numerical solution strategies for the current analytical approach

are given. Finally, several benchmark examples are analyzed to verify the validity of the proposed theory.

3.2. Assumptions

The following basic assumptions are adopted in the current study.

1) Euler-Bernoulli hypothesis is valid and the member is mainly under axial loads and the second-order effect due to axial loads is considered.
2) Strains are small but the deformation can be large.
3) Plane sections before deformation remain plane after deformation which implies a linear strain distribution exists across the section depth.
4) Material nonlinearity is considered by plastic hinge springs while the element is elastic.
5) Applied loads are nodal and conservative, which are assumed to be independent of the load path and proportionally increased.
6) Warping deformation, shear deformation as well as twisting effect are not considered.

The above assumptions are valid for most types of civil engineering structures and compatible with most codes requirements. Nevertheless, the consideration of lateral-torsional buckling is essential for design of slender beams, which can be achieved by checking according to the empirical formula provided in codes. This consideration is less likely to encounter in practical structures, and therefore does not have serious limitations on the use of the proposed element. If necessary, a complex

analysis allowing for beam buckling can be achieved by adoption of shell elements (Liu & Chan, 2009) at the expense of long computer time.

3.3. Curved beam-column element with an arbitrarily located hinge

3.3.1 Background

In this project, a new curved beam-column element with an arbitrarily located hinge (ALH Element) is proposed and shown in Figure 3.2, which is further extended from the three hinges beam element proposed by Chen and Chan (1995), with the improvements summarized as: (1) the location of internal hinge can be arbitrary; (2) second-order effect induced by the axial load is considered; (3) initial member imperfection is taken into account; and (4) plastic hinge model is refined for the gradual yielding.

In developing the element formulation, two sets of coordinate systems are introduced (e.g., a fixed global co-ordinates and a local convective system) as illustrated in Figure 3.3. In the local convective system, the member deflections are separated from the nodal translations that the element formula deviation can be simplified and concise. According to the minimum potential energy principle, it is assumed that the local member deflection is small. In order to analyze the member exhibiting large rotation, the formulation of the equilibrium equation can be established by an updated Lagrangian description.

Due to existence of the internal node, there are three more additional degrees of freedoms (DOFs) in the proposed element by comparison with the conventional beam-column element in a two-dimensional space. To incorporate efficiently into the existing computer program, the internal DOFs will be condensed before global stiffness assembly and decoupled in calculating the resisting forces. The member forces and DOFs in the various coordinate systems are illustrated in Figure 3.3.

3.3.2 Formulation of displacement function

The forces vs. displacements relations of the arbitrarily located hinge (ALH) element are illustrated in Figure 3.2. The initial member imperfection is assumed as:

$$v_0 = v_{mo}\frac{(L^2 - 4x^2)}{L^2} \qquad \text{and} \quad -\mathrm{L}/2 \le x \le L/2 \tag{3. 1}$$

where v_0 is the shape function of initial member imperfection; v_{mo} is the amplitude of initial imperfection at mid-span; L is the length of the member; x is the distance along the element (see Figure 3.2).

It is observed that, the finite element interpolation is a piecewise function, which can be expressed with eight coefficients of a_i and b_i with i = 0 to 3 respectively as given by,

$$\mathrm{v}=\begin{cases} v_1 = a_0 + a_1x + a_2x^2 + a_3x^3 & -\mathrm{L}/2 \le x \le \xi L \\ \text{and} & \\ v_2 = b_0 + b_1x + b_2x^2 + b_3x^3 & \xi L \le x \le L/2 \end{cases} \tag{3. 2}$$

where v is the lateral displacement function due to applied loads for the element; ξ is the location of the internal plastic hinge; a_i and b_i are the coefficients for the polynomial function which will be determined by the boundary conditions.

In order to solve the eight coefficients in the shape function, eight boundary conditions are introduced as follows,

$$\begin{cases} v = v_1 = 0 \\ \dot{v} = \dot{v_1} = \theta_{11} \end{cases} \quad \text{at} \quad x = -L/2 \tag{3. 3}$$

$$\begin{cases} v = v_1 = v_2 = \delta \\ \dot{v} = \dot{v_1} = \theta_{12} \\ \dot{v} = \dot{v_2} = \theta_{21} \end{cases} \quad \text{at} \quad x = \xi L \tag{3. 4}$$

$$\begin{cases} v = v_2 = 0 \\ \dot{v} = \dot{v_2} = \theta_{22} \end{cases} \quad \text{at} \quad x = L/2 \tag{3. 5}$$

in which θ_{11} and θ_{22} are the two external rotations at ends; δ, θ_{12} and θ_{21} are the internal lateral deflection and rotations at the junction between the two sub-elements respectively.

By solving the boundary conditions according to the equations above and the shape function can be written as,

$$v = \begin{cases} \{N_{11} \quad N_{12} \quad N_{13}\} \cdot \{\theta_{11} \quad \theta_{12} \quad \delta\}^T & -L/2 \le x \le \xi L \\ \{N_{21} \quad N_{22} \quad N_{23}\} \cdot \{\theta_{21} \quad \theta_{22} \quad \delta\}^T & \xi L \le x \le L/2 \end{cases} \quad \text{and} \tag{3. 6}$$

in which N_{11}, N_{12}, N_{13}, N_{21}, N_{22} and N_{23} are shape parameters for shape functions given by,

$$N_{11} = \frac{2(L + 2x)(x - L\xi)^2}{L^2(1 + 2\xi)^2} \tag{3. 7}$$

$$N_{12} = \frac{(L + 2x)^2(x - L\xi)}{L^2(1 + 2\xi)^2} \tag{3. 8}$$

$$N_{13} = \frac{(L+2x)^2(L-4x+6L\xi)}{L^3(1+2\xi)^3} \tag{3. 9}$$

$$N_{21} = \frac{(L-2x)^2(x-L\xi)}{L^2(1-2\xi)^2} \tag{3. 10}$$

$$N_{22} = -\frac{2(L-2x)(x-L\xi)^2}{L^2(1-2\xi)^2} \tag{3. 11}$$

$$N_{23} = \frac{(L-2x)^2(L+4x+6L\xi)}{L^3(1-2\xi)^3} \tag{3. 12}$$

For the axial compression and lengthening, the respective displacement function can be conventionally assumed to be linear and the shape function can be determined as,

$$\mathrm{u} = c_0 + c_1 x \tag{3. 13}$$

where, c_i is the coefficients for the linear function of axial deformation which will be determined by the boundary conditions.

And boundary conditions of axial deformation can be obtained as,

$$\mathrm{u} = 0 \quad \text{at} \quad x = -L/2 \tag{3. 14}$$

$$\mathrm{u} = e \quad \text{at} \quad x = L/2 \tag{3. 15}$$

By solving the boundary conditions the axial displacement function is,

$$\mathrm{u} = e\left(\frac{1}{2} + \frac{x}{L}\right) \tag{3. 16}$$

where e is the deformation along with axial force as illustration in Figure 3.2.

3.3.3 Bowing effects

Besides the axial shortening or lengthening occurs due to axial load, the distance between the two end nodes will be shortened due to bending moments. This bowing effect should be accounted for in the analysis, and it can be calculated as,

$$u_b = \frac{1}{2}\int_L \left(\frac{dv}{dx}\right)^2 \mathrm{dx} + \int_L \left(\frac{dv}{dx}\frac{dv_0}{dx}\right)^2 \mathrm{dx} \tag{3. 17}$$

By expressing the shape function in terms of the nodal displacement variables, the bowing effect can be expressed explicitly as,

$$\begin{aligned} u_b = {} & \delta\left(\frac{4v_{mo}}{L} + \frac{\theta_{21}}{10} + \frac{\theta_{22}}{10}\right) - \frac{1}{6}v_{mo}\theta_{22}(1-2\xi)^2 \\ & -\frac{1}{30}L{\theta_{21}}^2(-1+2\xi) - \frac{1}{30}L{\theta_{22}}^2(-1+2\xi) \\ & +\frac{1}{60}L{\theta_{11}}^2(2+4\xi) + \frac{1}{60}L{\theta_{12}}^2(2+4\xi) \\ & -\frac{12\delta^2}{5L(-1+4\xi^2)} + \theta_{21}\left[\frac{1}{6}v_{mo}(1-2\xi)^2 + \frac{1}{60}L\theta_{22}(-1+2\xi)\right] \\ & +\theta_{12}\left[-\frac{\delta}{10} - \frac{1}{6}v_{mo}(1+2\xi)^2\right] + \theta_{11}\left[-\frac{\delta}{10} - \frac{1}{60}L\theta_{12}(1+2\xi)\right. \\ & \left.+\frac{1}{6}v_{mo}(1+2\xi)^2\right] \end{aligned} \tag{3. 18}$$

3.3.4 Secant relations

The secant relations can be formulated by the principle of stationary potential energy, which is necessary for the numerical incremental-iterative type of analysis. The total potential energy function Π is given by,

$$\Pi = U - V \tag{3. 19}$$

where U is the strain energy and V is the external work done.

The degrees of freedom as presented in Figure 3.2 are as follows:

$$\begin{cases} u_1 = \theta_{11};\ u_2 = \theta_{12};\ u_3 = \delta \\ u_4 = \theta_{21};\ u_5 = \theta_{22};\ u_6 = \mathrm{e} \end{cases} \tag{3. 20}$$

$$\begin{cases} F_1 = \mathrm{M}_{11};\ F_2 = \mathrm{M}_{12};\ F_3 = \mathrm{F} \\ F_4 = \mathrm{M}_{21};\ F_5 = \mathrm{M}_{22};\ F_6 = \mathrm{P} \end{cases} \tag{3. 21}$$

The external work done can be expressed as,

$$V = \sum F_i u_i \qquad \text{and} \quad \mathrm{i}=1 \sim 6 \tag{3. 22}$$

The potential strain energy can be given by,

$$U = \frac{1}{2}\int_L EA\dot{u}^2 dx + \frac{1}{2}\int_L EI\ddot{v}^2 dx + \frac{1}{2}\int_L P(\dot{v}^2 + 2\dot{v}_0\dot{v})dx + \int_{\theta_m} S_m d\theta \tag{3. 23}$$

where S_m and θ_m are the stiffness and rotation at the internal hinge respectively and can be assumed as,.

$$\theta_m = \theta_{12} - \theta_{21} \tag{3. 24}$$

$$S_m = EI \cdot R_m \tag{3. 25}$$

in which, R_m is the plasticity parameter related to the loading state, which will be further discussed in the following sections.

It can be seen from the potential strain energy equation that, the first two terms are the elastic strain energy consumed by member flexural and axial deformations, while the third item is the second-order energy induced by axial force associated

with the initial member imperfection, and the last item is the plastic energy absorbed by plastic hinge rotation at the internal hinge.

The equilibrium condition can be obtained by the first variation of the potential energy function according to the minimum potential energy method as,

$$\delta\Pi = \frac{\partial \Pi}{\partial \mathrm{u}_i} + \frac{\partial \Pi}{\partial q}\frac{\partial \mathrm{q}}{\partial \mathrm{u}_i} = 0 \qquad \text{and} \qquad \mathrm{i}=1 \sim 6 \tag{3. 26}$$

Therefore, the secant relations can be obtained as follows,

$$\begin{aligned} \mathrm{M}_{11} = {} & \frac{8\mathrm{EI}}{L(1+2\xi)}\theta_{11} + \frac{4\mathrm{EI}}{L(1+2\xi)}\theta_{12} - \frac{24\mathrm{EI}}{L^2(1+2\xi)^2}\delta \\ & + P\left[\frac{1}{15}L(1+2\xi)\theta_{11} - \frac{1}{60}L(1+2\xi)\theta_{12} - \frac{1}{10}\delta + \frac{1}{6}(1+2\xi)^2 v_{mo}\right] \end{aligned} \tag{3. 27}$$

$$\begin{aligned} \mathrm{M}_{12} = {} & \frac{4\mathrm{EI}}{L(1+2\xi)}\theta_{11} + \frac{8\mathrm{EI}}{L(1+2\xi)}\theta_{12} - \frac{24\mathrm{EI}}{L^2(1+2\xi)^2}\delta \\ & + P\left[-\frac{1}{60}L(1+2\xi)\theta_{11} + \frac{1}{15}L(1+2\xi)\theta_{12} - \frac{1}{10}\delta - \frac{1}{6}(1+2\xi)^2 v_{mo}\right] \\ & + \mathrm{EI}\, R\, \theta_{12} - \mathrm{EI}\, R\, \theta_{21} \end{aligned} \tag{3. 28}$$

$$\begin{aligned} \mathrm{F} = {} & -\frac{24\mathrm{EI}}{L^2(1+2\xi)^2}\theta_{11} - \frac{24\mathrm{EI}}{L^2(1+2\xi)^2}\theta_{12} - \frac{192\mathrm{EI}(1+12\xi^2)}{L^3(-1+4\xi^2)^3}\delta \\ & + \frac{24\mathrm{EI}}{L^2(1-2\xi)^2}\theta_{21} + \frac{24\mathrm{EI}}{L^2(1-2\xi)^2}\theta_{22} \\ & + P\left[-\frac{1}{10}\theta_{11} - \frac{1}{10}\theta_{12} + \frac{24}{5L(1-4\xi^2)}\delta + \frac{1}{10}\theta_{21} + \frac{1}{10}\theta_{22} + \frac{4}{L}v_{mo}\right] \end{aligned} \tag{3. 29}$$

$$\begin{aligned} \mathrm{M}_{21} = {} & \frac{8\mathrm{EI}}{L(1-2\xi)}\theta_{21} + \frac{4\mathrm{EI}}{L(1-2\xi)}\theta_{22} + \frac{24\mathrm{EI}}{L^2(1-2\xi)^2}\delta \\ & + P\left[\frac{1}{15}L(1-2\xi)\theta_{21} - \frac{1}{60}L(1-2\xi)\theta_{22} + \frac{1}{10}\delta + \frac{1}{6}(1-2\xi)^2 v_{mo}\right] \\ & - \mathrm{EI}\, R\, \theta_{12} + \mathrm{EI}\, R\, \theta_{21} \end{aligned} \tag{3. 30}$$

$$\mathrm{M}_{22} = \frac{4\mathrm{EI}}{L(1-2\xi)}\theta_{21} + \frac{8\mathrm{EI}}{L(1-2\xi)}\theta_{22} + \frac{24\mathrm{EI}}{L^2(1-2\xi)^2}\delta \tag{3. 31}$$

$$+P\left[-\frac{1}{60}L(1-2\xi)\theta_{21}+\frac{1}{15}L(1-2\xi)\theta_{22}+\frac{1}{10}\delta-\frac{1}{6}(1-2\xi)^2 v_{mo}\right]$$

$$\begin{aligned}\mathrm{P} \quad &= \frac{\mathrm{EA}}{L}e+\frac{\mathrm{EA}}{10L}\delta(-\theta_{11}-\theta_{12}+\theta_{21}+\theta_{22})+\frac{EA}{60}[(2-4\xi){\theta_{21}}^2 \\ &+(2-4\xi){\theta_{22}}^2-\theta_{11}\theta_{12}(1+2\xi)-\theta_{21}\theta_{22}(1-2\xi)+{\theta_{11}}^2(2+4\xi) \\ &+{\theta_{12}}^2(2+4\xi)+\frac{144}{L^2(1-4\xi^2)}\delta^2]+\mathrm{EA}[\frac{(1+2\xi)^2}{6L}\theta_{11} \\ &-\frac{(1+2\xi)^2}{6L}\theta_{12}+\frac{4}{L^2}\delta+\frac{(1-2\xi)^2}{6L}\theta_{21}-\frac{(1-2\xi)^2}{6L}\theta_{22}]v_{mo}\end{aligned} \tag{3. 32}$$

3.3.5 Tangent stiffness matrix

In order to predict incremental displacements due to the corresponding forces, the tangent stiffness matrix is required and can be calculated by the second variation of the total potential energy function as,

$$\delta^2\Pi=\frac{\partial^2\Pi}{\partial u_i\partial u_j}\delta u_i\delta u_j=[\frac{\partial F_i}{\partial u_j}+\frac{\partial F_i}{\partial q}\frac{\partial q}{\partial u_j}]\delta u_i\delta u_j \quad \text{and} \quad \text{i,j=1 ~ 6} \tag{3. 33}$$

Therefore, the tangent stiffness of the element is determined and can be written in terms of three parts as,

$$k_e=k_L+k_G+k_S \tag{3. 34}$$

in which, k_e is the tangent stiffness of the element; k_L is the linear stiffness matrix; k_G is the geometric stiffness matrix; and k_S is the spring stiffness for the internal plastic hinge.

The linear stiffness matrix k_L is given by,

$$k_L = \begin{bmatrix} \mathrm{k11L} & \mathrm{k12L} & \mathrm{k13L} & \mathrm{k14L} & \mathrm{k15L} & \mathrm{k16L} \\ & \mathrm{k22L} & \mathrm{k23L} & \mathrm{k24L} & \mathrm{k25L} & \mathrm{k26L} \\ S. & & \mathrm{k33L} & \mathrm{k34L} & \mathrm{k35L} & \mathrm{k36L} \\ & Y. & & \mathrm{k44L} & \mathrm{k45L} & \mathrm{k46L} \\ & & M. & & \mathrm{k55L} & \mathrm{k56L} \\ & & & & & \mathrm{k66L} \end{bmatrix} \tag{3. 35}$$

where,

$$\mathrm{k11L} = \frac{8\mathrm{EI}}{L(1+2\xi)} \tag{3. 36}$$

$$\mathrm{k12L} = \frac{4\mathrm{EI}}{L(1+2\xi)} \tag{3. 37}$$

$$\mathrm{k13L} = -\frac{24\mathrm{EI}}{L^2(1+2\xi)^2} \tag{3. 38}$$

$$\mathrm{k22L} = \frac{8\mathrm{EI}}{L(1+2\xi)} \tag{3. 39}$$

$$\mathrm{k23L} = -\frac{24\mathrm{EI}}{L^2(1+2\xi)^2} \tag{3. 40}$$

$$\mathrm{k33L} = -\frac{192\mathrm{EI}(1+12\xi^2)}{L^3(-1+4\xi^2)^3} \tag{3. 41}$$

$$\mathrm{k34L} = \frac{24\mathrm{EI}}{L^2(1-2\xi)^2} \tag{3. 42}$$

$$\mathrm{k35L} = \frac{24\mathrm{EI}}{L^2(1-2\xi)^2} \tag{3. 43}$$

$$\mathrm{k44L} = \frac{8\mathrm{EI}}{L(1-2\xi)} \tag{3. 44}$$

$$\mathrm{k45L} = \frac{4\mathrm{EI}}{L(1-2\xi)} \tag{3. 45}$$

$$\mathrm{k55L} = \frac{8\mathrm{EI}}{L(1-2\xi)} \tag{3. 46}$$

$$\mathrm{k66L} = \frac{\mathrm{EA}}{L} \tag{3. 47}$$

$$\mathrm{k14L} = \mathrm{k15L} = \mathrm{k16L} = \mathrm{k24L} = \mathrm{k25L} = \mathrm{k26L} = \mathrm{k36L} = \mathrm{k46L} = \mathrm{k56L} = 0 \tag{3. 48}$$

The geometric stiffness matrix k_G is presented as,

$$k_G = \begin{bmatrix} \mathrm{k11G} & \mathrm{k12G} & \mathrm{k13G} & \mathrm{k14G} & \mathrm{k15G} & \mathrm{k16G} \\ & \mathrm{k22G} & \mathrm{k23G} & \mathrm{k24G} & \mathrm{k25G} & \mathrm{k26G} \\ S. & & \mathrm{k33G} & \mathrm{k34G} & \mathrm{k35G} & \mathrm{k36G} \\ & Y. & & \mathrm{k44G} & \mathrm{k45G} & \mathrm{k46G} \\ & & M. & & \mathrm{k55G} & \mathrm{k56G} \\ & & & & & \mathrm{k66G} \end{bmatrix} \tag{3. 49}$$

in which,

$$\mathrm{k11G} = \frac{1}{15}LP(1+2\xi) + \frac{\mathrm{EA}[-6\delta + L(4\theta_{11} - \theta_{12})(1+2\xi) + 10v_{mo}(1+2\xi)^2]^2}{3600L} \tag{3. 50}$$

$$\mathrm{k12G} = -\frac{1}{60}\mathrm{LP}(1+2\xi) \tag{3. 51}$$

$$-\frac{\mathrm{EA}[6\delta+\mathrm{L}(\theta_{11}-4\theta_{12})(1+2\xi)+10v_{mo}(1+2\xi)^2]}{3600\mathrm{L}}$$

$$*\ [-6\delta+\mathrm{L}(4\theta_{11}-\theta_{12})(1+2\xi)+10v_{mo}(1+2\xi)^2]$$

$$\mathrm{k13G}=-\frac{P}{10}$$

$$+\frac{\mathrm{EA}(-6\delta+L(4\theta_{11}-\theta_{12})(1+2\xi)+10v_{mo}(1+2\xi)^2)}{600L^2(-1+4\xi^2)}*[-48\delta \tag{3. 52}$$

$$+40v_{mo}(-1+4\xi^2)-L(\theta_{11}+\theta_{12}-\theta_{21}-\theta_{22})(-1+4\xi^2)]$$

$$\mathrm{k14G}=\frac{\mathrm{EA}[6\delta+10v_{mo}(1-2\xi)^2-L(4\theta_{21}-\theta_{22})(-1+2\xi)]}{3600L} \tag{3. 53}$$

$$*\ [-6\delta+L(4\theta_{11}-\theta_{12})(1+2\xi)+10v_{mo}(1+2\xi)^2]$$

$$\mathrm{k15G}=\frac{\mathrm{EA}[6\delta-10v_{mo}(1-2\xi)^2+L(\theta_{21}-4\theta_{22})(-1+2\xi)]}{3600L} \tag{3. 54}$$

$$*\ [-6\delta+L(4\theta_{11}-\theta_{12})(1+2\xi)+10v_{mo}(1+2\xi)^2]$$

$$\mathrm{k16G}=\frac{\mathrm{EA}[-6\delta+L(4\theta_{11}-\theta_{12})(1+2\xi)+10v_{mo}(1+2\xi)^2]}{60L} \tag{3. 55}$$

$$\mathrm{k22G}=\frac{1}{15}LP(1+2\xi)$$

$$+\frac{\mathrm{EA}[6\delta+L(\theta_{11}-4\theta_{12})(1+2\xi)+10v_{mo}(1+2\xi)^2]^2}{3600L} \tag{3. 56}$$

$$\mathrm{k23G}=-\frac{P}{10}$$

$$+\frac{\mathrm{EA}[6\delta+L(\theta_{11}-4\theta_{12})(1+2\xi)+10v_{mo}(1+2\xi)^2]}{600L^2(-1+4\xi^2)} \tag{3. 57}$$

$$*\ [48\delta-40v_{mo}(-1+4\xi^2)+L(\theta_{11}+\theta_{12}-\theta_{21}-\theta_{22})(-1+4\xi^2)]$$

$$\mathrm{k24G}=\frac{\mathrm{EA}[-6\delta-10v_{mo}(1-2\xi)^2+L(4\theta_{21}-\theta_{22})(-1+2\xi)]}{3600L} \tag{3. 58}$$

$$*\ [6\delta+L(\theta_{11}-4\theta_{12})(1+2\xi)+10v_{mo}(1+2\xi)^2]$$

$$\mathrm{k25G}=\frac{\mathrm{EA}[-6\delta+10v_{mo}(1-2\xi)^2-L(\theta_{21}-4\theta_{22})(-1+2\xi)]}{3600L} \tag{3. 59}$$

$$*\ [6\delta+L(\theta_{11}-4\theta_{12})(1+2\xi)+10v_{mo}(1+2\xi)^2]$$

$$\mathrm{k26G}=-\frac{\mathrm{EA}[6\delta+L(\theta_{11}-4\theta_{12})(1+2\xi)+10v_{mo}(1+2\xi)^2]}{60L} \tag{3. 60}$$

$$\mathrm{k33G} = \frac{24P}{5L - 20L\xi^2} + \frac{\mathrm{EA}[48\delta - 40v_{mo}(-1+4\xi^2) + L(\theta_{11}+\theta_{12}-\theta_{21}-\theta_{22})(-1+4\xi^2)]^2}{100L^3(1-4\xi^2)^2} \tag{3. 61}$$

$$\mathrm{k34G} = \frac{P}{10} + \frac{\mathrm{EA}[6\delta + 10v_{mo}(1-2\xi)^2 - L(4\theta_{21}-\theta_{22})(-1+2\xi)]}{600L^2(-1+4\xi^2)} * [-48\delta + 40v_{mo}(-1+4\xi^2) - L(\theta_{11}+\theta_{12}-\theta_{21}-\theta_{22})(-1+4\xi^2)] \tag{3. 62}$$

$$\mathrm{k35G} = \frac{P}{10} + \frac{\mathrm{EA}[6\delta - 10v_{mo}(1-2\xi)^2 + L(\theta_{21}-4\theta_{22})(-1+2\xi)]}{600L^2(-1+4\xi^2)} * [-48\delta + 40v_{mo}(-1+4\xi^2) - L(\theta_{11}+\theta_{12}-\theta_{21}-\theta_{22})(-1+4\xi^2)] \tag{3. 63}$$

$$\mathrm{k36G} = \frac{\mathrm{EA}}{10L}\left(\frac{40v_{mo}}{L} - \theta_{11} - \theta_{12} + \theta_{21} + \theta_{22} + \frac{48\delta}{L-4L\xi^2}\right) \tag{3. 64}$$

$$\mathrm{k44G} = -\frac{1}{15}LP(-1+2\xi) + \frac{\mathrm{EA}[6\delta + 10v_{mo}(1-2\xi)^2 - L(4\theta_{21}-\theta_{22})(-1+2\xi)]^2}{3600L} \tag{3. 65}$$

$$\mathrm{k45G} = \frac{1}{60}LP(-1+2\xi) - \frac{\mathrm{EA}[-6\delta + 10v_{mo}(1-2\xi)^2 - L(\theta_{21}-4\theta_{22})(-1+2\xi)]}{3600L} * [6\delta + 10v_{mo}(1-2\xi)^2 - L(4\theta_{21}-\theta_{22})(-1+2\xi)] \tag{3. 66}$$

$$\mathrm{k46G} = \frac{\mathrm{EA}[6\delta + 10v_{mo}(1-2\xi)^2 - L(4\theta_{21}-\theta_{22})(-1+2\xi)]}{60L} \tag{3. 67}$$

$$\mathrm{k55G} = -\frac{1}{15}LP(-1+2\xi) + \frac{\mathrm{EA}[6\delta - 10v_{mo}(1-2\xi)^2 + L(\theta_{21}-4\theta_{22})(-1+2\xi)]^2}{3600L} \tag{3. 68}$$

$$\mathrm{k56G} = \frac{\mathrm{EA}[6\delta - 10v_{mo}(1-2\xi)^2 + L(\theta_{21}-4\theta_{22})(-1+2\xi)]}{60L} \tag{3. 69}$$

$$\mathrm{k66G} = 0 \tag{3. 70}$$

The spring stiffness matrix k_S can be expressed as,

$$k_S = \begin{bmatrix} 0 & 0 & 0 & 0 & 0 & 0 \\ & \mathrm{EI} \cdot R_m & 0 & -\mathrm{EI} \cdot R_m & 0 & 0 \\ S. & & 0 & 0 & 0 & 0 \\ & Y. & & \mathrm{EI} \cdot R_m & 0 & 0 \\ & & M. & & 0 & 0 \\ & & & & & 0 \end{bmatrix} \tag{3. 71}$$

3.3.6 Condensed stiffness matrix and generalized nodal forces

In order to incorporate the proposed element into the existing program efficiently, the degree of freedoms (DOFs) of the internal node u_i will be condensed. The internal and external DOFs can be expressed as,

$$u_i = \{\theta_{12} \quad \delta \quad \theta_{21}\}^T \tag{3. 72}$$

$$u_e = \{\theta_{11} \quad \theta_{22} \quad e\}^T \tag{3. 73}$$

Therefore, the stiffness equation can be written as,

$$\begin{bmatrix} k_{ii} & k_{ie} \\ k_{ie}^T & k_{ee} \end{bmatrix} \begin{bmatrix} u_i \\ u_e \end{bmatrix} = \begin{bmatrix} F_i \\ F_e \end{bmatrix} \tag{3. 74}$$

where,

$$k_{ii} = \begin{bmatrix} k22 & k23 & k24 \\ k32 & k33 & k34 \\ k42 & k43 & k44 \end{bmatrix} \tag{3. 75}$$

$$k_{ee} = \begin{bmatrix} k11 & k15 & k16 \\ k51 & k55 & k56 \\ k61 & k65 & k66 \end{bmatrix} \tag{3. 76}$$

$$k_{ie} = \begin{bmatrix} k12 & k25 & k26 \\ k13 & k35 & k36 \\ k14 & k45 & k46 \end{bmatrix} \tag{3. 77}$$

$$F_i = \{\mathrm{M}_{12} \quad F \quad \mathrm{M}_{21}\}^T \tag{3. 78}$$

$$F_e = \{\mathrm{M}_{11} \quad M_{22} \quad \mathrm{P}\}^T \tag{3. 79}$$

The condensed stiffness k^* and generalized force f can be expressed as,

$$k^* u_e = f \tag{3. 80}$$

in which,

$$k^* = k_{ee} - k_{ie}^T k_{ii}^{-1} k_{ie} \tag{3. 81}$$

$$f = F_e - k_{ie}^T k_{ii}^{-1} F_i \tag{3. 82}$$

The internal DOFs u_i at hinge location can be decoupled by multiplying the incremental rotations at external DOFs, u_e, as,

$$u_i = k_{ii}^{-1}(F_i \ - k_{ie} u_e) \tag{3. 83}$$

3.3.7 Equivalent nodal forces

Except for the concentrated nodal forces directly applied to the element nodes, an arbitrarily lateral distributed force may be loaded along the element length and the loads are needed to be converted to the equivalent nodal forces as well as concentrated nodal forces in a finite-element analysis. Currently, due to the existence of one internal node along the element length, the equations for calculating the equivalent nodal forces for the conventional beam-column element cannot be directly utilized. Therefore, the corresponding equations should be derived. Since all forces are assumed applied at nodes only in a finite element analysis, the equivalent nodal forces (as shown in Figure 3.4) can be obtained by the principle that the work

done due to the equivalent nodal forces and the arbitrary lateral distribution forces should be balanced, which can be mathematically expressed as,

$$F^{EQV}u = \int_{-L/2}^{L/2} q(x)\, v(x)\, dx = \int_{-L/2}^{L/2} q(x)\, N(x) u\, dx \tag{3. 84}$$

where, F^{EQV} is a vector for the equivalent nodal forces; u is the DOFs in an element; $q(x)$ is an arbitrary lateral distribution force; and $N(x)$ is the shape functions of the proposed element.

For example, if a uniform distributed load q is applied along the member, the equivalent nodal forces can be obtained as follows,

$$M_{11} = \frac{1}{48} qL^2(1+2\xi)^2 \tag{3. 85}$$

$$M_{12} = -\frac{1}{48} qL^2(1+2\xi)^2 \tag{3. 86}$$

$$F = \frac{1}{2} qL \tag{3. 87}$$

$$M_{21} = \frac{1}{48} qL^2(1-2\xi)^2 \tag{3. 88}$$

$$M_{22} = -\frac{1}{48} qL^2(1-2\xi)^2 \tag{3. 89}$$

3.3.8 Transformation matrix [A] from member basic force displacement to member intermediate force / displacement

The forces and the element stiffness in the proposed element is formulated in a set of local coordinate axes parallel to the element principal axes as shown in Figure 3.3 (a). As aforementioned, DOFs in the internal hinge will be condensed as illustrated in Figure 3.3 (b). Usually, the element local coordinate system does not

have the same orientations with the global coordinate system, therefore, the element stiffness and forces must be transformed to the global axes in numerical analysis.

In order to consider large deformation of an element, the formulation of the equilibrium through an updated Lagrangian approach is adopted. Apart from the total Lagrangian formulation, which is expressed by referring to its original or unreformed geometry, the updated Lagrangian formulation uses the last known or step configuration as a reference. Therefore, the transform matrix is kept updating during the analysis.

Since the derivation of the proposed element formulation is still in two-dimensional space that only one joint angle is allowed in each node, the rotational degree of freedom can be described by the Euler angles. Consider the relations between the local coordinates and intermediate coordinates as shown in Figure 3.3 (b) and Figure 3.3 (c) respectively.

$$(L+e)^2 = (L+u')^2 + v'^2 \tag{3. 90}$$

in which, u' and v' are the horizontal and vertical displacement at the intermediate coordinates system.

Also, e can be rewritten as,

$$e = \sqrt{(L+u')^2 + v'^2} - L \tag{3. 91}$$

in which,

$$\theta_{11} = \theta_{11}{}' - \tan^{-1}\left(\frac{v'}{L+u'}\right) \tag{3. 92}$$

$$\theta_{22} = \theta_{22}{}' - \tan^{-1}\left(\frac{v'}{L+u'}\right) \tag{3. 93}$$

where, $\theta_{11}{}'$ and $\theta_{22}{}'$ are the rotations at the two ends of an element at the intermediate coordinates system.

Partial differentiating the equations (3. 91), (3. 92) and (3. 93), and have,

$$de = \frac{L+u'}{\mathrm{L+e}}du' + \frac{v'}{\mathrm{L+e}}dv' \tag{3. 94}$$

$$d\theta_{11} = \frac{v'}{(\mathrm{L+e})^2}du' - \frac{L+u'}{(\mathrm{L+e})^2}dv' + d\theta_{11}{}' \tag{3. 95}$$

$$d\theta_{22} = \frac{v'}{(\mathrm{L+e})^2}du' - \frac{L+u'}{(\mathrm{L+e})^2}dv' + d\theta_{22}{}' \tag{3. 96}$$

By writing in matrix form,

$$\Delta u = [A]\cdot\Delta u' \tag{3. 97}$$

where,

$$\Delta u = \{\theta_{11} \quad \theta_{22} \quad e\}^T \tag{3. 98}$$

$$\Delta u' = \{\theta_{11}{}' \quad \theta_{22}{}' \quad u' \quad v'\}^T \tag{3. 99}$$

$$[A] = \begin{bmatrix} 1 & 0 & \dfrac{v'}{(\mathrm{L+e})^2} & -\dfrac{L+u'}{(\mathrm{L+e})^2} \\ 0 & 1 & \dfrac{v'}{(\mathrm{L+e})^2} & -\dfrac{L+u'}{(\mathrm{L+e})^2} \\ 0 & 0 & \dfrac{L+u'}{\mathrm{L+e}} & \dfrac{v'}{\mathrm{L+e}} \end{bmatrix} \tag{3. 100}$$

According to the contragredient principle,

$$\mathrm{F}' = [A]^T\cdot f^* \tag{3. 101}$$

where,

$$f = \{M_1^* \quad M_2^* \quad P^*\}^T \tag{3. 102}$$

$$\mathrm{F}' = \{M_1' \quad M_2' \quad T \quad S\}^T \tag{3. 103}$$

Similarly, differentiating the equation (3. 101), and have,

$$\Delta\mathrm{F}' = [A]^T \cdot \Delta f^* + d([A]^T) \cdot f^* \tag{3. 104}$$

Also, the equation (3. 104) can be written as,

$$\Delta\mathrm{F}' = [A]^T \cdot \Delta f^* + [D] \cdot \Delta u' \tag{3. 105}$$

where

$$[\mathrm{D}] = \begin{bmatrix} 0 & 0 & 0 & 0 \\ 0 & 0 & 0 & 0 \\ 0 & 0 & d33 & d34 \\ 0 & 0 & d43 & d44 \end{bmatrix} \tag{3. 106}$$

and

$$d33 = \frac{1}{(L+e)^4}\left\{-T(L+u')v'^2 + Sv'\left[2(L+u')^2 + v'^2\right]\right\} \tag{3. 107}$$

$$\mathrm{d34} = d43 = \frac{1}{(L+e)^4}\left[-Tv'^3 - S(L+u')^3\right] \tag{3. 108}$$

$$\mathrm{d44} = \frac{1}{(L+e)^4}\left\{T(L+u')\left[(L+u')^2 + 2v'^2\right] - S(L+u')^2v'\right\} \tag{3. 109}$$

The derivation of matrix [D] is presented in Appendix I. The matrix [D] reflects the work done due to nodal displacements and initial stress.

3.3.9 Transformation matrix [T] from member intermediate force/ displacement to nodal global force/displacement

The member local displacements in intermediate coordinate system is related to the global nodal displacement given by,

$$u' = [T] \cdot u \tag{3. 110}$$

and it can be written as,

$$\begin{bmatrix} {\theta_{11}}' \\ {\theta_{22}}' \\ u' \\ v' \end{bmatrix} = \begin{bmatrix} 0 & 0 & 1 & 0 & 0 & 0 \\ 0 & 0 & 0 & 0 & 0 & 1 \\ -\cos\alpha & -\sin\alpha & 0 & \cos\alpha & \sin\alpha & 0 \\ \sin\alpha & -\cos\alpha & 0 & -\sin\alpha & \cos\alpha & 0 \end{bmatrix} \cdot \begin{bmatrix} u_1 \\ u_2 \\ u_3 \\ u_4 \\ u_5 \\ u_6 \end{bmatrix} \tag{3. 111}$$

also,

$$\Delta u' = [T] \cdot \Delta U \tag{3. 112}$$

By the contragredient principle,

$$\begin{aligned} \Delta F &= [T]^T \cdot \Delta \mathrm{F}' = [T]^T \cdot ([A]^T \cdot \Delta f^* + [D] \cdot \Delta u') \\ &= [T]^T \cdot ([A]^T \cdot \mathrm{k}_e \cdot \Delta \mathrm{u} + [D] \cdot \Delta u') \\ &= [T]^T \cdot ([A]^T \cdot \mathrm{k}_e \cdot [A] \cdot \Delta \mathrm{u}' + [D] \cdot \Delta u') \\ &= [T]^T \cdot ([A]^T \cdot \mathrm{k}_e \cdot [A] + [D]) \cdot \Delta \mathrm{u}' \\ &= [T]^T \cdot ([A]^T \cdot \mathrm{k}_e \cdot [A] + [D]) \cdot [T] \cdot \Delta U \\ &= K_e \cdot \Delta U \end{aligned} \tag{3. 113}$$

where, the K_e is the element stiffness in the global coordinate system.

3.4. Formulation of the three hinges element

3.4.1 Background

In order to represent the member plasticity at its end-nodes or end-zones, two section springs are further attached as illustrated in Figure 3.2, where the rotational stiffness for the left and right hinge springs are S_L and S_R respectively. The analysis

procedure for the refined plastic hinges element has been well-documented and studied by many researchers, such as Ho and Chan (1991), Yau and Chan (1994), Chen *et al*. (1995) and Liu *et al*.(2010) among others. The numerical algorithm is proven to be accurate and stable, and the procedure can be programmed simply and only requires the coefficients of the element stiffness. Thus, only a modest additional effort is needed to extend the ALH element to a three hinge element.

3.4.2 Element stiffness formulation

After condensation of the element stiffness matrix for the internal DOFs at the internal hinge, the incremental equilibrium can be written as,

$$\Delta f = k^* \cdot \Delta u_e \tag{3. 114}$$

or in matrix form,

$$\begin{Bmatrix} \Delta \mathrm{M}_1{}^* \\ \Delta \mathrm{M}_2{}^* \\ \Delta \mathrm{P}^* \end{Bmatrix} = \begin{bmatrix} k11^* & k12^* & k13^* \\ k21^* & k22^* & k23^* \\ k31^* & k32^* & k33^* \end{bmatrix} \cdot \begin{Bmatrix} \theta_{11} \\ \theta_{22} \\ e \end{Bmatrix} \tag{3. 115}$$

where, the Δf is the condensed incremental nodal forces; and k^* is the condensed tangent stiffness matrix.

Considering the moment equilibrium condition at a section spring, the incremental equation can be written as,

$$\begin{Bmatrix} \Delta \mathrm{M}_s \\ \Delta \mathrm{M}_b \end{Bmatrix} = \begin{bmatrix} S_s & -S_s \\ -S_s & S_s \end{bmatrix} \cdot \begin{Bmatrix} \Delta\theta_s \\ \Delta\theta_b \end{Bmatrix} \tag{3. 116}$$

in which, $\Delta \mathrm{M}_s$ and $\Delta \mathrm{M}_b$ are the internal nodal moments at the element node and the section spring respectively; $\Delta\theta_s$ and $\Delta\theta_b$ are the incremental rotations corresponding to the moments; and S_s is the rotational stiffness for the section spring.

Therefore, the incremental relations for an element and the section springs can be expressed as,

$$\begin{Bmatrix} \Delta \mathrm{M}_{s1} \\ \Delta \mathrm{M}_{b1} \\ \Delta \mathrm{M}_{b2} \\ \Delta \mathrm{M}_{s2} \end{Bmatrix} = \begin{Bmatrix} S_L & -S_L & 0 & 0 \\ -S_L & k11^* + S_L & k12^* & 0 \\ 0 & k21^* & k22^* + S_R & -S_R \\ 0 & 0 & -S_R & S_R \end{Bmatrix} \cdot \begin{Bmatrix} \Delta\theta_{s1} \\ \Delta\theta_{11} \\ \Delta\theta_{22} \\ \Delta\theta_{s2} \end{Bmatrix} \tag{3. 117}$$

where, S_L and S_R are the spring stiffness at left and right hinges, respectively.

By assuming the forces are applied at the external nodes, both $\Delta \mathrm{M}_{b1}$ and $\Delta \mathrm{M}_{b2}$ equals to zero and the equotation (3. 117) can be written as,

$$\begin{Bmatrix} \Delta\theta_{11} \\ \Delta\theta_{22} \end{Bmatrix} = \begin{bmatrix} k_{11}{}^* + S_L & k_{12}{}^* \\ k_{21}{}^* & k_{22}{}^* + S_R \end{bmatrix}^{-1} \cdot \begin{bmatrix} S_L & 0 \\ 0 & S_R \end{bmatrix} \cdot \begin{Bmatrix} \Delta\theta_{s1} \\ \Delta\theta_{s2} \end{Bmatrix} \tag{3. 118}$$

Submitting equation (3. 118) into equation (3. 117), the incremental stiffness relationships for the three-hinges element can be obtained as,

$$\Delta f_e = k_e \cdot \Delta u_e \tag{3. 119}$$

or, in matrix form,

$$\begin{Bmatrix} \Delta \mathrm{M}_{s1} \\ \Delta \mathrm{M}_{s2} \\ \Delta \mathrm{P} \end{Bmatrix} = \begin{Bmatrix} \tilde{k}11 & \tilde{k}12 & \tilde{k}13 \\ \tilde{k}21 & \tilde{k}22 & \tilde{k}23 \\ \tilde{k}31 & \tilde{k}32 & \tilde{k}33 \end{Bmatrix} \cdot \begin{Bmatrix} \Delta\theta_{s1} \\ \Delta\theta_{s2} \\ \Delta e \end{Bmatrix} \tag{3. 120}$$

where,

$$\tilde{k}11 = S_L - \frac{S_L^2(k22^* + S_R)}{\beta_s} \tag{3. 121}$$

$$\tilde{k}12 = \frac{S_L S_R k12^*}{\beta_s} \tag{3. 122}$$

$$\tilde{k}22 = S_R - \frac{S_R^2(k11^* + S_L)}{\beta_s} \tag{3. 123}$$

$$\tilde{k}21 = \frac{S_L S_R k21^*}{\beta_s} \tag{3. 124}$$

$$\tilde{k}13 = k13^*;\ \tilde{k}23 = k23^*;\ \tilde{k}33 = k33^*;\ \tilde{k}31 = k31^*;\ \tilde{k}32 = k32^* \tag{3. 125}$$

and,

$$\beta_s = \begin{vmatrix} k11^* + S_L & k12^* \\ k21^* & k22^* + S_R \end{vmatrix} = (k11^* + S_L)(k22^* + S_R) - k12^* k21^* > 0 \qquad (3.\ 126)$$

3.4.3 Refined plastic hinge model

The traditional plastic hinge model possesses an abrupt change from ideally elastic-to-perfectly-plastic states. In order to account for the gradual yielding behavior, the refined plastic hinge approach is introduced in this thesis. The rotational stiffness will be degraded along with the gradual plasticization of the cross section, providing a smooth transition during the elasto-plastic state. The formulation for the refined plastic hinge can be expressed as,

$$S_L = S_R = EIR/L \text{ and } S_M = EIR \qquad (3.\ 127)$$

where, the R is the plasticity parameter related to the loading state, which can be expressed as follows,

$$\mathrm{R} = 10^{10} \quad \text{for} \quad M_i^\zeta \le M_e^\zeta \qquad (3.\ 128)$$

$$\mathrm{R} = \left|\frac{M_p^\zeta - M_i^\zeta}{M_i^\zeta - M_e^\zeta}\right| \quad \text{for} \quad M_e^\zeta < M_i^\zeta < M_p^\zeta \qquad (3.\ 129)$$

$$\mathrm{R} = 10^{-10} \quad \text{for} \quad M_i^\zeta \ge M_p^\zeta \qquad (3.\ 130)$$

in which, M_i^ζ is the current moment at hinge location; M_e^ζ and M_p^ζ are the initial yield and plastic moment capacities under current axial load respectively, which will be discussed in the following chapters.

It can be seen from the equations (3. 128) to (3. 130) that the hinge stiffness is controlled by the magnitude of the current hinge moment. When the moment is smaller than the elastic moment capacities, the hinge stiffness is very large and no

plastic rotation occurs. Ideally, the hinge stiffness should be infinite in elastic state; however, this extreme value is usually assigned to be a large number in computer analysis, which is set to $10^{+10} \cdot EI/L$ in the present study. Similarly, in order to avoid numerical error, the hinge stiffness is set to be a small value equaling to $10^{-10} \cdot EI/L$ for representing the full plastic state.

3.4.4 Correction of force point movement after full plastic yielding

Once a plastic hinge is fully yielded, the equilibrium condition may be violated as the applied moments at the hinge location are greater than the plastic moments. This reflects the condition of the force point lying outside the failure surface. There is an infinite number of paths to bring back this force point onto the failure surface. In the current study, the path pointed to the origin or zero moment point is chosen as the recovery path. The new equilibrium force point will be therefore moved, the gradient of the force point coordinates is computed, and the corresponding point at the failure surface will be determined as the resisting moments.

3.5. Numerical solution strategies for nonlinear analysis

3.5.1 General

Newton-Raphson solution strategy for nonlinear analysis is the most frequently adopted method in conventional design practice. Besides the method is easy-understanding and has an acceptable performance for the analysis of the regular

structures, it also returns the extract structural response at the given load level such as the ultimate or serviceability design loads, where the structural responses and member internal forces and deflections at the corresponding design load levels are usually required. However, this method is unreliable when the solution point is close to the limit points, and it also causes difficulties in distinguishing whether it is a structural instability or numerical failure.

Since the nonlinearities and initial imperfections are taken into account in an advanced analysis, some types of behavior are very likely to occur during the numerical analysis such as in the post-buckling, stiffening and softening paths. In many occasions, the complete load vs. deflection response of a nonlinear structure is difficult to be obtained due to numerical divergence, especially in the situation that the tangent stiffness is ill-conditioned or even numerical-singular near the limit points. Therefore, the Newton-Raphson method, which only requires tangent stiffness in its incremental procedure with equilibrium iterations easily diverged, cannot fulfill performance analysis under some extreme conditions.

Several advanced numerical solution strategies have already been proposed for handling the highly nonlinear problems, and their feasibility and reliability are also verified by numerous examples in the last decades. Batoz and Dhatt (1979) proposed a displacement control algorithm by incrementing the displacement instead of the load. This method shows satisfactory performance in passing the limit points as well as the snap-through points but fails in the snap-back problem in which the equilibrium path is not increased in accordance with the monitored displacement. Riks (1979) introduced an additional constraint equation to the tangent stiffness

equations by controlling the arc-length of tracing the equilibrium path. This technique was later improved by Crisfield (1981) and Ramm (1981) to restore symmetry in the tangent stiffness matrix. The method is reliable and stable for all types of nonlinear problems; however, it requires the solutions of quadratic equations in each iteration. Chan (1988) noted the aim of an iterative process is to eliminate the unbalanced equilibrium error and proposed the minimum residual displacement method. This method is to minimize the unbalanced error in each iteration, which also means it follows the shortest path to the solution point. Moreover, the expressions for the minimum residual method are simple and avoid of solution the constraint equations such as the quadratic equations for the load factor in the arc-length method.

In this section, the Newton-Raphson solution method will be briefly reviewed, and the constraint equation for the incremental-iterative procedure is also presented. Sequentially, the iteration schemes by the minimum residual displacement, the displacement control and the Arc-length control methods are discussed. Finally, the summaries of the numerical solution strategies are given.

3.5.2 Newton-Raphson strategy

The Newton-Raphson solution strategy for nonlinear analysis is the most well-known method. The solution is to divide the nonlinear problem into a series of linear solutions. One or more times of iterations are required at each load increment ΔF to minimize the solution error, which can be measured by the norm of the unbalanced force vector ΔR. The vector of unbalanced forces ΔR is given by,

$$\Delta R = F - R \tag{3. 131}$$

in which, F is a vector of the external loads; and R is a vector of the internal resisting loads which can be calculated by the function of the nodal displacement u.

In the conventional type of Newton-Raphson method, the tangent stiffness matrix will be updated in iterations. Nevertheless, the tangent stiffness matrix is only needed to be updated once in the first iteration for the modified Newton-Raphson method. The illustrations for the two types of Newton-Raphson strategies are as shown in Figure 3.6.The corresponding interactive sequence can be expressed as follows,

$$\Delta R_i = F - R_i \tag{3. 132}$$

$$\Delta u_i = K_T^{-1} \cdot \Delta R_i \tag{3. 133}$$

$$u_{i+1} = u_i + \Delta u_i \tag{3. 134}$$

$$R_{i+1} = \text{Function of } u_{i+1} \tag{3. 135}$$

where, i is the iteration number; and K_T is tangent stiffness matrix and updated iteratively in the Newton-Raphson method.

3.5.3 Basic formulation and constraint equations

The incremental equilibrium equation can be written as,

$$\Delta F = K_T \cdot \Delta u \tag{3. 136}$$

in which ΔF is a vector of the unbalanced force; K_T is the tangent stiffness matrix; and Δu is a vector of the unbalanced displacement.

A constraint equation paralleled to the applied load vector is applied and can be expressed as,

$$\Delta\lambda \cdot \Delta\bar{\mathrm{F}} = \Delta\lambda(\mathrm{K}_T \cdot \Delta\bar{\mathrm{u}}) \tag{3. 137}$$

where, $\Delta\lambda$ is the load correction factor for imposing the constrain condition; $\Delta\bar{\mathrm{F}}$ is an arbitrary force vector parallel to the applied load; and $\Delta\bar{\mathrm{u}}$ is the corresponding displacement vector conjugate to $\Delta\bar{\mathrm{F}}$.

By substituting equations (3. 137) into (3. 136), the total equilibrium condition can be written as,

$$\Delta\mathrm{F} + \Delta\lambda \cdot \Delta\bar{\mathrm{F}} = \mathrm{K}_T(\Delta\mathrm{u} + \Delta\lambda \cdot \Delta\bar{\mathrm{u}}) \tag{3. 138}$$

and, the load and force vectors in each iteration can be updated as,

$$\mathrm{F}_{i+1} = \mathrm{F}_i + \Delta\lambda_{i+1} \cdot \Delta\bar{\mathrm{F}} \tag{3. 139}$$

$$\mathrm{u}_{i+1} = \mathrm{u}_i + \Delta\lambda_{i+1} \cdot \Delta\bar{\mathrm{u}} \tag{3. 140}$$

in which, the subscript i refers to the i-th iteration number within a load increment.

All numerical procedures for nonlinear finite element analysis can be formulated on the basic of the equation (3. 138) with the difference corrector factor $\Delta\lambda$. This equation was first proposed by Batoz and Dhatt (1979) for solving nonlinear problems by fixing the displacement increment at a chosen displacement degree of freedom. Obviously, when the corrector factor equals to zero, the equation will be reformulated to a conventional Newton-Raphson strategy.

3.5.4 Interaction scheme by minimum residual displacement method

Since the main objective for the iterative procedure is to eliminate the unbalanced residual displacements, it is more efficient and direct to utilize a corrector factor for finding the minimum residual displacement increment. Chan (1988) proposed a iteration scheme, named minimum residual displacement (MRD) method, to satisfy the convergence criterion rather than to satisfy the constraint arc-distance or work done, which is not the objective of an iteration for equilibrium.

In order to give an implemental description on the MRD method, the derivation will be briefly given. The residual displacement can be expressed as $\Delta \mathrm{u}_i + \Delta\lambda_i \cdot \Delta\bar{\mathrm{u}}$, where $\Delta\bar{\mathrm{u}}$ is the displacements due to the force vector $\Delta\bar{\mathrm{F}}$ paralleled to the applied forces F. Therefore, the minimum residual displacement can be obtained by differentiating the expression of convergence criterion with respect to the parameter $\Delta\lambda_i$ as,

$$\frac{\partial[(\Delta \mathrm{u}_i + \Delta\lambda_i \cdot \Delta\bar{\mathrm{u}})^T(\Delta \mathrm{u}_i + \Delta\lambda_i \cdot \Delta\bar{\mathrm{u}})]}{\partial\Delta\lambda_i} = 0 \tag{3. 141}$$

and it can be further written as,

$$\Delta\lambda_i = -\frac{\Delta \mathrm{u}_i{}^T \cdot \Delta\bar{\mathrm{u}}}{\Delta\bar{\mathrm{u}}^T \cdot \Delta\bar{\mathrm{u}}} \tag{3. 142}$$

This method follows the shortest path to the solution point in the iterative procedure as illustrated in Figure 3.7. The expression for this method is simple and also avoids the solution of the quadratic equations for the constraint load factor $\Delta\lambda_i$ as in the arc length method.

Except for the first iteration, the $\Delta\lambda_i$ can be calculated by the equation (3. 142). It is obvious to adopt a small value of load increment in the first step. However, as reported by Chan (1988), the current stiffness parameter proposed by Bergan *et al*. (1978) is one of the most logical and appropriate method to control the load size at the first iteration, which is given by,

$$\Delta\lambda_1 = \Delta\lambda_1(S_k)^{\gamma} \tag{3. 143}$$

where, γ is the user-defined parameter; S_k is current stiffness parameter expressed as,

$$S_k = \frac{\Delta\bar{\mathrm{F}}_1^{\,T} \cdot \Delta\bar{\mathrm{u}}_k}{\Delta\bar{\mathrm{F}}_k^{\,T} \cdot \Delta\bar{\mathrm{u}}_1} \quad \text{and} \quad 0.1 < (S_k)^{\gamma} < 2.0 \tag{3. 144}$$

3.5.5 Interaction scheme by displacement control method

The displacement control method adopted was firstly proposed by Batoz and Dhatt (1979). A single degree of freedom (DOF) is chosen to be the steering displacement that its incremental value is fixed. Apart from the load-controlled Newton-Raphson strategy, the method is displacement controlled, where the equilibrium is satisfied to a pre-defined deflection during each load increment. A graphical illustration of this method is presented in Figure 3.8.

Assume the *m*-th degree of freedom to be the steered, the corrector factor for the first iteration can be written as,

$$\Delta\lambda_1 = -\frac{\delta_0}{\Delta_m\bar{\mathrm{u}}_1} \tag{3. 145}$$

where, δ_0 is the pre-defined displacement increment at the steering DOF; and $\Delta_m \bar{u}_1$ is the displacement vector associated with an arbitrary load parallel to the applied loads.

For the second and later iteration within a load increment cycle, $\Delta_m \bar{u}_{i+1}$ will be the same as $\Delta_m \bar{u}_i$ for no displacement at steering DOF. The corrector factor can be further obtained as,

$$\Delta\lambda_i = -\frac{\Delta_m u_i}{\Delta_m \bar{u}_i} \qquad \text{and} \qquad i \geq 2 \tag{3. 146}$$

in which, $\Delta_m u_i$ is the load increment due to the unbalanced force at the iterations.

This solution strategy shows good performance at passing the limit points and suitable for obtaining the full load vs. deflection curve in an inelastic analysis. The method is also feasible for the snap-through problem, but it fails at the snap-back analysis. Moreover, it can be seen from the above equations that, the choice of the steering DOF is crucial for the analysis and has significant influence on the numerical stability. Usually, the steering DOF is chosen to be the largest displacement increment point in the structures.

3.5.6 Interaction scheme by arc-length control method

Arc-length control method is one of the most popular solution methods for nonlinear problems, which was firstly proposed by Riks (1979) and further improved by Crisfield (1983). In the Arc-length control method, an additional constraint equation is imposed on the load increment associated with an arc distance S.

Therefore, the corresponding constraint equation in the first iteration of a load cycle can be expressed as,

$$\Delta\lambda_1 = S/\sqrt{\Delta\bar{\mathrm{u}}_1{}^T \cdot \Delta\bar{\mathrm{u}}_1} \tag{3. 147}$$

where, S is the initial arc-length distance.

For the later iterations, the arc distance S is kept constant, thus the equation can be expressed as,

$$(\mathrm{u}_{i-1} + \Delta\mathrm{u}_i + \Delta\lambda_i\Delta\bar{\mathrm{u}}_i)^T(\mathrm{u}_{i-1} + \Delta\mathrm{u}_i + \Delta\lambda_i\Delta\bar{\mathrm{u}}_i) = S^2 \tag{3. 148}$$

Expanding the equation, we have,

$$\alpha_1\Delta\lambda_i^2 + \alpha_2\Delta\lambda_i + \alpha_3 = 0 \tag{3. 149}$$

in which,

$$\alpha_1 = \Delta\bar{\mathrm{u}}_i^T\Delta\bar{\mathrm{u}}_i \tag{3. 150}$$

$$\alpha_2 = 2(\mathrm{u}_{i-1} + \Delta\mathrm{u}_i)^T\Delta\bar{\mathrm{u}}_i \tag{3. 151}$$

$$\alpha_3 = (\mathrm{u}_{i-1} + \Delta\mathrm{u}_i)^T(\mathrm{u}_{i-1} + \Delta\mathrm{u}_i) - S^2 \tag{3. 152}$$

By solving the equation (3. 149) and choosing the root for maintaining a positive angle between the origin and the updated incremental displacement vector in equation (3. 153), the load increment factor for the *i*-th interaction can be obtained as,

$$\Delta\lambda_i = -\alpha_3/\alpha_2 \tag{3. 153}$$

The solution strategy for the Arc-length control method is illustrated in Figure 3.9. This method has been widely used and proved to be an effective and efficient

method for nonlinear analysis. However, in the iterative procedure, the quadratic equation as in (3. 149) needs to be solved, and the solution roots will be selected.

3.5.7 Convergence criteria

In an iterative solution procedure for the finite-element analysis, convergence criteria are needed to be introduced for the termination of the iteration. The criterion based on unbalanced forces is commonly adopted in engineering practice. In order to obtain an accurate analysis for both forces and displacements, the convergence criteria are checked using the unbalanced forces and displacements as,

$$\frac{\Delta \mathrm{u}_g{}^T \cdot \Delta \mathrm{u}_g}{\mathrm{u}_g{}^T \cdot \mathrm{u}_g} \leq TOL \tag{3. 154}$$

$$\frac{\left(\Delta \mathrm{F}_g{}^T \cdot \Delta \mathrm{F}_g\right) + \left(\Delta \mathrm{F}_i{}^T \cdot \Delta \mathrm{F}_i\right)}{\left(\mathrm{R}_g{}^T \cdot \mathrm{R}_g\right) + \left(\mathrm{R}_i{}^T \cdot \mathrm{R}_i\right)} \leq TOL \tag{3. 155}$$

where, TOL is a value for the acceptable accuracy and usually assumed to be 0.1% in conventional practice; $\Delta \mathrm{u}_g$ and u_g are the incremental and total displacements at external nodes in global directions respectively; $\Delta \mathrm{F}_g$ and $\Delta \mathrm{F}_i$ are the global and internal unbalanced forces respectively; while R_g and R_i are the external resisting forces at global axes and the local resisting forces at member local axes respectively.

3.5.8 Summaries

Due to the complexity of the nonlinear problem, versatile solution strategies are still required for different types of analysis. For the conventional second-order design, the Newton-Raphson method is generally adopted because the response at a

fixed load level is needed. However, for advanced analysis of a structure under ultimate limit state or some extreme scenarios, the minimum residual displacement method or arc-length method is recommended for the convergence of the analysis. Furthermore, in inelastic analysis of the regular structure or single member, the displacement control method is attractive with a proper selection of the steering degree of freedom.

3.6. Verification examples

Based on the proposed numerical algorithm, a computer program is developed to study the nonlinear behavior of two-dimensional frames and members. In order to determine the accuracy, efficiency and versatility of the proposed analytical model for the conventional second-order design and advanced analysis, several examples are selected. All the examples are limited to bare steel and the other material types of structure and members will be discussed in the following chapters.

3.6.1 Closed-form solutions of single initially curved members

The accurate simulation of geometric nonlinearity is fundamental for both second-order design and advanced analysis. Thus, to study the accuracy of elastic analysis, three single curved members with different boundary conditions are analyzed by the closed-form solutions and the proposed approach. As only the second-order effects as well as initial imperfections are studied, the rotational stiffness for the plastic hinges is set to be infinity that the material yielding is not

considered in the proposed element. Accordingly, the location of the middle hinge is assigned to be located at the middle span. Besides, the member end conditions are ideally assumed to be rigid or pinned and the semi-rigid connection is not considered.

The initial imperfection in member level is assumed to be as a sine function, which can be expressed as,

$$y_0 = \delta_0 sin\frac{\pi x}{L} \tag{3. 156}$$

where, y_0 is the variation of the initial imperfection along member length; x is the distance along the member; δ_0 is the magnitude of the initial curvature at mid-span; L is the member length.

The closed-form solution by the stability function can be expressed as,

$$y = \frac{M_1}{P}\left[\frac{\sin(kL-kx)}{sinkL} - \frac{L-x}{L}\right] - \frac{M_2}{P}\left[\frac{\sin kL}{sinkL} - \frac{x}{L}\right] + \frac{\delta_0}{1-P/P_{cr}} sin\frac{\pi x}{L} \tag{3. 157}$$

in which, P_{cr} is the Euler buckling load as $\pi^2 EI/L$; and k equals to $\sqrt{P/EI}$.

In the followings, three slender steel columns are analyzed and compared under different boundary conditions as “pinned-pinned”, “fixed-pinned” and “fixed-fixed” respectively. The section size is SHS300 × 10.0 with 300 mm for breadth and width and 10 mm for wall thickness. The material grade is S355 and the Young’s modulus is 205 GPa. The overall height of the column is 10 m with assuming the initial member imperfection of L/500 is assumed. The cross section area is 1.15×10^{-2} m^2 and the second moments of area about both the principal axes are 1.60×10^{-4} m^4.

In the pinned-pinned boundary condition, the end moment M_1=M_2=0, and therefore the deflection at mid-span can be expressed as,

$$\delta = \delta_0 \frac{1}{1 - P/P_{cr}} \tag{3. 158}$$

and the comparison between the analytical and present numerical results are plotted in Figure 3.10.

Moreover, the second column is pinned at its top end and fixed at its bottom end respectively. Therefore, due to M_2=0 and $\theta_1 = \delta_0 \pi / L$, the moment at the bottom end M_1 and rotation angle θ_2 at t he top can be written as,

$$M_1 = -\frac{\delta_0 \cdot \pi/L \cdot P/P_{cr}}{1 - P/P_{cr}} \cdot \frac{PL}{1 - kL/tan\, kL} \tag{3. 159}$$

$$\theta_2 = \frac{M_1}{PL}\left(1 - \frac{kL}{sin\, kL}\right) - \frac{\delta_0 \cdot \pi/L}{1 - P/P_{cr}} - \delta_0 \cdot \frac{\pi}{L} \tag{3. 160}$$

and the load vs. deflection curves are presented in Figure 3.11.

Herein, the third column is fixed at both ends, therefore, $\theta_1 = -\theta_2 = \delta_0 \pi / L$ and the equations can be written as,

$$M_1 = -M_2 = -\frac{\delta_0 \cdot \pi/L \cdot P/P_{cr}}{1 - P/P_{cr}} \cdot \frac{PL}{kLtan\,(kL/2)} \tag{3. 161}$$

$$y' = \frac{M_1}{PL} \frac{\mathrm{kL}}{sinkL} [cos\, kx - cos\,(kL - kx)] + \frac{\delta_0 \cdot \pi/L}{1 - P/P_{cr}} cos \frac{\pi x}{L} \tag{3. 162}$$

therefore, the vertical displacement can be calculated from the following equation as,

$$\Delta_y = \frac{PL}{EA} + \frac{1}{2} \int_L y'^2 dx \tag{3. 163}$$

and, the comparisons are illustrated in Figure 3.12.

These figures show that the numerical results from the proposed element using only one element per member are very accurate by comparing to the closed-form solutions.

3.6.2 Advanced analysis of a simply supported column

In this example, a simply supported column under different loading conditions is analyzed by advanced analysis method with the considerations of both geometric and material nonlinearities as well as initial member imperfection. The column studied is of length 20 m and its section size is CHS355.6 × 8.0. The design strength of steel is 275 MPa and the corresponding Young's modulus of elasticity is $205\ GPa$.The sectional area for the column is 8.74×10^{-3} m^2, second moment of area of 1.32×10^{-4} m^4, and the elastic and plastic section modulus are 7.42×10^{-4} m^3 and 9.67×10^{-4} m^3, respectively. The initial member imperfection is taken as L/500.

To model the initial imperfection by the traditional plastic hinge element, two and more elements must be required for a member and the middle node is needed to offset for simulate the member imperfection, as illustrated in Figure 3.13. Further, the initial imperfection shape recommended in design code is a sine curve which may need more elements for geometric modeling. For the circumstances that the imperfection value is small, this simplification is still valid and acceptable. However, when the initial imperfection is larger, the error induced by this modeling method becomes significant. This imperfection modeling method is hard to be adopted in actual practice when dealing with hundreds or even thousands of element and load cases. As the imperfection mode depends on loads, it varies with load case and

brings much inconvenience in practical design where hundreds of load cases may need to be combined. By utilizing the proposed element for advanced analysis, all members can be modeling by one element and the initial imperfection can be imposed on the element directly. This leads to much convenience and reliability in numerical convergence and efficiency.

In a purely axial loaded condition, the analysis results by the conventional plastic hinge element and the proposed element is illustrated in Figure 3.14. In order to obtain a full load vs. deflection curve, the displacement control method is adopted for determining the load increment and the minimum residual displacement method is introduced for the interactive procedure. The controlled displacement incremental at vertical translation is 0.001 m. From the comparisons, the result obtained by the proposed element is closed to the conventional analysis method by two plastic hinge elements.

The load vs. deflection curve for a uniform distributed load equal to 5 kN/m is shown in Figure 3.15. When the load-controlled Newton-Raphson method is introduced, the load incremental factor is taken as 0.01. In these pure bending conditions, both the material nonlinearity and large displacement effects are considered. The comparison shows high accuracy results by the proposed analytical method using one element per member can be achieved.

3.6.3 Second-order and advanced analysis of a cantilever column

In this example, a cantilever column with an axial and a lateral loads is analyzed by elastic second-order and advanced plastic analysis method. In order to evaluate the validity and accuracy of the proposed element for this large deflection and highly nonlinear problem, the PEP element (1994) and the advanced structural analysis software NIDA (2013) will be used for the comparisons, which have been approved to be accurate and efficient by numerous applications and studies. The column herein studied is 20 meter long and its section size is CHS323.9 × 16.0. The corresponding steel grade is S275, where the design yield strength is $275\ MPa$ and the Young's modulus is $205\ GPa$. The cross section area is 1.55×10^{-2} m^2, and the second moment of area is 1.84×10^{-4} m^4, and the elastic and plastic section moduli are 1.14×10^{-3} m^3 and 1.52×10^{-3} m^3, respectively. The initial member imperfection is taken as L/500.

The capability for large deflections and the geometric nonlinear analysis can be tested by a second-order elastic analysis of a cantilever column, where the comparison is plotted in Figure 3.16. All the analytical models in NIDA and the proposed program are modeled by one element per member. A vertical and a lateral concentrated loads equaling to -100 kN and 10 kN respectively are applied to the top of the cantilever column. It can be observed that, the analysis results by the proposed analytical model are very accurate by comparing with the mature software NIDA (2013).

Moreover, the inelastic behavior can be further taken into account by the refined plastic hinge method and the results for the advanced plastic analysis are presented

in Figure 3.17. The loading conditions are the same as the example in the second-order elastic analysis above.

From the comparisons, it shows the accuracy and validity of the proposed analytical model, which is not only suitable for second-order elastic analysis with large deflections, but also shows good performances in advanced plastic analysis with significant inelastic-softening behavior.

3.6.4 Advanced plastic analysis of a portal frame

In this example, a simple portal frame is shown in Figure 3.18 and analyzed by the advanced plastic analysis approach. The portal frame is made by bare steel members with the section type as RHS250 × 100 × 10.0 and the material grade as S275. All the members are assumed to be initially curved as a half sinusoidal shape of maximum in-plane deflection of L/500 at the mid-span, and the direction of the member initial imperfections is set to be opposite to the deflections due to applied loads. A uniform distributed loads equaling to -10 kN/m is applied at the beam, while two concentrated loads equaling to 10 kN are applied at the top of the two columns. The frame is pinned to the ground and only the connectivity between the beam and the columns are assumed to be perfectly rigid.

In order to study the performance of the proposed analytical model for the advanced analysis of the framed structure, the conventional beam-column element approach with refined plastic hinges at its ends is also introduced for the comparisons. In order to accurately reflect the inelastic behavior of the member, two

elements are required for modeling a member in the analysis by the conventional approach.

In the proposed analytical approach, the location of the middle hinge in the proposed element can be arbitrarily placed associated with the position in the most critical section. Usually, this critical location should be pre-determined by an elastic analysis. In this example, the middle hinge locations for all the members are assumed at the middle-span for an easy comparison purpose.

The comparison results for the two analytical approaches are presented in Figure 3.19 and Figure 3.20, where the first, second and third plastic hinges are observed at the load factors equaling to 1.1053, 1.1490 and 1.6624 respectively in the present study. It can be seen that the results by the two approaches are closed in tracing the horizontal and vertical deflections of the portal frame, and the collapse path of the structure can be also reflected.

3.6.5 Advanced analysis of Vogel's six story frame

This is a benchmark example reported by Vogel (1985) treated as an European calibration frame, which has been extensively studied by many researches for testing their inelastic analysis theories, as illustrated in Figure 3.21. The frame is applied by distributed gravity loads on beams and concentrated forces at the top of each floor. A global out-of-plumb straightness equaling to 1/450 is assumed while no member initial imperfections are taken into account. The yield strength of all members is 235 MPa and the Young's modulus is 205 GPa.

This frame has been analyzed by Vogel (1985), who used the plastic zone approach for tracing the entire load vs. deflection. Since the inelastic behavior is extremely significant in this example, two elements are still needed for modeling of each beam, while one element for a column is still valid. The comparison results are plotted in Figure 3.22.

From the comparison results, it shows the proposed analytical method is very accurate and valid for large deflections and inelastic analysis of steel frames. The ultimate load factor by the plastic zone method is 1.112, while the corresponding load factor by the proposed method is 1.152. A very slight different in the load vs. deflection relations is observed in the Figure 3.22, and the proposed refined plastic hinge method is more efficient and effective by comparing to the plastic-zone approach.

3.7. Concluding remarks

In order to develop a unified analytical model for advanced analysis of hybrid steel and concrete members, a new curved beam-column element with an arbitrarily-located and two end plastic hinges is proposed in this thesis. Moreover, for an easy incorporation of the proposed element into the existing software, the condensation approach for reducing the additional DOFs in the element is introduced. Sequentially, the formulation for the conventional refined plastic hinges can be added to the element ends. For the consideration of large deformation, the updated Lagrangian description is utilized that the equilibrium condition is established by referring to the

last known configuration in the interactive procedure. In conclusion, the proposed element is not only suitable for large deformation and stability analysis of the slender member such as steel columns, but also valid for the inelastic analysis of the stocky member such as reinforced concrete columns. Therefore, a unified analysis and design method can be then proposed for hybrid steel and concrete members by using this element, which will be further discussed in the following chapters.

3.8. Appendix I -the derivation of matrix [D]

Consider the force equilibrium between member local axes to intermediate coordinate system as,

$$\mathrm{F}' = [A]^T \cdot f^* \tag{3. 164}$$

or in matrix form,

$$\begin{bmatrix} M_1' \\ M_2' \\ T \\ S \end{bmatrix} = \begin{bmatrix} 1 & 0 & 0 \\ 0 & 1 & 0 \\ \dfrac{v'}{(\mathrm{L}+\mathrm{e})^2} & \dfrac{v'}{(\mathrm{L}+\mathrm{e})^2} & \dfrac{L+u'}{\mathrm{L}+\mathrm{e}} \\ -\dfrac{L+u'}{(\mathrm{L}+\mathrm{e})^2} & -\dfrac{L+u'}{(\mathrm{L}+\mathrm{e})^2} & \dfrac{v'}{\mathrm{L}+\mathrm{e}} \end{bmatrix} \cdot \begin{bmatrix} M_1{}^* \\ M_2{}^* \\ P^* \end{bmatrix} \tag{3. 165}$$

The equation (3. 165) can be rewritten as,

$$\tilde{\mathrm{F}}' = [\tilde{A}]^T \cdot f^* \tag{3. 166}$$

also written in matrix form,

$$\begin{bmatrix} M_{1'} \\ T \\ S \end{bmatrix} = \begin{bmatrix} 1 & 0 & 0 \\ \dfrac{v'}{(\mathrm{L}+\mathrm{e})^2} & \dfrac{v'}{(\mathrm{L}+\mathrm{e})^2} & \dfrac{L+u'}{\mathrm{L}+\mathrm{e}} \\ -\dfrac{L+u'}{(\mathrm{L}+\mathrm{e})^2} & -\dfrac{L+u'}{(\mathrm{L}+\mathrm{e})^2} & \dfrac{v'}{\mathrm{L}+\mathrm{e}} \end{bmatrix} \cdot \begin{bmatrix} M_1{}^* \\ M_2{}^* \\ P^* \end{bmatrix} \tag{3. 167}$$

Therefore, the expression for f^* can be obtained as,

$$f^* = ([\tilde{A}]^T)^{-1} \cdot \tilde{\mathrm{F}}' \tag{3. 168}$$

and presented in matrix form,

$$\begin{bmatrix} {M_1}^* \\ {M_2}^* \\ P^* \end{bmatrix} = \begin{bmatrix} 1 & 0 & 0 \\ -1 & v' & -L-u' \\ 0 & \dfrac{L+u'}{\mathrm{L+e}} & \dfrac{v'}{\mathrm{L+e}} \end{bmatrix} \cdot \begin{bmatrix} {M_1}' \\ T \\ S \end{bmatrix} \tag{3. 169}$$

Moreover, the differentiation of the transformation matrix [A] can be obtained as,

$$\begin{aligned} \mathrm{d}[\mathrm{A}^T] = {} & \frac{1}{(L+e)^4} \cdot \begin{bmatrix} 0 & 0 & 0 \\ 0 & 0 & 0 \\ -2(L+u')v' & -2(L+u')v' & {v'}^2(L+e) \\ (L+u')^2 - {v'}^2 & (L+u')^2 - {v'}^2 & -(L+u')v'(L+e) \end{bmatrix} du' \\ & + \frac{1}{(L+e)^4} \cdot \begin{bmatrix} 0 & 0 & 0 \\ 0 & 0 & 0 \\ (L+u')^2 - {v'}^2 & (L+u')^2 - {v'}^2 & -(L+u')v'(L+e) \\ 2(L+u')v' & 2(L+u')v' & (L+u')^2(L+e) \end{bmatrix} dv' \end{aligned} \tag{3. 170}$$

Therefore, the differentiation can be rewritten as,

$$\mathrm{d}[\mathrm{A}^T] \cdot f^* = \mathrm{d}[\mathrm{A}^T] \cdot ([\tilde{A}]^T)^{-1} \cdot \tilde{\mathrm{F}}' = [D] \cdot \Delta u' \tag{3. 171}$$

where,

$$[\mathrm{D}] = \begin{bmatrix} 0 & 0 & 0 & 0 \\ 0 & 0 & 0 & 0 \\ 0 & 0 & d33 & d34 \\ 0 & 0 & d43 & d44 \end{bmatrix} \tag{3. 172}$$

and,

$$d33 = \frac{1}{(L+e)^4}\left\{-T(L+u'){v'}^2 + Sv'\left[2(L+u')^2 + {v'}^2\right]\right\} \tag{3. 173}$$

$$\mathrm{d}34 = d43 = \frac{1}{(L+e)^4}\left[-T{v'}^3 - S(L+u')^3\right] \tag{3. 174}$$

$$\mathrm{d44} = \frac{1}{(L+e)^4}\left\{T(L+u')\left[(L+u')^2 + 2v'^2\right] - S(L+u')^2 v'\right\} \qquad (3.\ 175)$$

Figures

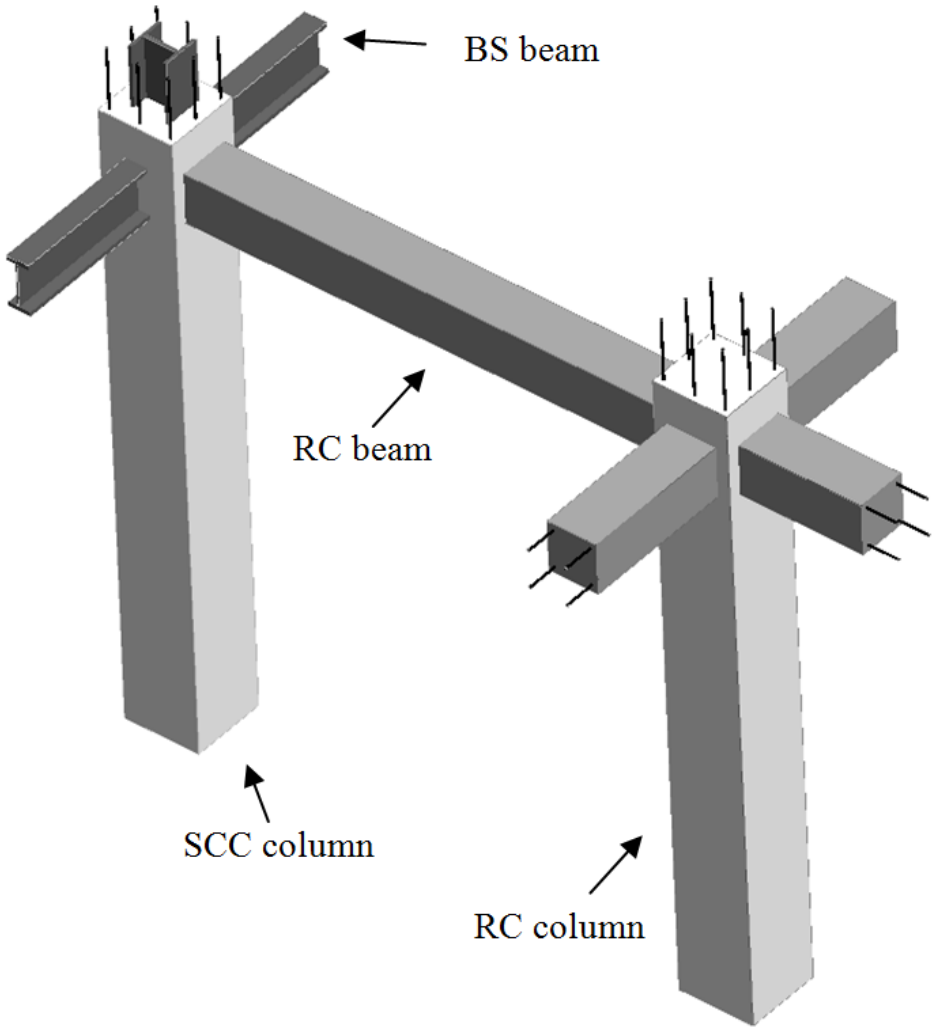

Figure 3.1 A typical hybrid steel and concrete framed structure.
(BS: Bare Steel; RC: Reinforced Concrete; SCC: Steel-Concrete Composite)

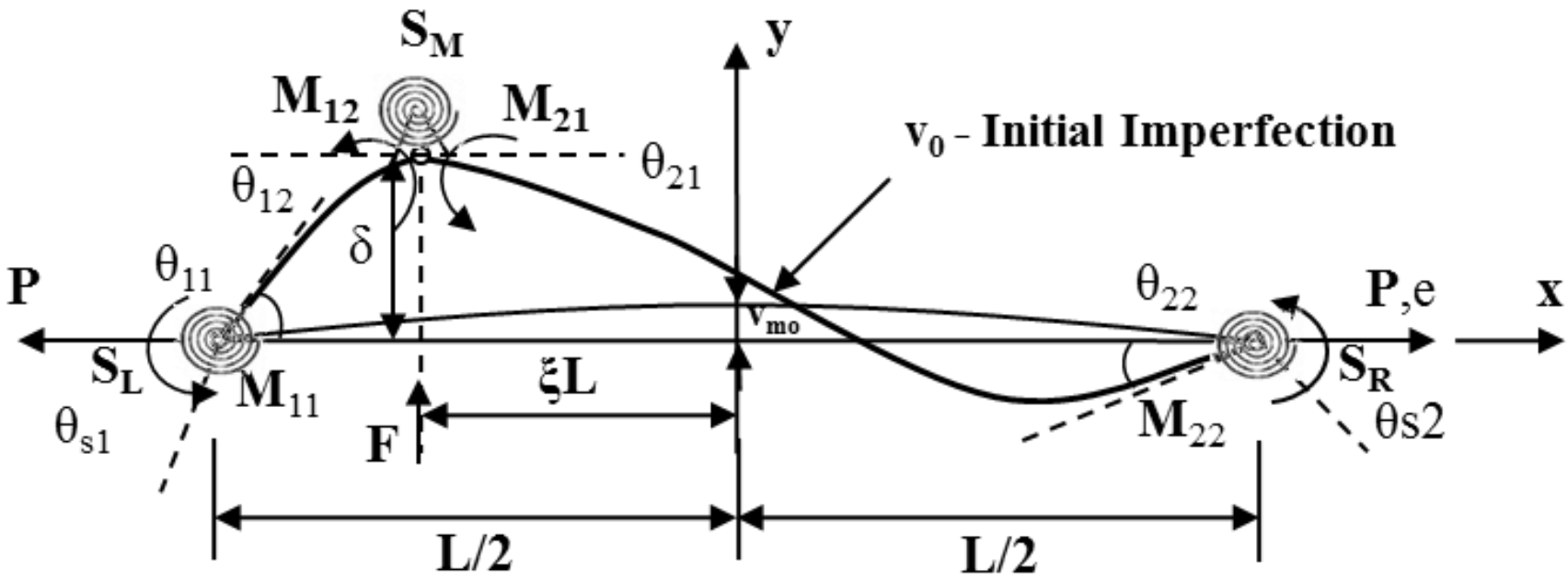

Figure 3.2 The forces vs. displacements relations of the ALH element

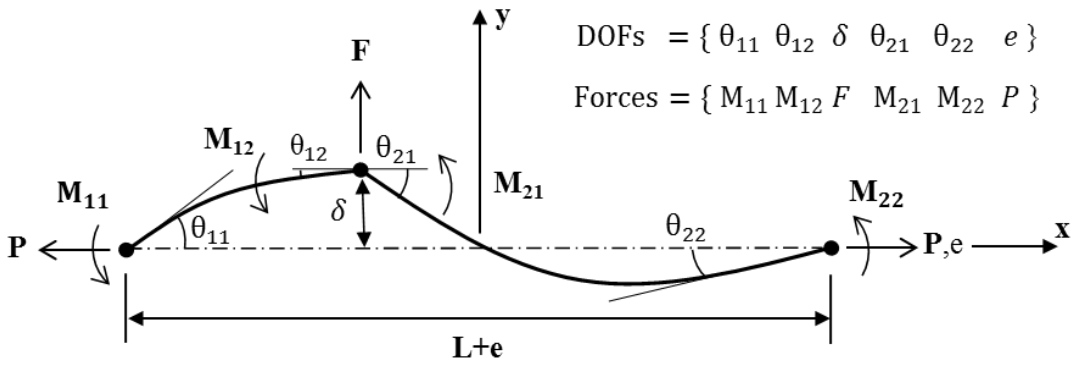

(a) Member basic displacements and forces
(Local coordinates)

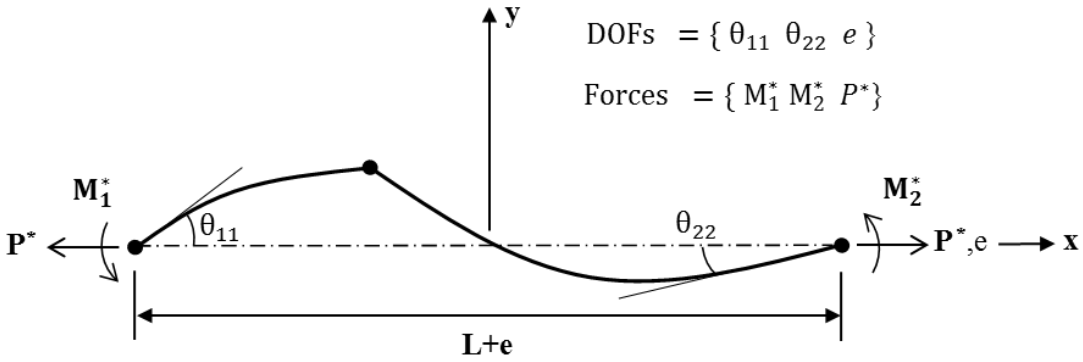

(b) Condensed member basic displacements and forces
(Local coordinates)

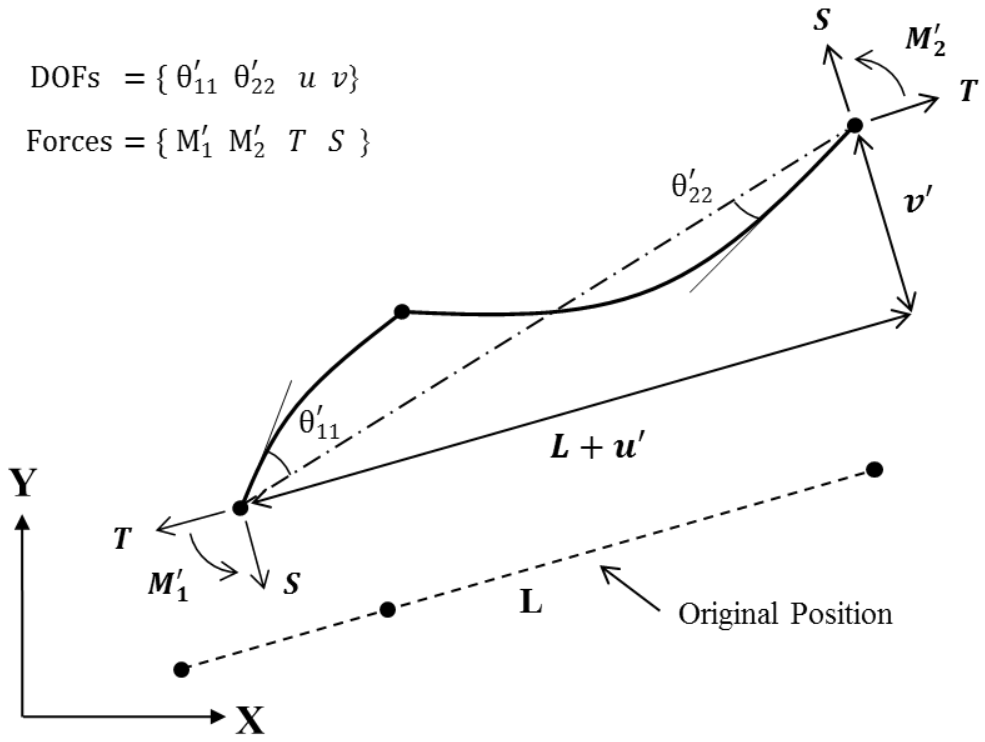

(c) Member intermediate displacements and forces
(Intermediate coordinates)

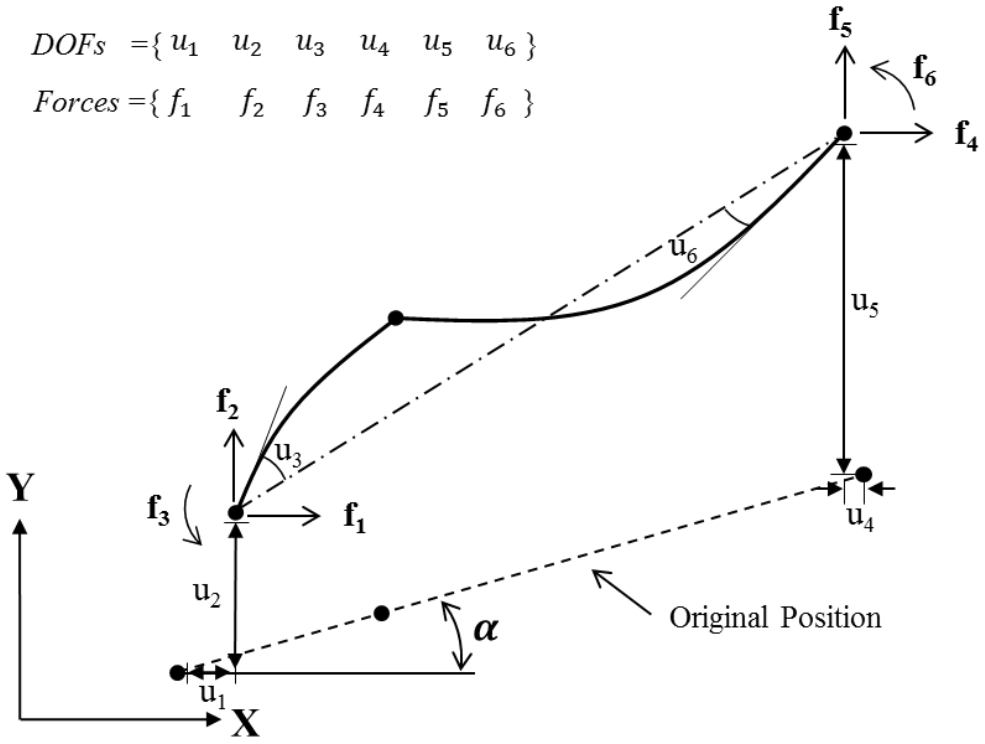

(d) Nodal displacements and forces
(Global coordinates)

Figure 3.3 Member deformations and associated forces

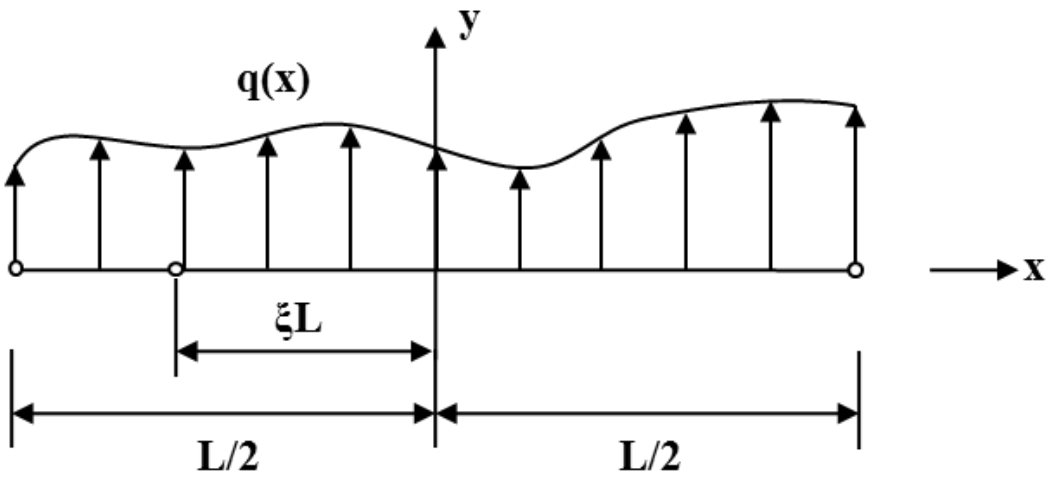

(a) Applied forces in local axes

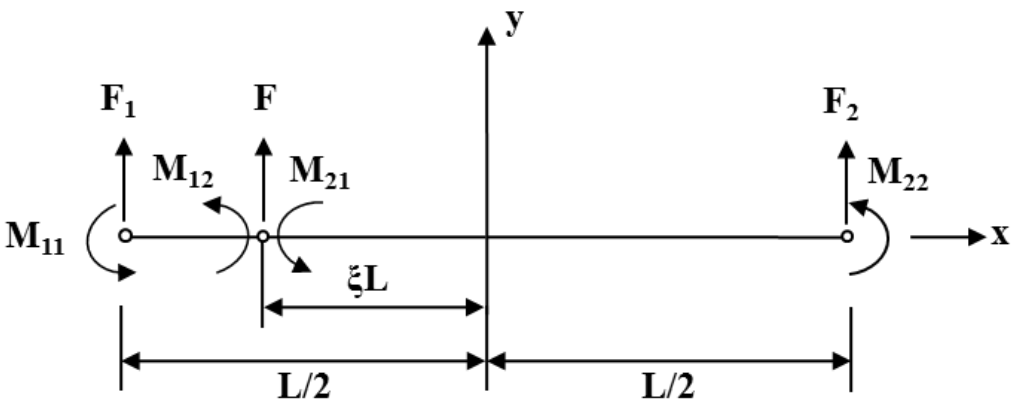

(b) Equivalent nodal forces

Figure 3.4 Equivalent nodal forces

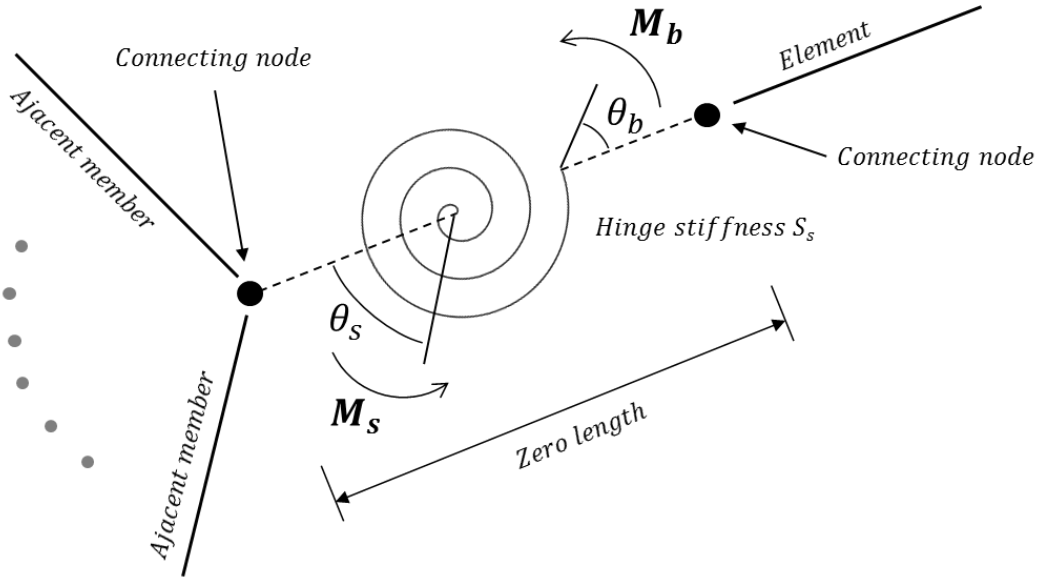

Figure 3.5 Rotational relationships in a plastic hinge at end-zone

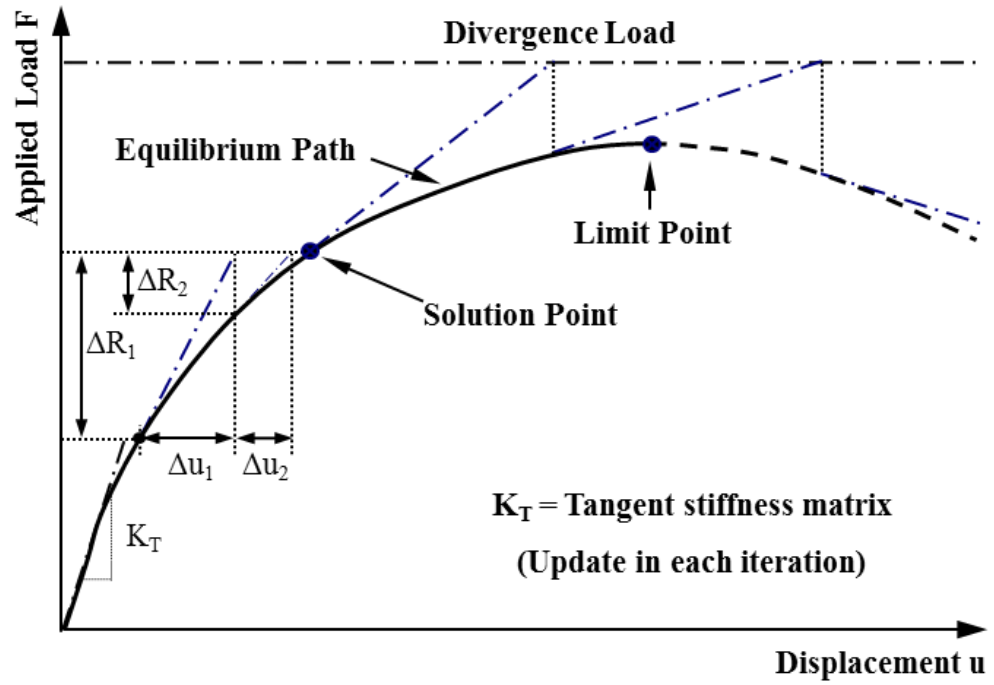

(a) Conventional Newton-Raphson solution method

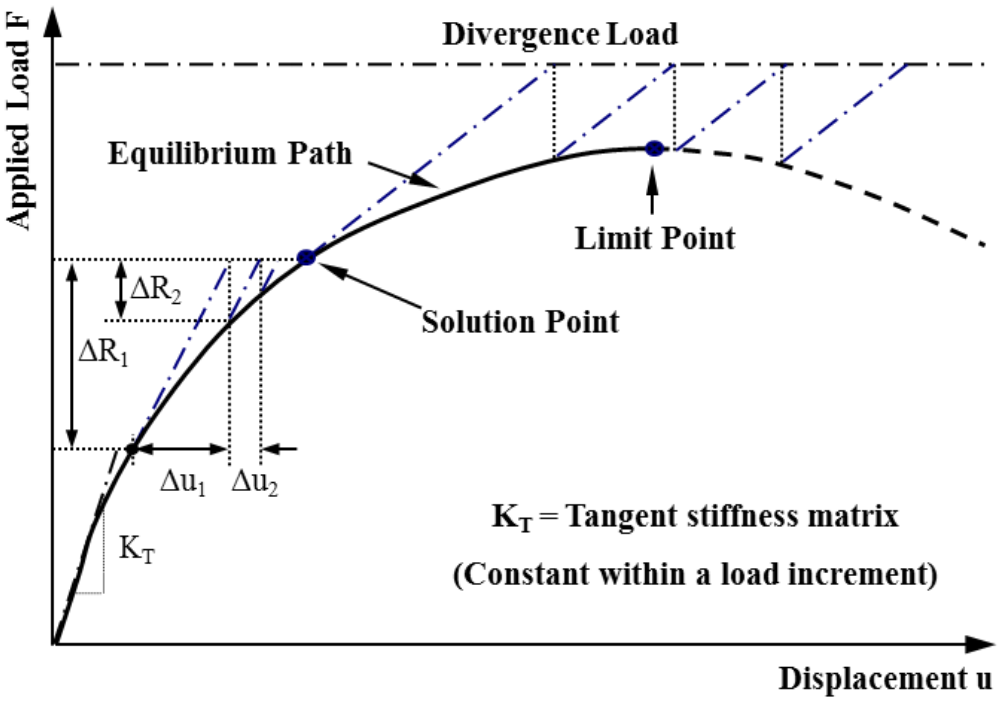

(b) Modified Newton-Raphson solution method

Figure 3.6 Two types of Newton-Raphson strategies

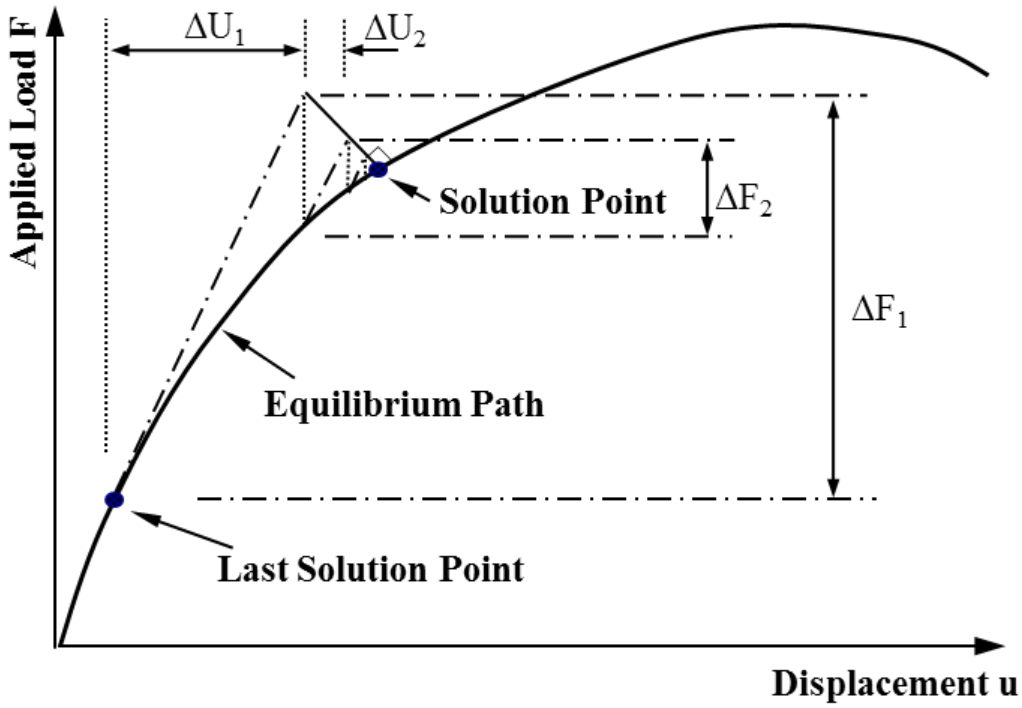

Figure 3.7 The Minimum Residual Displacement (MRD) Method

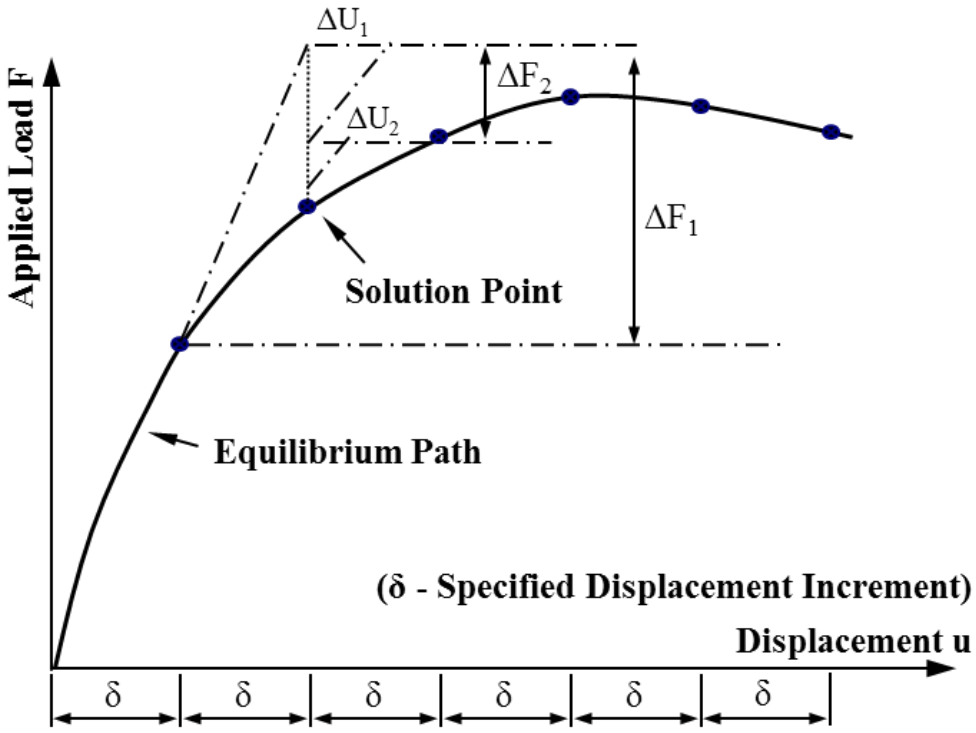

Figure 3.8 The displacement control method

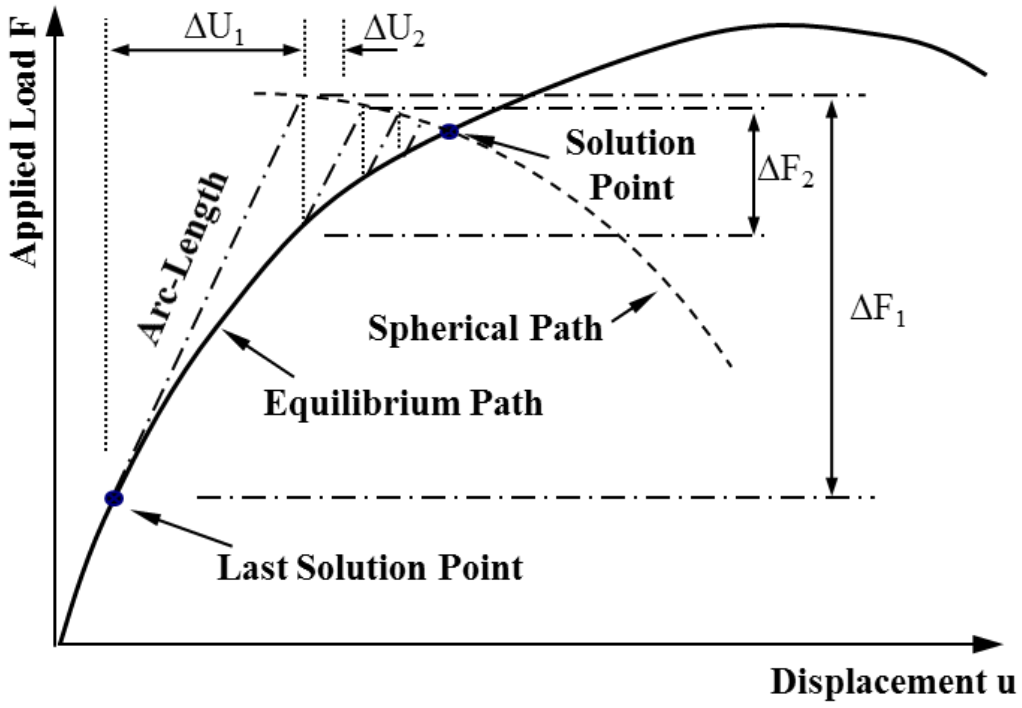

Figure 3.9 The Arc-length control method

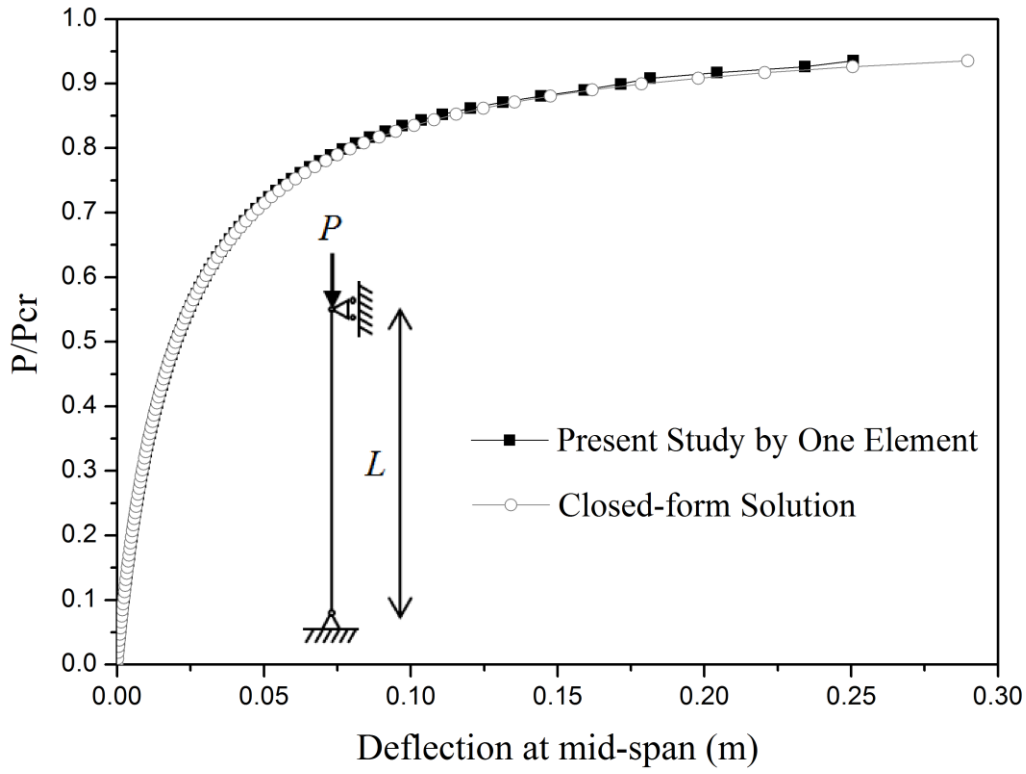

Figure 3.10 Comparison results of the pinned-pinned column

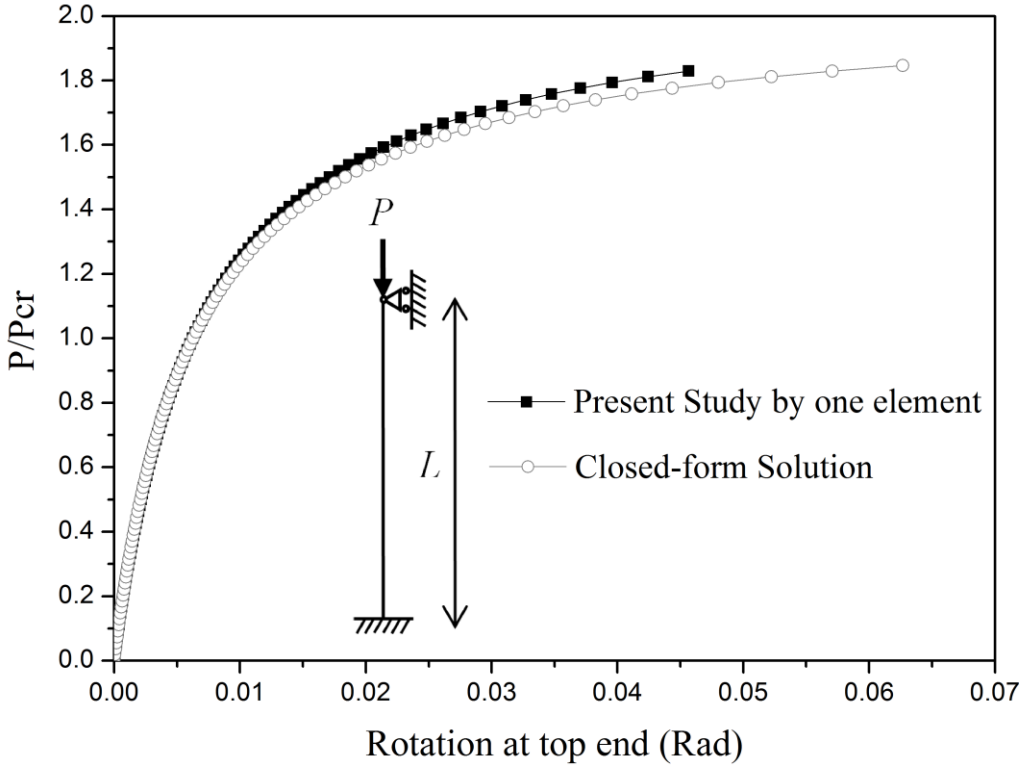

Figure 3.11 Comparison results of the fixed-pinned column

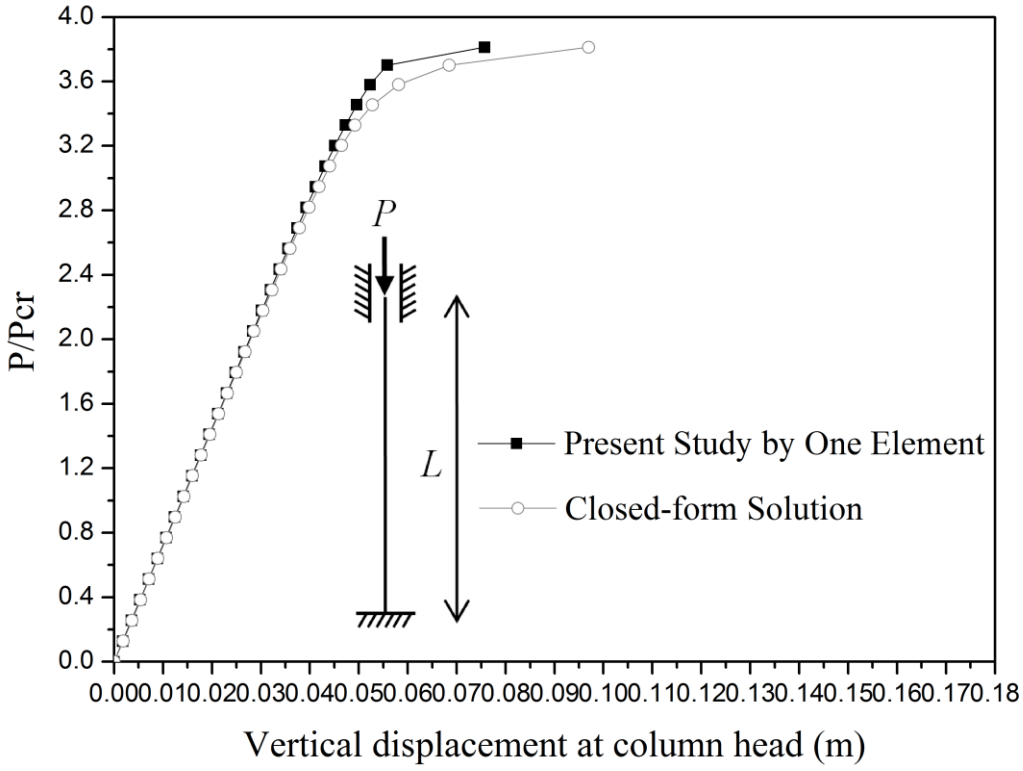

Figure 3.12 Comparison results of the fixed- fixed column

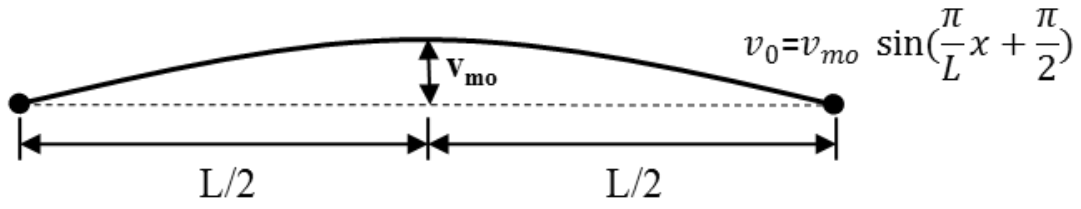

(a) Code recommended sine curve in one member

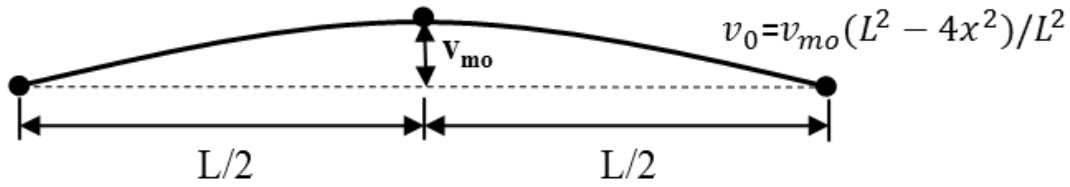

(b) Parabolic curve in the proposed one element

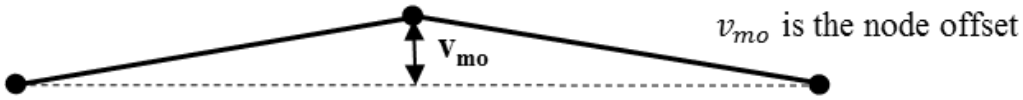

(c) Triangular shape in two conventional plastic hinge elements

Figure 3.13 Modeling of initial member imperfection

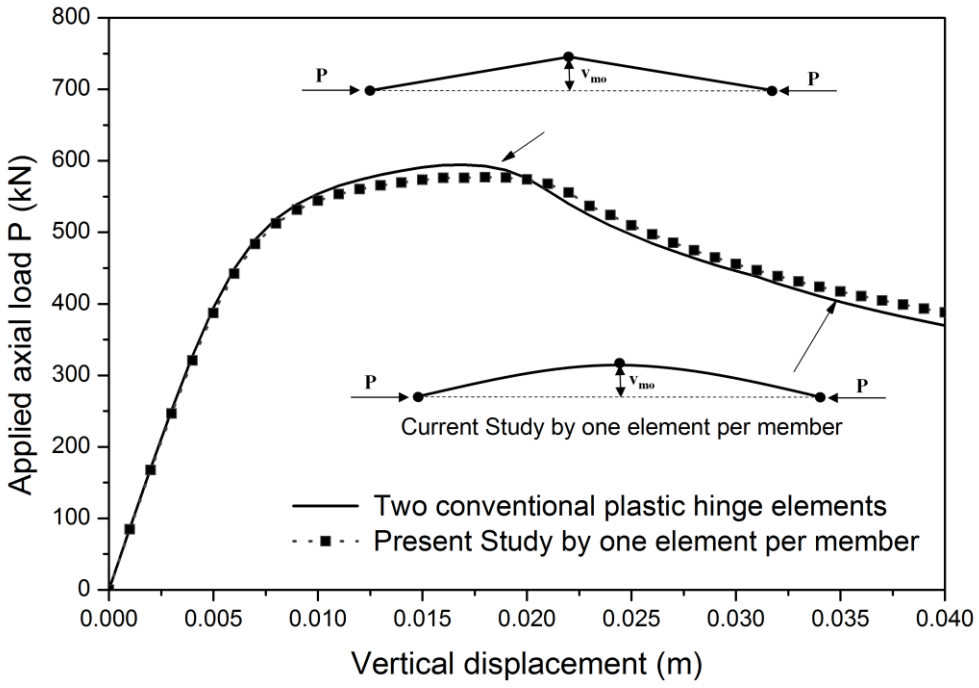

Figure 3.14 Advanced analysis of an axial-loaded simply supported column

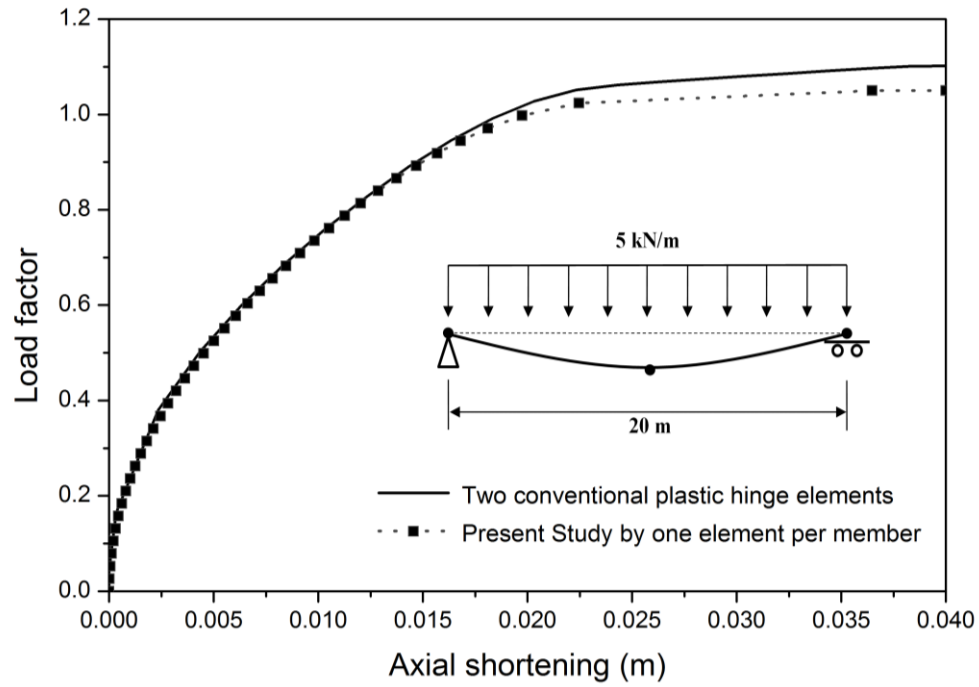

Figure 3.15 Advanced analysis of a simply supported column under UDL

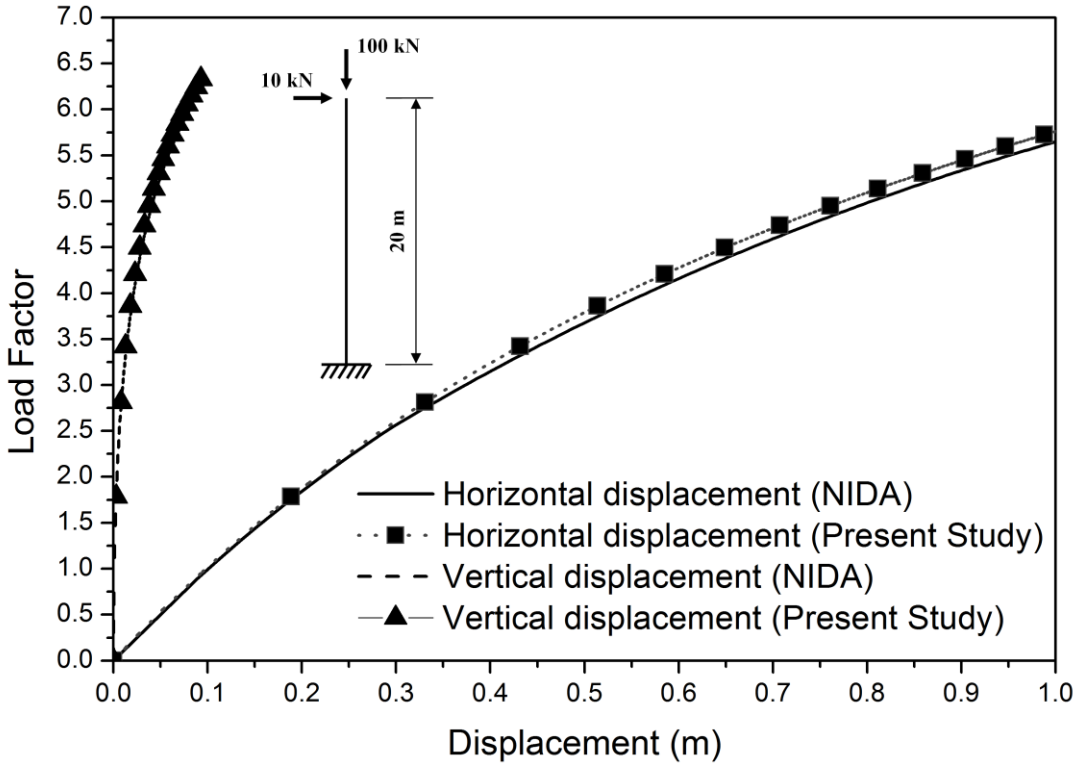

Figure 3.16 Second-order elastic analysis results of a cantilever column

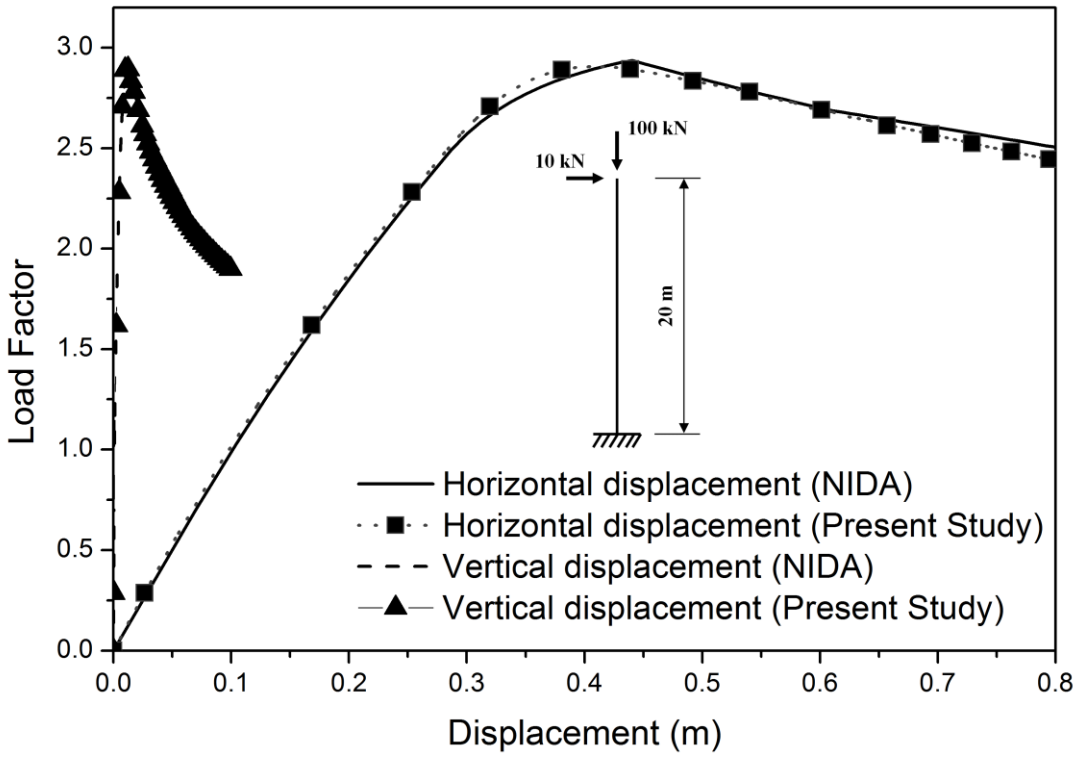

Figure 3.17 Advanced plastic analysis results of a cantilever column

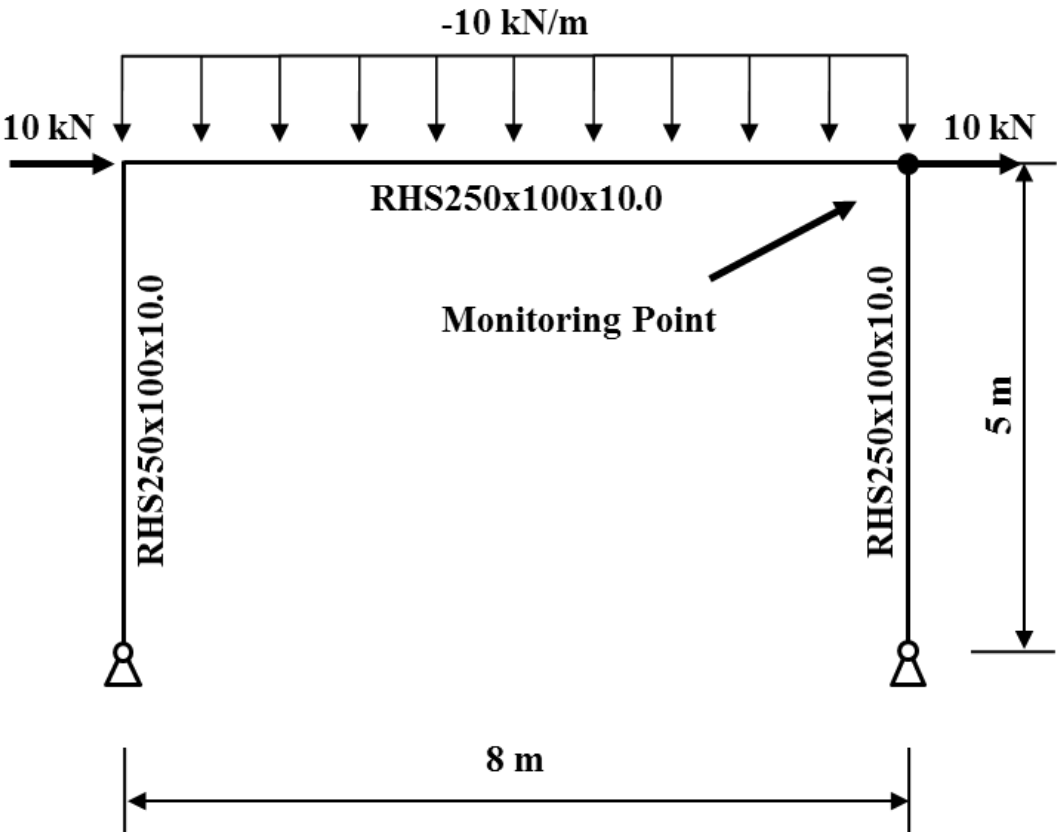

Figure 3.18 Geometry and loading pattern of the portal frame

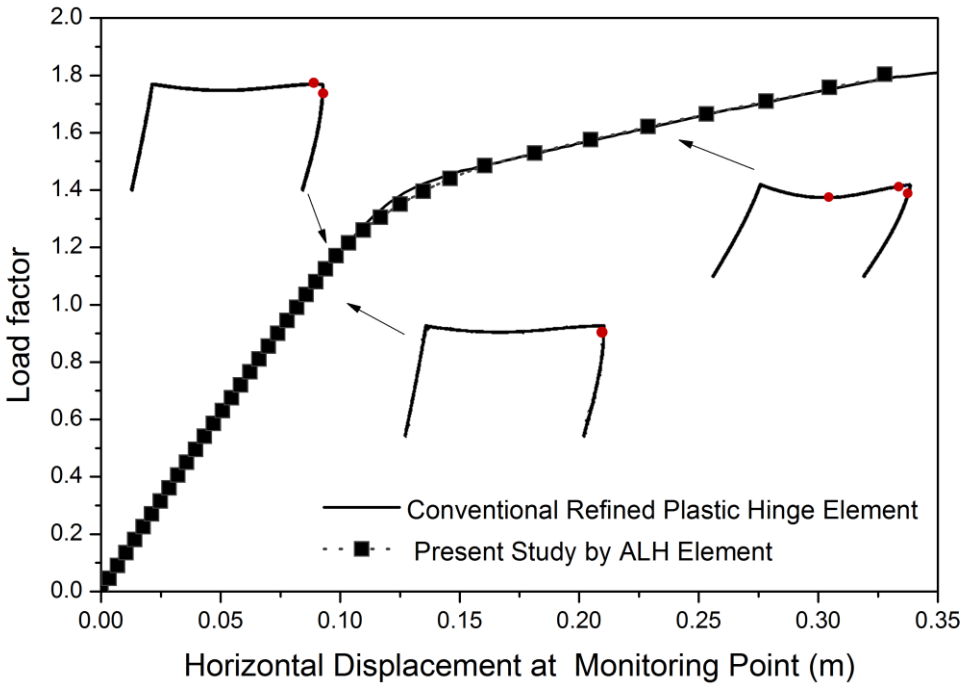

Figure 3.19 Horizontal displacement of the portal frame

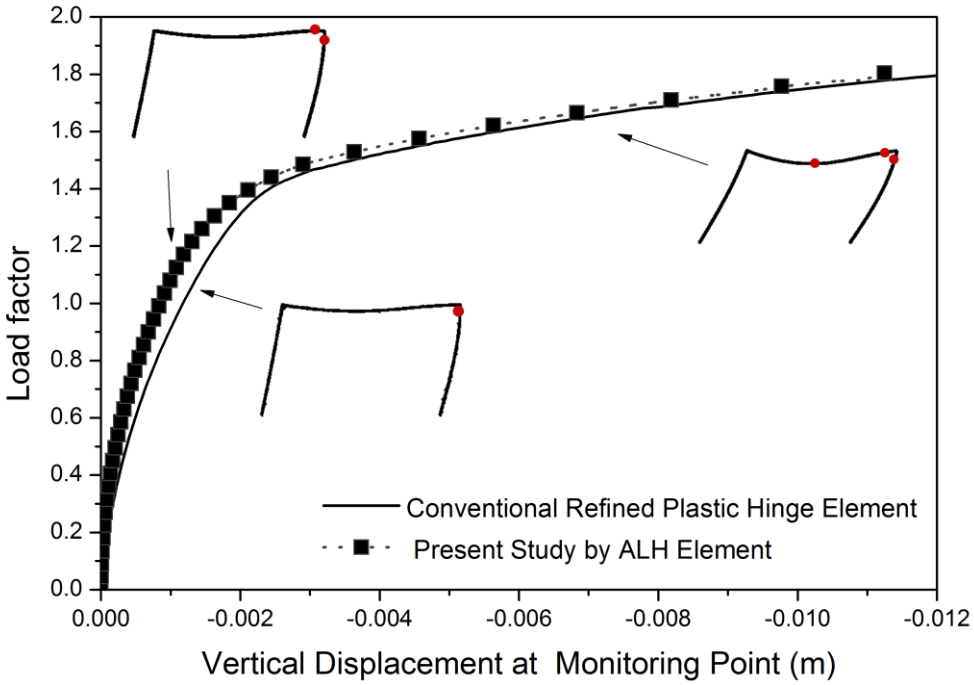

Figure 3.20 Vertical displacement of the portal frame

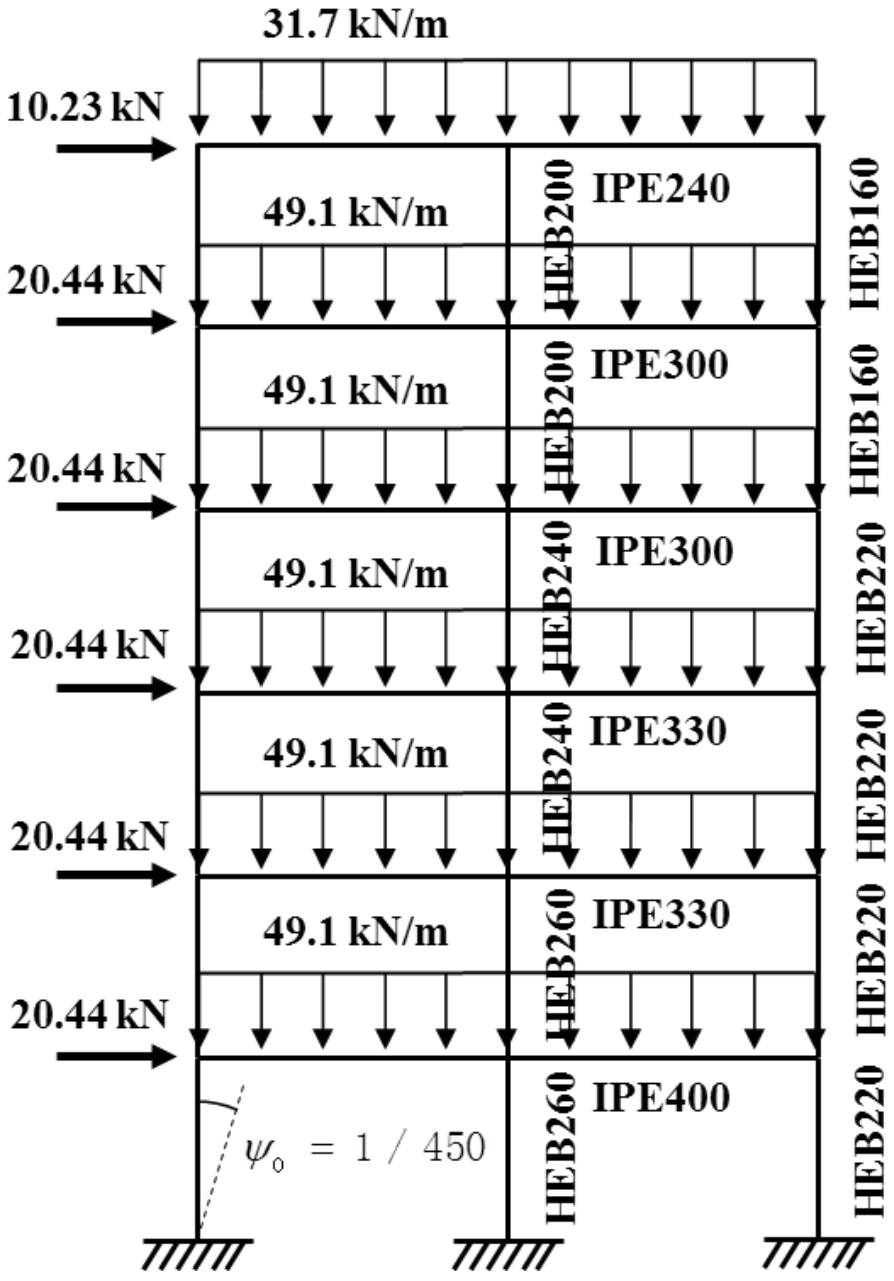

Figure 3.21 Geometry and loading pattern of the Vogel's six story frame

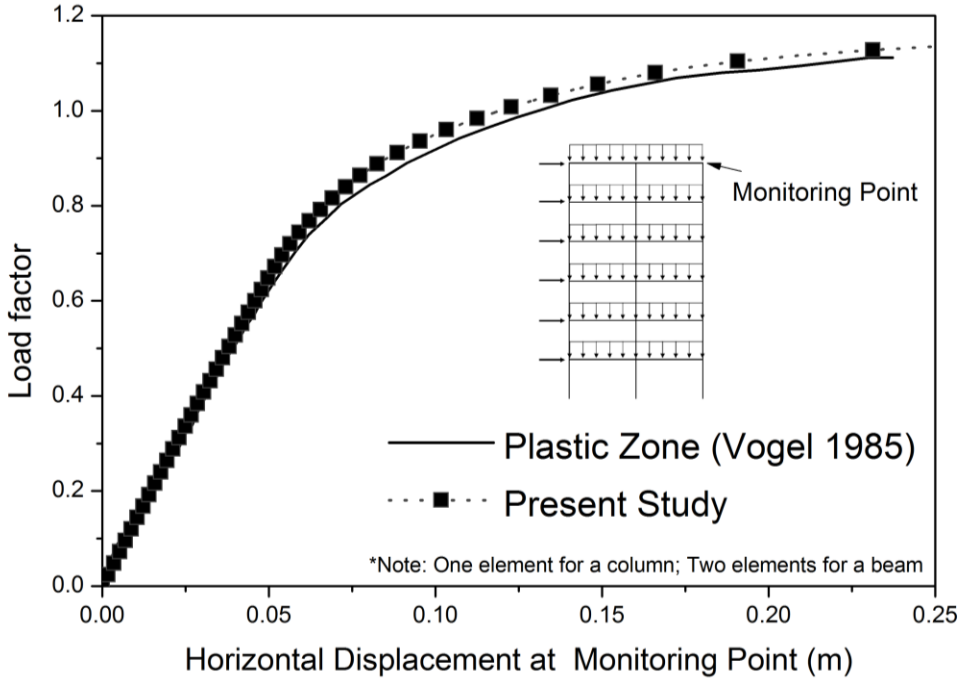

Figure 3.22 Horizontal displacement of the Vogel's six story frame

CHAPTER 4

ADVANCED ANALYSIS AND DESIGN OF THREE-DIMENSIONAL FRAMED STRUCTURES

This chapter extends the applications of the planar curved ALH (Arbitrarily Located Hinge) element as proposed previously to three-dimensional space for large deflections and inelastic analysis of the framed structure. Due to the non-vectorial property of rotations in a space and more degrees of freedom in a space, the three-dimensional analysis is more complex than its planar counterpart. A simplified approach, which assumes a space frame with finite but small rotations, is adopted for extending the planar element to the three-dimensional space. The updated Lagrangian description and the incremental secant stiffness method are introduced for considering large deflections in analysis, which is proven to be accurate and also efficient in the numerical interactive procedure. Since the internal degrees of freedom in the proposed element are condensed, a significant reduction on the size of the global stiffness matrix can be achieved with an apparent improvement in numerical efficiency. The element formulations and the corresponding kinematic descriptions of motion are detailed. Finally, verification examples are given for the validation and the accuracy of the proposed numerical method.

4.1. Introduction

In a planar frame analysis, it assumes the out-of-plane direction of a frame is fully restrained, where the corresponding deformations are perfectly prevented. However, due to the ineffective restraints, three-dimensional geometry of a structure and the existence of the imperfections in the out-of-plane direction, this simplified assumption is usually invalid in the actual practice. In order to propose a practical analysis method and reflect the overall stability a framed structure, the three-dimensional analysis approach must be adopted.

Analysis in three-dimensional space is usually more complex than that in a two-dimensional plane. Due to the non-vectorial property of rotations in the spatial dimension, as illustrated in Figure 4.1, the genuine large deflection analysis cannot be simply extended from a planar analysis. Argyris *et al*. (1978) studied this non-commutative nature of large rotations through an energy consideration, and found that no energy will be generated if two consecutive rotations are applied the y- and z-axes respectively. Therefore, this non-vectorial error can be minimized through a small rotational assumption and it is usually acceptable that if the rotations less than 15 °, this error is small.

For three-dimensional analysis with finite but small rotations, the analytical method can be extended from its counterpart formulations in the planar analysis as presented in the Chapter 3. This simplified approach has been adopted and tested by numerous practices in the past decades and proven to be effective and efficient. For example, Chan *et al*. (1994, 1995) successfully extended the PEP (Pointwise

Equilibrating Polynomial) element formulations from a two-dimensional plane to the three-dimensional space. However, this direct extension from a planar element to a space frame element can induce an underestimation in some coupling effects between the flexural and torsional displacements, as reported by Liew *et al*. (2000a). Nevertheless, in engineering practice, this induced torsional displacement is usually not as significant as the second-order or inelastic effects, which can be also further checked by the codified formulas.

In advanced analysis approach, both the large deflections and the inelastic behaviors of members and the overall frame should be captured. Moreover, the imperfections in local member and the overall structure should be considered. Since there are totally six degrees of freedom, e.g. three translations and three rotations, in each node of the structural model, the required computing expense and the storage for a global stiffness matrix in the three-dimensional space is considerably larger than those in a planar frame analysis. To minimize the numerical effort, the proposed element in the three-dimensional advanced analysis allows only one element to model a structural member such that the computer time can be dramatically reduced, and further, the plasticity along member length can also be considered as well.

In the plastic hinge approach, the inelastic behavior in a certain region along the member is considered to be lumped into a degradable spring, and the spread-of-plasticity cannot be directly considered. This plasticity spread could be considered by the plastic-zone method (S. E. Kim & W. F. Chen, 1996). However, as reported by Kim and Chen (1996), the plastic-zone solution cannot be actually adopted efficiently in daily engineering practice, since the computational time is too

excessive and it is therefore limited to research only. In order to propose a practical approach for advanced analysis, the refined plastic hinge method is adopted. Since three hinges have been already incorporated in the proposed element, the inelastic behavior can be more accurately simulated by using only one element per member.

To consider the large deflection effects of three-dimensional frames and to eliminate the limitation of small or moderately large rotations, the co-rotational formulation associated with the incremental secant stiffness method proposed by Chan (1989) is adopted. In this approach, a set of local axes is attached to an element and rotated simultaneously with the deformations of the element. Thus, the rotations relative to the chord and at the two ends of an element are then evaluated by subtracting the axis rotations. The final total rotations are obtained by a series of rotational transformations rather than by a summation process. Therefore, genius large rotations and deflection can be considered because infinitesimal rotations can be treated as vectorial quantities. Moreover, the incremental secant stiffness method and the updated Lagrangian description are adopted for establishing the equilibrium condition, which have been reported by Chan (1989) to be satisfactory in convergence and numerical stability.

In this chapter, the element formulations for the advanced analysis of the three-dimensional frame are presented. The kinematic description of motion is further discussed in the followings. Finally, several examples are used to illustrate and verify the accuracy and validity of the proposed analytical model.

4.2. Three-dimensional curved element with arbitrarily located hinge

In this section, the ALH element, as proposed in the previous chapter, is adopted and extended to three-dimensional space. A set of local axes parallel to the section principle axes is attached to the individual element as shown in Figure 4.2. The element rotations can be calculated by subtracting the rigid body rotations from the total rotations. Further, the element is usually not placed vertically or horizontally to the global axes, and inclined to a local orientation angle as shown in Figure 4.3. Therefore, the mapping relations between the element forces and displacements are needed. Similar to the planar element presented in the Chapter 3, the internal degrees of freedom (DOFs) in the three-dimensional element will be condensed for numerical efficiency and compatibility to the existing computer program which allows only six degrees of freedom in each node.

4.2.1 Basic force vs. displacement relations

The basic forces versus displacement relations for the three-dimensional element are presented in Figure 4.4. The initial imperfections along two principle axes can be expressed as,

$$\begin{cases} v_{0y}=v_{m0y}\dfrac{(L^2-4x^2)}{L^2} \\ v_{0z}=v_{m0z}\dfrac{(L^2-4x^2)}{L^2} \end{cases} \quad \text{and} \quad -L/2 \le x \le L/2 \qquad (4.1)$$

where v_{0y} and v_{0z} are the shape function of initial member imperfections along y-axis and z-axis respectively; v_{m0y} and v_{m0z} are the amplitude of initial imperfection at mid-span along y-axis and z-axis respectively; L is the length of the member; and x is the distance along the element.

The shape functions for the three-dimensional element can be given as,

$$v_y=\begin{cases}\{N_{11} \quad N_{12} \quad N_{13}\}\cdot\{\theta_{11y} \quad \theta_{12y} \quad \delta_z\}^T & -L/2 \le x \le \xi l \\ \{N_{21} \quad N_{22} \quad N_{23}\}\cdot\{\theta_{21y} \quad \theta_{22y} \quad \delta_z\}^T & \text{and} \quad \xi L \le x \le L/2\end{cases} \tag{4. 2}$$

and,

$$v_z=\begin{cases}\{N_{11} \quad N_{12} \quad N_{13}\}\cdot\{\theta_{11z} \quad \theta_{12z} \quad \delta_y\}^T & -L/2 \le x \le \xi l \\ \{N_{21} \quad N_{22} \quad N_{23}\}\cdot\{\theta_{21z} \quad \theta_{22z} \quad \delta_y\}^T & \text{and} \quad \xi L \le x \le L/2\end{cases} \tag{4. 3}$$

in which, v_y and v_z are the lateral displacement functions along y-axis and z-axis respectively; N_{11}, N_{12}, N_{13}, N_{21}, N_{22} and N_{23} are shape parameters for shape functions given in Chapter 3; θ_{11y}, θ_{11z}, θ_{22y} and θ_{22z} are the external rotations at ends about two principle axes; and δ_y, δ_z, θ_{12y}, θ_{12z}, θ_{21y} and θ_{21z} are the internal lateral deflections and rotations at two principle axes.

The displacement function for axial compression and lengthening can be introduced as,

$$u = e\left(\frac{1}{2}+\frac{x}{L}\right) \tag{4. 4}$$

where e is the deformation along with axial force.

Similarly, the twist angle can be expressed in linear interpolation as,

$$t = \theta_t(\frac{1}{2} + \frac{x}{L}) \tag{4. 5}$$

where θ_t is the twist angle along with torsional moment.

4.2.2 Total potential energy function

The potential strain energy function due to the deflections along two principle axes respectively, neglecting the shear strain, can be written as,

$$U = \frac{1}{2}\int_L EA\dot{u}^2 dx + \frac{1}{2}\int_L EI_y \ddot{v_y}^2 dx + \frac{1}{2}\int_L EI_z \ddot{v_z}^2 dx + \frac{1}{2}\int_L GJ\dot{t}^2 dx$$
$$+\frac{1}{2}\int_L P(\dot{v_y}^2 + 2\dot{v_{0y}}\dot{v_y})dx + \frac{1}{2}\int_L P(\dot{v_z}^2 + 2\dot{v_{0z}}\dot{v_z})dx \tag{4. 6}$$
$$+\int_{\theta_{my}} S_{my} d\theta + \int_{\theta_{mz}} S_{mz} d\theta$$

where, EA is the axial rigidity along x axis; EI_y and EI_z are the flexural rigidities about y- and z- axes respectively; GJ is the torsional rigidity; θ_{my}, θ_{mz}, S_{my} and S_{mz} are the hinge rotations and stiffness at middle hinge at y- and z- axes respectively, can be obtained as,

$$\theta_{my} = \theta_{12y} - \theta_{21y} \tag{4. 7}$$

$$\theta_{mz} = \theta_{12z} - \theta_{21z} \tag{4. 8}$$

$$S_{my} = EI \cdot R_{my} \tag{4. 9}$$

$$S_{mz} = EI \cdot R_{mz} \tag{4. 10}$$

in which, R_{my} and R_{mz} are the plasticity parameters related to the loading state.

The external work done by applied forces and moments can be expressed as,

$$
\begin{aligned}
V &= Pe + M_t\theta_{\mathrm{x}} \\
&+M_{11y}\theta_{11\mathrm{y}} + M_{12y}\theta_{12\mathrm{y}} + \mathrm{F_z}\delta_z + M_{21y}\theta_{21\mathrm{y}} + M_{22y}\theta_{22\mathrm{y}} \\
&+M_{11z}\theta_{11\mathrm{z}} + M_{12z}\theta_{12\mathrm{z}} + \mathrm{F_y}\delta_y + M_{21z}\theta_{21\mathrm{z}} + M_{22z}\theta_{22\mathrm{z}}
\end{aligned} \tag{4. 11}
$$

The total potential energy function Π is given by,

$$\Pi = U - V \tag{4. 12}$$

4.2.3 Bowing effects

The bowing effects due to the lateral displacements can be calculated as,

$$
\begin{aligned}
u_b &= \frac{1}{2}\int_L (\dot{v_y}^2 + 2\dot{v_{0y}}\dot{v_y})\,\mathrm{dx} + \frac{1}{2}\int_L (\dot{v_z}^2 + 2\dot{v_{0z}}\dot{v_z})\,\mathrm{dx} \\
&= \delta_{\mathrm{z}}\left(\frac{4\mathrm{v_{m0y}}}{L} + \frac{\theta_{21\mathrm{y}}}{10} + \frac{\theta_{22\mathrm{y}}}{10}\right) + \delta_{\mathrm{y}}\left(\frac{4\mathrm{v_{m0z}}}{L} + \frac{\theta_{21\mathrm{z}}}{10} + \frac{\theta_{22\mathrm{z}}}{10}\right) \\
&+\theta_{21\mathrm{y}}\left[-\frac{1}{60}L\theta_{22\mathrm{y}}(1-2\xi) + \frac{1}{6}\mathrm{v_{m0y}}(1-2\xi)^2\right] \\
&+\theta_{21\mathrm{z}}\left[-\frac{1}{60}L\theta_{22\mathrm{z}}(1-2\xi) + \frac{1}{6}\mathrm{v_{m0z}}(1-2\xi)^2\right] \\
&+\frac{1}{30}L{\theta_{21\mathrm{y}}}^2(1-2\xi) + \frac{1}{30}L{\theta_{21\mathrm{z}}}^2(1-2\xi) \\
&+\frac{1}{30}L{\theta_{22\mathrm{y}}}^2(1-2\xi) + \frac{1}{30}L{\theta_{22\mathrm{z}}}^2(1-2\xi) \\
&-\frac{1}{6}\mathrm{v_{m0y}}\theta_{22\mathrm{y}}(1-2\xi)^2 - \frac{1}{6}\mathrm{v_{m0z}}\theta_{22\mathrm{z}}(1-2\xi)^2 \\
&+\frac{1}{30}L{\theta_{11\mathrm{y}}}^2(1+2\xi) + \frac{1}{30}L{\theta_{11\mathrm{z}}}^2(1+2\xi) \\
&+\frac{1}{30}L{\theta_{12\mathrm{y}}}^2(1+2\xi) + \frac{1}{30}L{\theta_{12\mathrm{z}}}^2(1+2\xi) + \theta_{12\mathrm{y}}[-\frac{\delta_{\mathrm{z}}}{10} - \frac{1}{6}\mathrm{v_{m0y}}(1+2\xi)^2] \\
&+\theta_{12\mathrm{z}}\left[-\frac{\delta_{\mathrm{y}}}{10} - \frac{1}{6}\mathrm{v_{m0z}}(1+2\xi)^2\right] \\
&+\theta_{11\mathrm{y}}\left[-\frac{\delta_{\mathrm{z}}}{10} - \frac{1}{60}L\theta_{12\mathrm{y}}(1+2\xi) + \frac{1}{6}\mathrm{v_{m0y}}(1+2\xi)^2\right]
\end{aligned} \tag{4. 13}
$$

$$+\theta_{11z}\left[-\frac{\delta_y}{10}-\frac{1}{60}L\theta_{12z}(1+2\xi)+\frac{1}{6}v_{m0z}(1+2\xi)^2\right]$$

$$+\frac{1}{60}{\delta_y}^2\left[-\frac{72}{L(-1+2\xi)}+\frac{72}{L+2L\xi}\right]+\frac{1}{60}{\delta_z}^2\left[-\frac{72}{L(-1+2\xi)}+\frac{72}{L+2L\xi}\right]$$

4.2.4 Secant relations

The equilibrium condition can be obtained by the first variation of the potential energy function according to the minimum potential energy method as,

$$
\begin{aligned}
\mathrm{P} &= \frac{\partial \mathrm{U}}{\partial \mathrm{e}} + \frac{\partial \mathrm{U}}{\partial \mathrm{P}}\frac{\partial \mathrm{P}}{\partial \mathrm{e}} \\
&= \frac{e\mathrm{EA}}{L} + \frac{1}{60}\mathrm{EA}{\theta_{21\mathrm{y}}}^2(2-4\xi) + \frac{1}{60}\mathrm{EA}{\theta_{21\mathrm{z}}}^2(2-4\xi) \\
&+ \frac{1}{60}\mathrm{EA}{\theta_{22\mathrm{y}}}^2(2-4\xi) + \frac{1}{60}\mathrm{EA}{\theta_{22\mathrm{z}}}^2(2-4\xi) \\
&- \frac{\mathrm{EA}\mathrm{v}_{\mathrm{m0y}}\theta_{22\mathrm{y}}(1-2\xi)^2}{6L} - \frac{\mathrm{EA}\mathrm{v}_{\mathrm{m0z}}\theta_{22\mathrm{z}}(1-2\xi)^2}{6L} \\
&+ \frac{1}{60}\mathrm{EA}{\theta_{11\mathrm{y}}}^2(2+4\xi) + \frac{1}{60}\mathrm{EA}{\theta_{11\mathrm{z}}}^2(2+4\xi) \\
&+ \frac{1}{60}\mathrm{EA}{\theta_{12\mathrm{y}}}^2(2+4\xi) + \frac{1}{60}\mathrm{EA}{\theta_{12\mathrm{z}}}^2(2+4\xi) \\
&- \frac{12\mathrm{EA}{\delta_{\mathrm{y}}}^2}{5L^2(-1+4\xi^2)} - \frac{12\mathrm{EA}{\delta_{\mathrm{z}}}^2}{5L^2(-1+4\xi^2)} \\
&+ \theta_{21\mathrm{y}}\left[\frac{\mathrm{EA}\mathrm{v}_{\mathrm{m0y}}(1-2\xi)^2}{6L} + \frac{1}{60}\mathrm{EA}\theta_{22\mathrm{y}}(-1+2\xi)\right] \\
&+ \theta_{21\mathrm{z}}\left[\frac{\mathrm{EA}\mathrm{v}_{\mathrm{m0z}}(1-2\xi)^2}{6L} + \frac{1}{60}\mathrm{EA}\theta_{22\mathrm{z}}(-1+2\xi)\right] \\
&+ \theta_{12\mathrm{y}}\left[-\frac{\mathrm{EA}\delta_{\mathrm{z}}}{10L} - \frac{\mathrm{EA}\mathrm{v}_{\mathrm{m0y}}(1+2\xi)^2}{6L}\right] \\
&+ \theta_{11\mathrm{y}}\left[-\frac{\mathrm{EA}\delta_{\mathrm{z}}}{10L} + \frac{1}{60}\mathrm{EA}\theta_{12\mathrm{y}}(-1-2\xi) + \frac{\mathrm{EA}\mathrm{v}_{\mathrm{m0y}}(1+2\xi)^2}{6L}\right] \\
&+ \theta_{12\mathrm{z}}\left[-\frac{\mathrm{EA}\delta_{\mathrm{y}}}{10L} - \frac{\mathrm{EA}\mathrm{v}_{\mathrm{m0z}}(1+2\xi)^2}{6L}\right] \\
&+ \theta_{11\mathrm{z}}\left[-\frac{\mathrm{EA}\delta_{\mathrm{y}}}{10L} + \frac{1}{60}\mathrm{EA}\theta_{12\mathrm{z}}(-1-2\xi) + \frac{\mathrm{EA}\mathrm{v}_{\mathrm{m0z}}(1+2\xi)^2}{6L}\right] \\
&+ \delta_{\mathrm{z}}\left[\frac{\mathrm{EA}\theta_{21\mathrm{y}}}{10L} + \frac{\mathrm{EA}\theta_{22\mathrm{y}}}{10L} + \frac{1}{60}\mathrm{EA}\mathrm{v}_{\mathrm{m0y}}\left(-\frac{240}{L^2(-1+4\xi^2)} + \frac{960\xi^2}{L^2(-1+4\xi^2)}\right)\right] \\
&+ \delta_{\mathrm{y}}\left[\frac{\mathrm{EA}\theta_{21\mathrm{z}}}{10L} + \frac{\mathrm{EA}\theta_{22\mathrm{z}}}{10L} + \frac{1}{60}\mathrm{EA}\mathrm{v}_{\mathrm{m0z}}\left(-\frac{240}{L^2(-1+4\xi^2)} + \frac{960\xi^2}{L^2(-1+4\xi^2)}\right)\right]
\end{aligned}
\tag{4. 14}
$$

$$
\begin{aligned}
\mathrm{M}_{11\mathrm{y}} &= \frac{\partial \mathrm{U}}{\partial \theta_{11\mathrm{y}}} \\
&= -\frac{P\delta_{\mathrm{z}}}{10} + \frac{1}{15}LP\theta_{11\mathrm{y}}(1+2\xi) - \frac{1}{60}LP\theta_{12\mathrm{y}}(1+2\xi) + \frac{1}{6}P\mathrm{v}_{\mathrm{m0y}}(1+2\xi)^2 \\
&- \frac{24\mathrm{EI}_{\mathrm{y}}\delta_{\mathrm{z}}}{(L+2L\xi)^2} + \frac{8\mathrm{EI}_{\mathrm{y}}L\theta_{11\mathrm{y}}(1+2\xi)}{(L+2L\xi)^2} + \frac{4\mathrm{EI}_{\mathrm{y}}L\theta_{12\mathrm{y}}(1+2\xi)}{(L+2L\xi)^2}
\end{aligned}
\tag{4. 15}
$$

$$M_{11z} = \frac{\partial U}{\partial \theta_{11z}}$$

$$= -\frac{P\delta_y}{10} + \frac{1}{15}LP\theta_{11z}(1+2\xi) - \frac{1}{60}LP\theta_{12z}(1+2\xi) + \frac{1}{6}Pv_{m0z}(1+2\xi)^2 \quad (4.16)$$

$$-\frac{24EI_z\delta_y}{(L+2L\xi)^2} + \frac{8EI_zL\theta_{11z}(1+2\xi)}{(L+2L\xi)^2} + \frac{4EI_zL\theta_{12z}(1+2\xi)}{(L+2L\xi)^2}$$

$$M_{12y} = \frac{\partial U}{\partial \theta_{12y}}$$

$$= -\frac{P\delta_z}{10} - \frac{1}{60}LP\theta_{11y}(1+2\xi) + \frac{1}{15}LP\theta_{12y}(1+2\xi) - \frac{1}{6}Pv_{m0y}(1+2\xi)^2 \quad (4.17)$$

$$-\frac{24EI_y\delta z}{(L+2L\xi)^2} + \frac{4EI_yL\theta_{11y}(1+2\xi)}{(L+2L\xi)^2} + \frac{8EI_yL\theta_{12y}(1+2\xi)}{(L+2L\xi)^2}$$

$$M_{12z} = \frac{\partial U}{\partial \theta_{12z}}$$

$$= -\frac{P\delta_y}{10} - \frac{1}{60}LP\theta_{11z}(1+2\xi) + \frac{1}{15}LP\theta_{12z}(1+2\xi) - \frac{1}{6}Pv_{m0z}(1+2\xi)^2 \quad (4.18)$$

$$-\frac{24EI_z\delta_y}{(L+2L\xi)^2} + \frac{4EI_zL\theta_{11z}(1+2\xi)}{(L+2L\xi)^2} + \frac{8EI_zL\theta_{12z}(1+2\xi)}{(L+2L\xi)^2}$$

$$F_z = \frac{\partial U}{\partial \delta_z}$$

$$= \frac{P\left[-48\delta_z + L\left(\theta_{11y} + \theta_{12y} - \theta_{21y} - \theta_{22y}\right)(1-4\xi^2) + 40v_{m0y}(-1+4\xi^2)\right]}{10L(-1+4\xi^2)} \quad (4.19)$$

$$-\frac{24EI_y\left\{\delta_z(8+96\xi^2) + L(-1+4\xi^2)\left[\theta_{11y}(1-2\xi)^2 + \theta_{12y}(1-2\xi)^2 - \left(\theta_{21y} + \theta_{22y}\right)(1+2\xi)^2\right]\right\}}{L^3(-1+4\xi^2)^3}$$

$$F_y = \frac{\partial U}{\partial \delta_y}$$

$$= \frac{P\left[-48\delta_y + L(\theta_{11z} + \theta_{12z} - \theta_{21z} - \theta_{22z})(1-4\xi^2) + 40v_{m0z}(-1+4\xi^2)\right]}{10L(-1+4\xi^2)} \quad (4.20)$$

$$-\frac{24EI_z\left\{\delta_y(8+96\xi^2) + L(-1+4\xi^2)[\theta_{11z}(1-2\xi)^2 + \theta_{12z}(1-2\xi)^2 - (\theta_{21z} + \theta_{22z})(1+2\xi)^2]\right\}}{L^3(-1+4\xi^2)^3}$$

$$M_{21y} = \frac{\partial U}{\partial \theta_{21y}}$$

$$= \frac{P\delta_z}{10} + \frac{1}{6}Pv_{m0y}(1-2\xi)^2 - \frac{1}{15}LP\theta_{21y}(-1+2\xi) + \frac{1}{60}LP_{\theta 22y}(-1+2\xi) \quad (4.21)$$

$$+\frac{24EI_y\delta_z}{(L-2L\xi)^2} - \frac{8EI_yL\theta_{21y}(-1+2\xi)}{(L-2L\xi)^2} - \frac{4EI_yL\theta_{22y}(-1+2\xi)}{(L-2L\xi)^2}$$

$$M_{21z} = \frac{\partial U}{\partial \theta_{21z}} \quad (4.22)$$

$$= \frac{P\delta_y}{10} + \frac{1}{6}P\mathrm{v}_{m0z}(1-2\xi)^2 - \frac{1}{15}LP\theta_{21z}(-1+2\xi) + \frac{1}{60}LP\theta_{22z}(-1+2\xi)$$
$$+ \frac{24\mathrm{EI}_z\delta_y}{(L-2L\xi)^2} - \frac{8\mathrm{EPI}_zL\theta_{21z}(-1+2\xi)}{(L-2L\xi)^2} - \frac{4\mathrm{EI}_zL\theta_{22z}(-1+2\xi)}{(L-2L\xi)^2}$$

$$\mathrm{M}_{22y} = \frac{\partial \mathrm{U}}{\partial \theta_{22y}}$$
$$= \frac{P\delta_z}{10} - \frac{1}{6}P\mathrm{v}_{m0y}(1-2\xi)^2 + \frac{1}{60}LP\theta_{21y}(-1+2\xi) - \frac{1}{15}LP\theta_{22y}(-1+2\xi) \quad (4.\ 23)$$
$$+ \frac{24\mathrm{EI}_y\delta_z}{(L-2L\xi)^2} - \frac{4\mathrm{EI}_yL\theta_{21y}(-1+2\xi)}{(L-2L\xi)^2} - \frac{8\mathrm{EI}_yL\theta_{22y}(-1+2\xi)}{(L-2L\xi)^2}$$

$$\mathrm{M}_{22z} = \frac{\partial \mathrm{U}}{\partial \theta_{22z}}$$
$$= \frac{P\delta_y}{10} - \frac{1}{6}P\mathrm{v}_{m0z}(1-2\xi)^2 + \frac{1}{60}LP\theta_{21z}(-1+2\xi) - \frac{1}{15}LP\theta_{22z}(-1+2\xi) \quad (4.\ 24)$$
$$+ \frac{24\mathrm{EI}_z\delta_y}{(L-2L\xi)^2} - \frac{4\mathrm{EI}_zL\theta_{21z}(-1+2\xi)}{(L-2L\xi)^2} - \frac{8\mathrm{EI}_zL\theta_{22z}(-1+2\xi)}{(L-2L\xi)^2}$$

The secant relation in torsional direction can be evaluated as,

$$\mathrm{M}_t = \frac{GJ}{L}\theta_x \quad (4.\ 25)$$

in which, M_t is the torsional moment; GJ is the torsional rigidity.

4.2.5 Tangent stiffness matrix

In the incremental-iterative numerical procedure, the tangent stiffness is required to be formulated for the prediction of displacement increment due to an increased load vector. The tangent stiffness matrix can be obtained by the second variation of the total potential energy function and expressed as,

$$\delta^2\Pi = \frac{\partial^2\Pi}{\partial u_i \partial u_j}\delta u_i \delta u_j = [\frac{\partial F_i}{\partial u_j} + \frac{\partial F_i}{\partial P}\frac{\partial P}{\partial u_j}]\delta u_i \delta u_j \quad \text{and} \quad \text{i,j=1 ~ 12} \quad (4.\ 26)$$

where, F_i and u_i are the force and displacement vectors respectively, and expressed as follows,

$$F = \{P \quad M_{11y} \quad M_{11z} \quad M_x \quad M_{12y} \quad M_{12z} \quad F_z \quad F_y \quad M_{21y} \quad M_{21z} \quad M_{22y} \quad M_{22z}\}^T \tag{4. 27}$$

$$u = \{e \quad \theta_{11y} \quad \theta_{11z} \quad \theta_x \quad \theta_{12y} \quad \theta_{12z} \quad \delta_z \quad \delta_y \quad \theta_{21y} \quad \theta_{21z} \quad \theta_{22y} \quad \theta_{22z}\}^T \tag{4. 28}$$

Therefore, the tangent stiffness of the element is determined and can be written in terms of three parts as,

$$[k_e] = [k_L] + [k_G] + [k_S] \tag{4. 29}$$

in which, k_e is the tangent stiffness of the element; k_L is the linear stiffness matrix; k_G is the geometric stiffness matrix; and k_S is the spring stiffness matrix for the internal plastic hinge.

The linear stiffness matrix k_L is given by,

$$[k_L] = \begin{bmatrix} \text{KA1L} & 0 & 0 & 0 & 0 & 0 & 0 & 0 & 0 & 0 & 0 & 0 \\ & \text{KB2L} & 0 & 0 & \text{KB5L} & 0 & \text{KB7L} & 0 & 0 & 0 & 0 & 0 \\ & & \text{KC3L} & 0 & 0 & \text{KC6L} & 0 & \text{KC8L} & 0 & 0 & 0 & 0 \\ & & & \text{KD4L} & 0 & 0 & 0 & 0 & 0 & 0 & 0 & 0 \\ & S & & & \text{KE5L} & 0 & \text{KE7L} & 0 & 0 & 0 & 0 & 0 \\ & & & & & \text{KF6L} & 0 & \text{KF8L} & 0 & 0 & 0 & 0 \\ & & Y & & & & \text{KG7L} & 0 & \text{KG9L} & 0 & \text{KG11L} & 0 \\ & & & & & & & \text{KH8L} & 0 & \text{KH10L} & 0 & \text{KH12L} \\ & & & M & & & & & \text{KI9L} & 0 & \text{KI11L} & 0 \\ & & & & & & & & & \text{KJ10L} & 0 & \text{KJ12L} \\ & & & & & & & & & & \text{KK11L} & 0 \\ & & & & & & & & & & & \text{KL12L} \end{bmatrix} \tag{4. 30}$$

where,

$$\text{KA1L} = \frac{\text{EA}}{L} \tag{4. 31}$$

$$\text{KB2L} = \frac{8\text{EI}_\text{y}}{L + 2L\xi} \tag{4. 32}$$

$$\text{KB5L} = \frac{4\text{EI}_\text{y}}{L + 2L\xi} \tag{4. 33}$$

$$\text{KB7L} = -\frac{24\text{EI}_\text{y}}{(L + 2L\xi)^2} \tag{4. 34}$$

$$\text{KC3L} = \frac{8\text{EI}_\text{z}}{L + 2L\xi} \tag{4. 35}$$

$$\text{KC6L} = \frac{4\text{EI}_\text{z}}{L + 2L\xi} \tag{4. 36}$$

$$KC8L = -\frac{24EI_z}{(L+2L\xi)^2} \quad (4.37)$$

$$KD4L = \frac{GJ}{L} \quad (4.38)$$

$$KE5L = \frac{8EI_y}{L+2L\xi} \quad (4.39)$$

$$KE7L = -\frac{24EI_y}{(L+2L\xi)^2} \quad (4.40)$$

$$KF6L = \frac{8EI_z}{L+2L\xi} \quad (4.41)$$

$$KF8L = -\frac{24EI_z}{(L+2L\xi)^2} \quad (4.42)$$

$$KG7L = -\frac{24EI_y(8+96\xi^2)}{L^3(-1+4\xi^2)^3} \quad (4.43)$$

$$KG9L = \frac{24EI_y}{L^2(1-2\xi)^2} \quad (4.44)$$

$$KG11L = \frac{24EI_y}{L^2(1-2\xi)^2} \quad (4.45)$$

$$KH8L = -\frac{24EI_z(8+96\xi^2)}{L^3(-1+4\xi^2)^3} \quad (4.46)$$

$$KH10L = \frac{24EI_z}{L^2(1-2\xi)^2} \quad (4.47)$$

$$KH12L = \frac{24EI_z}{L^2(1-2\xi)^2} \quad (4.48)$$

$$KI9L = \frac{8EI_y}{L-2L\xi} \quad (4.49)$$

$$KI11L = \frac{4EI_y}{L-2L\xi} \quad (4.50)$$

$$KJ10L = \frac{8EI_z}{L-2L\xi} \quad (4.51)$$

$$KJ12L = \frac{4EI_z}{L-2L\xi} \quad (4.52)$$

$$KK11L = \frac{8EI_y}{L-2L\xi} \quad (4.53)$$

$$KL12L = \frac{8EI_z}{L-2L\xi} \quad (4.54)$$

Similarly, the geometric stiffness matrix can be obtained as,

$$[k_G] = \begin{bmatrix} 0 & \mathrm{KA2G} & \mathrm{KA3G} & 0 & \mathrm{KA5G} & \mathrm{KA6G} & \mathrm{KA7G} & \mathrm{KA8G} & \mathrm{KA9G} & \mathrm{KA10G} & \mathrm{KA11G} & \mathrm{KA12G} \\ & \mathrm{KB2G} & \mathrm{KB3G} & 0 & \mathrm{KB5G} & \mathrm{KB6G} & \mathrm{KB7G} & \mathrm{KB8G} & \mathrm{KB9G} & \mathrm{KB10G} & \mathrm{KB11G} & \mathrm{KB12G} \\ & & \mathrm{KC3G} & 0 & \mathrm{KC5G} & \mathrm{KC6G} & \mathrm{KC7G} & \mathrm{KC8G} & \mathrm{KC9G} & \mathrm{KC10G} & \mathrm{KC11G} & \mathrm{KC12G} \\ & & & 0 & \mathrm{KD5G} & \mathrm{KD6G} & \mathrm{KD7G} & \mathrm{KD8G} & \mathrm{KD9G} & \mathrm{KD10G} & \mathrm{KD11G} & \mathrm{KD12G} \\ & S & & & \mathrm{KE5G} & \mathrm{KE6G} & \mathrm{KE7G} & \mathrm{KE8G} & \mathrm{KE9G} & \mathrm{KE10G} & \mathrm{KE11G} & \mathrm{KE12G} \\ & & & & & \mathrm{KF6G} & \mathrm{KF7G} & \mathrm{KF8G} & \mathrm{KF9G} & \mathrm{KF10G} & \mathrm{KF11G} & \mathrm{KF12G} \\ & & Y & & & & \mathrm{KG7G} & \mathrm{KG8G} & \mathrm{KG9G} & \mathrm{KG10G} & \mathrm{KG11G} & \mathrm{KG12G} \\ & & & & & & & \mathrm{KH8G} & \mathrm{KH9G} & \mathrm{KH10G} & \mathrm{KH11G} & \mathrm{KH12G} \\ & & & M & & & & & \mathrm{KI9G} & \mathrm{KI10G} & \mathrm{KI11G} & \mathrm{KI12G} \\ & & & & & & & & & \mathrm{KJ10G} & \mathrm{KJ11G} & \mathrm{KJ12G} \\ & & & & & & & & & & \mathrm{KK11G} & \mathrm{KK12G} \\ & & & & & & & & & & & \mathrm{KL12G} \end{bmatrix} \tag{4. 55}$$

in which,

$$\mathrm{KA2G} = \frac{\mathrm{EA}(-6\delta_{\mathrm{z}} + L(4\theta_{11\mathrm{y}} - \theta_{12\mathrm{y}})(1+2\xi) + 10\mathrm{v}_{\mathrm{m0y}}(1+2\xi)^2)}{60L} \tag{4. 56}$$

$$\mathrm{KA3G} = \frac{\mathrm{EA}(-6\delta_{\mathrm{y}} + L(4\theta_{11\mathrm{z}} - \theta_{12\mathrm{z}})(1+2\xi) + 10\mathrm{v}_{\mathrm{m0z}}(1+2\xi)^2)}{60L} \tag{4. 57}$$

$$\mathrm{KA5G} = -\frac{\mathrm{EA}(6\delta_{\mathrm{z}} + L(\theta_{11\mathrm{y}} - 4\theta_{12\mathrm{y}})(1+2\xi) + 10\mathrm{v}_{\mathrm{m0y}}(1+2\xi)^2)}{60L} \tag{4. 58}$$

$$\mathrm{KA6G} = -\frac{\mathrm{EA}(6\delta_{\mathrm{y}} + L(\theta_{11\mathrm{z}} - 4\theta_{12\mathrm{z}})(1+2\xi) + 10\mathrm{v}_{\mathrm{m0z}}(1+2\xi)^2)}{60L} \tag{4. 59}$$

$$\mathrm{KA7G} = \frac{\mathrm{EA}\left(-48\delta_{\mathrm{z}} + L\left(\theta_{11\mathrm{y}} + \theta_{12\mathrm{y}} - \theta_{21\mathrm{y}} - \theta_{22\mathrm{y}}\right)(1-4\xi^2) + 40\mathrm{v}_{\mathrm{m0y}}(-1+4\xi^2)\right)}{10L^2(-1+4\xi^2)} \tag{4. 60}$$

$$\mathrm{KA8G} = \frac{\mathrm{EA}\left(-48\delta_{\mathrm{y}} + L(\theta_{11\mathrm{z}} + \theta_{12\mathrm{z}} - \theta_{21\mathrm{z}} - \theta_{22\mathrm{z}})(1-4\xi^2) + 40\mathrm{v}_{\mathrm{m0z}}(-1+4\xi^2)\right)}{10L^2(-1+4\xi^2)} \tag{4. 61}$$

$$\mathrm{KA9G} = \frac{\mathrm{EA}\left(6\delta_{\mathrm{z}} + 10\mathrm{v}_{\mathrm{m0y}}(1-2\xi)^2 - L\left(4\theta_{21\mathrm{y}} - \theta_{22\mathrm{y}}\right)(-1+2\xi)\right)}{60L} \tag{4. 62}$$

$$\mathrm{KA10G} = \frac{\mathrm{EA}\left(6\delta_{\mathrm{y}} + 10\mathrm{v}_{\mathrm{m0z}}(1-2\xi)^2 - L(4\theta_{21\mathrm{z}} - \theta_{22\mathrm{z}})(-1+2\xi)\right)}{60L} \tag{4. 63}$$

$$\mathrm{KA11G} = \frac{\mathrm{EA}\left(6\delta_{\mathrm{z}} - 10\mathrm{v}_{\mathrm{m0y}}(1-2\xi)^2 + L\left(\theta_{21\mathrm{y}} - 4\theta_{22\mathrm{y}}\right)(-1+2\xi)\right)}{60L} \tag{4. 64}$$

$$\mathrm{KA12G} = \frac{\mathrm{EA}\left(6\delta_{\mathrm{y}} - 10\mathrm{v}_{\mathrm{m0z}}(1-2\xi)^2 + L(\theta_{21\mathrm{z}} - 4\theta_{22\mathrm{z}})(-1+2\xi)\right)}{60L} \tag{4. 65}$$

$$\mathrm{KB2G} = \frac{1}{15}LP(1+2\xi) + \frac{\mathrm{EA}\left(-6\delta_{\mathrm{z}} + L\left(4\theta_{11\mathrm{y}} - \theta_{12\mathrm{y}}\right)(1+2\xi) + 10\mathrm{v}_{\mathrm{m0y}}(1+2\xi)^2\right)^2}{3600L} \tag{4. 66}$$

KB3G

$$= \frac{\mathrm{EA}\left(-6\delta_z + L\left(4\theta_{11y} - \theta_{12y}\right)(1+2\xi) + 10\mathrm{v}_{m0y}(1+2\xi)^2\right)\left(-6\delta_y + L(4\theta_{11z} - \theta_{12z})(1+2\xi) + 10\mathrm{v}_{m0z}(1+2\xi)^2\right)}{3600L} \tag{4. 67}$$

$$\mathrm{KB5G} = -\frac{1}{60}LP(1+2\xi) - \frac{\mathrm{EA}\left(6\delta_z + L\left(\theta_{11y} - 4\theta_{12y}\right)(1+2\xi) + 10\mathrm{v}_{m0y}(1+2\xi)^2\right)\left(-6\delta_z + L\left(4\theta_{11y} - \theta_{12y}\right)(1+2\xi) + 10\mathrm{v}_{m0y}(1+2\xi)^2\right)}{3600L} \tag{4. 68}$$

KB6G

$$= -\frac{\mathrm{EA}\left(-6\delta_z + L\left(4\theta_{11y} - \theta_{12y}\right)(1+2\xi) + 10\mathrm{v}_{m0y}(1+2\xi)^2\right)\left(6\delta_y + L(\theta_{11z} - 4\theta_{12z})(1+2\xi) + 10\mathrm{v}_{m0z}(1+2\xi)^2\right)}{3600L} \tag{4. 69}$$

$$\mathrm{KB7G} = \frac{1}{600}\left(-60P + \frac{\mathrm{EA}\left(-6\delta_z + L\left(4\theta_{11y} - \theta_{12y}\right)(1+2\xi) + 10\mathrm{v}_{m0y}(1+2\xi)^2\right)\left(-48\delta_z + L\left(\theta_{11y} + \theta_{12y} - \theta_{21y} - \theta_{22y}\right)(1-4\xi^2) + 40\mathrm{v}_{m0y}(-1+4\xi^2)\right)}{L^2(-1+4\xi^2)}\right) \tag{4. 70}$$

$$\mathrm{KB8G} = \frac{\mathrm{EA}\left(-6\delta_z + L\left(4\theta_{11y} - \theta_{12y}\right)(1+2\xi) + 10\mathrm{v}_{m0y}(1+2\xi)^2\right)\left(-48\delta_y + L(\theta_{11z} + \theta_{12z} - \theta_{21z} - \theta_{22z})(1-4\xi^2) + 40\mathrm{v}_{m0z}(-1+4\xi^2)\right)}{600L^2(-1+4\xi^2)} \tag{4. 71}$$

$$\mathrm{KB9G} = \frac{\mathrm{EA}\left(6\delta_z + 10\mathrm{v}_{m0y}(1-2\xi)^2 - L\left(4\theta_{21y} - \theta_{22y}\right)(-1+2\xi)\right)\left(-6\delta_z + L\left(4\theta_{11y} - \theta_{12y}\right)(1+2\xi) + 10\mathrm{v}_{m0y}(1+2\xi)^2\right)}{3600L} \tag{4. 72}$$

$$\mathrm{KB10G} = \frac{\mathrm{EA}\left(6\delta_y + 10\mathrm{v}_{m0z}(1-2\xi)^2 - L(4\theta_{21z} - \theta_{22z})(-1+2\xi)\right)\left(-6\delta_z + L\left(4\theta_{11y} - \theta_{12y}\right)(1+2\xi) + 10\mathrm{v}_{m0y}(1+2\xi)^2\right)}{3600L} \tag{4. 73}$$

$$\mathrm{KB11G} = \frac{\mathrm{EA}\left(6\delta_z - 10\mathrm{v_{m0y}}(1-2\xi)^2 + L\left(\theta_{21y} - 4\theta_{22y}\right)(-1+2\xi)\right)\left(-6\delta_z + L\left(4\theta_{11y} - \theta_{12y}\right)(1+2\xi) + 10\mathrm{v_{m0y}}(1+2\xi)^2\right)}{3600L} \tag{4. 74}$$

$$\mathrm{KB12G} = \frac{\mathrm{EA}\left(6\delta_y - 10\mathrm{v_{m0z}}(1-2\xi)^2 + L(\theta_{21z} - 4\theta_{22z})(-1+2\xi)\right)\left(-6\delta_z + L\left(4\theta_{11y} - \theta_{12y}\right)(1+2\xi) + 10\mathrm{v_{m0y}}(1+2\xi)^2\right)}{3600L} \tag{4. 75}$$

$$\mathrm{KC3G} = \frac{1}{15}LP(1+2\xi) + \frac{\mathrm{EA}\left(-6\delta_y + L(4\theta_{11z} - \theta_{12z})(1+2\xi) + 10\mathrm{v_{m0z}}(1+2\xi)^2\right)^2}{3600L} \tag{4. 76}$$

$$\mathrm{KC5G} = -\frac{\mathrm{EA}\left(6\delta_z + L\left(\theta_{11y} - 4\theta_{12y}\right)(1+2\xi) + 10\mathrm{v_{m0y}}(1+2\xi)^2\right)\left(-6\delta_y + L(4\theta_{11z} - \theta_{12z})(1+2\xi) + 10\mathrm{v_{m0z}}(1+2\xi)^2\right)}{3600L} \tag{4. 77}$$

$$\mathrm{KC6G} = -\frac{1}{60}LP(1+2\xi) - \frac{\mathrm{EA}\left(6\delta_y + L(\theta_{11z} - 4\theta_{12z})(1+2\xi) + 10\mathrm{v_{m0z}}(1+2\xi)^2\right)\left(-6\delta_y + L(4\theta_{11z} - \theta_{12z})(1+2\xi) + 10\mathrm{v_{m0z}}(1+2\xi)^2\right)}{3600L} \tag{4. 78}$$

$$\mathrm{KC7G} = \frac{\mathrm{EA}\left(-6\delta_y + L(4\theta_{11z} - \theta_{12z})(1+2\xi) + 10\mathrm{v_{m0z}}(1+2\xi)^2\right)\left(-48\delta_z + L\left(\theta_{11y} + \theta_{12y} - \theta_{21y} - \theta_{22y}\right)(1-4\xi^2) + 40\mathrm{v_{m0y}}(-1+4\xi^2)\right)}{600L^2(-1+4\xi^2)} \tag{4. 79}$$

$$\mathrm{KC8G} = \frac{1}{600}\left(-60P + \frac{\mathrm{EA}\left(-6\delta_y + L(4\theta_{11z} - \theta_{12z})(1+2\xi) + 10\mathrm{v_{m0z}}(1+2\xi)^2\right)\left(-48\delta_y + L(\theta_{11z} + \theta_{12z} - \theta_{21z} - \theta_{22z})(1-4\xi^2) + 40\mathrm{v_{m0z}}(-1+4\xi^2)\right)}{L^2(-1+4\xi^2)}\right) \tag{4. 80}$$

$$\mathrm{KC9G} = \frac{\mathrm{EA}\left(6\delta_z + 10\mathrm{v_{m0y}}(1-2\xi)^2 - L\left(4\theta_{21y} - \theta_{22y}\right)(-1+2\xi)\right)\left(-6\delta_y + L(4\theta_{11z} - \theta_{12z})(1+2\xi) + 10\mathrm{v_{m0z}}(1+2\xi)^2\right)}{3600L} \tag{4. 81}$$

$$\mathrm{KC10G} = \frac{\mathrm{EA}\left(6\delta_y + 10\mathrm{v_{m0z}}(1-2\xi)^2 - L(4\theta_{21z} - \theta_{22z})(-1+2\xi)\right)\left(-6\delta_y + L(4\theta_{11z} - \theta_{12z})(1+2\xi) + 10\mathrm{v_{m0z}}(1+2\xi)^2\right)}{3600L} \tag{4. 82}$$

$$\mathrm{KC11G}=\frac{\mathrm{EA}\left(6\delta_{\mathrm{z}}-10\mathrm{v}_{\mathrm{m0y}}(1-2\xi)^2+L\left(\theta_{21\mathrm{y}}-4\theta_{22\mathrm{y}}\right)(-1+2\xi)\right)\left(-6\delta_{\mathrm{y}}+L(4\theta_{11\mathrm{z}}-\theta_{12\mathrm{z}})(1+2\xi)+10\mathrm{v}_{\mathrm{m0z}}(1+2\xi)^2\right)}{3600L} \tag{4. 83}$$

$$\mathrm{KC12G}=\frac{\mathrm{EA}\left(6\delta_{\mathrm{y}}-10\mathrm{v}_{\mathrm{m0z}}(1-2\xi)^2+L(\theta_{21\mathrm{z}}-4\theta_{22\mathrm{z}})(-1+2\xi)\right)\left(-6\delta_{\mathrm{y}}+L(4\theta_{11\mathrm{z}}-\theta_{12\mathrm{z}})(1+2\xi)+10\mathrm{v}_{\mathrm{m0z}}(1+2\xi)^2\right)}{3600L} \tag{4. 84}$$

$$\mathrm{KE5G}=\frac{1}{15}LP(1+2\xi)+\frac{\mathrm{EA}\left(6\delta_{\mathrm{z}}+L\left(\theta_{11\mathrm{y}}-4\theta_{12\mathrm{y}}\right)(1+2\xi)+10\mathrm{v}_{\mathrm{m0y}}(1+2\xi)^2\right)^2}{3600L} \tag{4. 85}$$

$$\mathrm{KE6G}=\frac{\mathrm{EA}\left(6\delta_{\mathrm{z}}+L\left(\theta_{11\mathrm{y}}-4\theta_{12\mathrm{y}}\right)(1+2\xi)+10\mathrm{v}_{\mathrm{m0y}}(1+2\xi)^2\right)\left(6\delta_{\mathrm{y}}+L(\theta_{11\mathrm{z}}-4\theta_{12\mathrm{z}})(1+2\xi)+10\mathrm{v}_{\mathrm{m0z}}(1+2\xi)^2\right)}{3600L} \tag{4. 86}$$

$$\mathrm{KE7G}=\frac{1}{600}\left(-60P+\frac{\mathrm{EA}\left(6\delta_{\mathrm{z}}+L\left(\theta_{11\mathrm{y}}-4\theta_{12\mathrm{y}}\right)(1+2\xi)+10\mathrm{v}_{\mathrm{m0y}}(1+2\xi)^2\right)\left(48\delta_{\mathrm{z}}+40\mathrm{v}_{\mathrm{m0y}}(1-4\xi^2)+L\left(\theta_{11\mathrm{y}}+\theta_{12\mathrm{y}}-\theta_{21\mathrm{y}}-\theta_{22\mathrm{y}}\right)(-1+4\xi^2)\right)}{L^2(-1+4\xi^2)}\right) \tag{4. 87}$$

$$\mathrm{KE8G}=\frac{\mathrm{EA}\left(6\delta_{\mathrm{z}}+L\left(\theta_{11\mathrm{y}}-4\theta_{12\mathrm{y}}\right)(1+2\xi)+10\mathrm{v}_{\mathrm{m0y}}(1+2\xi)^2\right)\left(48\delta_{\mathrm{y}}+40\mathrm{v}_{\mathrm{m0z}}(1-4\xi^2)+L(\theta_{11\mathrm{z}}+\theta_{12\mathrm{z}}-\theta_{21\mathrm{z}}-\theta_{22\mathrm{z}})(-1+4\xi^2)\right)}{600L^2(-1+4\xi^2)} \tag{4. 88}$$

$$\mathrm{KE9G}=\frac{\mathrm{EA}\left(-6\delta_{\mathrm{z}}-10\mathrm{v}_{\mathrm{m0y}}(1-2\xi)^2+L\left(4\theta_{21\mathrm{y}}-\theta_{22\mathrm{y}}\right)(-1+2\xi)\right)\left(6\delta_{\mathrm{z}}+L\left(\theta_{11\mathrm{y}}-4\theta_{12\mathrm{y}}\right)(1+2\xi)+10\mathrm{v}_{\mathrm{m0y}}(1+2\xi)^2\right)}{3600L} \tag{4. 89}$$

$$\mathrm{KE10G}=\frac{\mathrm{EA}\left(-6\delta_{\mathrm{y}}-10\mathrm{v}_{\mathrm{m0z}}(1-2\xi)^2+L(4\theta_{21\mathrm{z}}-\theta_{22\mathrm{z}})(-1+2\xi)\right)\left(6\delta_{\mathrm{z}}+L\left(\theta_{11\mathrm{y}}-4\theta_{12\mathrm{y}}\right)(1+2\xi)+10\mathrm{v}_{\mathrm{m0y}}(1+2\xi)^2\right)}{3600L} \tag{4. 90}$$

$$\mathrm{KE11G}=\frac{\mathrm{EA}\left(-6\delta_{\mathrm{z}}+10\mathrm{v}_{\mathrm{m0y}}(1-2\xi)^2-L\left(\theta_{21\mathrm{y}}-4\theta_{22\mathrm{y}}\right)(-1+2\xi)\right)\left(6\delta_{\mathrm{z}}+L\left(\theta_{11\mathrm{y}}-4\theta_{12\mathrm{y}}\right)(1+2\xi)+10\mathrm{v}_{\mathrm{m0y}}(1+2\xi)^2\right)}{3600L} \tag{4. 91}$$

$$\mathrm{KE12G} = -\frac{\mathrm{EA}\left(6\delta_{\mathrm{y}} - 10\mathrm{v}_{\mathrm{m0z}}(1-2\xi)^2 + L(\theta_{21\mathrm{z}} - 4\theta_{22\mathrm{z}})(-1+2\xi)\right)\left(6\delta_{\mathrm{z}} + L\left(\theta_{11\mathrm{y}} - 4\theta_{12\mathrm{y}}\right)(1+2\xi) + 10\mathrm{v}_{\mathrm{m0y}}(1+2\xi)^2\right)}{3600L} \tag{4. 92}$$

$$\mathrm{KF6G} = \frac{1}{15}LP(1+2\xi) + \frac{\mathrm{EA}\left(6\delta_{\mathrm{y}} + L(\theta_{11\mathrm{z}} - 4\theta_{12\mathrm{z}})(1+2\xi) + 10\mathrm{v}_{\mathrm{m0z}}(1+2\xi)^2\right)^2}{3600L} \tag{4. 93}$$

$$\mathrm{KF7G} = \frac{\mathrm{EA}\left(6\delta_{\mathrm{y}} + L(\theta_{11\mathrm{z}} - 4\theta_{12\mathrm{z}})(1+2\xi) + 10\mathrm{v}_{\mathrm{m0z}}(1+2\xi)^2\right)\left(48\delta_{\mathrm{z}} + 40\mathrm{v}_{\mathrm{m0y}}(1-4\xi^2) + L\left(\theta_{11\mathrm{y}} + \theta_{12\mathrm{y}} - \theta_{21\mathrm{y}} - \theta_{22\mathrm{y}}\right)(-1+4\xi^2)\right)}{600L^2(-1+4\xi^2)} \tag{4. 94}$$

$$\mathrm{KF8G} = \frac{1}{600}\left(-60P + \frac{\mathrm{EA}\left(6\delta_{\mathrm{y}} + L(\theta_{11\mathrm{z}} - 4\theta_{12\mathrm{z}})(1+2\xi) + 10\mathrm{v}_{\mathrm{m0z}}(1+2\xi)^2\right)\left(48\delta_{\mathrm{y}} + 40\mathrm{v}_{\mathrm{m0z}}(1-4\xi^2) + L(\theta_{11\mathrm{z}} + \theta_{12\mathrm{z}} - \theta_{21\mathrm{z}} - \theta_{22\mathrm{z}})(-1+4\xi^2)\right)}{L^2(-1+4\xi^2)}\right) \tag{4. 95}$$

$$\mathrm{KF9G} = \frac{\mathrm{EA}\left(-6\delta_{\mathrm{z}} - 10\mathrm{v}_{\mathrm{m0y}}(1-2\xi)^2 + L\left(4\theta_{21\mathrm{y}} - \theta_{22\mathrm{y}}\right)(-1+2\xi)\right)\left(6\delta_{\mathrm{y}} + L(\theta_{11\mathrm{z}} - 4\theta_{12\mathrm{z}})(1+2\xi) + 10\mathrm{v}_{\mathrm{m0z}}(1+2\xi)^2\right)}{3600L} \tag{4. 96}$$

$$\mathrm{KF10G} = \frac{\mathrm{EA}\left(-6_{\delta\mathrm{y}} - 10\mathrm{v}_{\mathrm{m0z}}(1-2\xi)^2 + L(4\theta_{21\mathrm{z}} - \theta_{22\mathrm{z}})(-1+2\xi)\right)\left(6\delta_{\mathrm{y}} + L(\theta_{11\mathrm{z}} - 4\theta_{12\mathrm{z}})(1+2\xi) + 10\mathrm{v}_{\mathrm{m0z}}(1+2\xi)^2\right)}{3600L} \tag{4. 97}$$

$$\mathrm{KF11G} = \frac{\mathrm{EA}\left(-6\delta_{\mathrm{z}} + 10\mathrm{v}_{\mathrm{m0y}}(1-2\xi)^2 - L\left(\theta_{21\mathrm{y}} - 4\theta_{22\mathrm{y}}\right)(-1+2\xi)\right)\left(6\delta_{\mathrm{y}} + L(\theta_{11\mathrm{z}} - 4\theta_{12\mathrm{z}})(1+2\xi) + 10\mathrm{v}_{\mathrm{m0z}}(1+2\xi)^2\right)}{3600L} \tag{4. 98}$$

$$\mathrm{KF12G} = \frac{\mathrm{EA}\left(-6\delta_{\mathrm{y}} + 10\mathrm{v}_{\mathrm{m0z}}(1-2\xi)^2 - L(\theta_{21\mathrm{z}} - 4\theta_{22\mathrm{z}})(-1+2\xi)\right)\left(6\delta_{\mathrm{y}} + L(\theta_{11\mathrm{z}} - 4\theta_{12\mathrm{z}})(1+2\xi) + 10\mathrm{v}_{\mathrm{m0z}}(1+2\xi)^2\right)}{3600L} \tag{4. 99}$$

$$\mathrm{KG7G} = \frac{-48P + \frac{\mathrm{EA}\left(48\delta_{\mathrm{z}} + 40\mathrm{v}_{\mathrm{m0y}}(1-4\xi^2) + L\left(\theta_{11\mathrm{y}} + \theta_{12\mathrm{y}} - \theta_{21\mathrm{y}} - \theta_{22\mathrm{y}}\right)(-1+4\xi^2)\right)^2}{10L^2(-1+4\xi^2)}}{10L(-1+4\xi^2)} \tag{4. 100}$$

$$\mathrm{KG8G} = \frac{\mathrm{EA}\left(48\delta_{\mathrm{z}} + 40\mathrm{v}_{\mathrm{m0y}}(1-4\xi^2) + L\left(\theta_{11\mathrm{y}} + \theta_{12\mathrm{y}} - \theta_{21\mathrm{y}} - \theta_{22\mathrm{y}}\right)(-1+4\xi^2)\right)\left(48\delta_{\mathrm{y}} + 40\mathrm{v}_{\mathrm{m0z}}(1-4\xi^2) + L(\theta_{11\mathrm{z}} + \theta_{12\mathrm{z}} - \theta_{21\mathrm{z}} - \theta_{22\mathrm{z}})(-1+4\xi^2)\right)}{100L^3(1-4\xi^2)^2} \tag{4. 101}$$

$$\mathrm{KG9G} = \frac{P(-1+4\xi^2) + \frac{\mathrm{EA}(6\delta\_\mathrm{z} + 10\mathrm{v\_m0y}(1-2\xi)^2 - L(4\theta\_21\mathrm{y} - \theta\_22\mathrm{y})(-1+2\xi))(-48\delta\_\mathrm{z} + L(\theta\_11\mathrm{y} + \theta\_12\mathrm{y} - \theta\_21\mathrm{y} - \theta\_22\mathrm{y})(1-4\xi^2) + 40\mathrm{vm0y}(-1+4\xi^2))}{60L^2}}{10(-1+4\xi^2)} \tag{4. 102}$$

$$\mathrm{KG10G} = \frac{\mathrm{EA}(-6\delta\mathrm{y} - 10\mathrm{vm0z}(1-2\xi)^2 + L(4\theta21\mathrm{z} - \theta22\mathrm{z})(-1+2\xi))(48\delta\mathrm{z} + 40\mathrm{vm0y}(1-4\xi^2) + L(\theta11\mathrm{y} + \theta12\mathrm{y} - \theta21\mathrm{y} - \theta22\mathrm{y})(-1+4\xi^2))}{600L^2(-1+4\xi^2)} \tag{4. 103}$$

$$\mathrm{KG11G} = \frac{P(-1+4\xi^2) + \frac{\mathrm{EA}\left(6\delta\mathrm{z} - 10\mathrm{v}_{\mathrm{m0y}}(1-2\xi)^2 + L(\theta21\mathrm{y} - 4\theta22\mathrm{y})(-1+2\xi)\right)\left(-48\delta\mathrm{z} + L(\theta11\mathrm{y} + \theta12\mathrm{y} - \theta21\mathrm{y} - \theta22\mathrm{y})(1-4\xi^2) + 40\mathrm{v}_{\mathrm{m0y}}(-1+4\xi^2)\right)}{60L^2}}{10(-1+4\xi^2)} \tag{4. 104}$$

$$\mathrm{KG12G} = \frac{\mathrm{EA}\left(-6\delta_{\mathrm{y}} + 10\mathrm{v}_{\mathrm{m0z}}(1-2\xi)^2 - L(\theta_{21\mathrm{z}} - 4\theta_{22\mathrm{z}})(-1+2\xi)\right)\left(48\delta_{\mathrm{z}} + 40\mathrm{v}_{\mathrm{m0y}}(1-4\xi^2) + L\left(\theta_{11\mathrm{y}} + \theta_{12\mathrm{y}} - \theta_{21\mathrm{y}} - \theta_{22\mathrm{y}}\right)(-1+4\xi^2)\right)}{600L^2(-1+4\xi^2)} \tag{4. 105}$$

$$\mathrm{KH8G} = \frac{-48P + \frac{\mathrm{EA}\left(48\delta_{\mathrm{y}} + 40\mathrm{v}_{\mathrm{m0z}}(1-4\xi^2) + L(\theta_{11\mathrm{z}} + \theta_{12\mathrm{z}} - \theta_{21\mathrm{z}} - \theta_{22\mathrm{z}})(-1+4\xi^2)\right)^2}{10L^2(-1+4\xi^2)}}{10L(-1+4\xi^2)} \tag{4. 106}$$

$$\mathrm{KH9G} = \frac{\mathrm{EA}\left(-6\delta_{\mathrm{z}} - 10\mathrm{v}_{\mathrm{m0y}}(1-2\xi)^2 + L\left(4\theta_{21\mathrm{y}} - \theta_{22\mathrm{y}}\right)(-1+2\xi)\right)\left(48\delta_{\mathrm{y}} + 40\mathrm{v}_{\mathrm{m0z}}(1-4\xi^2) + L(\theta_{11\mathrm{z}} + \theta_{12\mathrm{z}} - \theta_{21\mathrm{z}} - \theta_{22\mathrm{z}})(-1+4\xi^2)\right)}{600L^2(-1+4\xi^2)} \tag{4. 107}$$

$$\mathrm{KH10G}=\frac{P(-1+4\xi^2)+\frac{\mathrm{EA}\left(6\delta_{\mathrm{y}}+10\mathrm{v}_{\mathrm{m0z}}(1-2\xi)^2-L(4\theta_{21\mathrm{z}}-\theta_{22\mathrm{z}})(-1+2\xi)\right)\left(-48\delta_{\mathrm{y}}+L(\theta_{11\mathrm{z}}+\theta_{12\mathrm{z}}-\theta_{21\mathrm{z}}-\theta_{22\mathrm{z}})(1-4\xi^2)+40\mathrm{v}_{\mathrm{m0z}}(-1+4\xi^2)\right)}{60L^2}}{10(-1+4\xi^2)} \tag{4.108}$$

$$\mathrm{KH11G}=\frac{\mathrm{EA}\left(-6\delta_{\mathrm{z}}+10\mathrm{v}_{\mathrm{m0y}}(1-2\xi)^2-L\left(\theta_{21\mathrm{y}}-4\theta_{22\mathrm{y}}\right)(-1+2\xi)\right)\left(48\delta_{\mathrm{y}}+40\mathrm{v}_{\mathrm{m0z}}(1-4\xi^2)+L(\theta_{11\mathrm{z}}+\theta_{12\mathrm{z}}-\theta_{21\mathrm{z}}-\theta_{22\mathrm{z}})(-1+4\xi^2)\right)}{600L^2(-1+4\xi^2)} \tag{4.109}$$

$$\mathrm{KH12G}=\frac{P(-1+4\xi^2)+\frac{\mathrm{EA}\left(6\delta_{\mathrm{y}}-10\mathrm{v}_{\mathrm{m0z}}(1-2\xi)^2+L(\theta_{21\mathrm{z}}-4\theta_{22\mathrm{z}})(-1+2\xi)\right)\left(-48\delta_{\mathrm{y}}+40\mathrm{v}_{\mathrm{m0z}}(-1+4\xi^2)-L(\theta_{11\mathrm{z}}+\theta_{12\mathrm{z}}-\theta_{21\mathrm{z}}-\theta_{22\mathrm{z}})(-1+4\xi^2)\right)}{60L^2}}{10(-1+4\xi^2)} \tag{4.110}$$

$$\mathrm{KI9G}=\frac{1}{15}LP(1-2\xi)+\frac{\mathrm{EA}\left(6\delta_{\mathrm{z}}+10\mathrm{v}_{\mathrm{m0y}}(1-2\xi)^2-L\left(4\theta_{21\mathrm{y}}-\theta_{22\mathrm{y}}\right)(-1+2\xi)\right)^2}{3600L} \tag{4.111}$$

$$\mathrm{KI10G}=\frac{\mathrm{EA}\left(-6\delta_{\mathrm{z}}-10\mathrm{v}_{\mathrm{m0y}}(1-2\xi)^2+L\left(4\theta_{21\mathrm{y}}-\theta_{22\mathrm{y}}\right)(-1+2\xi)\right)\left(-6\delta_{\mathrm{y}}-10\mathrm{v}_{\mathrm{m0z}}(1-2\xi)^2+L(4\theta_{21\mathrm{z}}-\theta_{22\mathrm{z}})(-1+2\xi)\right)}{3600L} \tag{4.112}$$

$$\mathrm{KI11G}=\frac{1}{60}LP(-1+2\xi)-\frac{\mathrm{EA}\left(-6\delta_{\mathrm{z}}+10\mathrm{v}_{\mathrm{m0y}}(1-2\xi)^2-L\left(\theta_{21\mathrm{y}}-4\theta_{22\mathrm{y}}\right)(-1+2\xi)\right)\left(6\delta_{\mathrm{z}}+10\mathrm{v}_{\mathrm{m0y}}(1-2\xi)^2-L\left(4\theta_{21\mathrm{y}}-\theta_{22\mathrm{y}}\right)(-1+2\xi)\right)}{3600L} \tag{4.113}$$

$$\mathrm{KI12G}=\frac{\mathrm{EA}\left(6\delta_{\mathrm{z}}+10\mathrm{v}_{\mathrm{m0y}}(1-2\xi)^2-L\left(4\theta_{21\mathrm{y}}-\theta_{22\mathrm{y}}\right)(-1+2\xi)\right)\left(6\delta_{\mathrm{y}}-10\mathrm{v}_{\mathrm{m0z}}(1-2\xi)^2+L(\theta_{21\mathrm{z}}-4\theta_{22\mathrm{z}})(-1+2\xi)\right)}{3600L} \tag{4.114}$$

$$\mathrm{KJ10G}=\frac{1}{15}LP(1-2\xi)+\frac{\mathrm{EA}\left(6\delta_{\mathrm{y}}+10\mathrm{v}_{\mathrm{m0z}}(1-2\xi)^2-L(4\theta_{21\mathrm{z}}-\theta_{22\mathrm{z}})(-1+2\xi)\right)^2}{3600L} \tag{4.115}$$

$$\mathrm{KJ11G} = \frac{\mathrm{EA}\left(-6\delta_{\mathrm{z}} + 10\mathrm{v}_{\mathrm{m0y}}(1-2\xi)^2 - L\left(\theta_{21\mathrm{y}} - 4\theta_{22\mathrm{y}}\right)(-1+2\xi)\right)\left(-6\delta_{\mathrm{y}} - 10\mathrm{v}_{\mathrm{m0z}}(1-2\xi)^2 + L(4\theta_{21\mathrm{z}} - \theta_{22\mathrm{z}})(-1+2\xi)\right)}{3600L} \tag{4. 116}$$

$$\mathrm{KJ12G} = \frac{1}{60}LP(-1+2\xi) - \frac{\mathrm{EA}\left(-6\delta_{\mathrm{y}} + 10\mathrm{v}_{\mathrm{m0z}}(1-2\xi)^2 - L(\theta_{21\mathrm{z}} - 4\theta_{22\mathrm{z}})(-1+2\xi)\right)\left(6\delta_{\mathrm{y}} + 10\mathrm{v}_{\mathrm{m0z}}(1-2\xi)^2 - L(4\theta_{21\mathrm{z}} - \theta_{22\mathrm{z}})(-1+2\xi)\right)}{3600L} \tag{4. 117}$$

$$\mathrm{KK11G} = \frac{1}{15}LP(1-2\xi) + \frac{\mathrm{EA}\left(6\delta_{\mathrm{z}} - 10\mathrm{v}_{\mathrm{m0y}}(1-2\xi)^2 + L\left(\theta_{21\mathrm{y}} - 4\theta_{22\mathrm{y}}\right)(-1+2\xi)\right)^2}{3600L} \tag{4. 118}$$

$$\mathrm{KK12G} = \frac{\mathrm{EA}\left(6\delta_{\mathrm{z}} - 10\mathrm{v}_{\mathrm{m0y}}(1-2\xi)^2 + L\left(\theta_{21\mathrm{y}} - 4\theta_{22\mathrm{y}}\right)(-1+2\xi)\right)\left(6\delta_{\mathrm{y}} - 10\mathrm{v}_{\mathrm{m0z}}(1-2\xi)^2 + L(\theta_{21\mathrm{z}} - 4\theta_{22\mathrm{z}})(-1+2\xi)\right)}{3600L} \tag{4. 119}$$

$$\mathrm{KL12G} = \frac{1}{15}LP(1-2\xi) + \frac{\mathrm{EA}\left(6\delta_{\mathrm{y}} - 10\mathrm{v}_{\mathrm{m0z}}(1-2\xi)^2 + L(\theta_{21\mathrm{z}} - 4\theta_{22\mathrm{z}})(-1+2\xi)\right)^2}{3600L} \tag{4. 120}$$

The internal spring stiffness matrix k_S can be expressed as,

$$[k_S] = \begin{bmatrix} 0 & 0 & 0 & 0 & 0 & 0 & 0 & 0 & 0 & 0 & 0 & 0 \\ & 0 & 0 & 0 & 0 & 0 & 0 & 0 & 0 & 0 & 0 & 0 \\ & & 0 & 0 & 0 & 0 & 0 & 0 & 0 & 0 & 0 & 0 \\ & & & 0 & 0 & 0 & 0 & 0 & 0 & 0 & 0 & 0 \\ & S & & & \mathrm{EI_y \cdot R_y} & 0 & 0 & 0 & -\mathrm{EI_y \cdot R_y} & 0 & 0 & 0 \\ & & & & & \mathrm{EI_z \cdot R_z} & 0 & 0 & 0 & -\mathrm{EI_z \cdot R_z} & 0 & 0 \\ & & Y & & & & 0 & 0 & 0 & 0 & 0 & 0 \\ & & & & & & & 0 & 0 & 0 & 0 & 0 \\ & & & M & & & & & \mathrm{EI_y \cdot R_y} & 0 & 0 & 0 \\ & & & & & & & & & \mathrm{EI_z \cdot R_z} & 0 & 0 \\ & & & & & & & & & & 0 & 0 \\ & & & & & & & & & & & 0 \end{bmatrix} \quad (4.\ 121)$$

where, $\mathrm{R_y}$ and $\mathrm{R_z}$ are the plasticity parameters at the internal hinges at two principle axes respectively.

4.2.6 Condensed stiffness matrix and generalized nodal forces

Similar to the two-dimensional element as presented in Chapter 3, the internal degree of freedoms (DOFs) are needed to be condensed for the compatibility to the existing computer program as well as the numerical efficiency. Therefore, the internal and external DOFs and the corresponding forces can be expressed as.

$$u_i = \{\theta_{12y} \quad \theta_{12z} \quad \delta_z \quad \delta_y \quad \theta_{21y} \quad \theta_{21z}\}^T \quad (4.\ 122)$$

$$u_e = \{e \quad \theta_{11y} \quad \theta_{11z} \quad \theta_x \quad \theta_{22y} \quad \theta_{22z}\}^T \quad (4.\ 123)$$

$$F_i = \{M_{12y} \quad M_{12z} \quad F_z \quad F_y \quad M_{21y} \quad M_{21z}\}^T \quad (4.\ 124)$$

$$F_e = \{P \quad M_{11y} \quad M_{11z} \quad M_x \quad M_{22y} \quad M_{22z}\}^T \quad (4.\ 125)$$

The condensed stiffness k^* and generalized force f can be expressed as,

$$[k^*] = [k_{ee}] - [k_{ie}]^T \left[k_{ii}\right]^{-1} [k_{ie}] \quad (4.\ 126)$$

$$f = F_e - k_{ie}^T k_{ii}^{-1} F_i \tag{4. 127}$$

where,

$$[k_{ee}] = \begin{bmatrix} KA1 & KA2 & KA3 & KA4 & KA11 & KA12 \\ KB1 & KB2 & KB3 & KB4 & KB11 & KB12 \\ KC1 & KC2 & KC3 & KC4 & KC11 & KC12 \\ KD1 & KD2 & KD3 & KD4 & KD11 & KD12 \\ KK1 & KK2 & KK3 & KK4 & KK11 & KK12 \\ KL1 & KL2 & KL3 & KL4 & KL11 & KL12 \end{bmatrix} \tag{4. 128}$$

$$[k_{ii}] = \begin{bmatrix} KE5 & KE6 & KE7 & KE8 & KE9 & KE10 \\ KF5 & KF6 & KF7 & KF8 & KF9 & KF10 \\ KG5 & KG6 & KG7 & KG8 & KG9 & KG10 \\ KH5 & KH6 & KH7 & KH8 & KH9 & KH10 \\ KI5 & KI6 & KI7 & KI8 & KI9 & KI10 \\ KJ5 & KJ6 & KJ7 & KJ8 & KJ9 & KJ10 \end{bmatrix} \tag{4. 129}$$

$$[k_{ie}] = \begin{bmatrix} KA5 & KB5 & KC5 & KD5 & KE11 & KE12 \\ KA6 & KB6 & KC6 & KD6 & KF11 & KF12 \\ KA7 & KB7 & KC7 & KD7 & KG11 & KG12 \\ KA8 & KB8 & KC8 & KD8 & KH11 & KH12 \\ KA9 & KB9 & KC9 & KD9 & KI11 & KI12 \\ KA10 & KB10 & KC10 & KD10 & KJ11 & KJ12 \end{bmatrix} \tag{4. 130}$$

The internal DOFs u_i at hinge location can be decoupled by multiplying the incremental rotations at external DOFs, u_e, as,

$$u_i = k_{ii}^{-1}(F_i \ - k_{ie} u_e) \tag{4. 131}$$

4.2.7 Incorporation of two end plastic hinges

The plastic hinges at the element ends are needed to be incorporated into the formulations, and the derivation has been already given in Chapter 3. After the condensation of the internal DOFs, the stiffness matrix and the generalized load vector can be written as,

$$[k^*] = \begin{bmatrix} k11^* & k12^* & k13^* & k14^* & k15^* & k16^* \\ & k22^* & k23^* & k24^* & k25^* & k26^* \\ S. & & k33^* & k34^* & k35^* & k36^* \\ & Y. & & k44^* & k45^* & k46^* \\ & & M. & & k55^* & k56^* \\ & & & & & k66^* \end{bmatrix} \quad (4.\ 132)$$

$$f = \{P^* \quad {M_{1y}}^* \quad {M_{1z}}^* \quad {M_x}^* \quad {M_{2y}}^* \quad {M_{2z}}^*\}^T \quad (4.\ 133)$$

The incorporation of the two end hinges at two principle directions can be achieved by updating the stiffness matrix. The

$$\tilde{k}22 = S_{Ly} - \frac{S_{Ly}^2\left(k55^* + S_{Ry}\right)}{\beta_{sy}} \quad (4.\ 134)$$

$$\tilde{k}25 = \frac{S_{Ly}S_{Ry}k25^*}{\beta_{sy}} \quad (4.\ 135)$$

$$\tilde{k}55 = S_{Ry} - \frac{S_{Ry}^2\left(k22^* + S_{Ly}\right)}{\beta_{sy}} \quad (4.\ 136)$$

$$\tilde{k}33 = S_{Lz} - \frac{S_{Lz}^2(k66^* + S_{Rz})}{\beta_{sz}} \quad (4.\ 137)$$

$$\tilde{k}36 = \frac{S_{Lz}S_{Rz}k36^*}{\beta_{sz}} \quad (4.\ 138)$$

$$\tilde{k}66 = S_{Rz} - \frac{S_{Rz}^2(k33^* + S_{Lz})}{\beta_{sz}} \quad (4.\ 139)$$

in which,

$$\beta_{sy} = \left(k22^* + S_{Ly}\right)\left(k55^* + S_{Ry}\right) - k25^*k52^* > 0 \quad (4.\ 140)$$

$$\beta_{sz} = (k33^* + S_{Lz})(k66^* + S_{Rz}) - k36^*k63^* > 0 \quad (4.\ 141)$$

where, S_{Ly} and S_{Ry} are the spring stiffness at y-axis for the left and right hinges, respectively; and S_{Lz} and S_{Rz} are the spring stiffness at z-axis for the left and right hinges, respectively.

Therefore, the member stiffness matrix can be eventually obtained as,

$$[\widetilde{k}] = \begin{bmatrix} k11^* & k12^* & k13^* & k14^* & k15^* & k16^* \\ & \tilde{k}22 & k23^* & k24^* & \tilde{k}25 & k26^* \\ S. & & \tilde{k}33 & k34^* & k35^* & \tilde{k}36 \\ & Y. & & k44^* & k45^* & k46^* \\ & & M. & & \tilde{k}55 & k56^* \\ & & & & & \tilde{k}66 \end{bmatrix} \tag{4. 142}$$

And the rotations at the element ends can be calculated as,

$$\begin{Bmatrix} \Delta\theta_{11y} \\ \Delta\theta_{22y} \end{Bmatrix} = \begin{bmatrix} k22^* + S_{Ly} & k25^* \\ k52^* & k55^* + S_{Ry} \end{bmatrix}^{-1} \cdot \begin{bmatrix} S_{Ly} & 0 \\ 0 & S_{Ry} \end{bmatrix} \cdot \begin{Bmatrix} \Delta\theta_{s1y} \\ \Delta\theta_{s2y} \end{Bmatrix} \tag{4. 143}$$

$$\begin{Bmatrix} \Delta\theta_{11z} \\ \Delta\theta_{22z} \end{Bmatrix} = \begin{bmatrix} k33^* + S_{Lz} & k36^* \\ k63^* & k66^* + S_{Rz} \end{bmatrix}^{-1} \cdot \begin{bmatrix} S_{Lz} & 0 \\ 0 & S_{Rz} \end{bmatrix} \cdot \begin{Bmatrix} \Delta\theta_{s1z} \\ \Delta\theta_{s2z} \end{Bmatrix} \tag{4. 144}$$

4.3. Kinematic descriptions of motion

In order to consider large deflections of a beam-column element in a three-dimensional space, three common kinematic descriptions of motion, such as total secant stiffness method, joint orientation matrix method and incremental secant stiffness method, are commonly introduced. Chan (1992) has conducted an extensive study on these three kinematic formulations and found the incremental secant stiffness method to be the most stability, efficient and suitable for nonlinear beam-column finite element analysis. In the present study, the incremental secant stiffness method is adopted, which has been successfully used by numerous research and actual practice. Similar to the analytical approach given in Chapter 3, the updated Lagrangian description is also employed.

4.3.1 The incremental secant stiffness method

The incremental secant stiffness method is similar to the total incremental secant counterpart, where the equilibrium conditions are established by the last-known configuration in the former approach and the original configuration in the latter method respectively. However, the incremental rotations in each step should be limited to be small, but the element can exhibit moderately large rotations by considering the infinitesimal rotations as vectorial quantities. Furthermore, the convergence speed of the incremental secant stiffness method is considerably better than the total secant stiffness approach.

This method has been successfully adopted by numerous researchers and approved to be efficient and effective for large deflection and inelastic analysis. Chan (1989) used the incremental secant stiffness method for inelastic post-buckling analysis of the tubular member and found to be very stable and efficient in the numerical iterative procedure. Yang and Chiou (1987) utilized this approach for the large deflections of the planar frame. Argyris *et al*. (1978) extended this method to the three-dimensional frame with large member rotations. Chan and Zhou (1994, 1995) also introduced this algorithm in their high-order beam-column element and proved it to be accurate and feasible.

Therefore, the goal of the analysis at each load-increment is to find the resisting forces at the $i+1^{th}$ position by referring to the last-known configuration at the i^{th} position, as shown in Figure 4.5. The natural incremental rotations in an element can be calculated as,

$$\Delta\theta_{y1i} = \Delta\alpha_{y1i} + \Delta\beta_{yi} \quad (4.145)$$

$$\Delta\theta_{y2i} = \Delta\alpha_{y2i} + \Delta\beta_{yi} \quad (4.146)$$

$$\Delta\theta_{z1i} = \Delta\alpha_{z1i} - \Delta\beta_{zi} \quad (4.147)$$

$$\Delta\theta_{z2i} = \Delta\alpha_{z2i} - \Delta\beta_{zi} \quad (4.148)$$

in which, $\Delta\alpha_{y1i}$, $\Delta\alpha_{y2i}$, $\Delta\alpha_{z1i}$ and $\Delta\alpha_{z2i}$ are the incremental rotations about the last known configuration; and $\Delta\beta_{yi}$ and $\Delta\beta_{zi}$ are the rigid body rotations given by,

$$\Delta\beta_{yi} = \frac{\Delta w_{2i} - \Delta w_{1i}}{L_i} \quad (4.149)$$

$$\Delta\beta_{zi} = \frac{\Delta v_{2i} - \Delta v_{1i}}{L_i} \quad (4.150)$$

where, L_i is the member length at the last known configuration; Δw_{1i}, Δw_{2i}, Δv_{1i} and Δv_{2i} are the displacement at member local axes along z- and y- axes respectively.

The relative incremental twist about the shear center can be simply evaluated as,

$$\Delta\theta_{xi} = \Delta\theta_{x2i} - \Delta\theta_{x1i} \quad (4.151)$$

The incremental axial lengthening can be determined as,

$$\Delta e_i = \Delta \mathrm{u_b} - \Delta u_{ni} \quad (4.152)$$

where,

$$\Delta u_{ni} = \mathrm{L}_{i+1} - \mathrm{L}_i \quad (4.153)$$

and the $\Delta \mathrm{u_b}$ can be obtained by the first deviation of the expressions of $\mathrm{u_b}$ as,

$$\begin{aligned}\Delta \mathrm{u_b} = {} & \frac{1}{60}\Delta\theta_{22\mathrm{y}}\left(6\delta_{\mathrm{z}} - 10\mathrm{v_{m0y}}(1-2\xi)^2 + L\left(\theta_{21\mathrm{y}} - 4\theta_{22\mathrm{y}}\right)(-1+2\xi)\right) \\ & + \frac{1}{60}\Delta\theta_{21\mathrm{y}}\left(6\delta_{\mathrm{z}} + 10\mathrm{v_{m0y}}(1-2\xi)^2 - L\left(4\theta_{21\mathrm{y}} - \theta_{22\mathrm{y}}\right)(-1+2\xi)\right) \\ & + \frac{1}{60}\Delta\theta_{22\mathrm{z}}\left(6\delta_{\mathrm{y}} - 10\mathrm{v_{m0z}}(1-2\xi)^2 + L(\theta_{21\mathrm{z}} - 4\theta_{22\mathrm{z}})(-1+2\xi)\right)\end{aligned} \quad (4.154)$$

$$+\frac{1}{60}\Delta\theta_{21z}\left(6\delta_y+10v_{m0z}(1-2\xi)^2-L(4\theta_{21z}-\theta_{22z})(-1+2\xi)\right)$$

$$-\frac{1}{60}\Delta\theta_{12y}\left(6\delta_z+L\left(\theta_{11y}-4\theta_{12y}\right)(1+2\xi)+10v_{m0y}(1+2\xi)^2\right)$$

$$+\frac{1}{60}\Delta\theta_{11y}\left(-6\delta_z+L\left(4\theta_{11y}-\theta_{12y}\right)(1+2\xi)+10v_{m0y}(1+2\xi)^2\right)$$

$$-\frac{1}{60}\Delta\theta_{12z}\left(6\delta_y+L(\theta_{11z}-4\theta_{12z})(1+2\xi)+10v_{m0z}(1+2\xi)^2\right)$$

$$+\frac{1}{60}\Delta\theta_{11z}\left(-6\delta_y+L(4\theta_{11z}-\theta_{12z})(1+2\xi)+10v_{m0z}(1+2\xi)^2\right)$$

$$+\frac{\Delta\delta_z\left(-48\delta_z+L\left(\theta_{11y}+\theta_{12y}-\theta_{21y}-\theta_{22y}\right)(1-4\xi^2)+40v_{m0y}(-1+4\xi^2)\right)}{10L(-1+4\xi^2)}$$

$$+\frac{\Delta\delta_y\left(-48\delta_y+L(\theta_{11z}+\theta_{12z}-\theta_{21z}-\theta_{22z})(1-4\xi^2)+40v_{m0z}(-1+4\xi^2)\right)}{10L(-1+4\xi^2)}$$

The consideration of the incremental bowing effect is very vital for an accurate analysis by only one element per member, which is usually ignored by some researchers and more elements are needed for minimizing the corresponding errors. The comparison results of the included and excluded this incremental bowing effect has been reported by Chan (1992).

Once the natural deformations are obtained, the incremental forces and moments can be evaluated as,

$$\Delta R_i = [Ke]_i \Delta u_i \tag{4. 155}$$

$$R_{i+1} = R_i + \Delta R_i \tag{4. 156}$$

where, $[Ke]_i$ is the element stiffness matrix at the i^{th} configuration; and R is the internal resisting forces and given by

$$R = \{P \quad M_{1y} \quad M_{1z} \quad M_x \quad M_{2y} \quad M_{2z}\}^T \tag{4. 157}$$

4.3.2 Transformation matrix [T] from member basic force/displacements to member local axes

A three dimensional element contains six degree of freedoms at each ends in its member local axes as shown in Figure 4.6. The twelve forces and moments can be calculated by the six internal and independent member forces and moments by the transformation matrix [T] expressed as,

$$\bar{F} = [T]f \tag{4. 158}$$

$$u = [T]^T \bar{u} \tag{4. 159}$$

$$[\mathrm{T}] = \begin{bmatrix} -1 & 0 & 0 & 0 & 0 & 0 \\ 0 & 0 & 1/L & 0 & 0 & 1/L \\ 0 & -1/L & 0 & 0 & -1/L & 0 \\ 0 & 0 & 0 & -1 & 0 & 0 \\ 0 & 1 & 0 & 0 & 0 & 0 \\ 0 & 0 & 1 & 0 & 0 & 0 \\ 1 & 0 & 0 & 0 & 0 & 0 \\ 0 & 0 & -1/L & 0 & 0 & -1/L \\ 0 & 1/L & 0 & 0 & 1/L & 0 \\ 0 & 0 & 0 & 1 & 0 & 0 \\ 0 & 0 & 0 & 0 & 1 & 0 \\ 0 & 0 & 0 & 0 & 0 & 1 \end{bmatrix} \tag{4. 160}$$

where, $\bar{F}$ and $\bar{u}$ are the forces and corresponding displacements at the member local axes as shown in Figure 4.6.

4.3.3 Matrix [N] for the rigid body movement

In the co-rotational formulation, the rigid body movement is extracted from the element derivation and can be calculated by introducing the matrix [N] as,

$$[\mathrm{N}] = \begin{bmatrix} 0 & N_z & -N_y & 0 & 0 & 0 & 0 & -N_z & N_y & 0 & 0 & 0 \\ & N_p & 0 & 0 & 0 & 0 & -N_z & -N_p & 0 & 0 & 0 & 0 \\ & & N_p & 0 & 0 & 0 & N_y & 0 & -N_p & 0 & 0 & 0 \\ & S. & & 0 & 0 & 0 & 0 & 0 & 0 & 0 & 0 & 0 \\ & & & & 0 & 0 & 0 & 0 & 0 & 0 & 0 & 0 \\ & & Y. & & & 0 & 0 & 0 & 0 & 0 & 0 & 0 \\ & & & & & & 0 & N_z & -N_y & 0 & 0 & 0 \\ & & & M. & & & & N_p & 0 & 0 & 0 & 0 \\ & & & & & & & & N_p & 0 & 0 & 0 \\ & & & & & & & & & 0 & 0 & 0 \\ & & & & & & & & & & 0 & 0 \\ & & & & & & & & & & & 0 \end{bmatrix} \quad (4.\ 161)$$

where,

$$N_z = \frac{{M_{1z}}^* + {M_{2z}}^*}{L^2} \quad (4.\ 162)$$

$$N_y = \frac{{M_{1y}}^* + {M_{2y}}^*}{L^2} \quad (4.\ 163)$$

$$N_p = \frac{P^*}{L} \quad (4.\ 164)$$

in which, P^*, ${M_{1z}}^*$, ${M_{2z}}^*$, ${M_{1y}}^*$ and ${M_{2y}}^*$ are the condensed member resisting forces and moments in the last known configuration.

4.3.4 Transformation matrix [L] from member local to global axes

The element formulations are given in a set of member local axes as shown in Figure 4.7, and needed to be transferred to the global axes before assembling.

$$[\mathrm{L}]_{i+1} = [\mathrm{L}]_i[\Delta\mathrm{L}]_i \quad (4.\ 165)$$

where,

$$[\mathrm{L}]_i = \begin{bmatrix} [\mathrm{L}']_i & 0 & 0 & 0 \\ 0 & [\mathrm{L}']_i & 0 & 0 \\ 0 & 0 & [\mathrm{L}']_i & 0 \\ 0 & 0 & 0 & [\mathrm{L}']_i \end{bmatrix} \quad (4.\ 166)$$

The initial transformation matrix can be obtained as,

$$[\mathrm{L}]_0 = \begin{bmatrix} \mathrm{Cx} & \dfrac{-CxCy\cos\beta - Cz\sin\beta}{\sqrt{\mathrm{Cx}^2+\mathrm{Cz}^2}} & \dfrac{CxCy\sin\beta - Cz\cos\beta}{\sqrt{\mathrm{Cx}^2+\mathrm{Cz}^2}} \\ Cy & \sqrt{\mathrm{Cx}^2+\mathrm{Cz}^2}\cos\beta & -\sqrt{\mathrm{Cx}^2+\mathrm{Cz}^2}\sin\beta \\ Cz & \dfrac{-CyCz\cos\beta + Cx\sin\beta}{\sqrt{\mathrm{Cx}^2+\mathrm{Cz}^2}} & \dfrac{CyCz\sin\beta + Cx\cos\beta}{\sqrt{\mathrm{Cx}^2+\mathrm{Cz}^2}} \end{bmatrix} \quad (4.\ 167)$$

where,

$$\mathrm{L}_0 = \sqrt{(X2_0 - X1_0)^2 + (Y2_0 - Y1_0)^2 + (Z2_0 - Z1_0)^2} \quad (4.\ 168)$$

$$\mathrm{Cx} = \frac{X2_0 - X1_0}{\mathrm{L}_0} \quad (4.\ 169)$$

$$\mathrm{Cy} = \frac{Y2_0 - Y1_0}{\mathrm{L}_0} \quad (4.\ 170)$$

$$\mathrm{Cz} = \frac{Z2_0 - Z1_0}{\mathrm{L}_0} \quad (4.\ 171)$$

in which, L_0 is the original member length; and $X1_0$, $X2_0$, $Y1_0$, $Y2_0$, $Z1_0$ and $Z2_0$ are the coordinates in original position.

For particular condition that Cx and Cz are both 0 that, the transformation matrix can be rewritten as,

$$[\mathrm{L}]_0 = \begin{bmatrix} 0 & -Cy\cos\beta & Cy\sin\beta \\ Cy & 0 & 0 \\ 0 & \sin\beta & \cos\beta \end{bmatrix} \quad (4.\ 172)$$

$$[\Delta\mathrm{L}]_i = \begin{bmatrix} \mathrm{Dx}_i & \dfrac{-\mathrm{Dx}_i Dy_i}{\sqrt{{\mathrm{Dx}_i}^2 + {Dz_i}^2}} & \dfrac{-Dz_i}{\sqrt{{\mathrm{Dx}_i}^2 + {Dz_i}^2}} \\ Dy_i & \sqrt{{\mathrm{Dx}_i}^2 + {Dz_i}^2} & 0 \\ Dz_i & \dfrac{-\mathrm{Dy}_i Dz_i}{\sqrt{{\mathrm{Dx}_i}^2 + {Dz_i}^2}} & \dfrac{Dx_i}{\sqrt{{\mathrm{Dx}_i}^2 + {Dz_i}^2}} \end{bmatrix} \quad (4.\ 173)$$

where,

$$\mathrm{Dy}_i = \frac{\Delta Y2_i - \Delta Y1_i}{\mathrm{L}_i} \tag{4. 174}$$

$$\mathrm{Dz}_i = \frac{\Delta Z2_i - \Delta Z1_i}{\mathrm{L}_i} \tag{4. 175}$$

$$\mathrm{Dx}_i = \sqrt{1 - (\mathrm{Dy}_i)^2 - (\mathrm{Dz}_i)^2} \tag{4. 176}$$

in which, L_i is the current member length at the ith iteration; and $\Delta X1_i$, $\Delta X2_i$, $\Delta Y1_i$, $\Delta Y2_i$, $\Delta Z1_i$ and $\Delta Z2_i$ are the incremental displacements in global axes.

4.3.5 Relations between member local axes and global axes

With the availability of the above transformation matrix, the complete 12 by 12 element stiffness matrix can be calculated by the following process as,

$$[\mathrm{Kt}]_e = [L]([T][k_e][T]^T + [N])[L]^T \tag{4. 177}$$

in which, $[\mathrm{Kt}]_e$ is the rotated member stiffness matrix; and $[k_e]$ is the element stiffness matrix in element local axes.

Therefore, the global tangent stiffness matrix can be obtained by assembling the rotated element stiffness matrix as,

$$[\mathrm{Kt}]_g = \sum_1^{NELE} [\mathrm{Kt}]_e^i \tag{4. 178}$$

where, $[\mathrm{Kt}]_g$ is the global tangent stiffness matrix of the whole system; and NELE is the total number of the element.

The member incremental displacement in global axes is needed to be transferred to member local displacements as,

$$\Delta[\mathrm{u}]_e = [L]^T[T]^T\Delta[\mathrm{U}]_e \tag{4. 179}$$

The element resisting forces are needed to transferred to global axes as,

$$\mathrm{R}_e = [L][T]r \tag{4. 180}$$

4.4. Verification examples

The computer program as presented in Chapter 3 has been further extended to the analysis of three-dimensional problems. In order to give an extensive evaluation of the accuracy and validity on the proposed analytical model for large deflection and inelastic analysis of the space frames and members, several examples are constructed and presented in this section.

4.4.1 Biaxially-loaded cantilever column

In this example, the capacity for large deflection analysis of the proposed element is tested and verified. A cantilever column under a purely axial load, as shown in Figure 4.8, is analyzed by the second-order elastic analysis method. The section of this column is UB305 × 127 × 42, with the initial imperfections equaling to L/500 and L/400 along its minor and major axes respectively. The material of this column is S275, where the Young's modulus is 2.05×10^8 kN/m^2 and the yield strength is 2.50×10^4 kN/m^2. The column is 10 meters long and a concentrated load along Z-axis as -18 kN is applied at the top of the column.

To evaluate the accuracy of the proposed element in large deflection analysis and the simulations on initial member imperfections, the imperfect PEP (Pointwise Equilibrating Polynomial) element as proposed by Chan and Zhou (1995) is introduced for comparing purpose. The PEP element is possessed of high-order shape function and initial imperfections, which capable to simulate very large member deflections by one element per member and is widely recognized to be one of the best elements for second-order nonlinear analysis. In the second-order elastic analysis by the proposed element, the stiffness for the three hinges are set to be infinity and the internal hinge is assigned to be placed at the half length.

This example is essential for testing the element formulations for second-order analysis and the use for the actual design purpose. The results by the proposed element and the PEP element (Chan & Zhou, 1995) are presented in Figure 4.9. From the comparisons, it shows that the two curves are closed and the maximum differences between the two elements are within 0.3%. This indicates the accuracy of the proposed element formulations and the kinematic descriptions for the large deflections.

4.4.2 Two story space steel frame with I sections

This example presents a two story and two bay space steel frame with I sections for both beams and columns, as shown in Figure 4.10, which is originally studied and analyzed by the Finite Element Method (FEM) by Cuong and Kim (2007). The section size of the steel frame is H150 × 160 × 10 × 6.5 and the yield stress, Young's modulus and shear modulus are 350 MPa, 221 GPa and 85 GPa

respectively. The concentrated loads are applied at the nodes only, where P equals to 80 kN. The out-of-plumpness imperfection is directly modeled by offsetting the coordinates of the nodes as tabulated in Table 4.1, and no member initial imperfections are included in analysis. The frame is fixed to the ground and all the members are rigidly connected. All the members are modeled by one element in the present study.

The comparison results are presented in Figure 4.11 and Figure 4.12 for the displacements at the roof and second floor levels respectively. The results by the proposed analytical model is only slightly stiffed than the FEM results and very closed. The ultimate load factors are 0.94 and 0.92 for the FEM and the proposed analytical model, respectively. This indicates the high accuracy can be achieved by adopting the proposed numerical method by using only one element per member for advanced inelastic analysis of space steel frames.

4.4.3 Harrison's space frame

In this example, an equilateral triangular space frame is introduced as shown in Figure 4.13, which has been originally studied by Harrison (1965) by the experiments. All members in the frame are circular hollow sections with diameter and wall-thickness equaling to 42.72 mm and 4.47 mm, respectively. This frame has been latterly studied by Teh and Clarke (1999) by using the plastic-zone approach. All members in the proposed analytical method are modeled by one element only.

The comparison results are plotted in Figure 4.14, where the results from the experiment, plastic-zone analysis and the proposed analytical model are presented and compared. It can be seen that, the results among the three approaches are closed. The results from the proposed analytical model are identical as those from the plastic-zone analysis in the elastic range while a slightly different is noticed in the elasto-plastic range. Both the plastic zone method and the proposed analytical model are capable to reflect the inelastic and large deflections of the frame under increasing loads, however, the latter method is much more efficient and easily-formulated.

4.4.4 Two story space steel frame with rectangular sections

This example is firstly proposed and analyzed by Argyris *et al*. (1982) as presented in Figure 4.15, and later it was analyzed by the forced-based element proposed by De Souza (2000), which is introduced for the comparisons. The geometry of the two story space frame is illustrated in Figure 4.15, where the frame is with 400 cm width, 300cm depth and 400cm height at each floor respectively. The sections for both the beams and the columns are solid rectangular and the sizes are 400 mm × 200mm and 200mm × 400mm, respectively. The Young's modulus for the steel is 19613 MPa and yield stress is 98 MPa. Since two concentrated loads are applied at the mid-span of the two roof beams, these two beams are modeled by two elements and the other members are simulated by one element per member.

The load vs. deflection along X-axis at the roof level is plotted in Figure 4.16. From the comparisons, it shows that the results from the two analytical methods are

closed, where the forced-based element is usually considered to be essentially suitable for inelastic analysis.

4.4.5 Six story space steel frame

This is a famous example and initially proposed by Orbison *et al*. (1982) by the conventional plastic hinge approach, which is one of the famous examples for calibrating and verifying the validity of the analytical method in practice. Liew *et al*. (2000a) introduced the improved plastic hinge analysis method for the advanced analysis of this frame. And later Jiang *et al*. (2002) proposed a spread-of-analysis approach for the inelastic analysis and also studied this example. More recently, Iu and Bradford (2012a, 2012b) used their high-order element associated with the refined plastic hinge method and selected this frame for calibrating their theories.

The geometry of the six story frame is illustrated in Figure 4.17, where the overall width, depth and height of the frame is 14.63 m, 7.315 m and 21.948 m, respectively. The yield stress of all members is 250 MPa, while the Young's modulus is 206850 MPa. Uniform floor loads equaling to 9.6 kN/m^2 are converted into concentrated loads applied at the top of the columns. Wind loads are treated as joint loads as 51.376 kN and applied in the Y-direction at the beam-column joints. All the members are modeled by one element per member only.

The comparison results are plotted in Figure 4.18 and Figure 4.19 for the load vs. deflection along Y-axis and X-axis, respectively. It can be noticed that, the differences from the three analytical approaches are slight in the load vs. deflection

curve in Y-axis direction. However, the differences are obvious in the deflections in X-direction. This might be properly induced by the miss-consideration of the shear deformation in the proposed element, which will be further improved in the later study.

In the plastic zone analysis proposed by Jiang *et al*. (2002), all the sections are needed to discretized into three layers in the web and flanges respectively, and nine integral points along both the major and minor axes are required. Therefore, the computing expense for the plastic-zone analysis is huger than the required expense in the plastic hinge analysis approach. Although the spread-of-plastic behavior in the in the member locally cannot be accurately reflected by the plastic hinge approach, from the view of the overall structural system, the differences between the plastic-zone and plastic-hinge methods are not significant. Therefore, the plastic hinge method is regarded to be the first choice in actual engineering practice.

4.4.6 Twenty story space steel frame

In this example, a twenty story space frame is selected and analyzed, which is firstly studied by Liew *et al*. (2000a), which is a large-scale size problem closed to reality. The geometry and the section assignments of this twenty story space frame are illustrated in Figure 4.20. There are totally 460 members and 210 joints in this frame. All the members are steel sections and A50 steel is used with the yield stress equaling to 344.8 MPa. The gravity loads on all the floors are 4.8 kN/m^2 and concentrated into joints loads applied at the top of the columns. Wind loads of 0.96

kN/m^2 are applied at the beam-column joints. All the members are modeled by one element per member in the proposed analytical model.

The results obtained by the improved plastic hinge method from Liew *et al.* (2000a) are selected for the comparison and given in Figure 4.21. From the comparison, the two curves are identical in the elastic range, while the differences are noticed in the gradually yielding stage, which might be due to the disparities in the refined plastic hinge model in the two analytical approaches. The ultimate load factors are 1.022 and 1.032 from the present study and the improved plastic hinge model by Liew *et al.* (2000a), respectively.

4.5. Concluding remarks

In this chapter, the analytical model as presented in the previous chapter for planar frame analysis has been extended to three-dimensional space analysis. The element formulations are further derived and given in details. In order to consider the large deflections, the updated Lagrangian description associated with the incremental secant stiffness method is introduced and approved to be efficient and effective. Since the internal degrees of freedom have been condensed, the overall size of the global stiffness matrix has been dramatically reduced as well as the significant improvements on numerical efficiency. Finally, verification examples are given and the proposed analytical model is approved to be accurate and valid for advanced analysis of space frames.

Figures

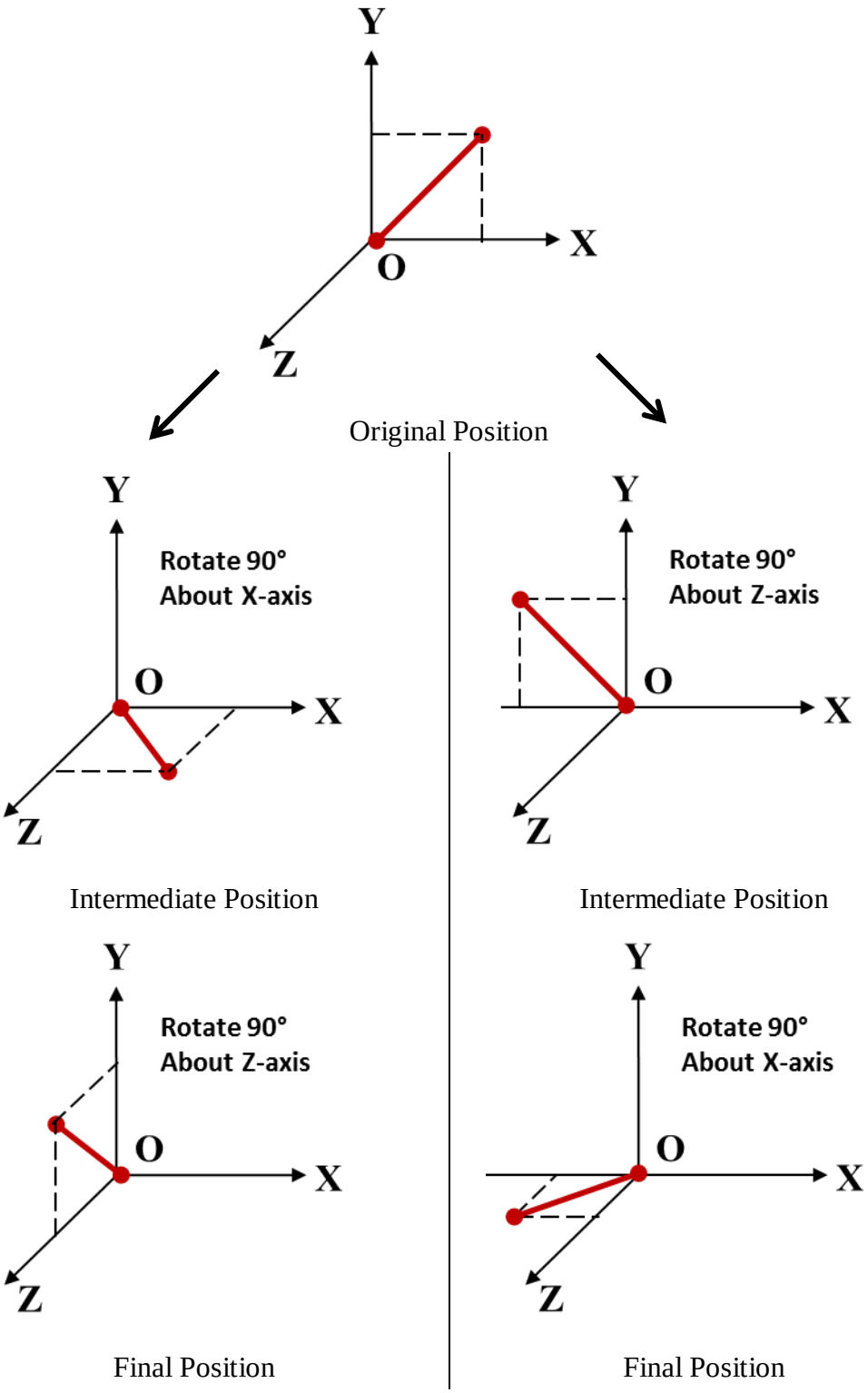

Figure 4.1 Non-vectorial property of large rotations in three-dimensional space

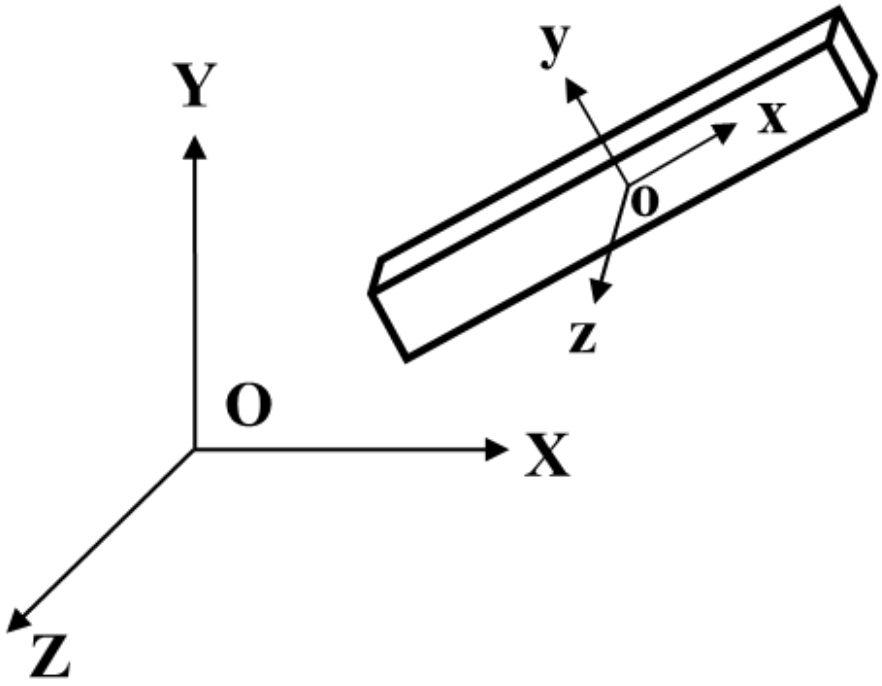

Figure 4.2 The element local coordinate system

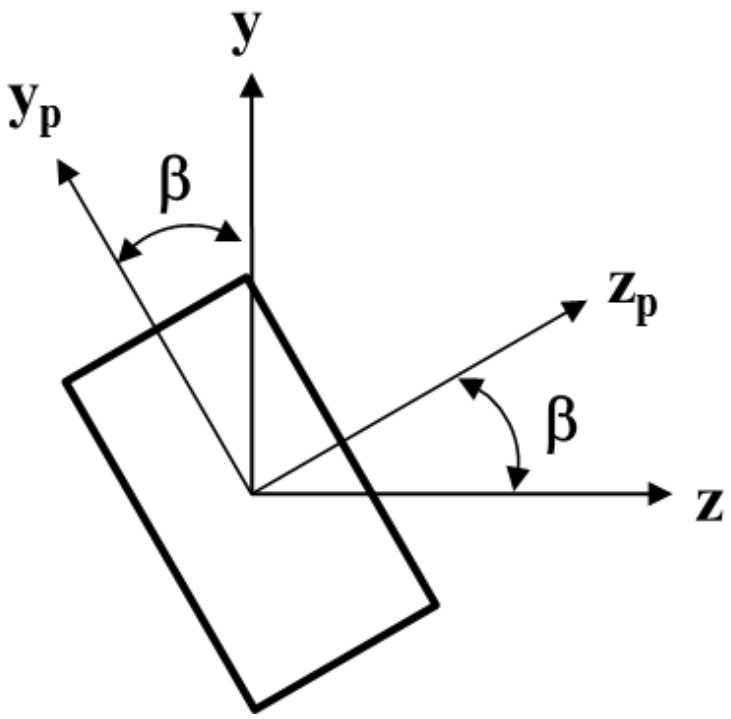

Figure 4.3 The inclination of principle axes

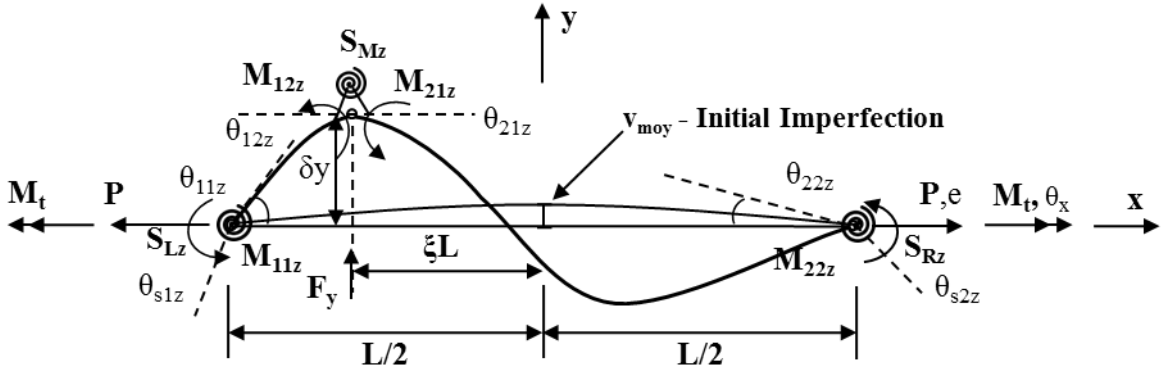

(a) Along y-axis

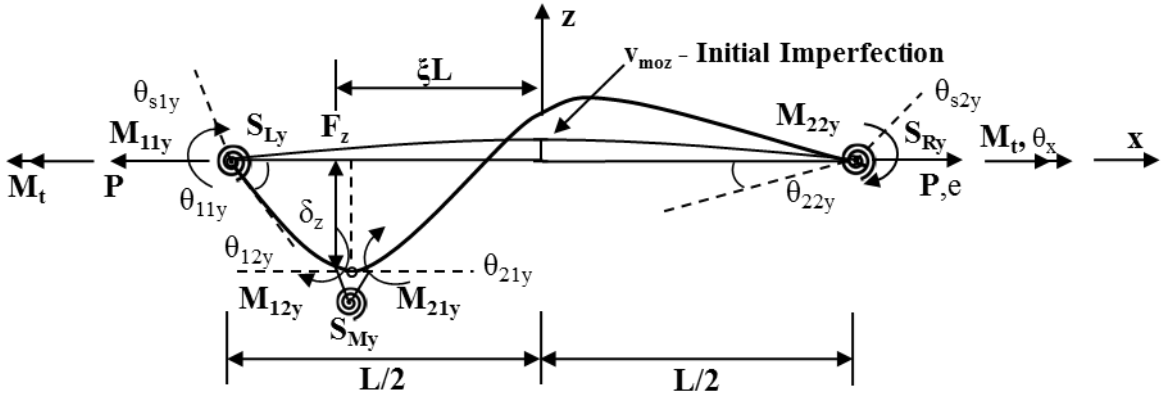

(b) Along z-axis

Figure 4.4 Relative member basic forces and deformations

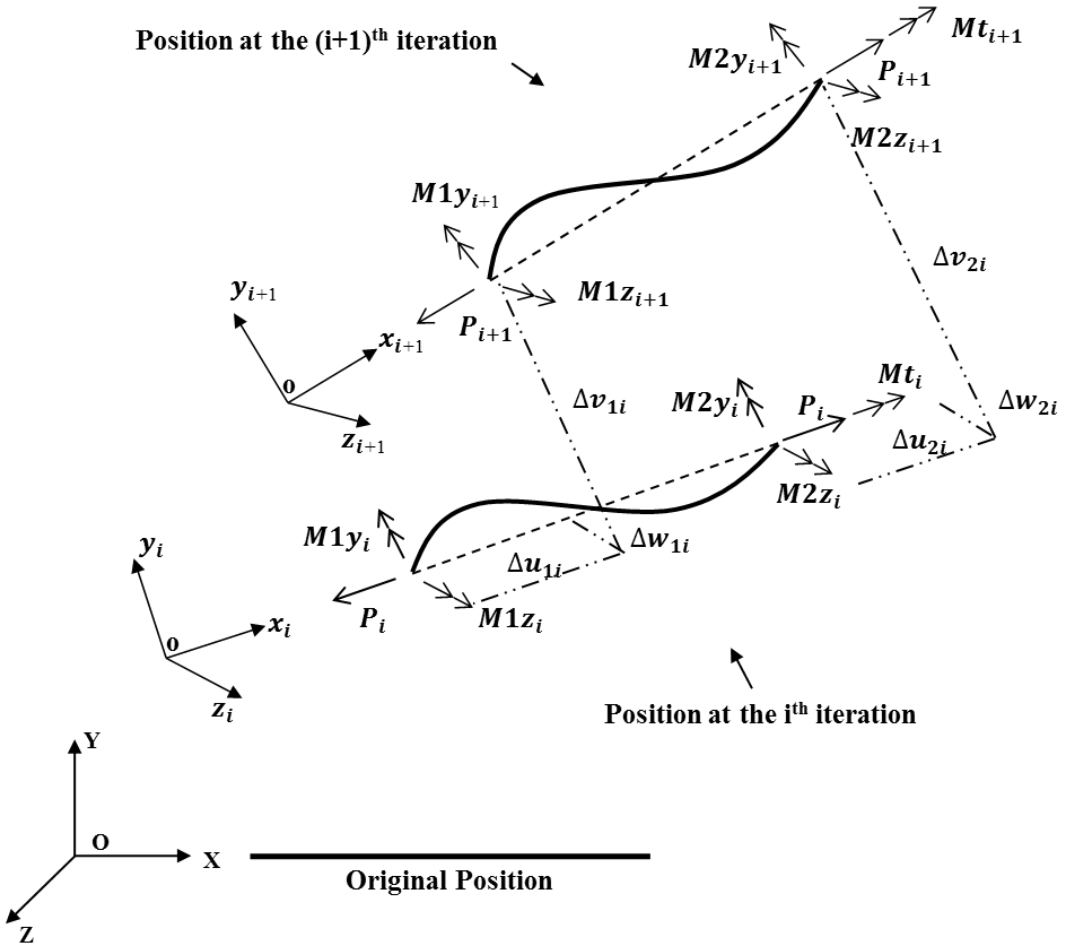

Figure 4.5 Incremental kinematics of an element in three-dimensional space

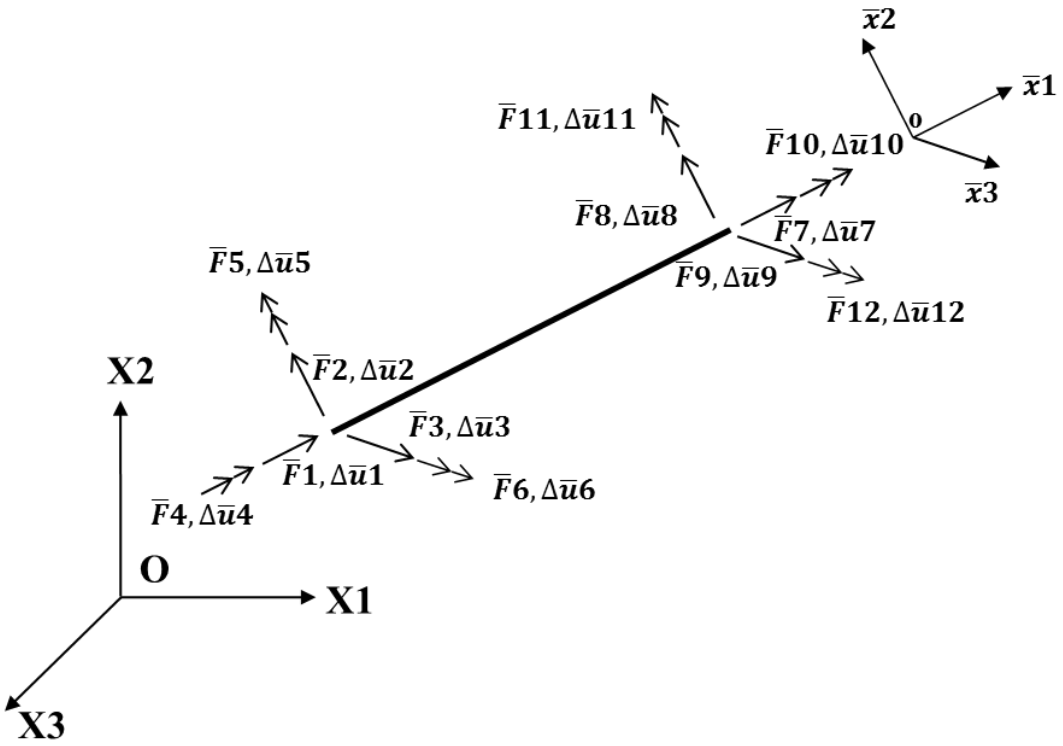

Figure 4.6 Member deformations and associated forces in local axes

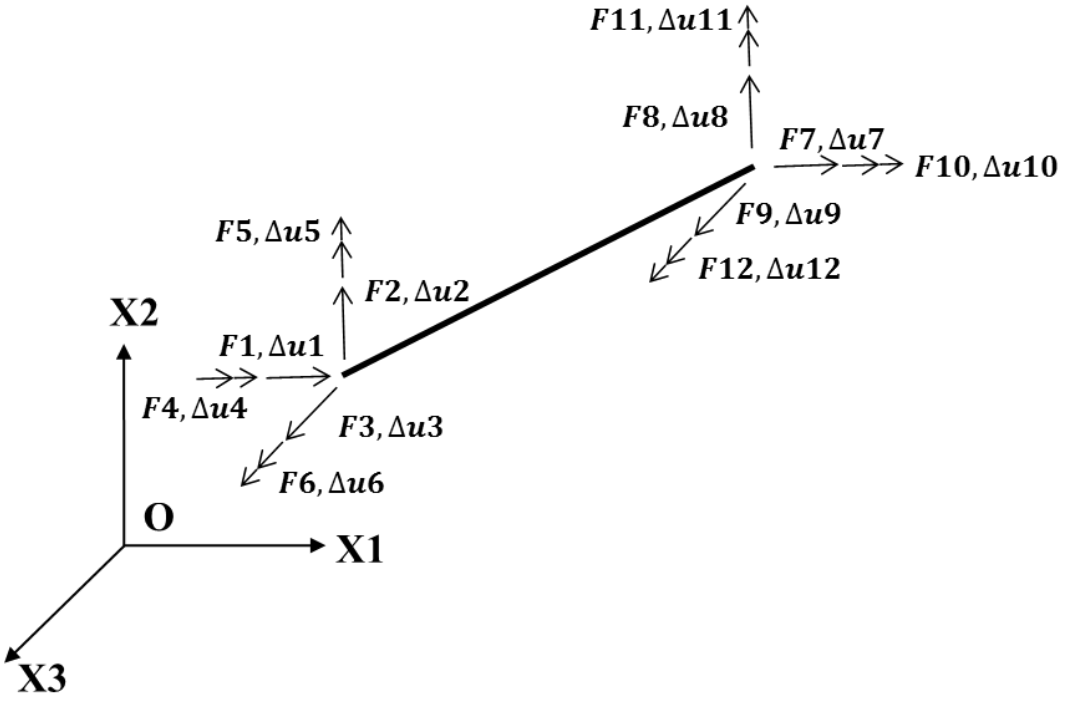

Figure 4.7 Member deformations and associated forces in global axes

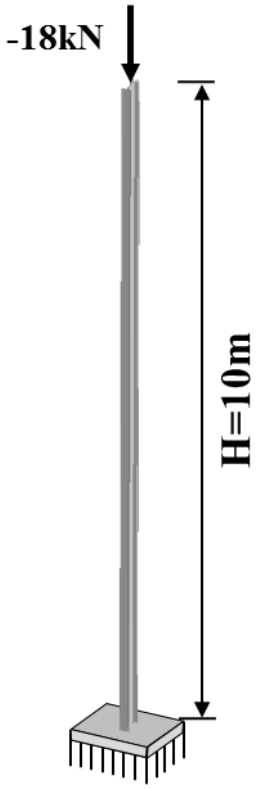

Figure 4.8 Geometry and loadings of the cantilever column

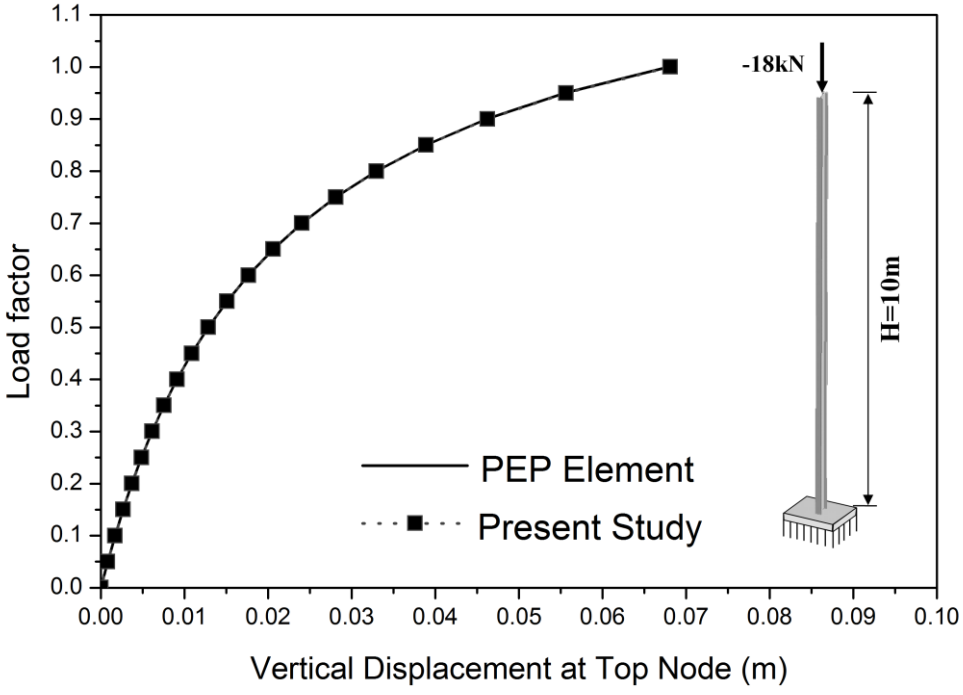

Figure 4.9 Vertical displacement at the top node

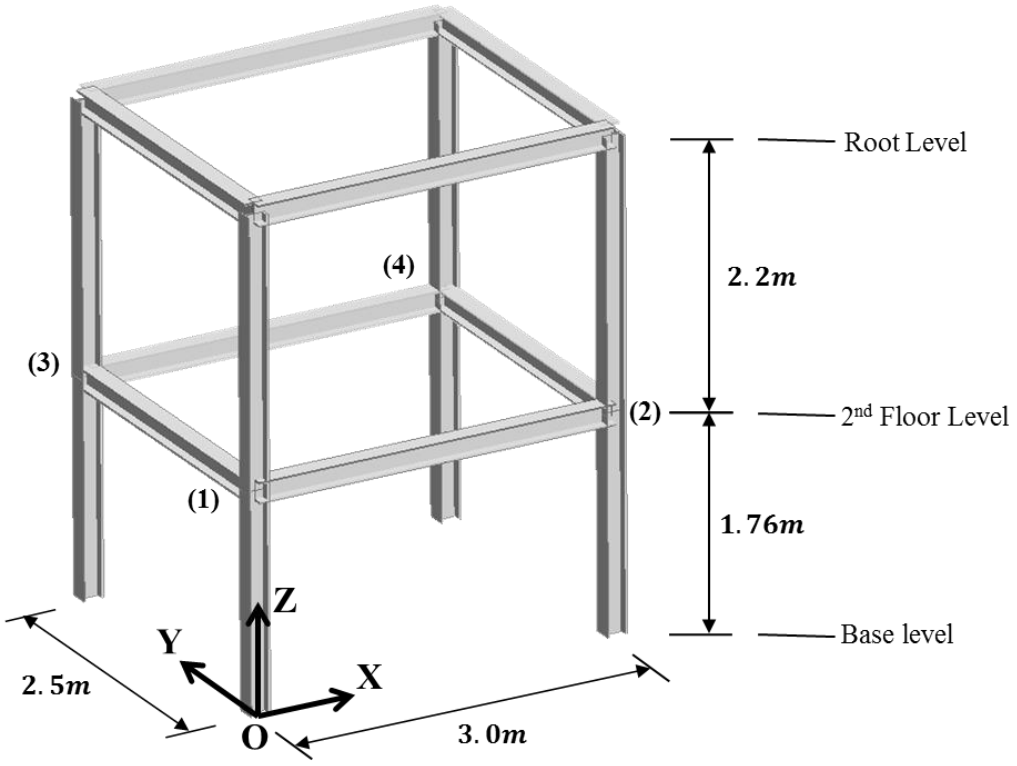

(a) Dimensions and section layout

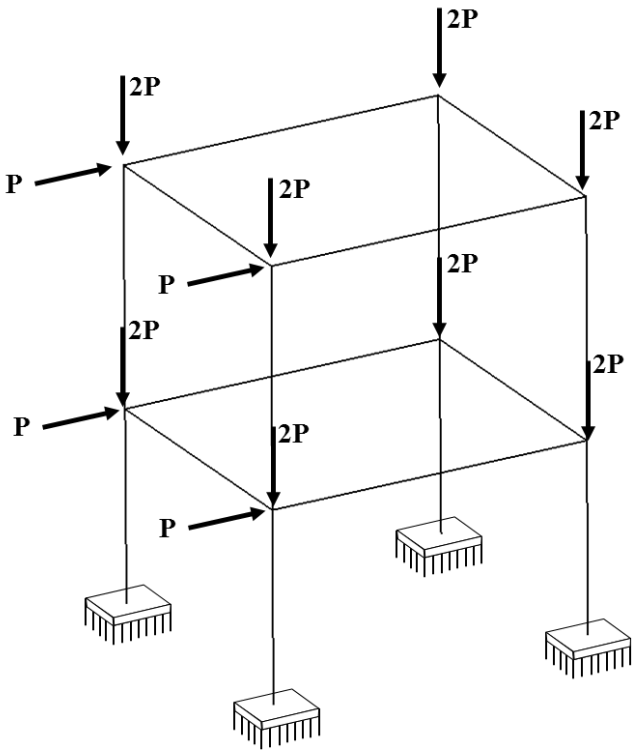

(b) Loadings and boundary conditions

Figure 4.10 Geometry and loadings of two story space frame with I section

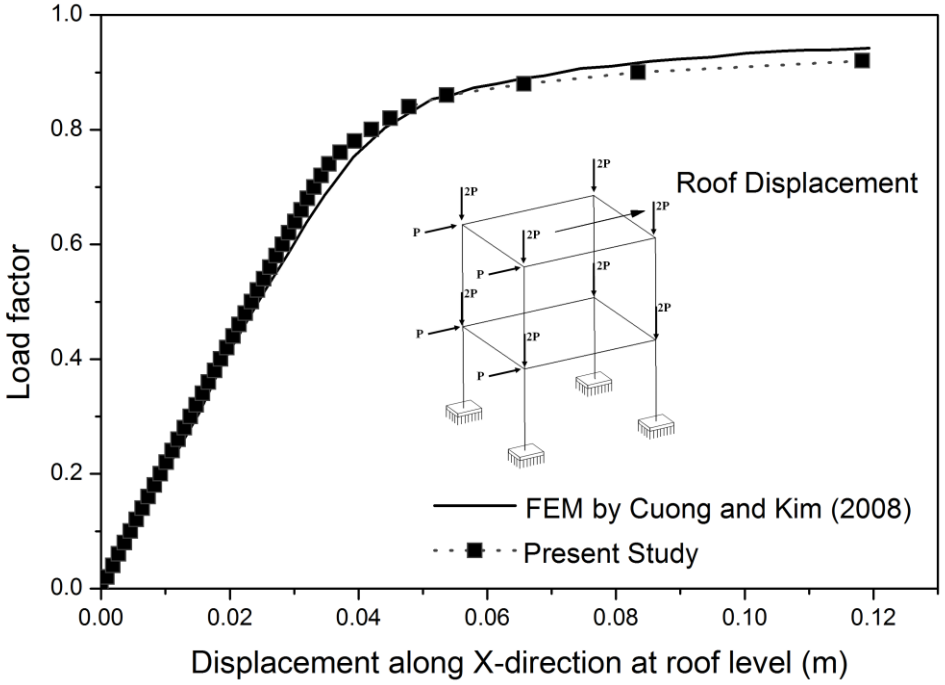

Figure 4.11 Displacement along X-direction at the roof level

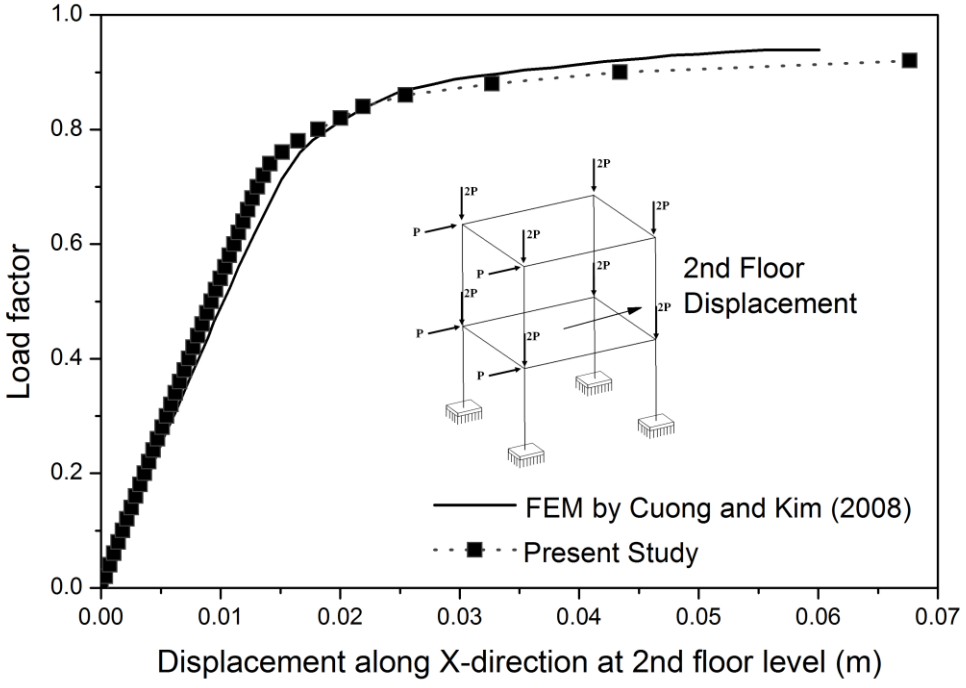

Figure 4.12 Displacement along X-direction at the 2nd floor level

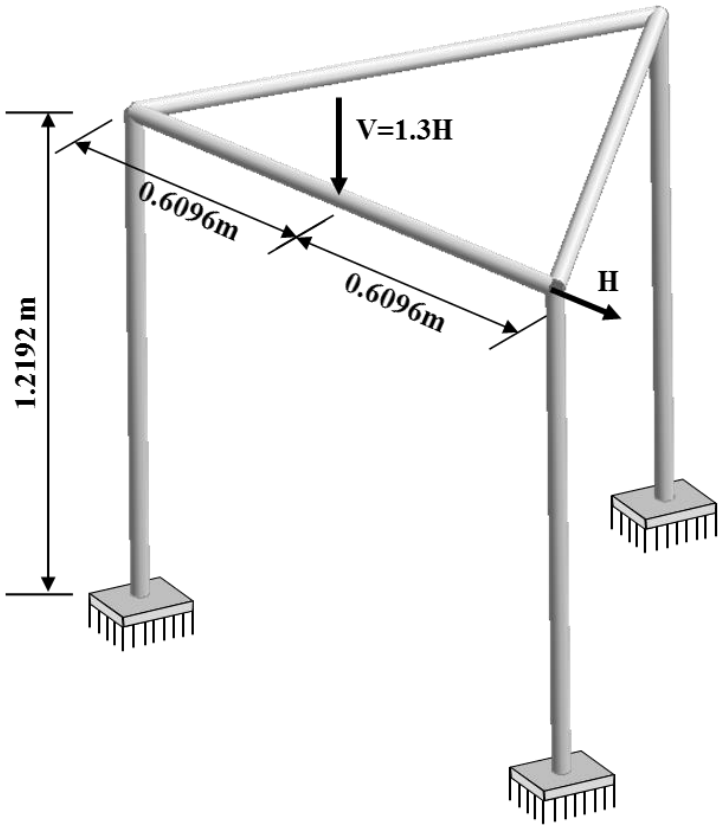

Figure 4.13 Geometry and loadings of the Harrison's space frame

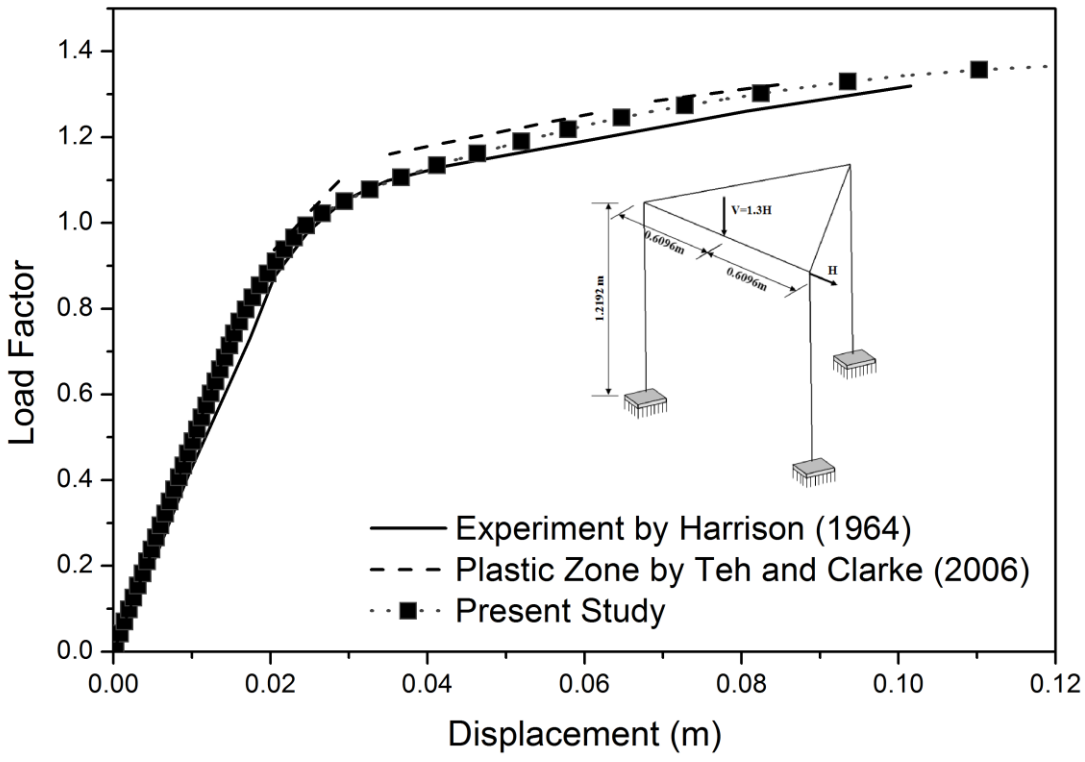

Figure 4.14 Horizontal sway of the Harrison's space frame

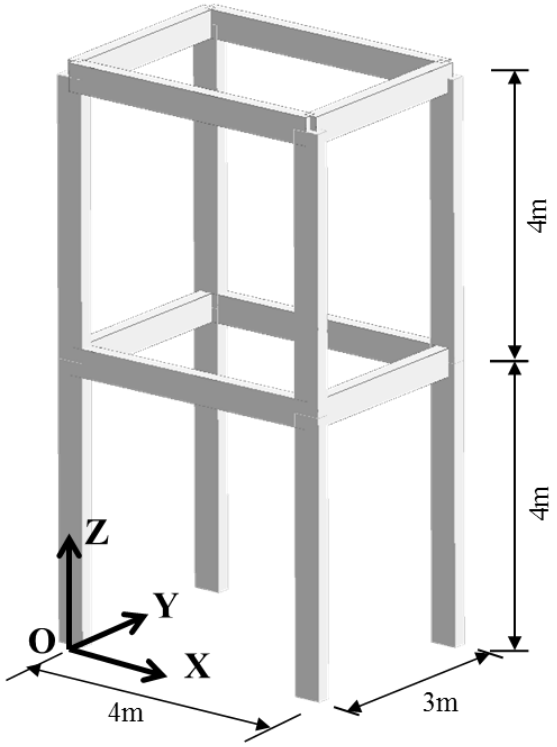

(a) Dimensions and section layout

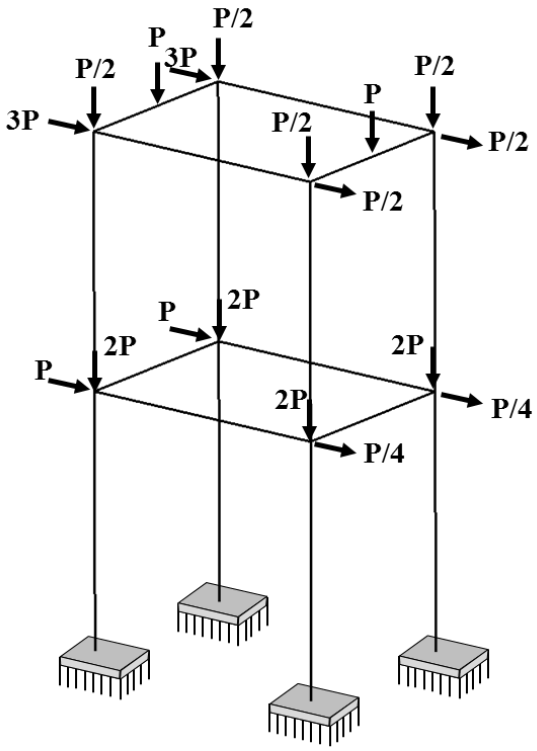

(b) Loadings and boundary conditions

Figure 4.15 Geometry and loadings of two story frame with rectangular section

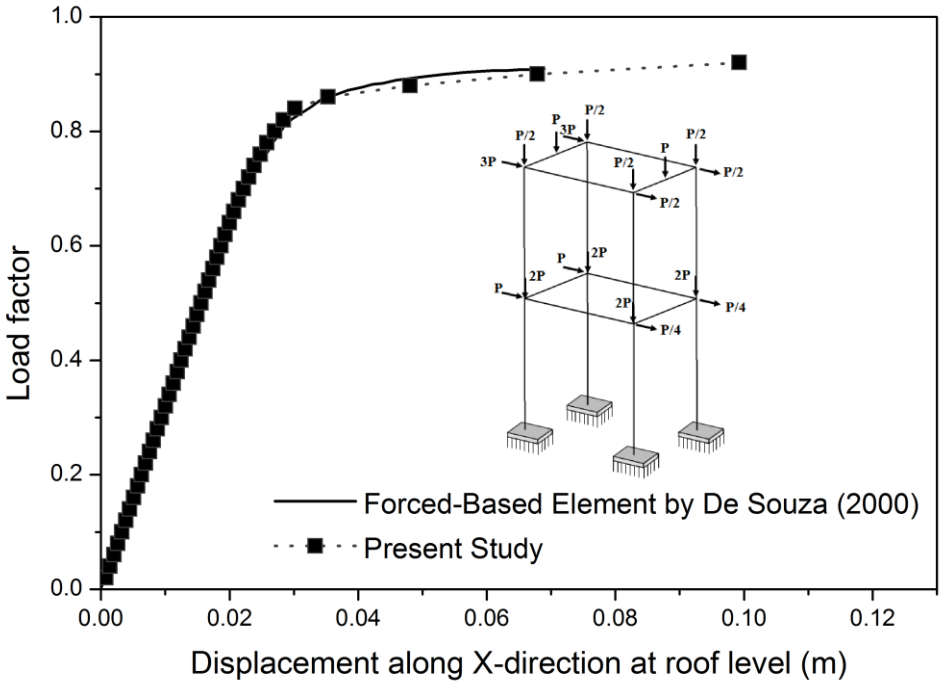

Figure 4.16 Horizontal displacement of the two story frame

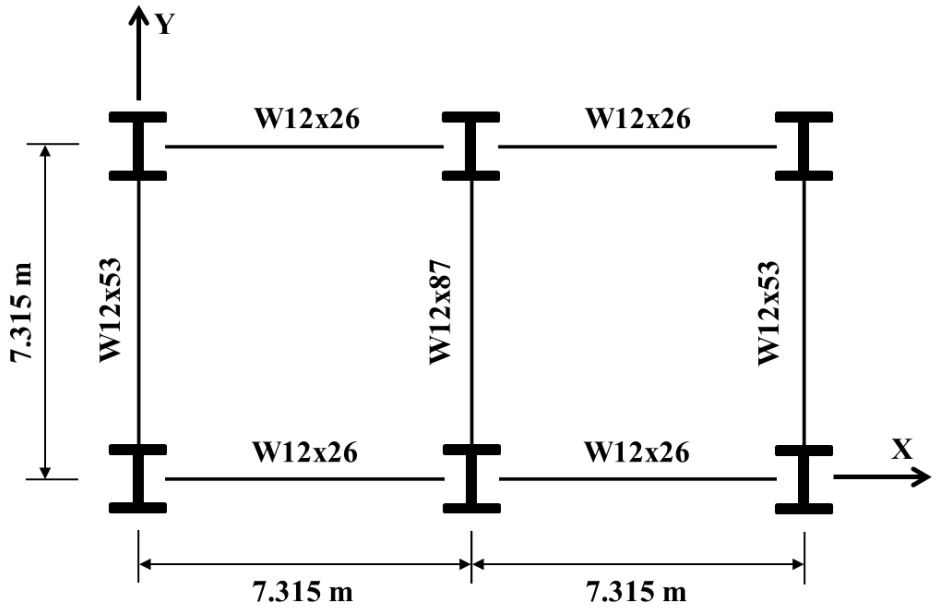

(a) Plan view

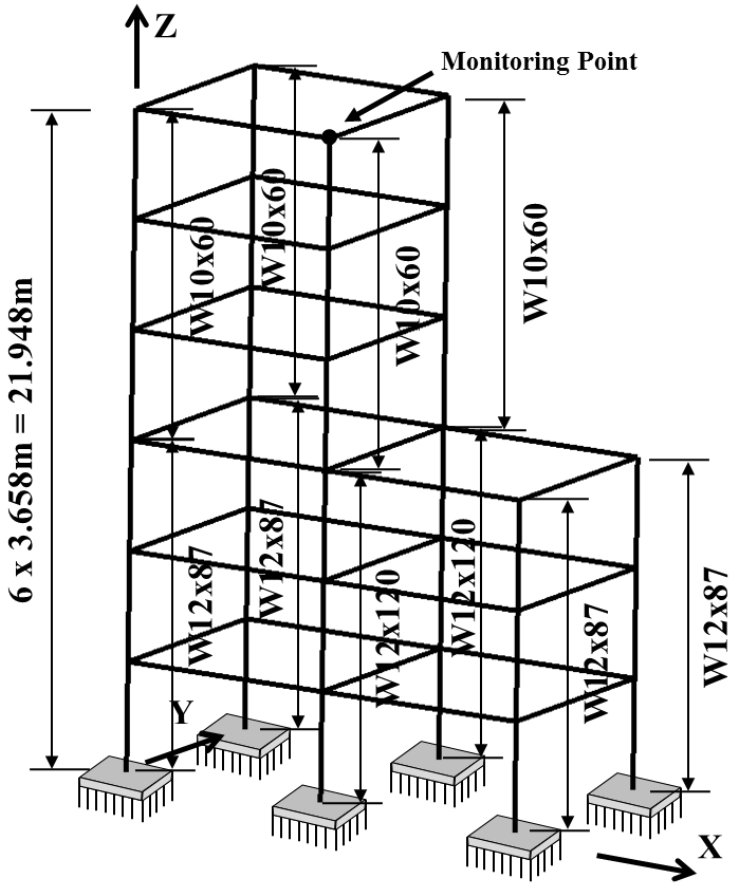

(b) Perspective view

Figure 4.17 Geometry of the six story space frame

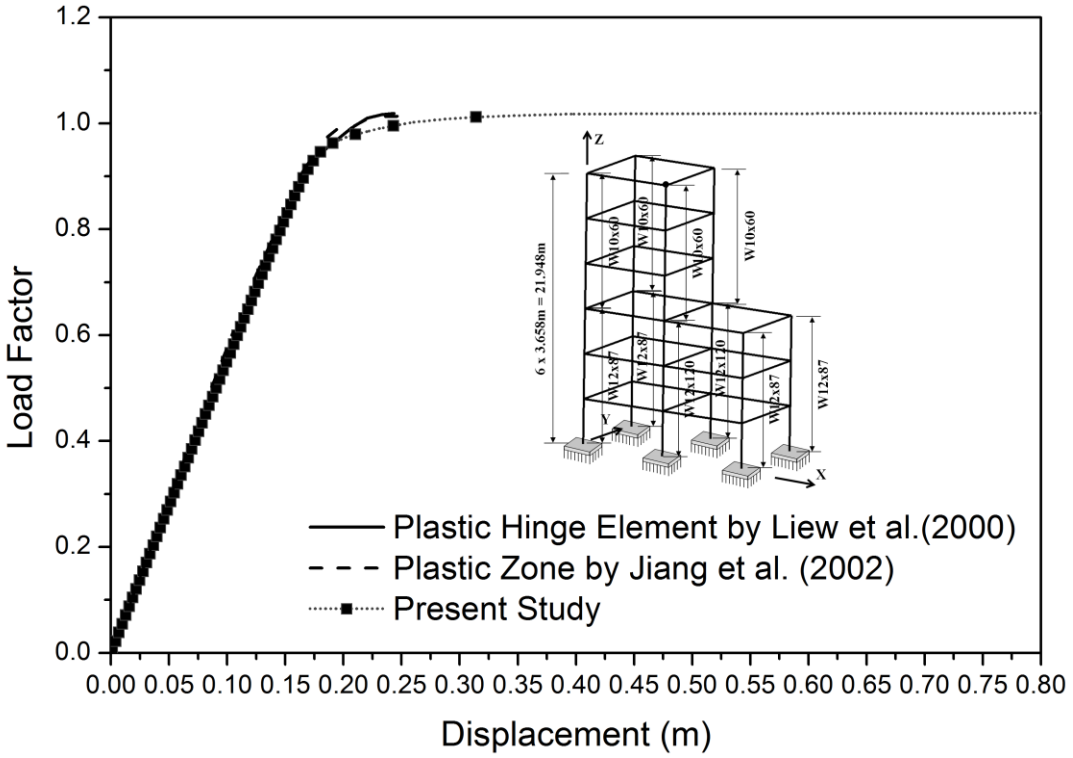

Figure 4.18 Load vs. displacement along Y-axis of the six story space frame

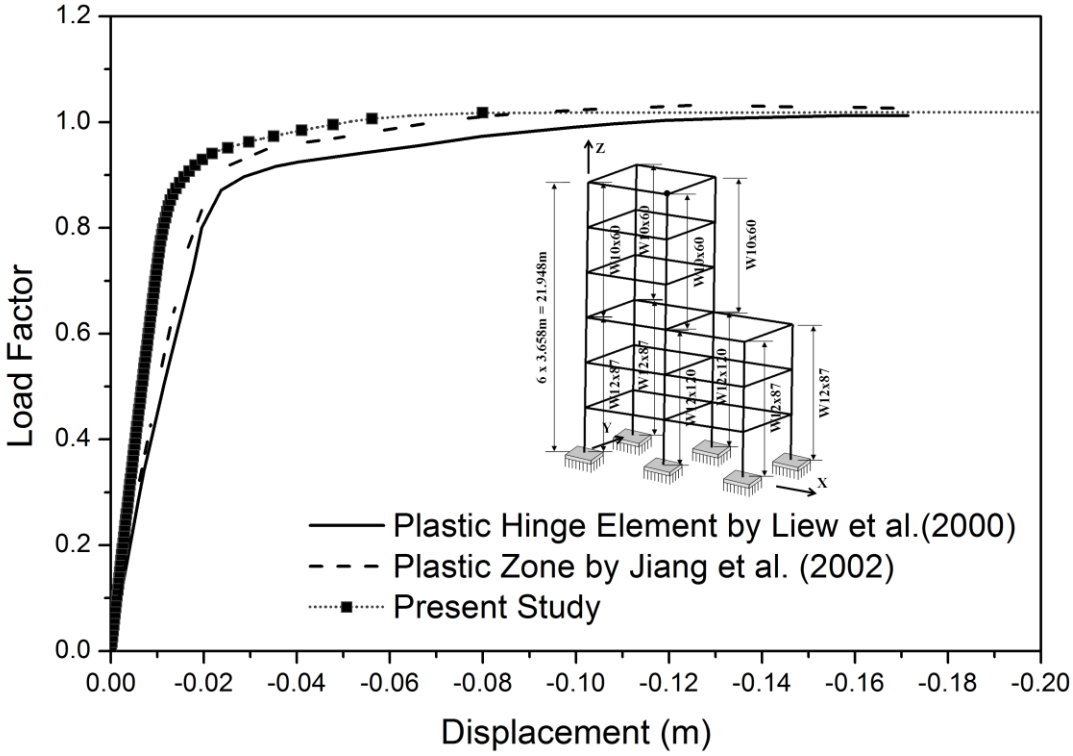

Figure 4.19 Load vs. displacement along X-axis of the six story space frame

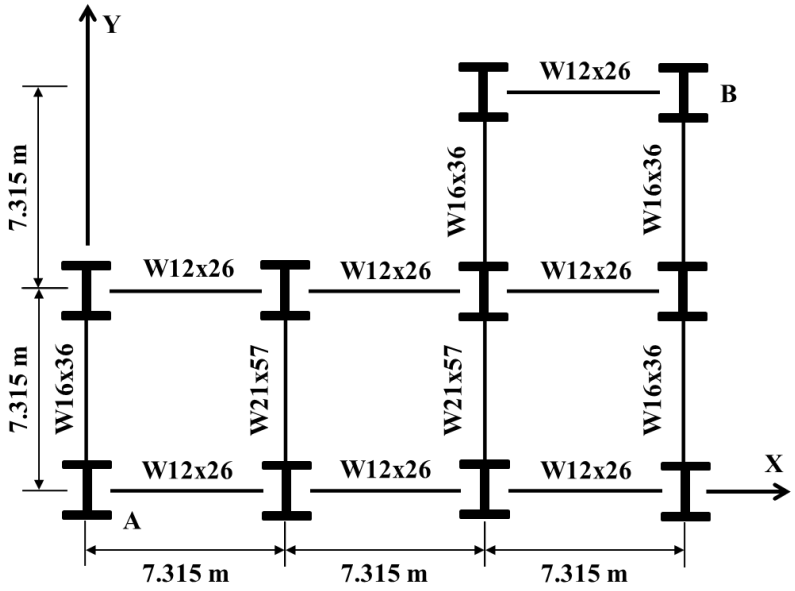

(a) Plan view

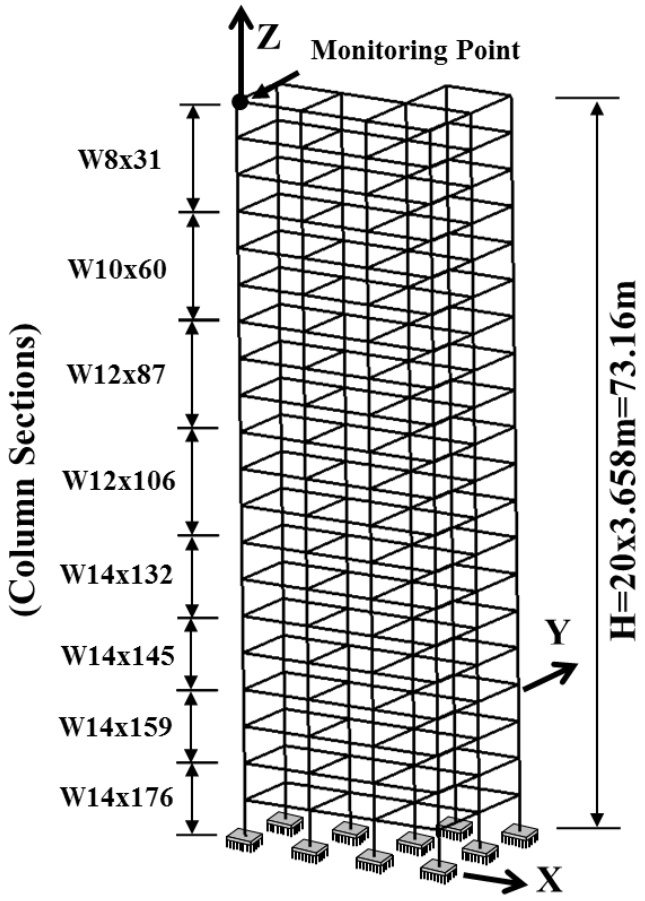

(b) Perspective view

Figure 4.20 Geometry of the twenty story space frame

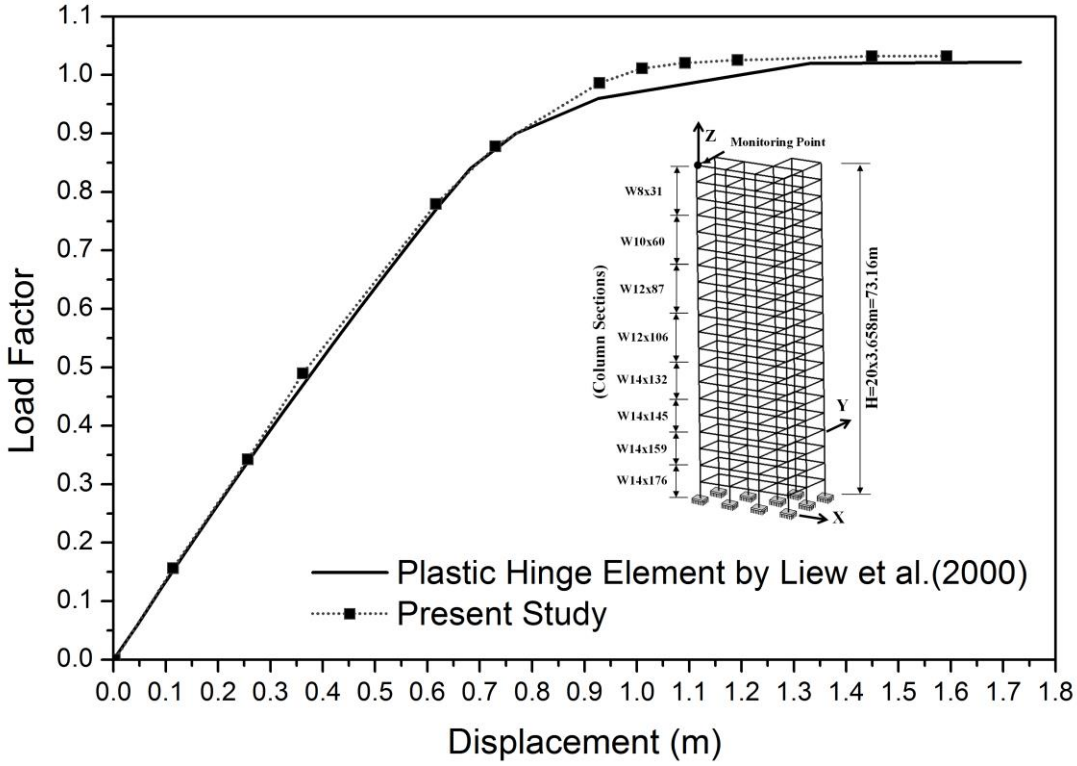

Figure 4.21 Roof displacement of the twenty story space frame

Tables

Table 4.1 Out-of-plumpness imperfection of two story space frame

Level	**Imperfection (mm)**							
	Column (1)		Column (2)		Column (3)		Column (4)	
	X	Y	X	Y	X	Y	X	Y
Roof	4.51	11.08	5.49	11.41	-8.17	6.58	-4.31	12.04
Second Floor	1.39	6.88	-0.68	6.77	-5.11	2.11	-3.96	6.19
Base	0	0	0	0	0	0	0	0

CHAPTER 5

SECTIONAL YIELD SURFACES FOR SECOND-ORDER DESIGN AND ADVANCED ANALYSIS

This chapter discusses a proposed cross-section analysis technique for arbitrary sections in a hybrid steel and concrete frame. To calculate sectional capacity, a quasi-Newton iterative scheme is adopted in determining the neutral axis of a section. This study puts forward two types of stress resultant approaches for concrete components, namely, the equivalent stress block method and elaborated layer-integration method. The former is limited to the ultimate limit state, whereas the latter is valid for any specified conditions. A structural steel component is automatically meshed into small fibers and each rebar is lumped into a point that occupies a certain area. The openings and voids occupied by other components are removed by the negative area approach. Three types of sectional yield surfaces, i.e. failure, initial yield and concrete fracture surfaces, are introduced for further use in the proposed second-order design and advanced analysis. This analysis technique is discussed in the succeeding chapters. Finally, the effectiveness of the cross-section analysis technique is verified on the basis of published works and design codes.

5.1. Introduction

Sectional states are to be examined for both the second-order design and advanced analysis. To this end, the evaluation approach based on sectional yield surfaces is adopted. Sequentially, three types of strength interaction surfaces (Figure 2.1) for a section of a beam-column element are introduced; these surfaces are the failure, initial yield and concrete fracture surfaces. A failure surface defines the ultimate limit state of a cross-section and can be easily found in conventional design charts; it is commonly used in elastic analysis to verify member strength. An initial yield surface is the controlling boundary condition that determines elastic limit. These two surfaces divide a loading space into elastic, elasto-plastic and plastic zones, which represent different states of sectional strength. These surfaces are also further used in the present refined plastic hinge model. A concrete fracture surface (Figure 5.2) is used to determine the limits for crushing or cracking fractures. Figure 5.2 shows that the upper zone of the concrete fracture surface is controlled by concrete crushing, whereas the lower zone is the crack surface controlled by tensile fracture.

The ultimate capacity of a section usually describes a failure surface, which is also usually called a full yield surface; this capacity is extensively adopted in design practice. The concept of a failure surface was proposed by Dafalias *et al*. (1975), who incorporated it into the construction of a model that describes material behavior under complex multi-axial loading. This model is particularly suitable for cyclic loading conditions and has been extended to soil analysis (Dafalias, 1979). Sfakianakis (1991; 1997, 1998), De Vivo *et al*. (1998) and El-Tawil *et al*. (2001a,

2001b) used this concept as basis for constructing the failure surfaces of regular and irregular reinforced concrete sections. Their research shows that the sizes and shapes of failure surfaces are significantly influenced by reinforcing bar arrangement and sectional geometry. Attalla *et al*. (1994), Chan *et al*. (1997), Liew *et al*. (2000a) and Jiang *et al*. (2002) carried out beam-column finite element analysis to propose similar methods for the conventional design and advanced plastic analysis of structural steel sections associated with use of the failure surface. Moreover, Chen *et al*. (2001), Sfakianakis *et al*. (2002) and Charalampakis *et al*. (2008) developed several cross-section analysis techniques for irregular composite sections with arbitrarily arranged structural steels and reinforcing bars.

In the present study, a quasi-Newton method is introduced to determine the height of the neutral axis of a section and the capacity of arbitrary cross-sections can be obtained. An entire steel section is meshed into small fibers for stress integration, and the openings and voids occupied by steel sections and reinforcing bars are removed by the negative area approach. To calculate the stress resultants of concrete components, either the equivalent stress block method or the elaborated layer integration method can be used. The first approach is simple and has been widely employed in concrete design codes, but is limited to the determination of ultimate sectional capacity. The second approach is more rigorous, accurate and suitable for use under any sectional state; this flexibility is attributed to the fact that the concrete zone is divided into parallel layers. Given that only a slight difference in derived ultimate sectional capacity occurs between these two approaches, the equivalent stress block method is recommended for failure surfaces because of its simplicity

and the elaborated layer-integration method is suggested for other limit states, such as initial yield or cracking onset.

In this chapter, the cross-section analysis technique is presented in detail and the proposed sectional yield surfaces are briefly explained. Finally, the effectiveness of the proposed analysis technique for arbitrary sections is verified on the basis of published works.

5.2. Assumptions

For the cross-section analysis in this research, the following basic assumptions are adopted:

1) Plane sections before deformation remain in plane after deformation, suggesting linear strain distribution across section depth. This observation corresponds to the classical Bernoulli–Navier hypothesis in line with the assumption for analysis by beam-column elements.
2) The bond slip between concrete and steel is prevented and full strain compatibility between steel and surrounding concrete is assumed.
3) Steel reinforcement embedded in concrete does not buckle under compression.
4) Compressive stresses and strains are positive, as typically assumed in cross-section analysis.

5) The tensile strength of concrete is considered only in the calculation of sectional strength before cracking. Except for this calculation, such tensile strength is disregarded.

The definition of the positive direction of the axial compression in cross-section analysis contrasts with that in the beam-column element assumptions presented in the previous chapters. This assumption for the positive direction is commonly found in conventional design practice for cross-section analysis. Therefore, the forces and moments obtained from the analysis by beam-column elements should be revised in the section strength checks. Accordingly, tensile stress and strain are assumed negative in cross-section analysis.

5.3. Cross-section analysis technique

This segment of the thesis discusses the sectional analysis of arbitrarily shaped sections, which may consist of four components: unconfined and confined concrete, rebars, structural steels and openings. An arbitrarily shaped cross-section with arbitrarily arranged reinforcing bars and structural steels subjected to bi-axially eccentric loading is shown in Figure 5.3. All the concrete and opening components are inputted by the vertices, which have the coordinates Y_i, Z_i with respect to the global Y-, Z-axes. For curved or circular components, the boundary line is approximated as a polygon, in which accuracy depends on the number of vertices. The steel component is automatically meshed into a given number of small triangular

fibers, each treated in the same manner as an individual rebar in the analysis. The mesh algorithm proposed by Niceno (2002) for steel components is introduced.

5.3.1 Referenced loading axes

Figure 5.3 shows that the location of the neutral axis can be determined by two variables, i.e. orientation angle θ_n and the depth d_n of the neutral axis. Brondum-Nielsen (1985) and Yen (1991) used a quasi-Newton method to identify θ_n and d_n; this method effectively and efficiently determines the neutral axes and failure surfaces of regularly shaped cross-sections. The authors adopted the geometric centroid as the origin of reference loading axes, which can be calculated as,

$$Z_{gc} = \frac{A_c Z_c + A_r Z_r + A_s Z_s - A_o Z_o}{A_c + A_r + A_s - A_o} \tag{5. 1}$$

$$Y_{gc} = \frac{A_c Y_c + A_r Y_r + A_s Y_s - A_o Y_o}{A_c + A_r + A_s - A_o} \tag{5. 2}$$

where A_c, A_r, A_s and A_o are the areas of concrete, reinforcing bars, structural steels and openings, respectively; Z_c, Y_c, Z_r, Y_r, Z_s, Y_s, Z_o and Y_o are the centroid coordinates of each component; and Z_{gc} and Y_{gc} are the coordinates of the geometric centroid of an entire section.

Conversely, Chen *et al*. (2001) reported that this technique does not always converge when it is applied to irregularly shaped cross-sections, especially when the arrangement of reinforcing bars and structural steels is highly eccentric. Chen *et al*. (2001) proposed that the aforementioned convergence problem can be overcome by using the plastic centroid as the origin of reference loading axes; meanwhile, the

number of iterations for convergence can be reduced. For an arbitrarily shaped composite cross-section, the plastic centroid may be determined thus (Roik & Bergmann, 1990):

$$Z_{pc} = \frac{A_c Z_c f_c / \gamma_c + A_r Z_r f_r / \gamma_r + A_s Z_s f_s / \gamma_s - A_o Z_o f_c / \gamma_c}{A_c f_c / \gamma_c + A_r f_r / \gamma_r + A_s f_s / \gamma_s - A_o f_c / \gamma_c} \tag{5. 3}$$

$$Y_{pc} = \frac{A_c Y_c f_c / \gamma_c + A_r Y_r f_r / \gamma_r + A_s Y_s f_s / \gamma_s - A_o Y_o f_c / \gamma_c}{A_c f_c / \gamma_c + A_r f_r / \gamma_r + A_s f_s / \gamma_s - A_o f_c / \gamma_c} \tag{5. 4}$$

in which f_c, f_r and f_s denote the characteristic strengths of concrete, reinforcing bars and structural steels, respectively; γ_c, γ_r and γ_s represent the corresponding partial safety factors; and Z_{pc} and Y_{pc} are the coordinates of the plastic centroid of the entire section.

Given the Euler–Bernoulli hypothesis in beam-column finite element analysis, the generalized force and moments should correspond to the origin of the geometric centroid. To ensure consistency, the moment capacities calculated at the plastic centroid should be converted into values by corresponding to the geometric centroid. The conversion of moments is described in the succeeding sections.

5.3.2 Coordinate systems

Three coordinate systems, namely ZCY, zoy and uov, are used to describe the analysis procedure. The ZCY system is intended to describe a cross-section defined by designers. The zoy and uov systems have the same origin as the plastic centroid of the cross-section. The geometric and plastic centroid can be readily determined. Thus, the entire iterative process involves only two rounds of coordinate conversion:

conversion from the global ZCY system to the load reference zoy system and that from the zoy system to the uov system, in which the u-axis is parallel to the neutral axis.

The coordinate conversion equations are written as,

$$z = Z - Z_{pc} \tag{5. 5}$$

$$y = Y - Y_{pc} \tag{5. 6}$$

$$u = z\cos\theta_n + y\sin\theta_n \tag{5. 7}$$

$$v = y\cos\theta_n - z\sin\theta_n \tag{5. 8}$$

where Z and Y, z and y and u and v are the coordinates in the ZCY, zoy and uov systems, respectively.

5.3.3 Stress resultants in concrete by equivalent stress block method

In calculating the stress resultant of concrete under ultimate crushing, Whitney's stress block (1965) (Figure 5.4) is introduced in the integration of parabola stress distribution, which is widely adopted in many national concrete codes. The strain of the most externally located fiber is taken as crushing strain ε_{cu} and tensile strength is usually disregarded at the ultimate state.

The equivalent stress block method is limited to the generation of stress resultants under the ultimate failure state. The stress resultants of other limit states can be obtained by more comprehensively elaborated layer-integration approaches. The difference between these two methods is minimal under ultimate limit state, as

demonstrated in the verification examples. The equivalent stress block method is more suitable for calculating the stress resultant of concrete under the ultimate limit state. The mathematical expressions for such calculation are as follows:

$$N_{xc} = \left| \sum_{i=1}^{n_c} N_{xci}^{e} \right| = \left| \sum_{i=1}^{n_c} \int_{u_i}^{u_{i+1}} \int_{0}^{\bar{v}(u)} \alpha f_c \, du d\bar{v} \right| \tag{5. 9}$$

$$M_{uc} = \rho \sum_{i=1}^{n_c} M_{uci}^{e} = \rho \sum_{i=1}^{n_c} \int_{u_i}^{u_{i+1}} \int_{0}^{\bar{v}(u)} [-\alpha f_c (\bar{v} + v_n)] du d\bar{v} \tag{5. 10}$$

$$M_{vc} = \rho \sum_{i=1}^{n_c} M_{vci}^{e} = \rho \sum_{i=1}^{n_c} \int_{u_i}^{u_{i+1}} \int_{0}^{\bar{v}(u)} \alpha f_c u du d\bar{v} \tag{5. 11}$$

where n_c is the number of vertices of the compression zone; $\bar{v}(u)$ is the linear equation of the boundary line equal to $v(u) - v_n$, with v_n being the coordinate of the neutral axis in the v-axis; ρ is equal to +1 when $N_{zc} > 0$ and –1 when $N_{zc} < 0$.

5.3.4 Stress resultants in concrete by elaborated integration method

As previously stated, the concrete zone is divided into several layer segments (Figure 5.5) for a more accurate integration of stress in concrete components. Given that stress and strain distributions are the same under identical vertical levels in a local rotation axis, the fibers in each layer segment are of the same strain value and the method for dividing layer segments involves less computation, making it more efficient than conventional sectional fiber discretization. Except for the generation of the concrete fracture surface of a section, the entire concrete zone should be divided into sub-zones; the tension zone of concrete is disregarded.

The proposed approach for layer segment integration is applicable to the generation of any yield or control surface, with the approach implemented through adjustments in strain value at the most externally located fiber. A stress vs. strain model should be used to determine stress distribution. Adequate segments are required for acceptable accuracy. The mathematical formulae are as follows:

$$N_{xc} = \sum_{i=1}^{n_L} N_{xci}^{L} = \sum_{i=1}^{n_L} \sum_{j=1}^{n_v(i)} \int_{u_j^i}^{u_{j+1}^i} \int_0^{\bar{v}(n)} \sigma_c^i \, du d\bar{v} \tag{5. 12}$$

$$M_{uc} = \rho \sum_{i=1}^{n_L} M_{uci}^{L} = \rho \sum_{i=1}^{n_L} \sum_{j=1}^{n_v(i)} \int_{u_j^i}^{u_{j+1}^i} \int_0^{\bar{v}(n)} [-\sigma_c^i (\bar{v} + v_n)] du d\bar{v} \tag{5. 13}$$

$$M_{vc} = \rho \sum_{i=1}^{n_L} M_{vci}^{L} = \rho \sum_{i=1}^{n_L} \sum_{j=1}^{n_v(i)} \int_{u_j^i}^{u_{j+1}^i} \int_0^{\bar{v}(n)} \sigma_c^i u \, du d\bar{v} \tag{5. 14}$$

where n_L is the number of sectional layers and $n_v(i)$ denotes the number of intersection points in the corresponding layers.

5.3.5 Stress resultants in steel

Each rebar is treated as an individual fiber as structural steel is meshed into fibers with rectangular areas. The stress resultants of steel sections and reinforcements can be computed thus:

$$N_{xs} = \sum_{j=1}^{n_r} \sigma_{rj} A_{rj} + \sum_{k=1}^{n_s} \sigma_{sk} A_{sk} \tag{5. 15}$$

$$M_{us} = -\sum_{j=1}^{n_r} \sigma_{rj} A_{rj} v_{rj} - \sum_{k=1}^{n_s} \sigma_{sk} A_{sk} v_{sk} \tag{5. 16}$$

$$M_{vs} = \sum_{j=1}^{n_r} \sigma_{rj} A_{rj} u_{rj} + \sum_{k=1}^{n_s} \sigma_{sk} A_{sk} u_{sk} \tag{5. 17}$$

where A_{rj} and A_{sk} are the areas of discrete fibers and reinforcing bar respectively; and σ_{rj} and σ_{sk} are the corresponding stress values.

5.3.6 Opening area

The negative area approach is used to remove the voids occupied by the steel components and openings in a section.

5.3.7 Total force and moments

The bending moments obtained from the above-mentioned equations are summed and then converted into the xoy system by the transformations below. The moments generated from the cross-section analysis are based on the origin of the plastic centroid, which should be converted into reference loading axes, i.e. the origin of the geometric centroid:

$$N_x = N_{xc} + N_{xs} - N_{xo} \tag{5. 18}$$

$$M_u = M_{uc} + M_{us} - M_{uo} \tag{5. 19}$$

$$M_v = M_{vc} + M_{vs} - M_{vo} \tag{5. 20}$$

$$M_{pz} = M_u \cos\theta_n - M_v \sin\theta_n \tag{5. 21}$$

$$M_{py} = M_u \sin\theta_n + M_v \cos\theta_n \tag{5. 22}$$

$$M_z = M_{pz} + N_x(Z_{gc} - Z_{pc}) \tag{5. 23}$$

$$M_y = M_{py} + N_x(Y_{gc} - Y_{pc}) \tag{5. 24}$$

where N_x, M_u and M_v are the axial force and bending moments with reference to uov axes; M_{py} and M_{pz} are the bending moments in relation to local yoz axes with the origin of the plastic centroid; and M_y and M_z are the output moments with reference to the geometric centroid.

5.3.8 Iteration scheme

Section capacity can be precisely determined by rotating the orientation θ_n of the neutral axis from $0°$ to $360°$ with changing depth d_n. The Regula–Falsi numerical method is used to derive equilibrium, compatibility and constitutive relationships. The procedure for sectional analysis is illustrated in Figure 5.6.

Axial force capacity N_x is iterated with respect to d_n by the following equation, with θ_n kept constant:

$$d_{n,k} = d_n + \frac{d_n^{'} - d_n}{N_x^{'} - N_x}(N_{xd} - N_x) \tag{5. 25}$$

where $d_{n,k}$ is the depth of the updated neutral axis; d_n and d_n' are the depths of the neutral axis with axial capacity being smaller and greater than the design value, respectively; N_x and N_x' are the axial force capacities calculated at d_n and d_n'; and N_{xd} is the current design axial loading.

5.4. Sectional yield surfaces

Any specified bending moment capacity under a given axial force can be obtained by adopting the cross-section analysis technique presented in the above-

mentioned section. Thus, tri-axial strength interaction surfaces are introduced in the second-order design and advanced analysis. These surfaces, also called the sectional yield surfaces of a cross-section, are defined by axial loads and corresponding moments. Three section yield surfaces are introduced: failure, initial yield and concrete fracture surfaces (Figure 2.1).

5.4.1 Failure surface

The outermost surface in Figure 2.1 is a failure surface. The points in the figure define the ultimate limit state of a cross-section to which the loads at these points cause sectional damage by either concrete crushing or steel fracture. This surface is essential for determining individual load-bearing states in conventional designs.

Many national codes provide the basic formulae for generating failure surfaces under normal situations. A uni-axial bending condition can be treated as a specific plane that intersects the sectional yield surface. Some researchers have put forward simplified equations that describe these planar failure surfaces to avoid complexity and save on computational time in generating failure surfaces for bi-axial analysis. Such avoidance is not adopted in the present research because yield surfaces can be pre-constructed and interaction points are specifically indexed by the proposed indexing method, thereby dramatically reducing computational time.

5.4.2 Initial yield surface

Apart from the failure surface, the initial yield surface is also a fundamental strength control criterion for the plastic hinge method proposed in this study. The initial yield surface is the boundary surface within a particular load combination; it has no material yielding and its cross-section remains elastic. This elastic limit is an approximate assumption for numerical analysis, causing slight deviations in the tracing of load versus deflection path in a gradual yield range. In this study, the elastic limit strains of concrete and steel are ε_{ce} and ε_{se}, respectively.

In generating initial yield surfaces, all sectional fibers are monitored and the onset of the strain of either concrete or steel components exceeding their elastic limits is detected. Sectional capacity is obtained from the state at initial yield and the stress along the cross-section is integrated to compute the internal force and moments. The upper limit of the initial yield surface is therefore controlled by concrete, whereas the lower limit is governed by steel.

5.4.3 Concrete fracture surface

In contrast to metal materials, which have isotropic properties, concrete weakens under tension and cracks under low tensile stress. In the inelastic analysis of RC and SCC members or frames, therefore, cracking-induced influence on the flexural stiffness of members should be considered. This incorporation into the analysis can be realized by reducing moments of inertia (discussed in the subsequent chapters).

As an extension of initial yield surface application, the fracture surface of concrete is first introduced in the consideration of cracking in beam-column element

analysis. The cracking surface is illustrated in Figure 5.2, which shows that the upper zone of the concrete fracture surface is controlled by concrete crushing, thereby causing overlap with the failure surface given that the same controlling criteria are used. The lower zone is the crack surface controlled by tensile fracture strain ε_{tu}.

5.4.4 Index of surfaces

This type of cross-section analysis has been criticized as more complicated and time consuming than the use of simplified equations in codes or certain studies. However, completely generating all yield surfaces in every iteration is impossible because such operation involves huge computational time. These two methods can be combined for optimally efficient and accurate design and analysis. One approach is to pre-generate failure surfaces prior to frame analysis and design. The other approach is to index interaction points to accelerate search speed, with minimal storage required for recording strength interaction surfaces. The index approach and search technique are discussed in this section.

The index vector is denoted as $\vec{\Gamma}(\varsigma,\eta)$ and the position coordinates ς and η are expressed as,

$$\varsigma_i = N_{xi} / \Delta N \tag{5. 26}$$

$$\eta_i = \tan^{-1}(M_{yi} / M_{zi}) / \Delta\theta \tag{5. 27}$$

Here, ΔN is the axial load increment of the yield surfaces and $\Delta\theta$ is the rotation increment of the moment capacity curve under axial force N_{xi}. Then the strength of interaction surfaces can be expressed as follows:

$$\Omega = \left(\vec{\Gamma}(\varsigma,\eta), m\right) \text{ and } m=1,2,3 \tag{5. 28}$$

where Ω is the indexed strength interaction surface and the failure, initial yield and concrete fracture surfaces can be written as Ω_f, Ω_e and Ω_c respectively. The corresponding axial force and moments can be obtained, thus:

$$N_{xi} = \Omega\left\{\vec{\Gamma}(\varsigma_i,\eta_i),1\right\} \tag{5. 29}$$

$$M_{yi} = \Omega\left\{\vec{\Gamma}(\varsigma_i,\eta_i),2\right\} \tag{5. 30}$$

$$M_{zi} = \Omega\left\{\vec{\Gamma}(\varsigma_i,\eta_i),3\right\} \tag{5. 31}$$

The applied force vector is expressed as $(N_{xa}, M_{ya}, M_{za})^T$ and converted into the index vector as $(\varsigma_a, \eta_a)^T$ using the equations above. Intersection point $(N_{xn}, M_{yn}, M_{zn})^T$ can be obtained by the following equations:

$$N_{xn} = N_{xa} \tag{5. 32}$$

$$\Omega\left\{\vec{\Gamma}(\varsigma_a,\eta_i),m\right\} = \Omega\left\{\vec{\Gamma}(\varsigma_i,\eta_i),m\right\} + \frac{\varsigma_a-\varsigma_i}{\varsigma_{i+1}-\varsigma_i}\left(\Omega\left\{\vec{\Gamma}(\varsigma_{i+1},\eta_i),m\right\} - \Omega\left\{\vec{\Gamma}(\varsigma_i,\eta_i),m\right\}\right) \tag{5. 33}$$

$$\Omega\left\{\vec{\Gamma}(\varsigma_a,\eta_{i+1}),m\right\} = \Omega\left\{\vec{\Gamma}(\varsigma_i,\eta_{i+1}),m\right\} + \frac{\varsigma_a-\varsigma_i}{\varsigma_{i+1}-\varsigma_i}\left(\Omega\left\{\vec{\Gamma}(\varsigma_{i+1},\eta_{i+1}),m\right\} - \Omega\left\{\vec{\Gamma}(\varsigma_i,\eta_{i+1}),m\right\}\right) \tag{5. 34}$$

$$M_{yn} = \Omega\left\{\vec{\Gamma}(\varsigma_a,\eta_i),m\right\} + \frac{\eta_a-\eta_i}{\eta_{i+1}-\eta_i}\left(\Omega\left\{\vec{\Gamma}(\varsigma_a,\eta_{i+1}),m\right\} - \Omega\left\{\vec{\Gamma}(\varsigma_a,\eta_i),m\right\}\right) \text{ when m = 2} \tag{5. 35}$$

$$M_{zn} = \Omega\left\{\vec{\Gamma}(\varsigma_a,\eta_i),m\right\} + \frac{\eta_a-\eta_i}{\eta_{i+1}-\eta_i}\left(\Omega\left\{\vec{\Gamma}(\varsigma_a,\eta_{i+1}),m\right\} - \Omega\left\{\vec{\Gamma}(\varsigma_a,\eta_i),m\right\}\right) \text{ when m = 3} \tag{5. 36}$$

5.5. Verifications of the cross-section analysis technique

Computer software with a completely user-friendly interface (called RCD-2013) is developed on the basis of the analytical algorithm presented in this chapter. The core and user interface of the software are written using Fortran-90/95 and C#/C++, respectively (Figure 5.8). To illustrate the accuracy and efficiency of the analytical method and software, several benchmark examples are presented and compared.

5.5.1 Bi-axially loaded and doubly symmetric steel sections

In this example, three typical steel sections (i.e. wide flange, double web and circular hollow sections) subjected to bi-axial loading are analyzed. The results are compared with the benchmark solutions reported by Chen and Atsuta (1972). The steel grade and design yield stress adopted in the current work are A36 and 250 MPa, respectively. The steel sections are meshed into small fibers, a task that can be automatically executed in RCD-2013. The dimensions and meshed fibers are illustrated in Figure 5.9(a, b)–Figure 5.11(a, b). Because the sections are doubly symmetric, only a quarter of strength interaction curves are plotted.

The analysis results are shown in Figure 5.9(c)–Figure 5.11(c). The solid lines represent exact solutions and the dotted lines are the results obtained by the proposed analytical method. The findings exhibit minimal differences, which may be attributed to the length of the sectional fibers. In practice, fiber length is usually assumed as one-fifth of plate thickness, so that sufficient accuracy is guaranteed. The three sections are representative of other types of steel sections and can therefore be analyzed in the same manner.

The comparison of the results for the three sections confirms the feasibility and accuracy of the proposed method for complex loading conditions associated with axial loading and bi-axial bending. In design codes, bi-axial interactions are usually idealized as linear interpolation, leading to an overly conservative design in some instances. The proposed method generates more economical and safe designs.

5.5.2 Bi-axial analysis of an irregular composite cross-section

The bi-axial analysis of irregular composite cross-sections is another benchmark example given by Chen *et al*. (2001). Such complex composite cross-sections comprise an opening and structural steel section in an irregular concrete component (Figure 5.12). This example is useful for demonstrating the analytical performance and feasibility of the method for arbitrarily shaped sections. Obtaining a converged analysis result necessitates the use of the iteration scheme based on the reference point taken as the plastic centroid.

Figure 5.12 indicates that the complex cross-section consists of a polygonal concrete, a circular opening, 15 reinforcement bars of 18-mm diameter and a structural steel I-section. The characteristic strengths of concrete, reinforcing bars and structural steels are f_c=30, f_r=460 and f_s=355 N/mm^2, respectively, and the corresponding partial safety factors of the material are γ_c=1.50, γ_r=1.15 and γ_s=1.10, respectively. For easy comparison, the presents study uses the concrete stress vs. strain curve used by Chen *et al*. (2001):

$$\sigma_c = f_c\left(2\frac{\varepsilon}{\varepsilon_0} - \frac{\varepsilon^2}{\varepsilon_0{}^2}\right), \text{ for } \varepsilon \le \varepsilon_0 \qquad (5.\ 37)$$

$$\sigma_c = f_c, \text{ for } \varepsilon_0 \le \varepsilon \le \varepsilon_{cu} \quad (5.38)$$

where σ_c is the concrete compressive stress; ε is the concrete compressive strain; ε_0 and ε_{cu} represent the initial yield and fracture strains of concrete, respectively; and f_c denotes the design compressive stress of concrete.

Given the high irregularity of the present composite section, the plastic centroid is regarded as the origin of the reference loading axis in the iterative scheme to reduce the number of iterations and improve numerical convergence, as discussed by Chen *et al*. (2001) . The M_y-M_z interaction curve under a given axial load N_x=4120 kN is shown in Figure 5.13.

Figure 5.13 shows that the proposed method can produce almost the same results as those of Chen *et al*. (2001), indicating the accuracy of the proposed method for highly irregular composite sections. The complete three-dimensional view of the failure surface of the section is shown in Figure 5.14. Any loading point outside the surface reflects the failure of the section to resist applied load.

5.5.3 Rectangular reinforced concrete section analyzed by Eurocode 2

To demonstrate the advantages of the proposed analytical approach in conventional design practice, a typical rectangular reinforced concrete section is selected and designed in accordance with Eurocode 2 (2004) (Figure 5.15). In calculating the stress resultant by the proposed method, both the equivalent stress block method and elaborated layer-integration method are used. The failure surfaces

of the major and minor axes obtained by the proposed method are compared with those designed using Eurocode 2 (2004) (Figure 5.16 and Figure 5.17). The stress vs. strain curves of concrete and steel, as specified in Eurocode 2 (2004), are adopted in the proposed sectional analysis.

As shown in Figure 5.16, the proposed method produces almost the same results as those derived by manual calculation using the RC design code. The slight difference is due to the concrete area occupied by reinforcing bars: this area is commonly disregarded in manual calculation, but is considered in the proposed approach through the removal of voids. Thus, the latter generates more accurate results. Furthermore, the equivalent stress block method (Figure 5.16) and elaborated layer-integration approach (Figure 5.17) exhibit small differences at the ultimate failure state. Because the equivalent stress block method is much simpler and requires less computation time, it is recommended for design under the ultimate limit state.

5.5.4 Extensive testing of six typical RC sections

To validate the effectiveness of the proposed algorithms, six typical RC sections are extensively investigated. These sections are rectangular, T-shaped, L-shaped, C-shaped, G-shaped and multi-cell sections, which represent most of the commonly used sections in actual practice. The analysis results are compared with the data reported by De Vivo and Rosati (1998). The dimensions of each section are presented in Figure 5.18 to Figure 5.23, which indicate that the failure surfaces obtained by the proposed analysis method are close to the reported values. Moreover,

the iterative procedure is highly stable and no divergence amongst the sections occurs.

5.5.5 Typical composite sections analyzed by Eurocode 4

Two typical SCC sections, namely, concrete-encased and rectangular concrete-filled sections, are used to verify the accuracy of the proposed approach. The dimensions and material properties of these sections are shown in Figure 5.24 and Figure 5.26, respectively. The failure surfaces of the major and minor axes obtained by the proposed method are compared with those designed on the basis of Eurocode 4 (2004) (Figure 5.25 and Figure 5.27).

The results derived on the basis of the design code (Figure 5.25 and Figure 5.27) are obtained by the simplified design equations in Eurocode 4 (2004); such equations are limited to simple cases, including regular sections with doubly symmetrical structural steel. The proposed method, similar to the general method in Eurocode 4 (2004), can be applied to any composite sections characterized by arbitrary shapes, as well as arbitrary structural steel and rebar arrangements. The main difference between the two approaches lies in the assumption on the cross-sectional ultimate limit state. In the general method, the failure of the cross-section is controlled by concrete crushing; i.e. when the most externally located fiber of concrete reaches its crushing strain, the section is assumed failed. By contrast, the simplified method assumes that all components can reach their ultimate strains towards developing fully plastic moment capacity—a phenomenon that rarely occurs. This assumption also causes the over-estimation of moment capacity. Figure 5.25 and Figure 5.27

show that the moment capacities obtained by the simplified method are larger than those derived by the proposed method. For the encased composite section, the two curves exhibit a small difference under major bending but a large difference under minor bending. For the concrete-filled rectangular hollow section, the two results are very close because the confinement effect enlarges the concrete crushing strain. The discussion above demonstrates that the proposed cross-sectional analysis technique is accurate and efficient.

5.6. Concluding remarks

The cross-section technique with a divergence-proof iterative procedure precisely calculates the sectional yield surfaces of arbitrary sections subjected to bi-axial bending. Initial yield, failure and concrete fracture surfaces are analyzed and discussed. At the end of this chapter, several benchmarks and examples are presented, and the proposed cross-section analysis method is validated as accurate, efficient and reliable for any types of hybrid steel and concrete sections.

Figures

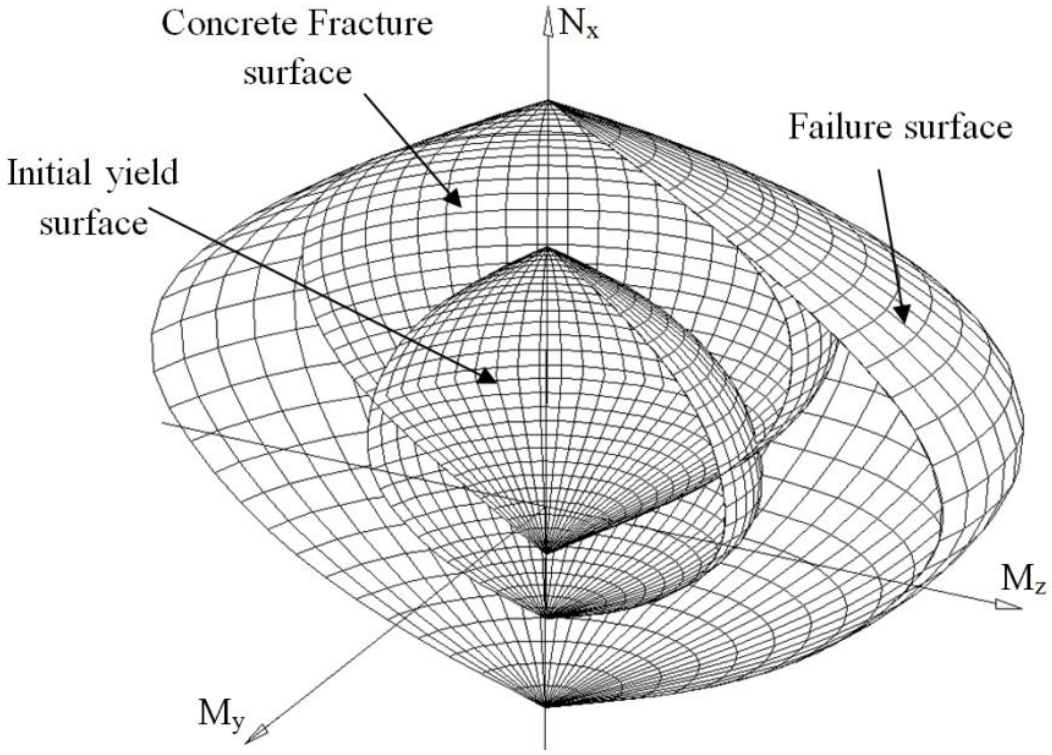

Figure 5.1 Illustration of failure, initial yield, concrete fracture surfaces

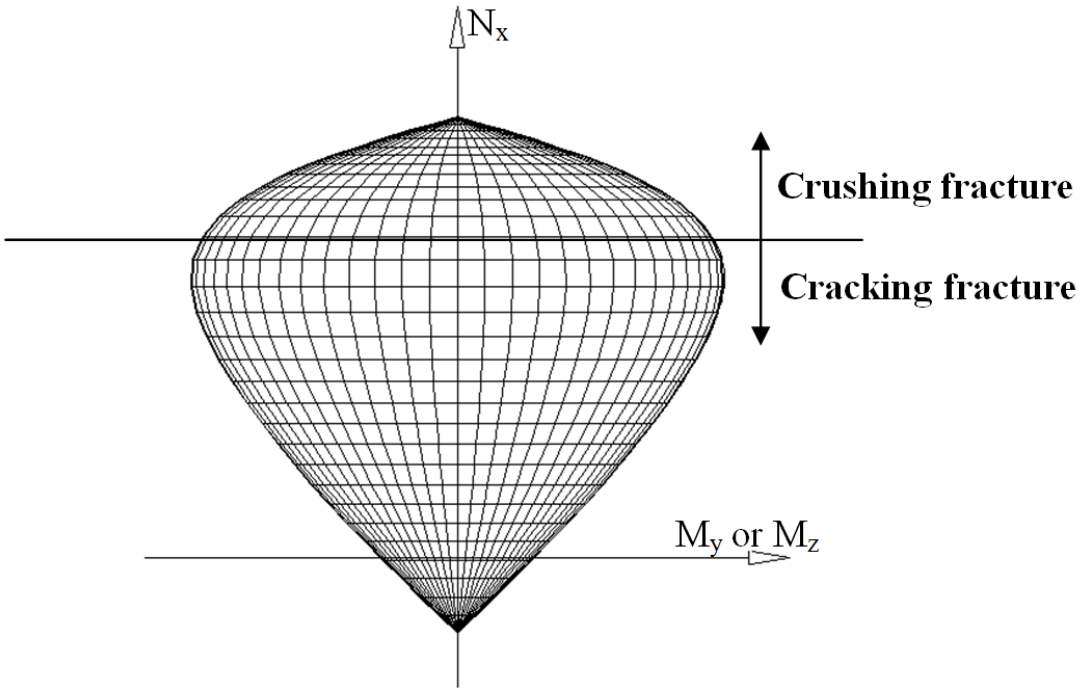

Figure 5.2 Illustration of concrete fracture surface

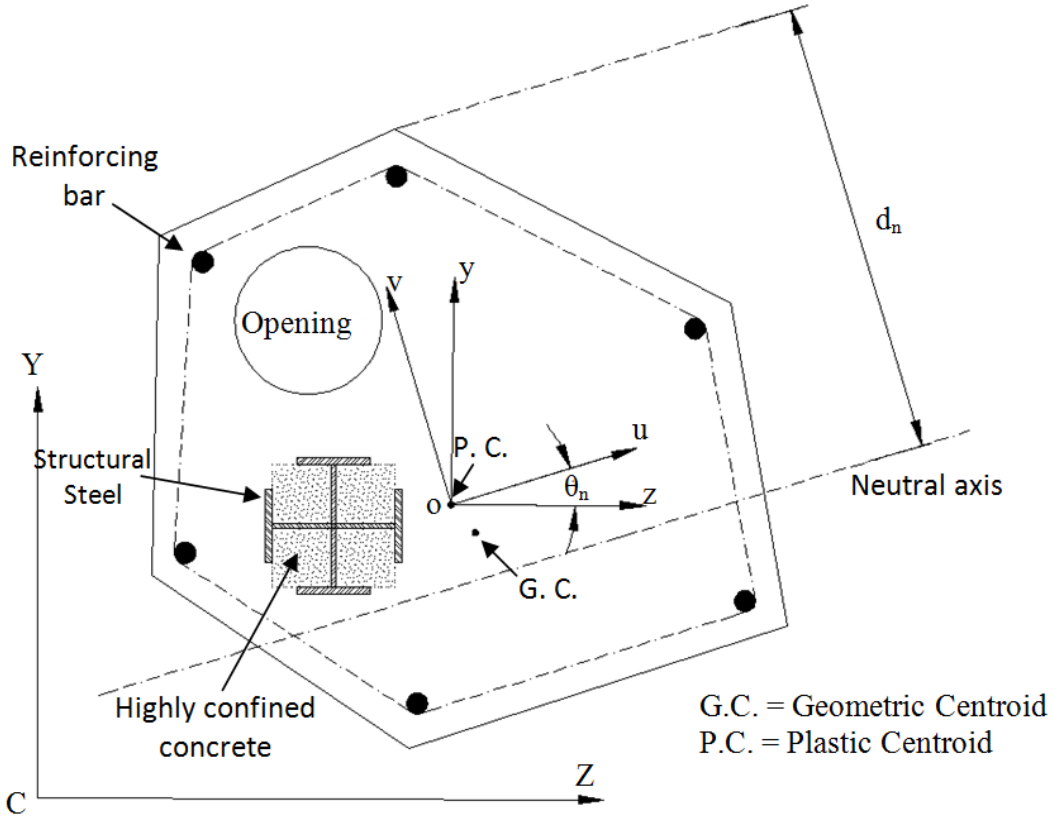

Figure 5.3 Arbitrarily shaped composite cross-section

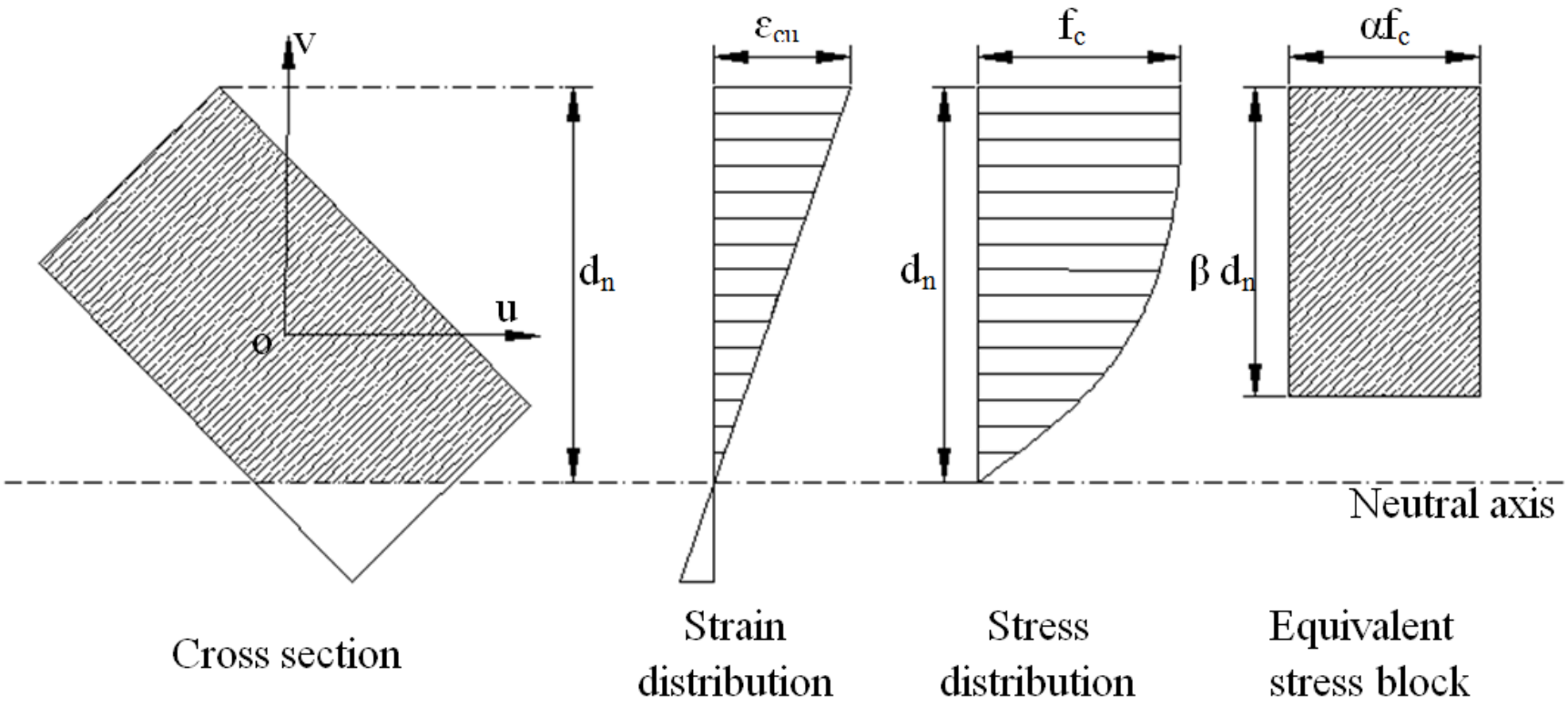

Figure 5.4 Stress resultants by the equivalent stress block method

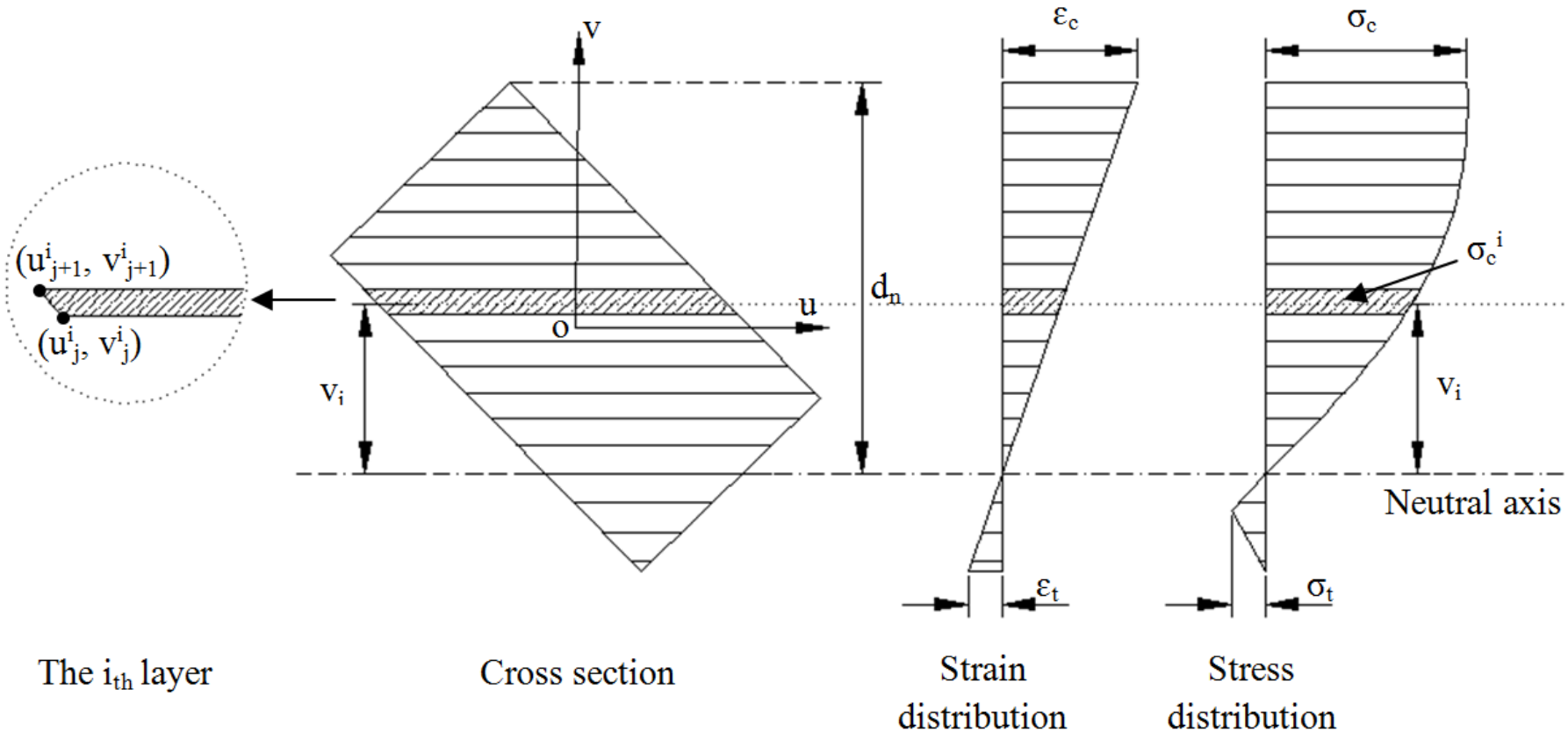

Figure 5.5 Stress resultants by the elaborated layer-integration method

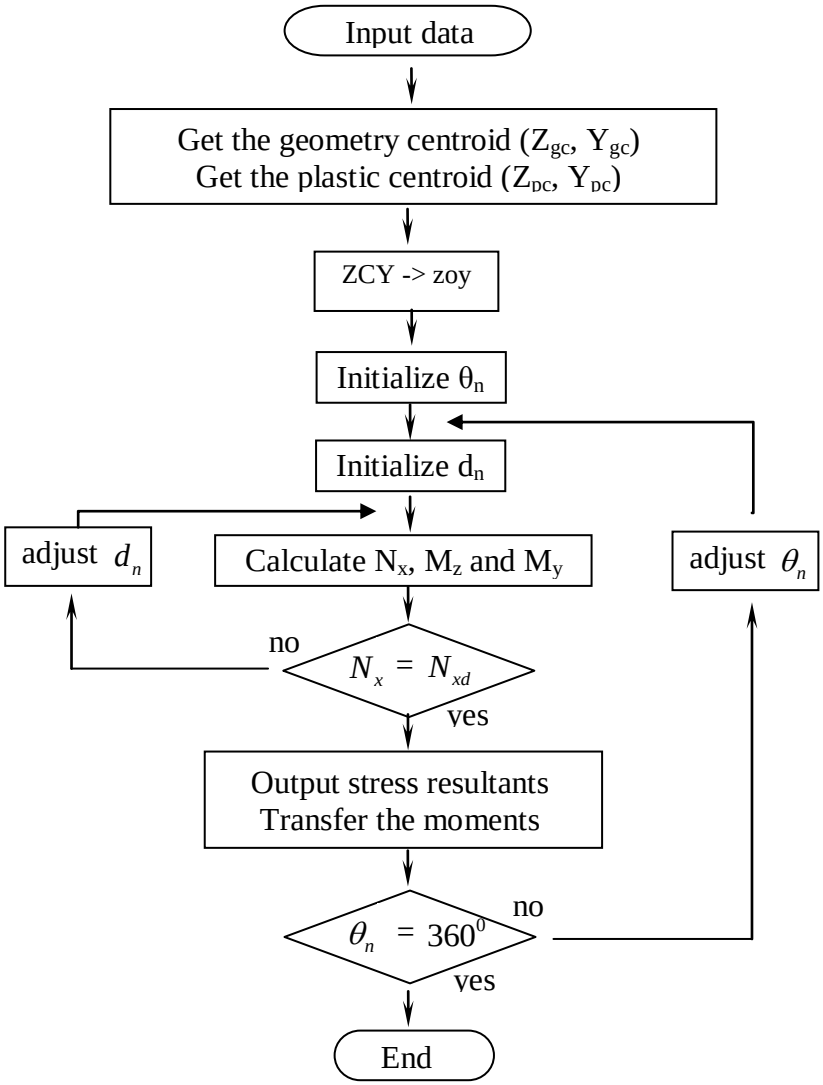

Figure 5.6 Flowchart of generating the yield surfaces under given axial load

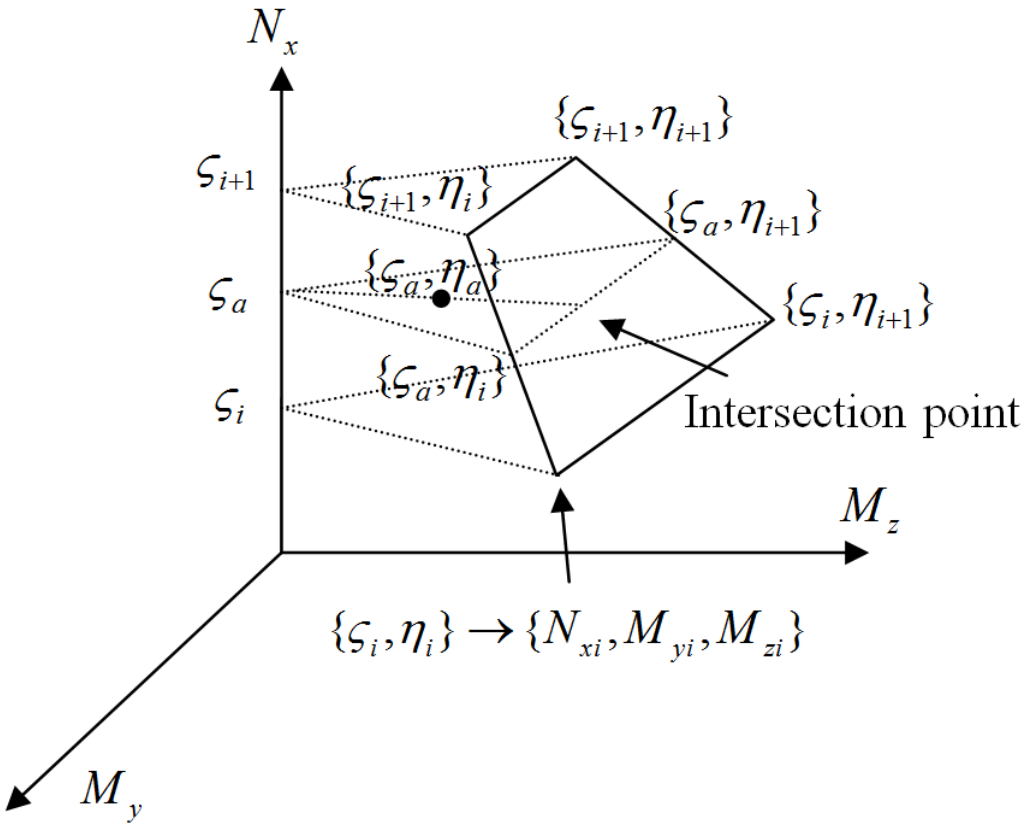

Figure 5.7 Indexed interaction strength suface

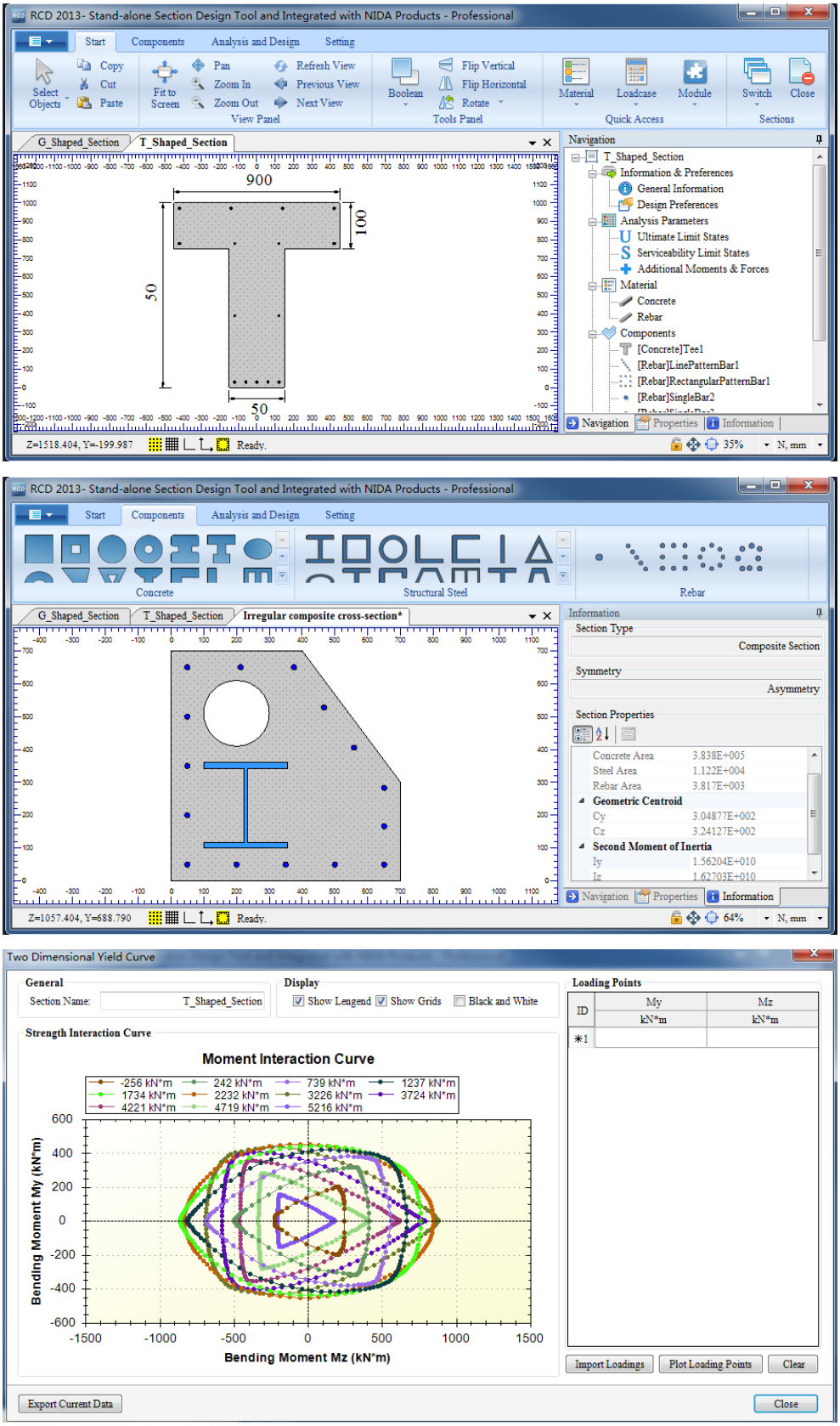

Figure 5.8 Screenshots of RCD 2013

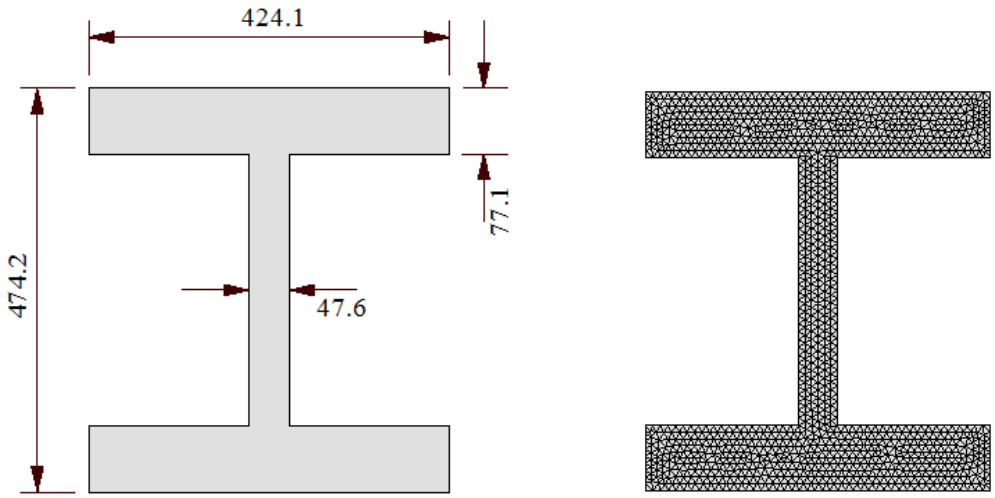

(a) Dimensions

(b) Sectional fibres

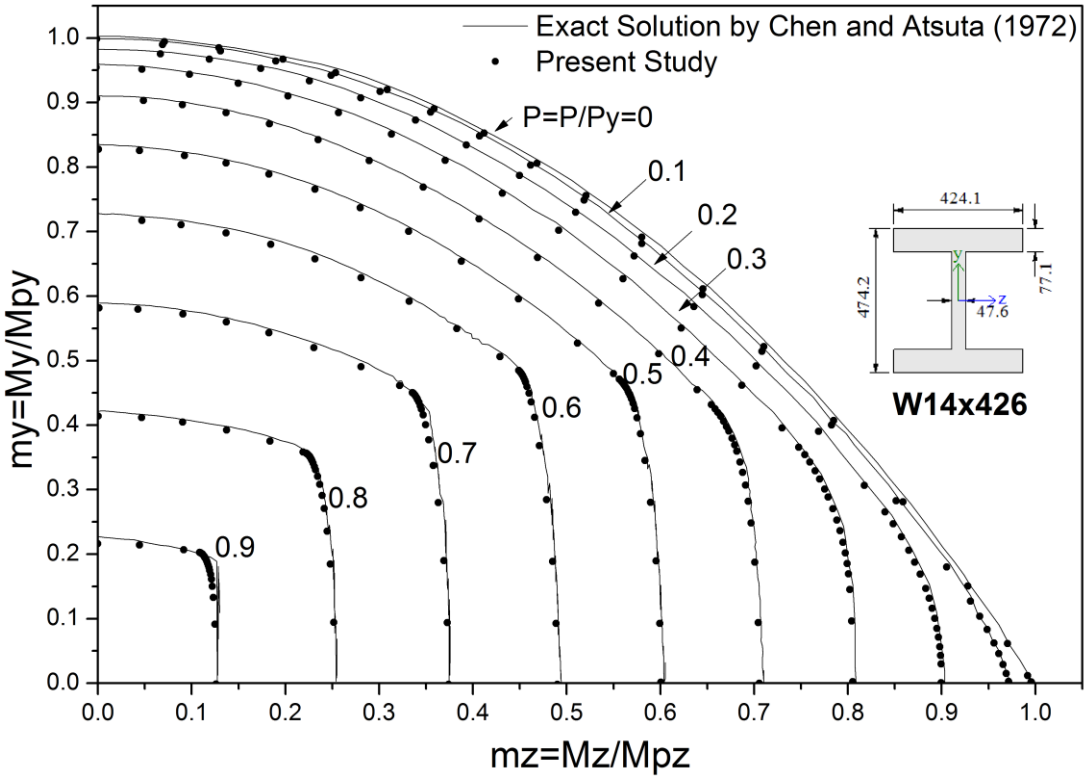

(c) Interaction curve for a wide flange section

Figure 5.9 Comparison results for a wide flange steel section

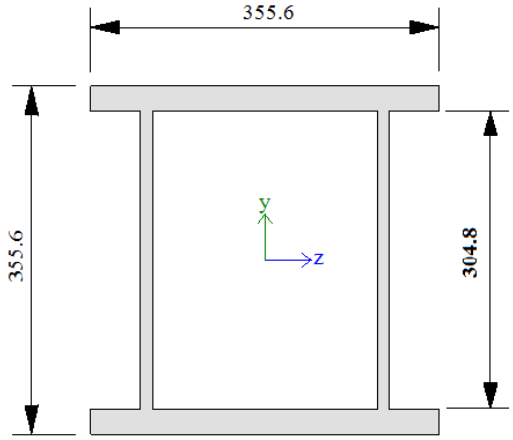

(a) Dimensions

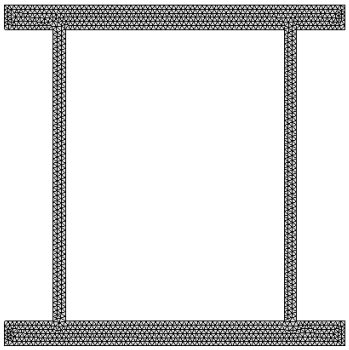

(b) Sectional fibres

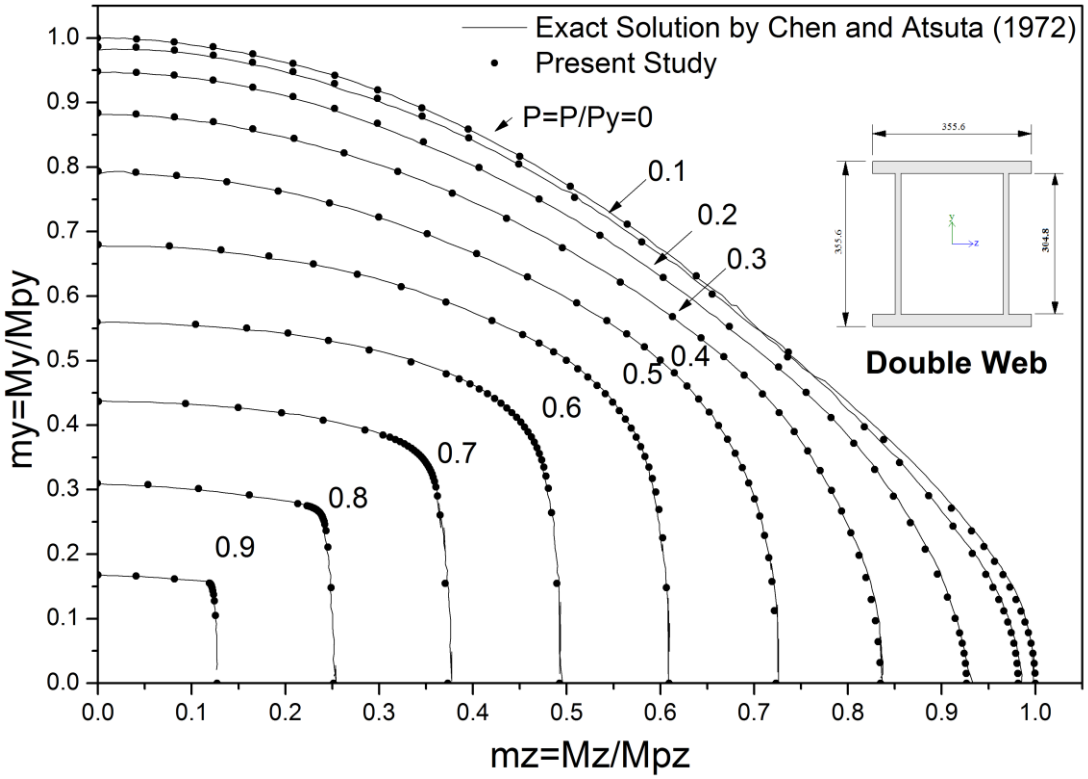

(c) Interaction curve for a double web steel section

Figure 5.10 Comparison results for a double web steel section

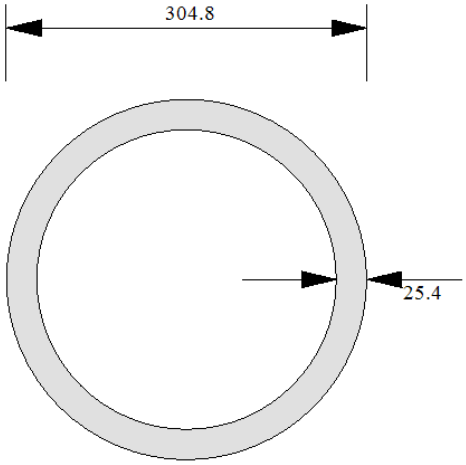

(a) Dimensions

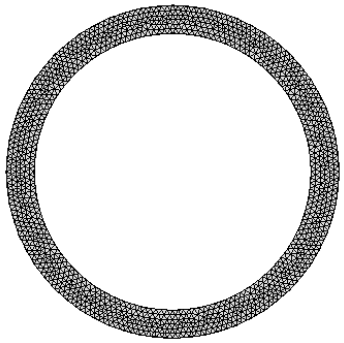

(b) Sectional fibres

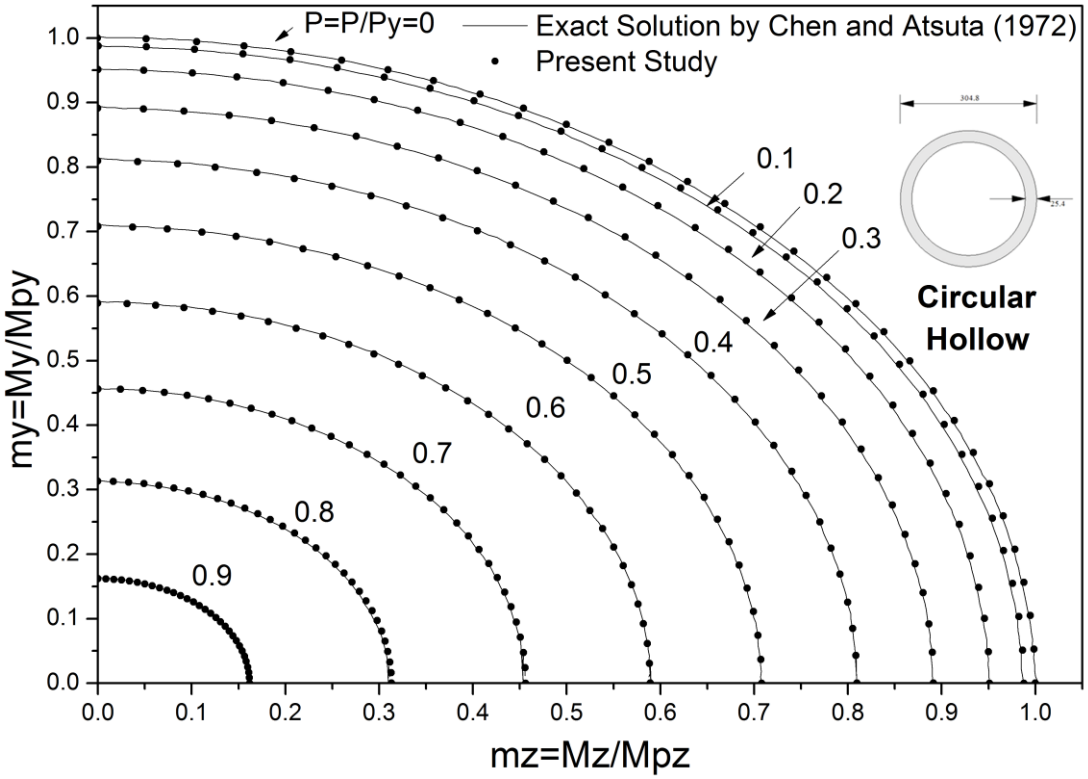

(c) Interaction curve for a circular hollow steel section

Figure 5.11 Comparison results for a circular hollow steel section

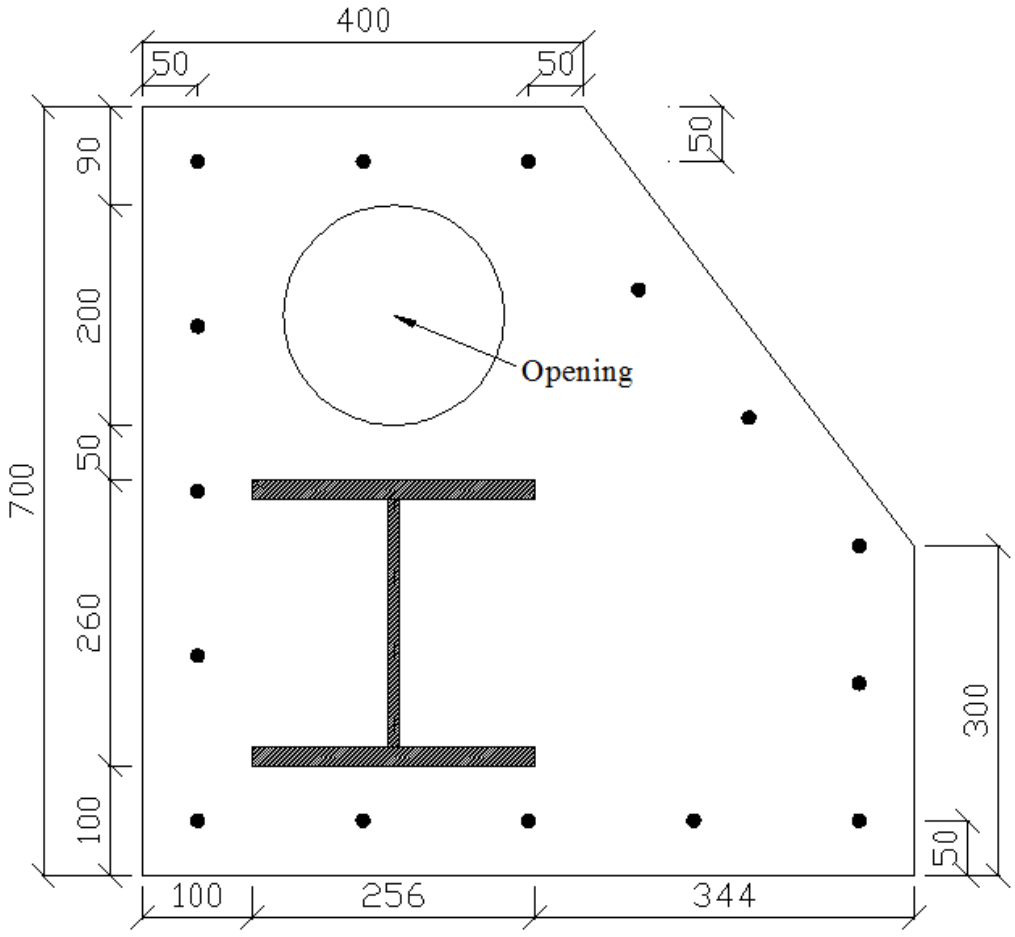

Figure 5.12 Irregular composite cross-section

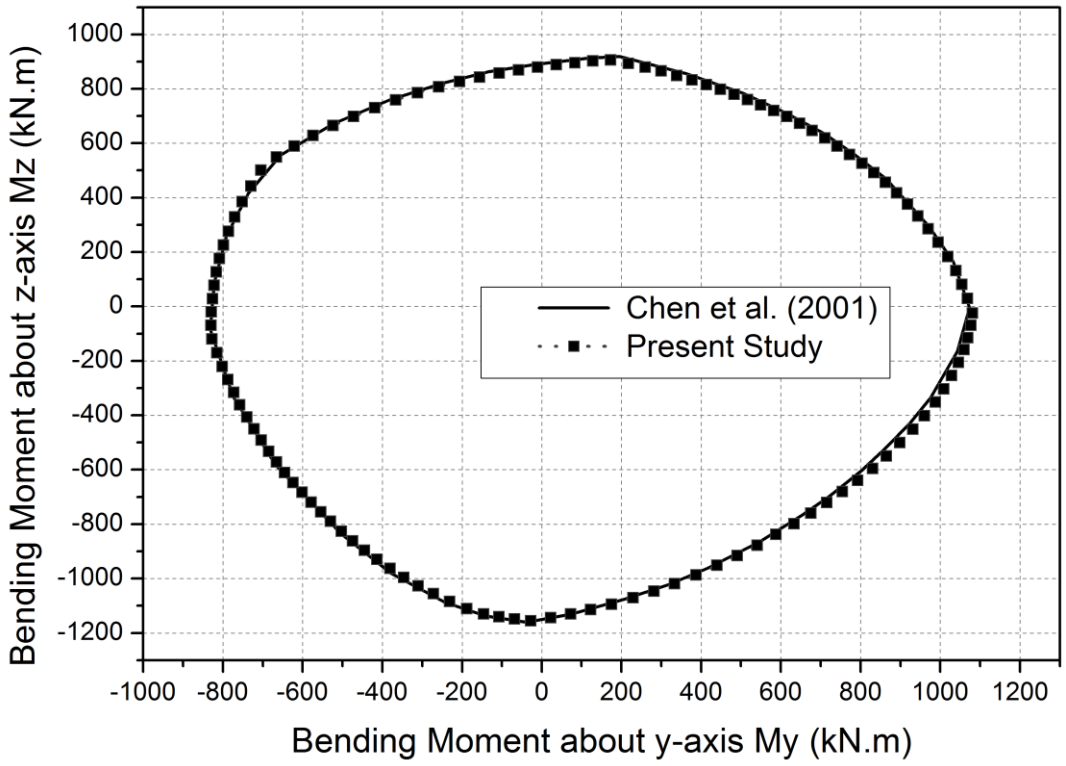

Figure 5.13 My vs. Mz interaction curve under axial load Nx=4120kN

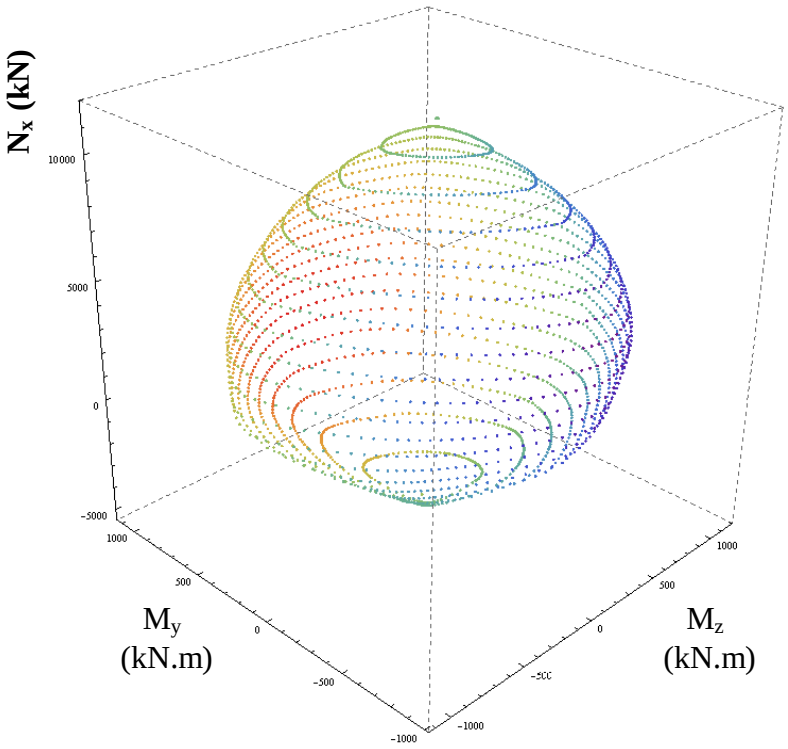

Figure 5.14 Three dimensional yield surface of the irregular composite section

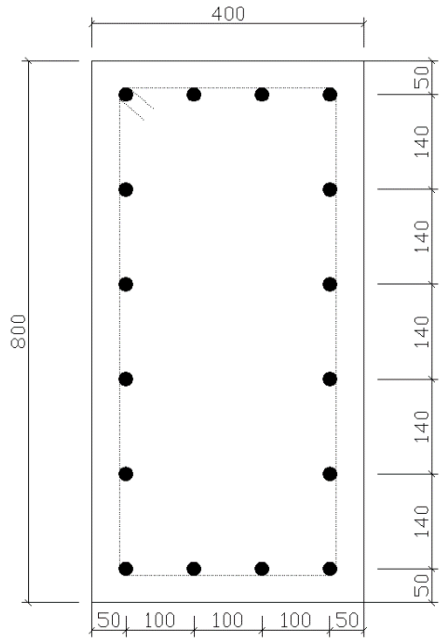

(a) Overview of section

Concrete: fck=40 MPa ; ϒc=1.5

Reinforcement Bars: fy=355 MPa; ; ϒb=1.15
(ϕ20 at corners; ϕ20 on faces ; Cover is 50 mm)

Stress vs. strain curve of concrete:

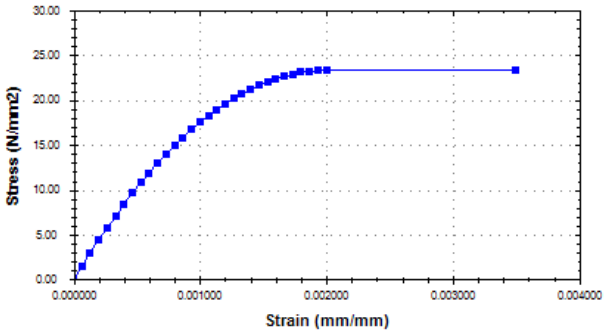

(b) Concrete Properties

Figure 5.15 Typical rectangular reinforced concrete section

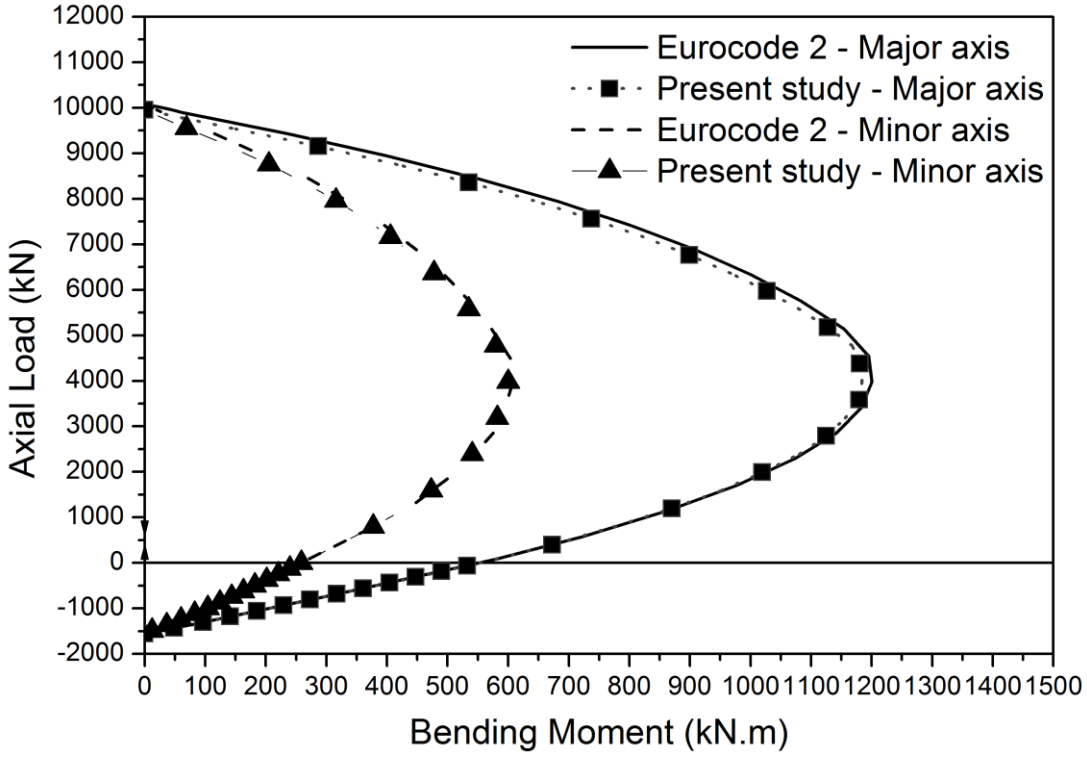

Figure 5.16 Results of the RC section by equivalent stress block method

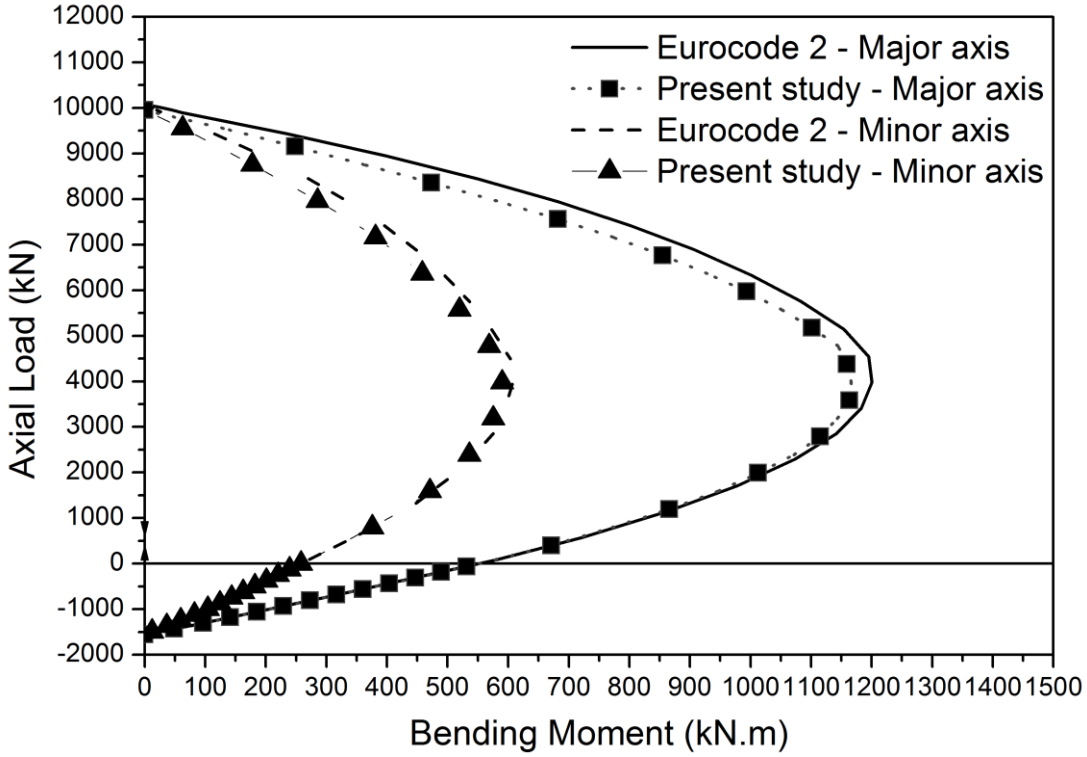

Figure 5.17 Results of the RC section by elaborated layer-integration method

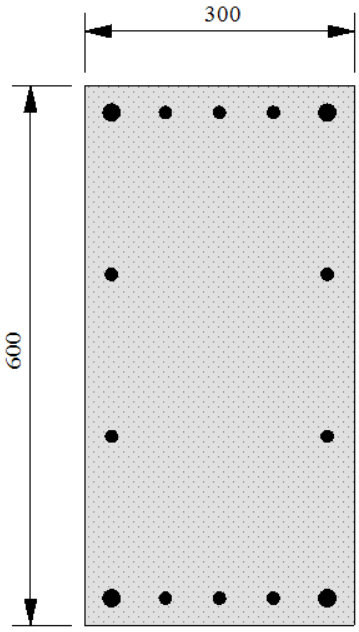

(a) Overview of section

Concrete: fck=20.75 MPa ; ϒc=1.6

Reinforcement Bars: fyk=375 MPa; ; ϒb=1.15
(ϕ20 at corners; ϕ14 on faces ; Cover is 30 mm)

Stress vs. strain curve of concrete:

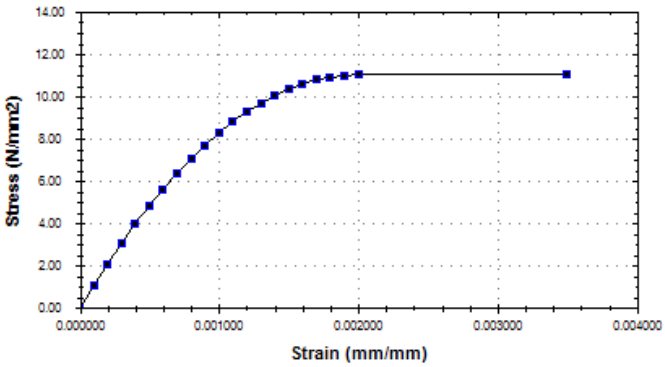

(b) Concrete Properties

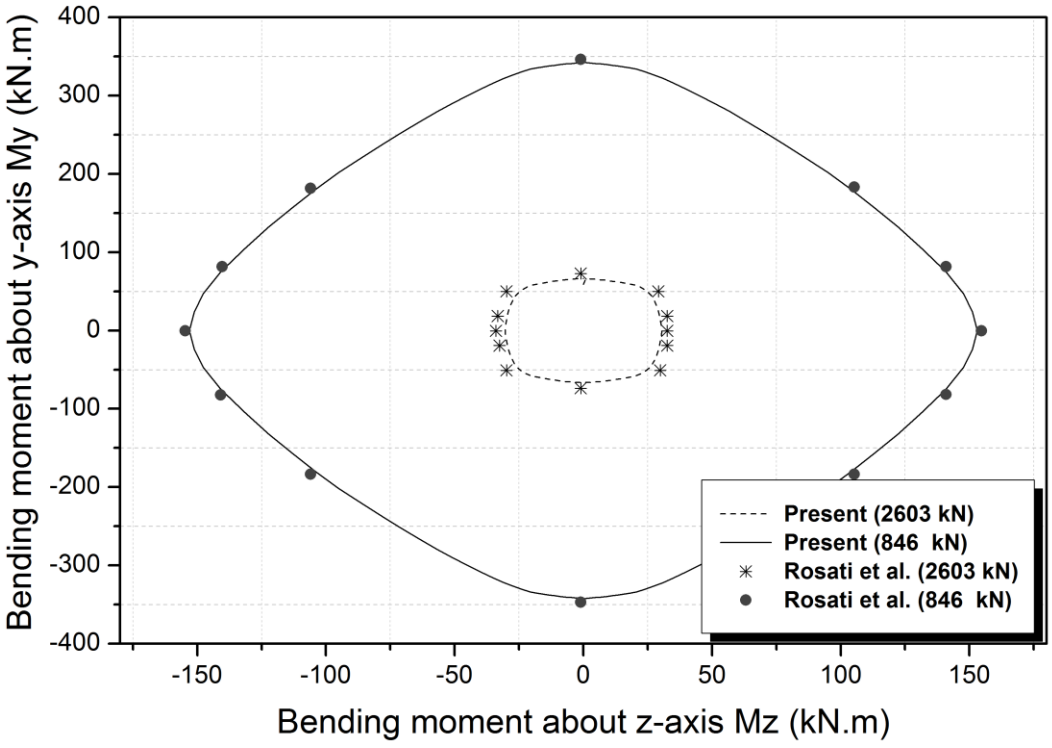

(c) Comparison results – Group 1

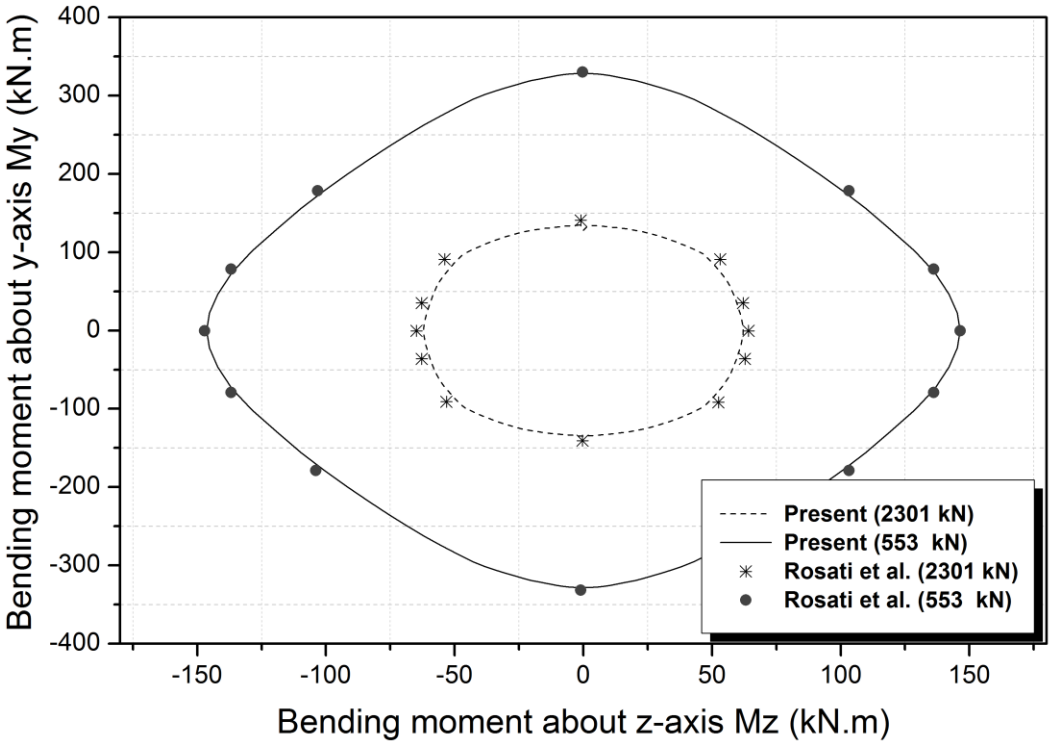

(d) Comparison results – Group 2

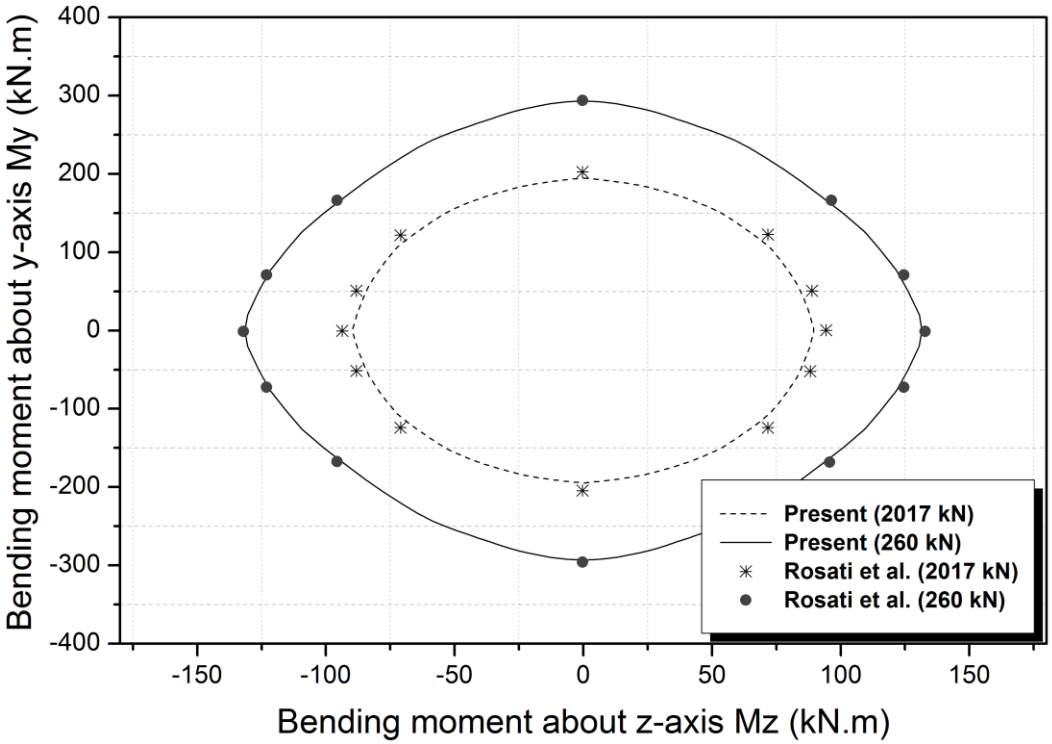

(e) Comparison results – Group 3

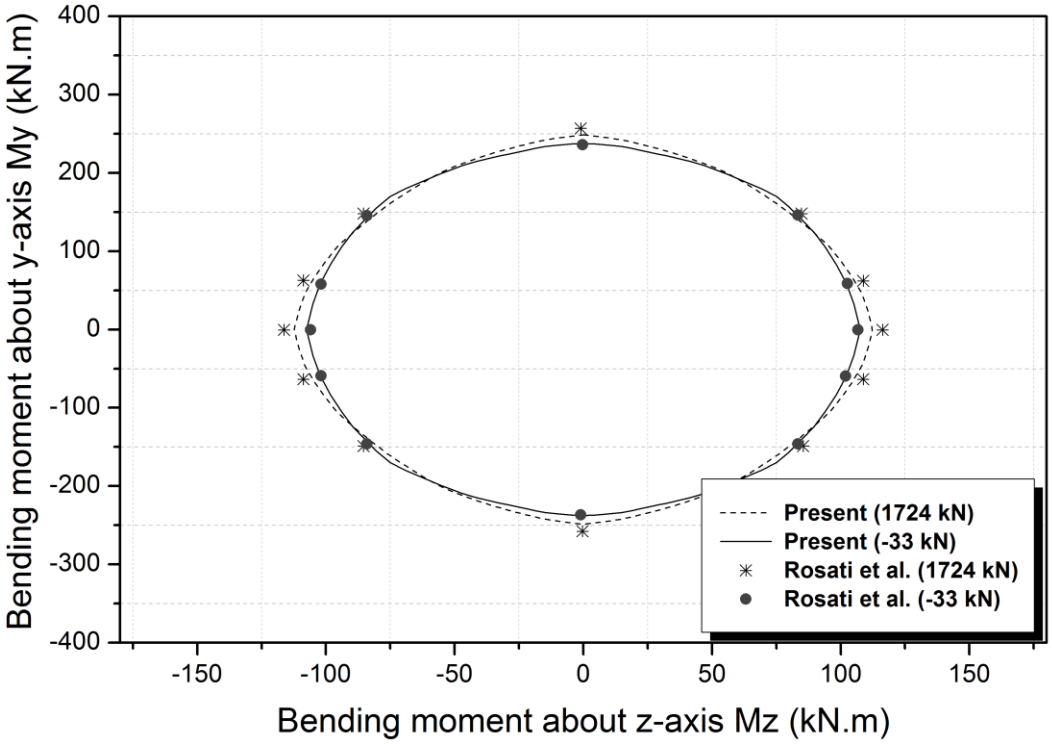

(f) Comparison results – Group 4

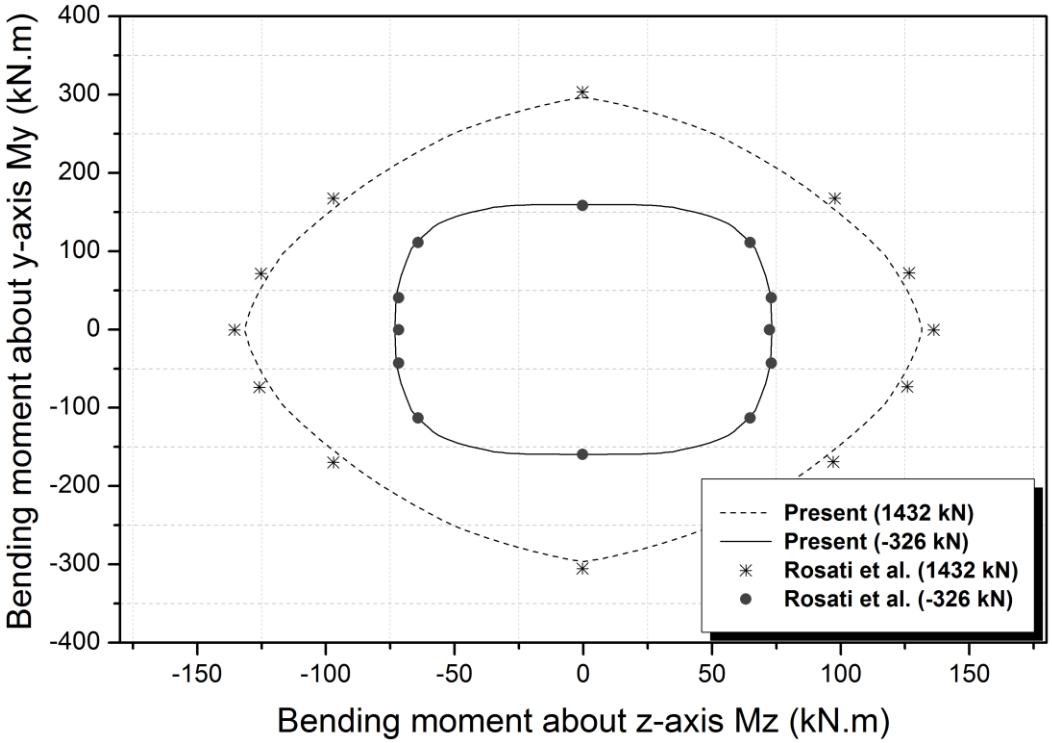

(g) Comparison results – Group 5

Figure 5.18 Comparison results of Rosati's RC Section - Rectangular

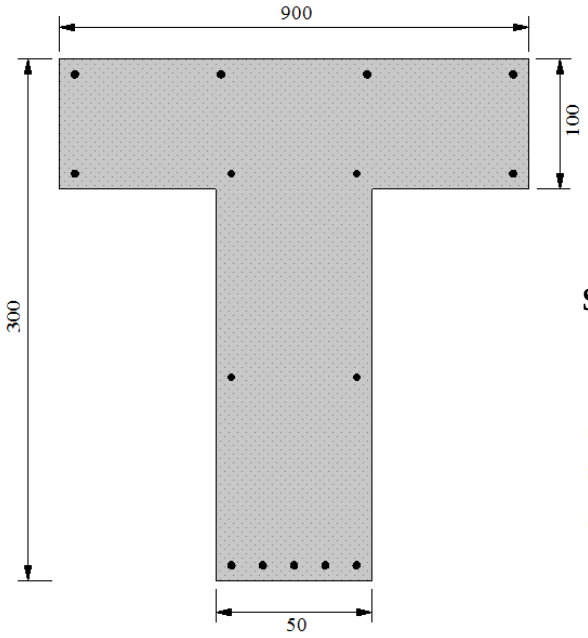

Concrete: fck=20.75 MPa ; ϒc=1.6

Reinforcement Bars:
fyk=375 MPa; ; ϒb=1.15
(ϕ20 at corners; ϕ14 on faces ;
Cover is 30 mm)

Stress vs. strain curve of concrete:

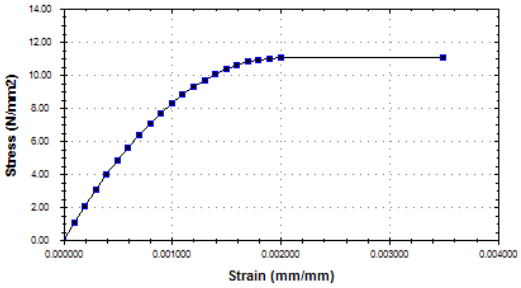

(a) Overview of section

(b) Concrete Properties

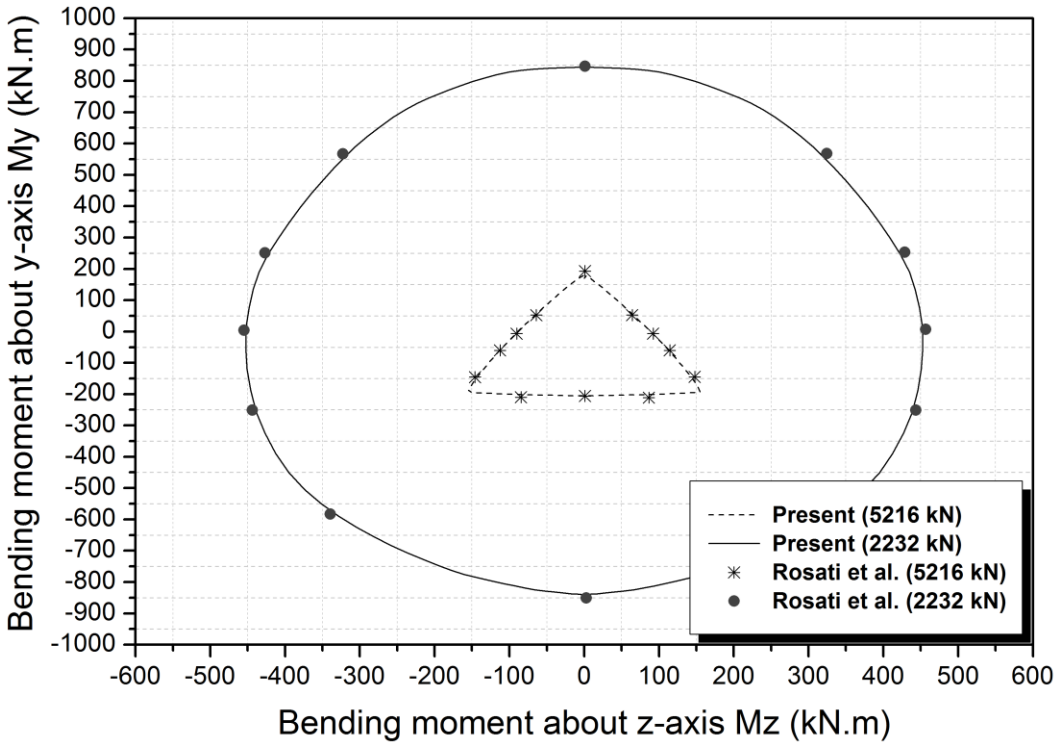

(c) Comparison results – Group 1

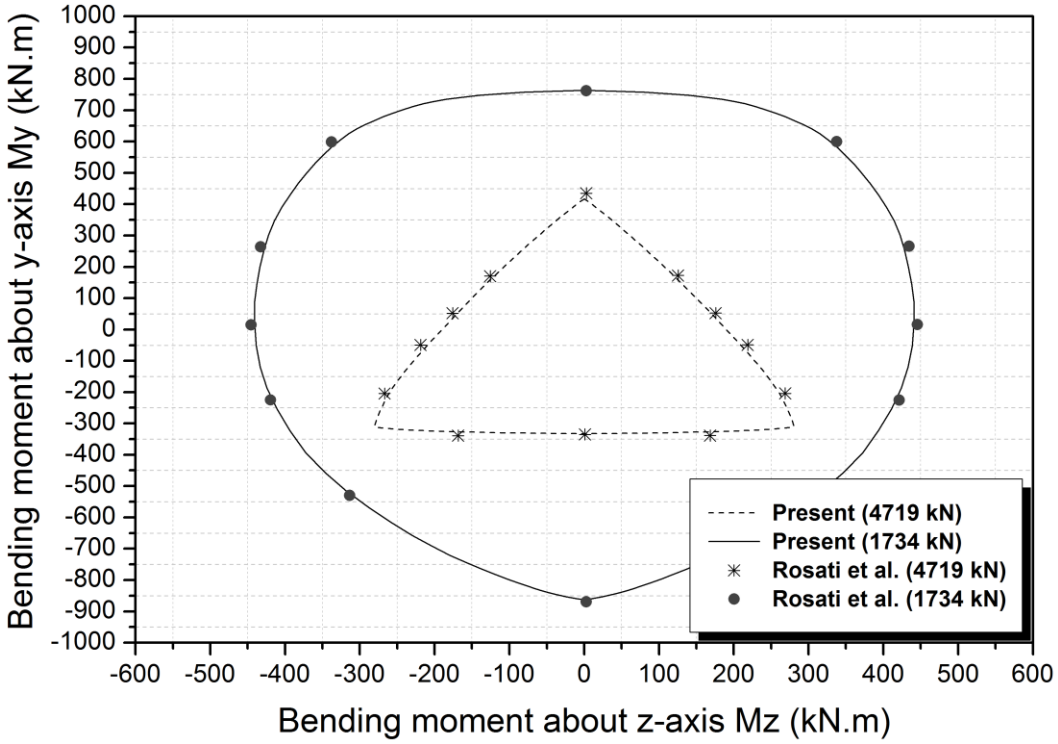

(d) Comparison results – Group 2

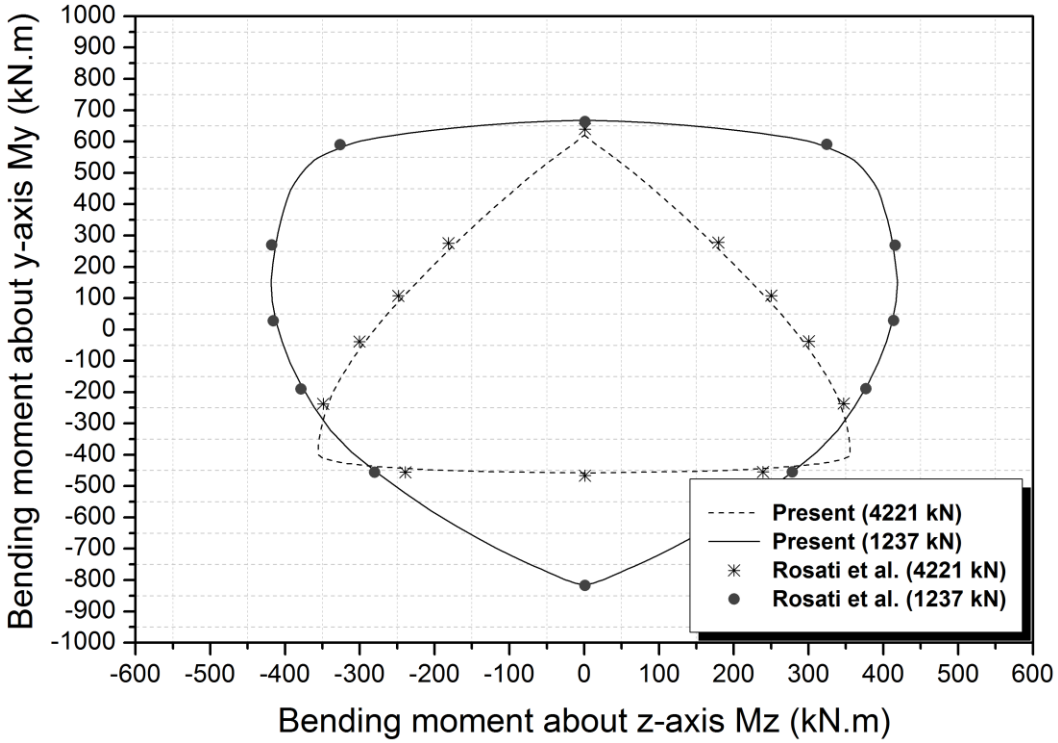

(e) Comparison results – Group 3

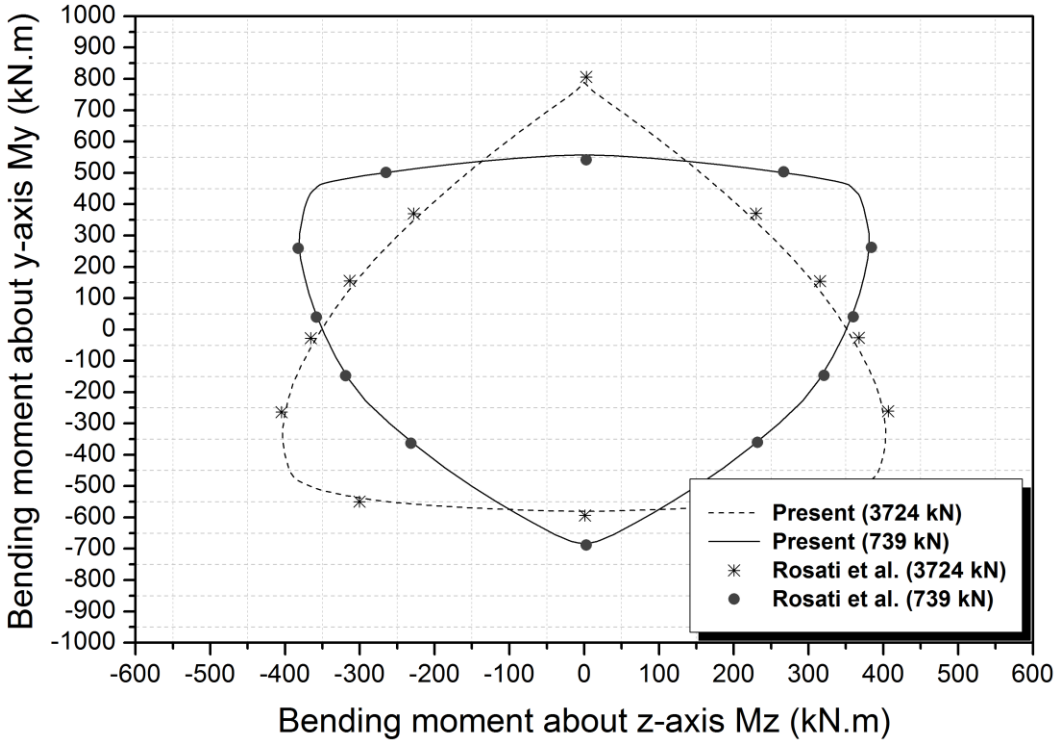

(f) Comparison results – Group 4

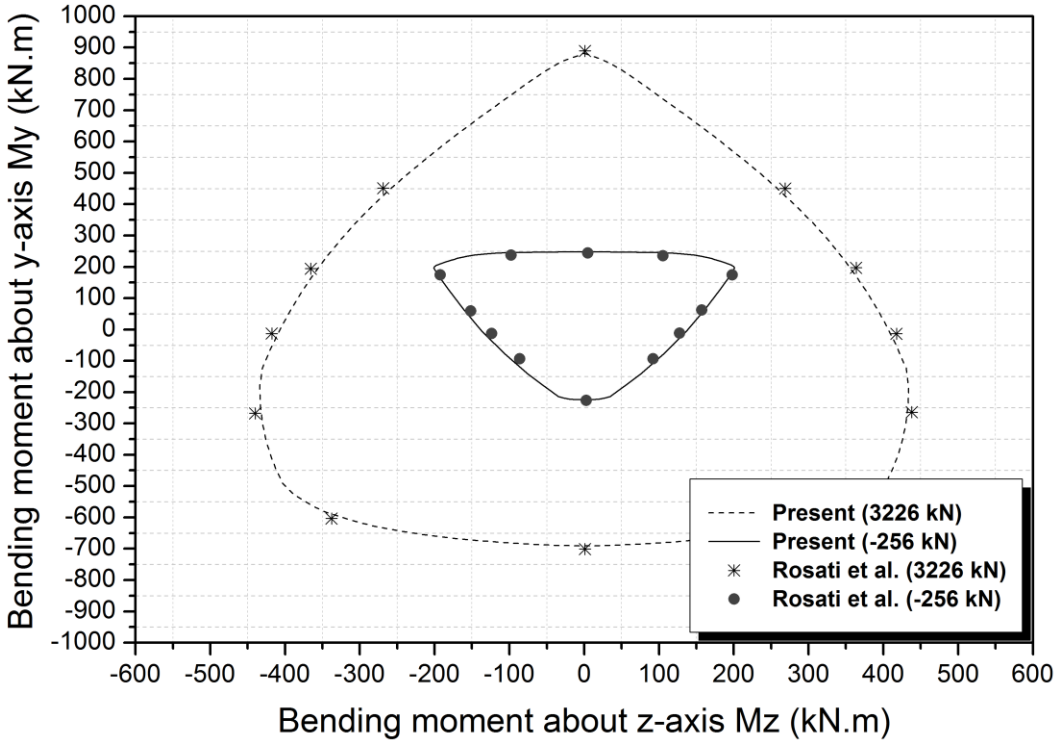

(g) Comparison results – Group 5

Figure 5.19 Comparison results of Rosati's RC Section – T Shaped Section

Concrete: fck=20.75 MPa ;ϒc=1.6 ; Cover is 30 mm

Reinforcement Bars: fyk=375 MPa; ; ϒb=1.15(ϕ24 at corners; ϕ20 on faces)

Stress vs. strain curve :

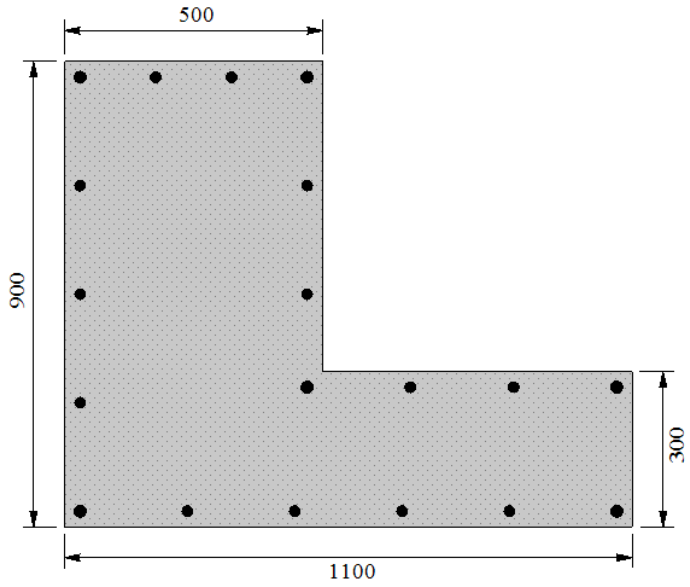

(a) Overview of section

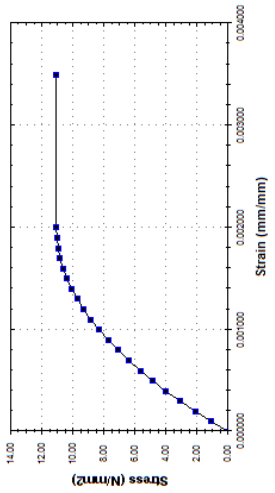

(b) Concrete Properties

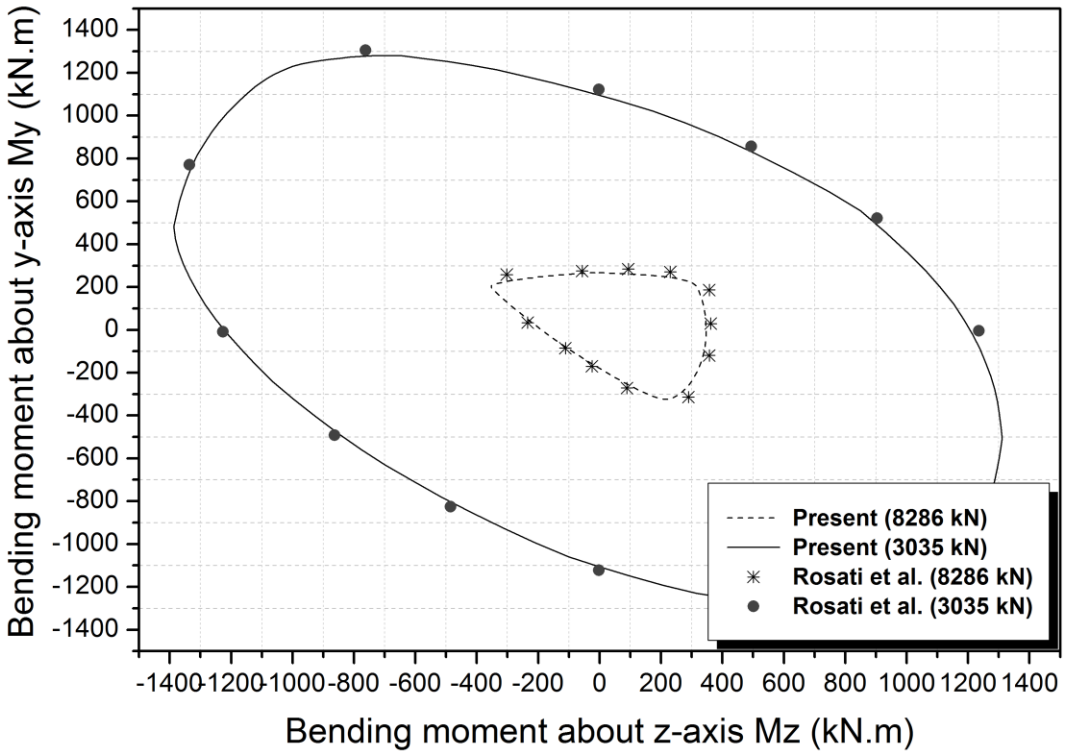

(c) Comparison results – Group 1

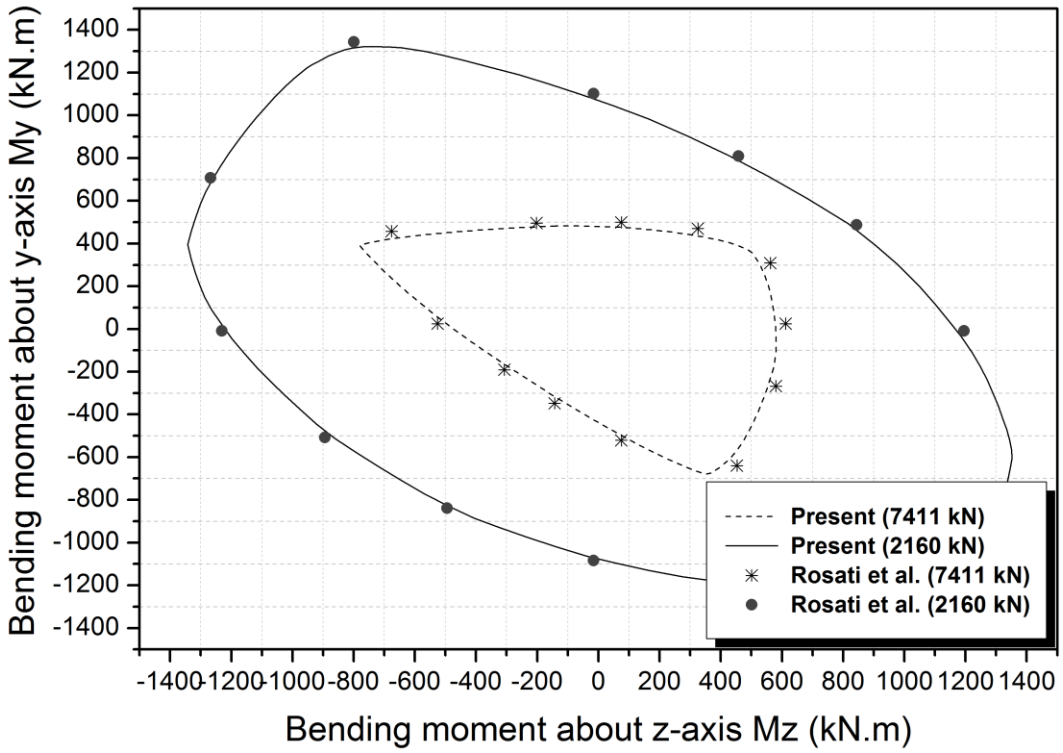

(d) Comparison results – Group 2

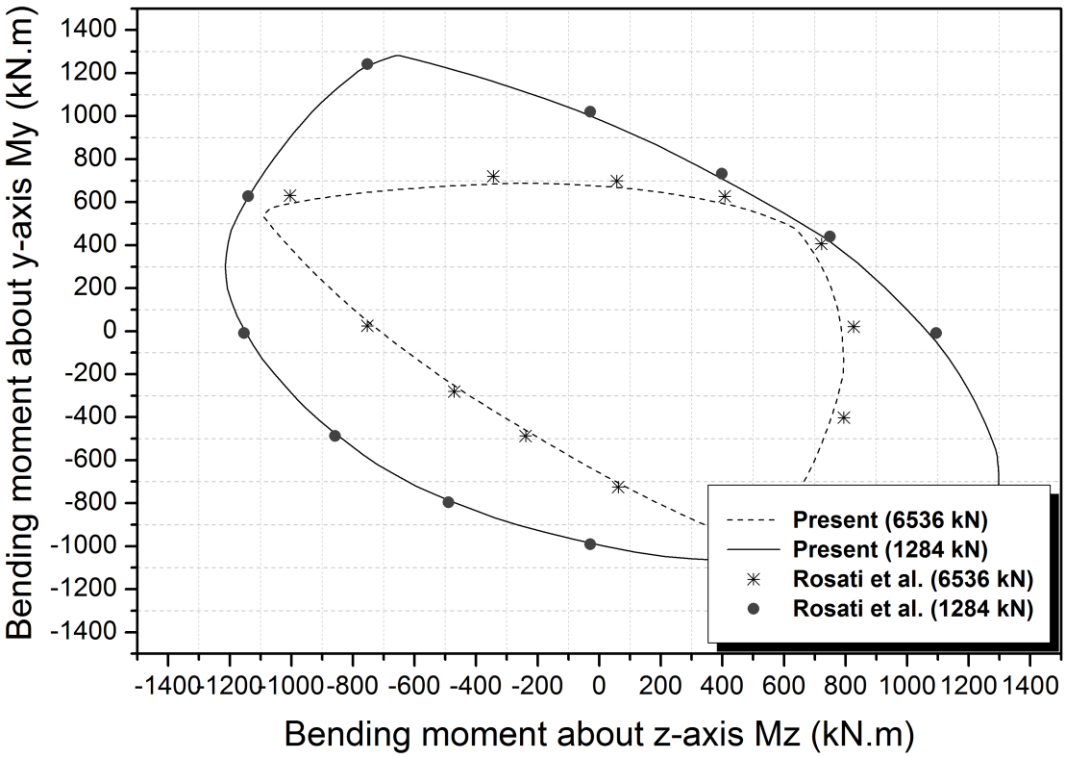

(e) Comparison results – Group 3

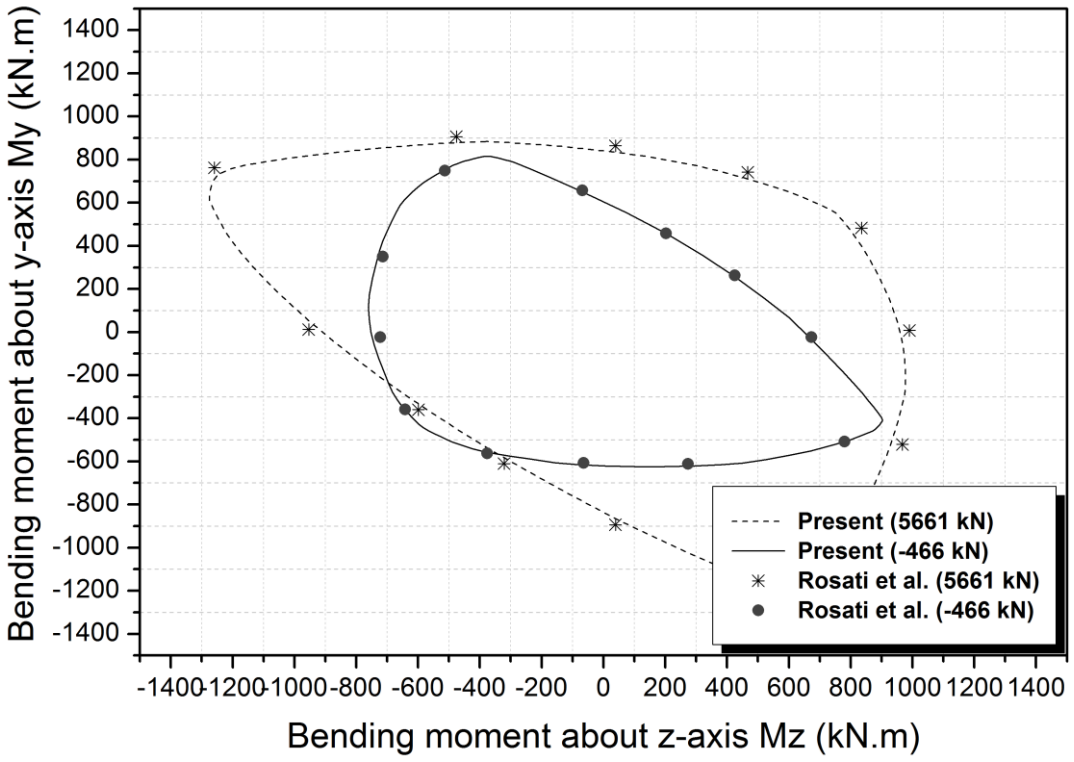

(f) Comparison results – Group 4

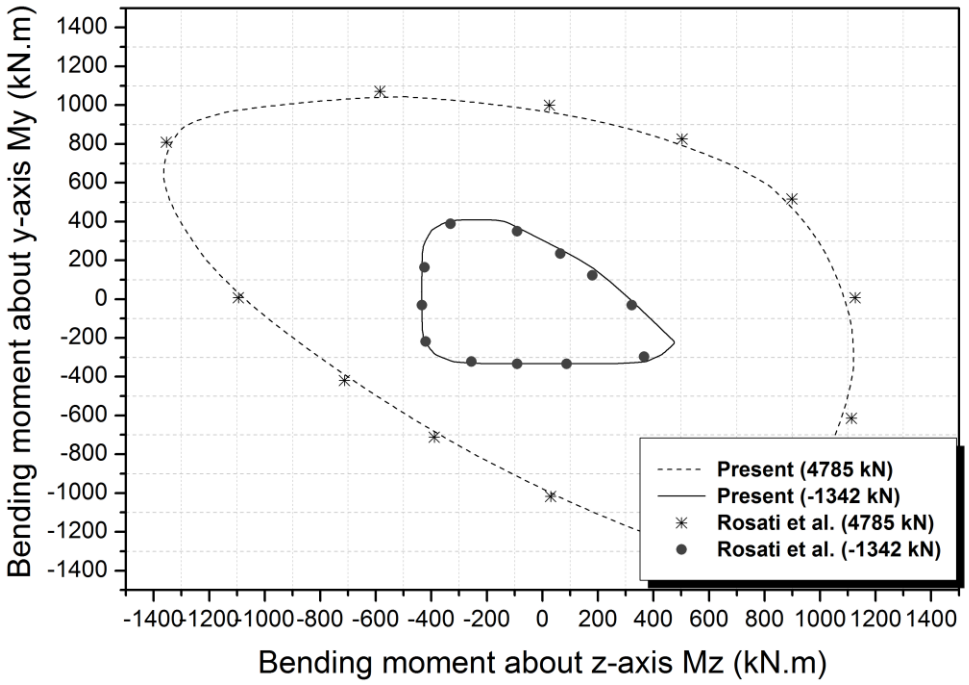

(g) Comparison results – Group 5

Figure 5.20 Comparison results of Rosati's RC Section – L Shaped Section

Concrete: fck=20.75 MPa ;ϒc=1.6 ; Cover is 30 mm

Reinforcement Bars: fyk=375 MPa; ; ϒb=1.15(ϕ20 at corners; ϕ20 on faces)

Stress vs. strain curve of concrete:

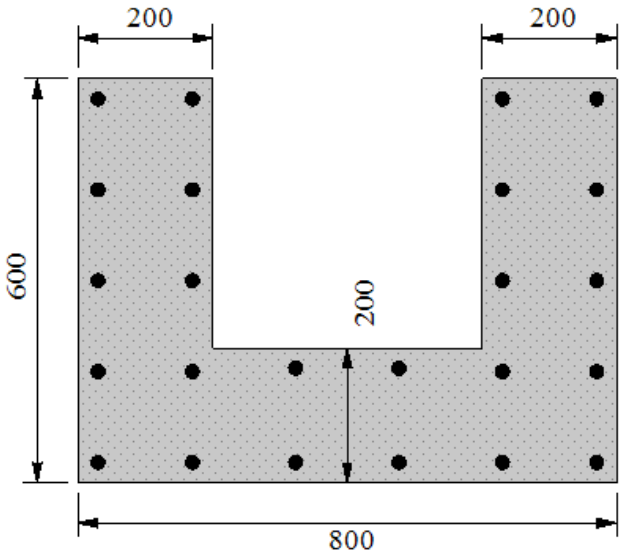

(a) Overview of section

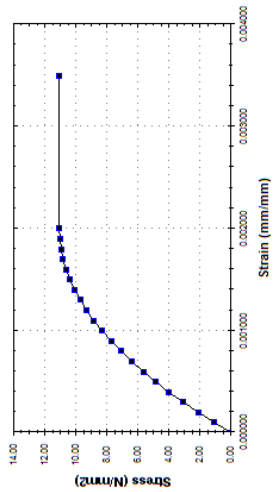

(b) Concrete Properties

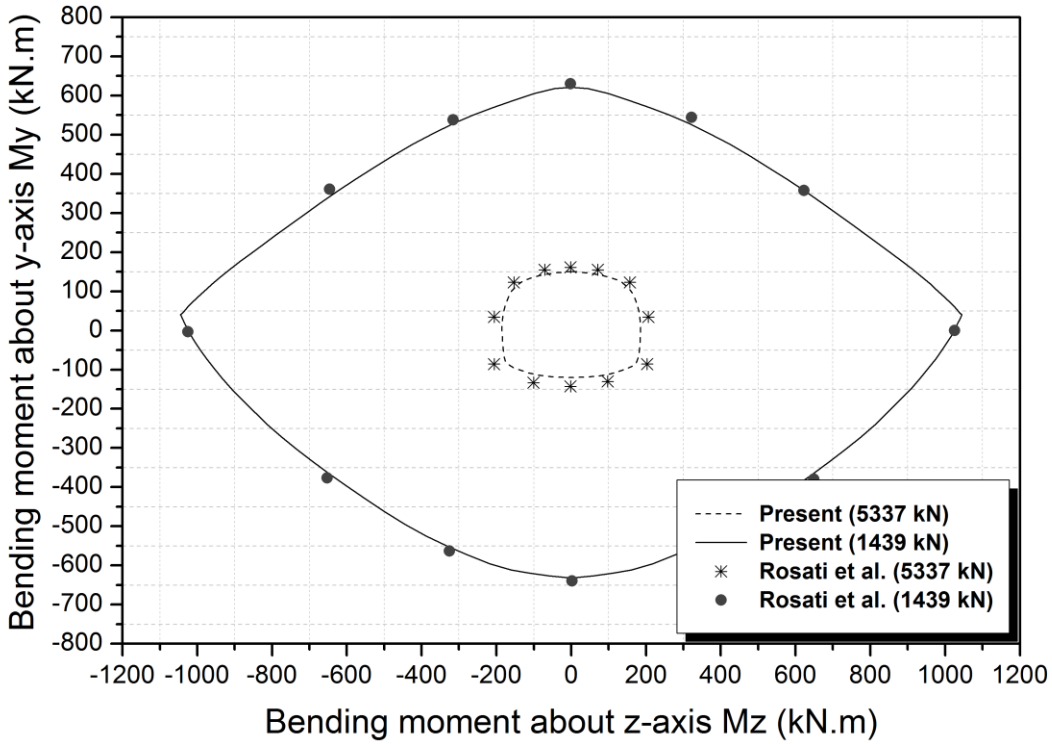

(c) Comparison results – Group 1

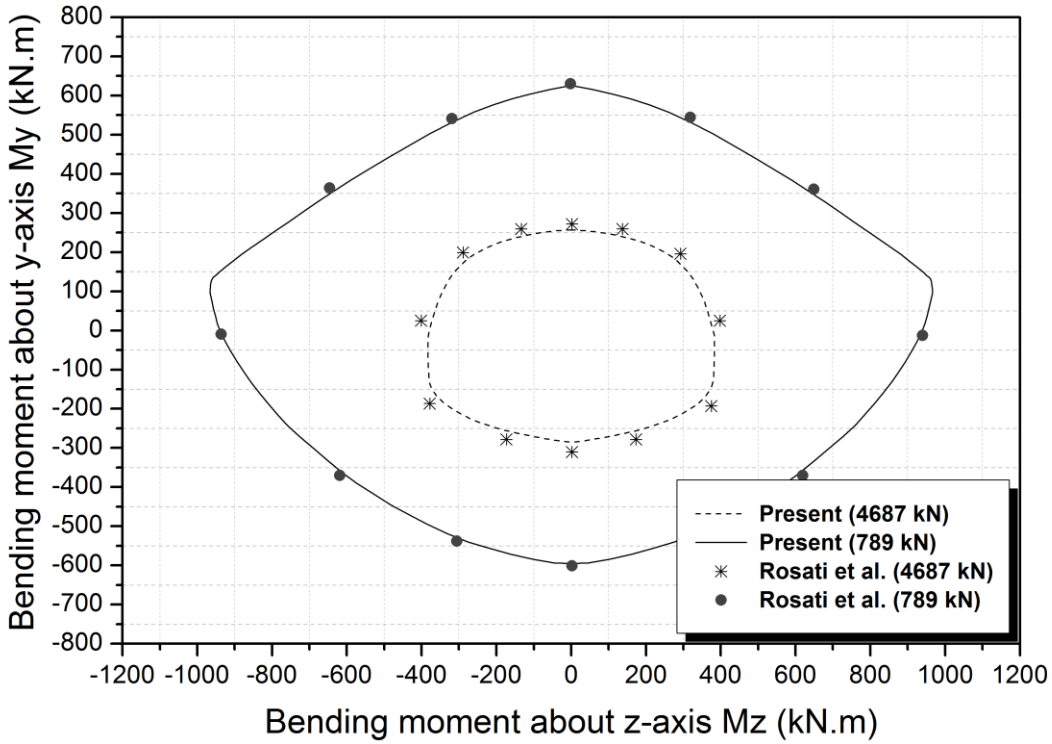

(d) Comparison results – Group 2

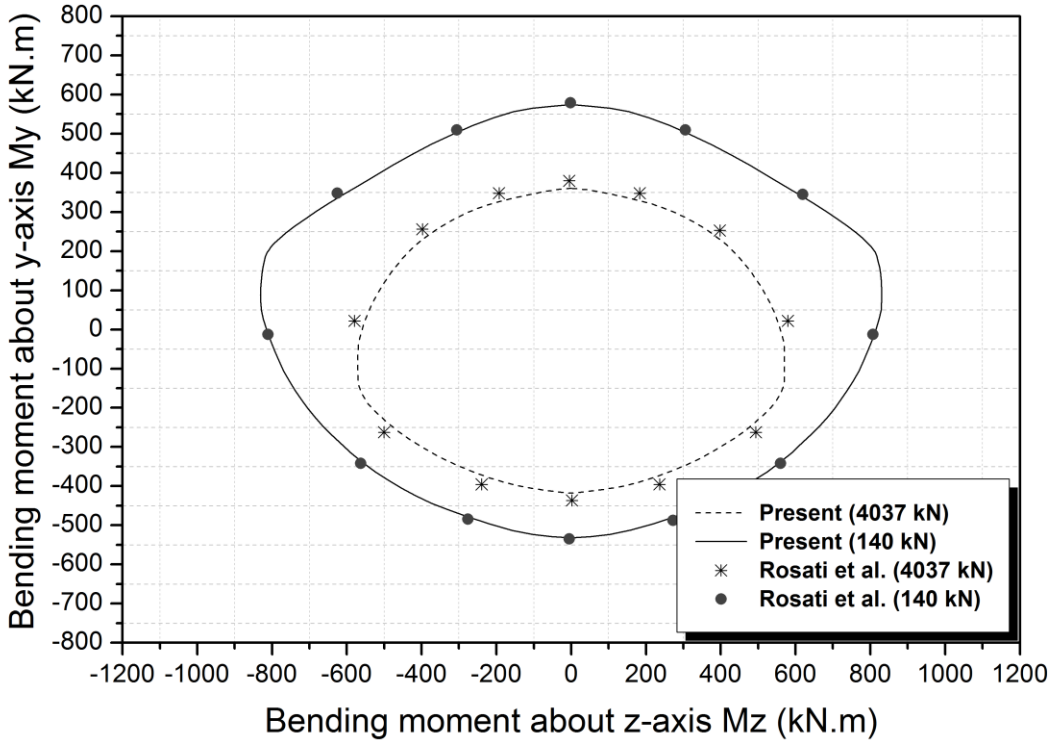

(e) Comparison results – Group 3

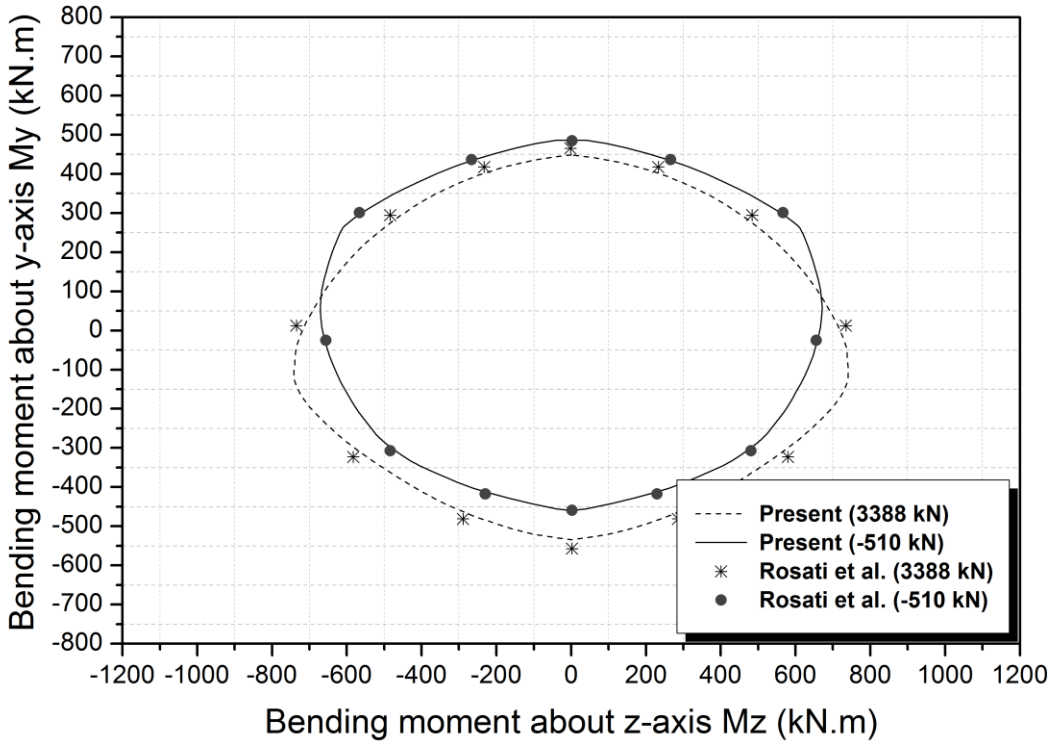

(f) Comparison results – Group 4

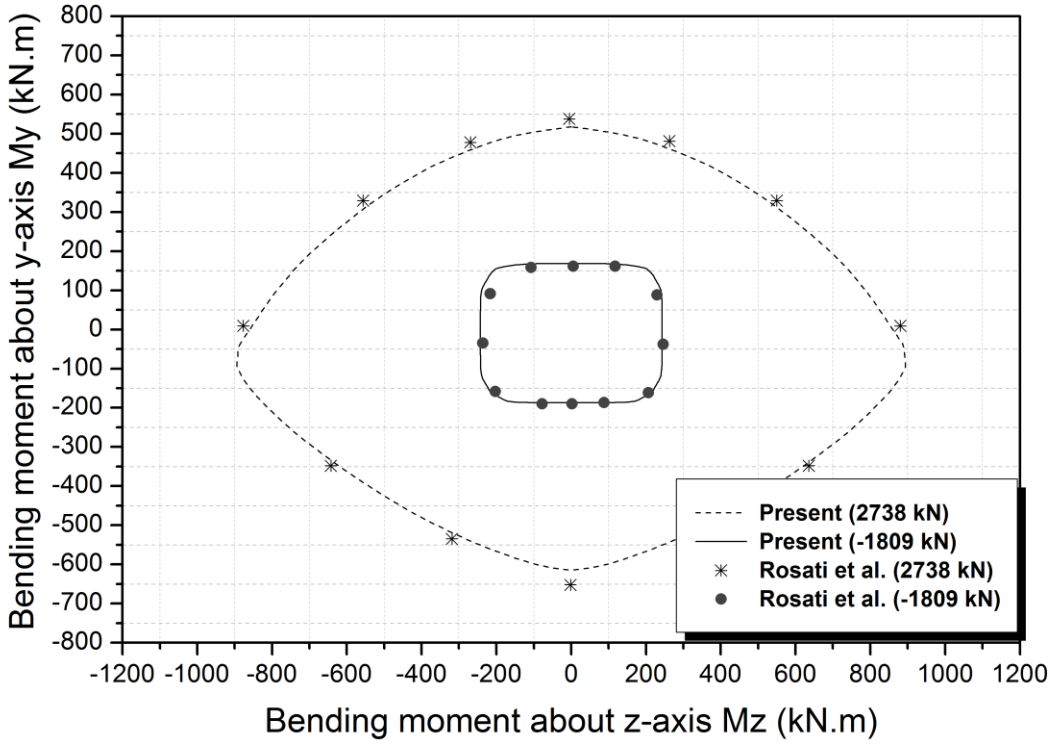

(g) Comparison results – Group 5

Figure 5.21 Comparison results of Rosati's RC Section – C Shaped Section

Concrete: fck=20.75 MPa ;ϒc=1.6 ; Cover is 30 mm

Reinforcement Bars: fyk=375 MPa; ; ϒb=1.15(ϕ24 at corners; ϕ24 on faces)

Stress vs. strain curve of concrete:

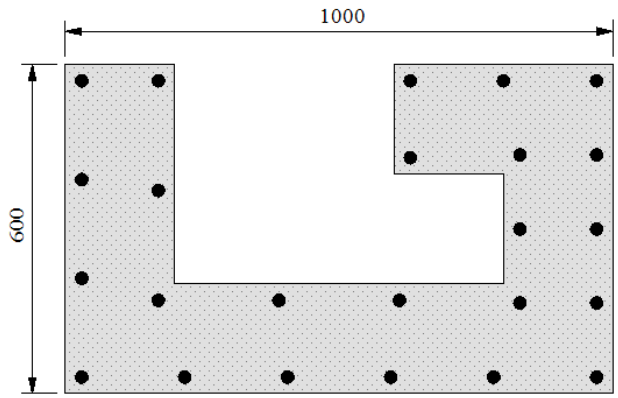

(a) Overview of section

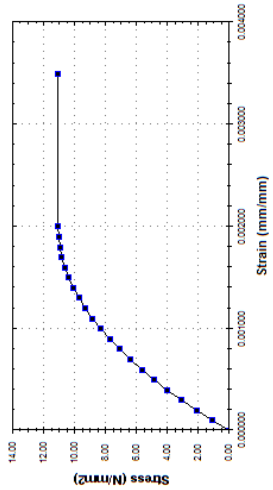

(b) Concrete Properties

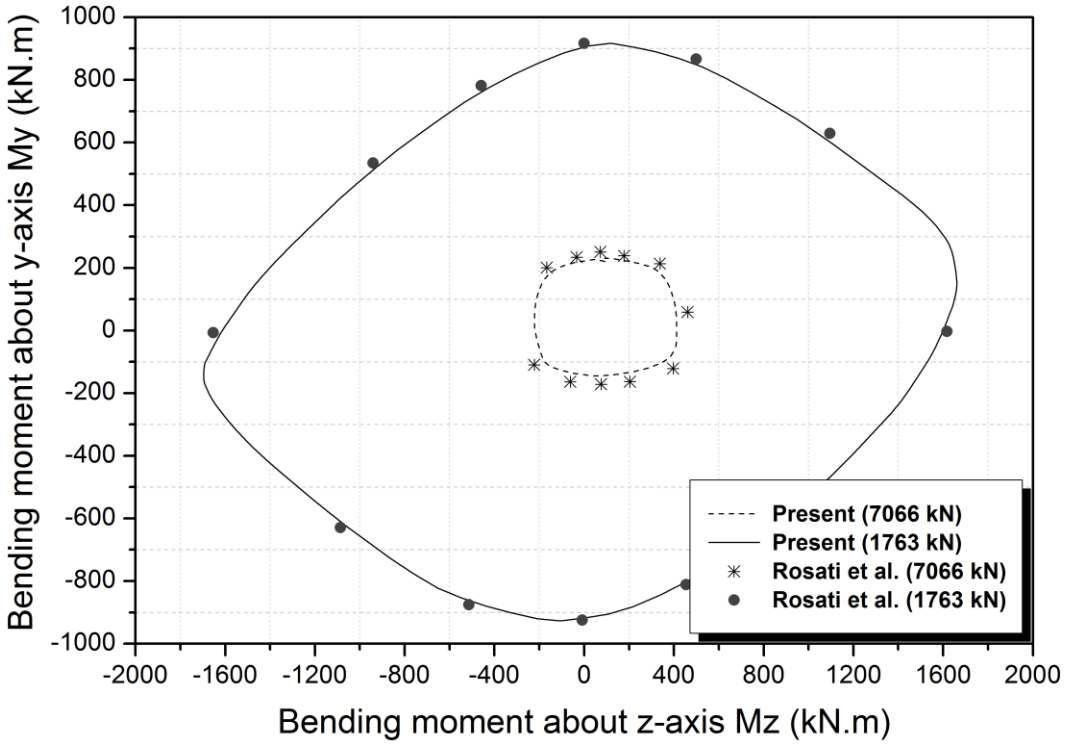

(c) Comparison results – Group 1

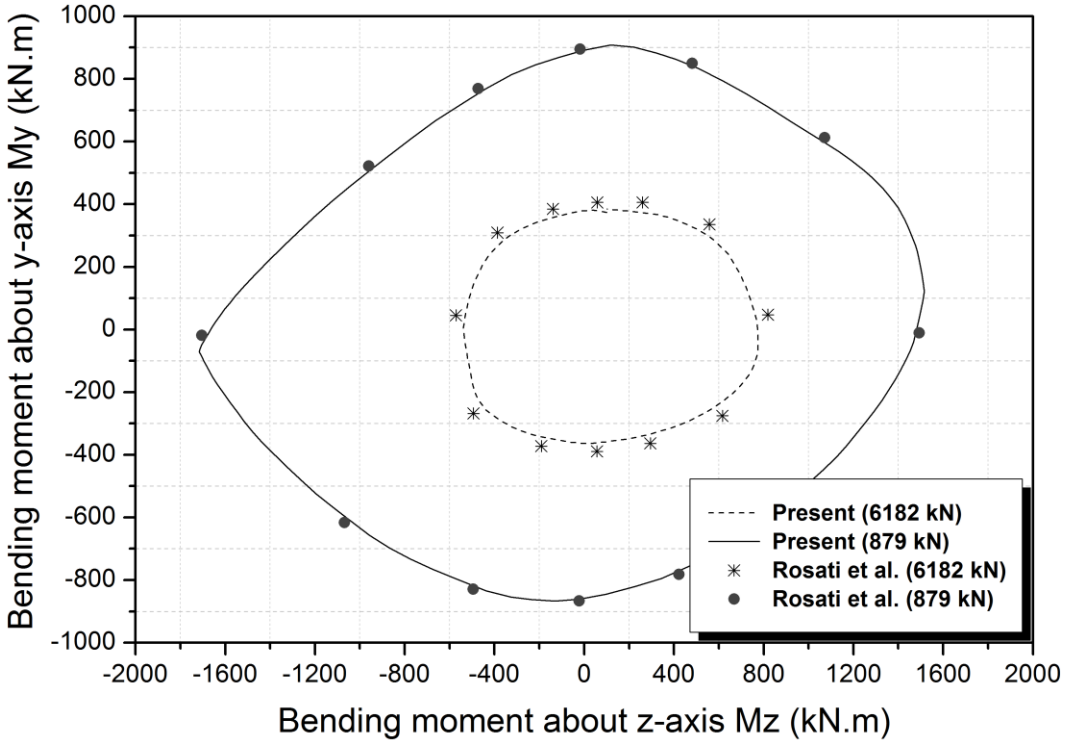

(d) Comparison results – Group 2

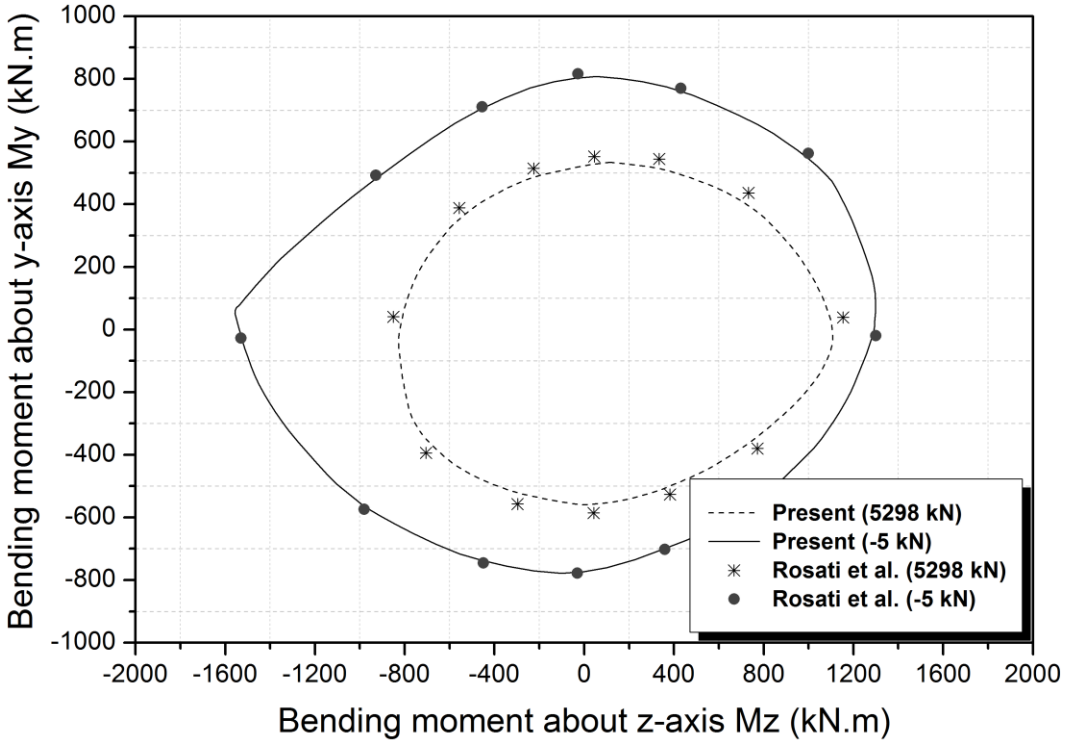

(e) Comparison results – Group 3

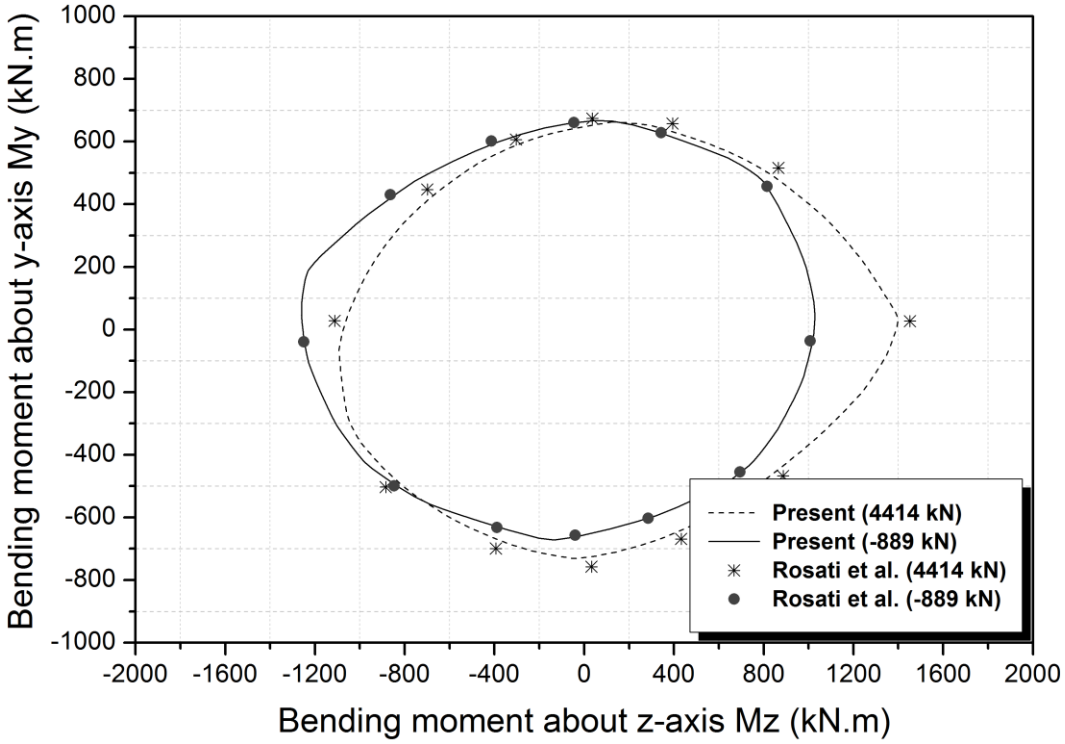

(f) Comparison results – Group 4

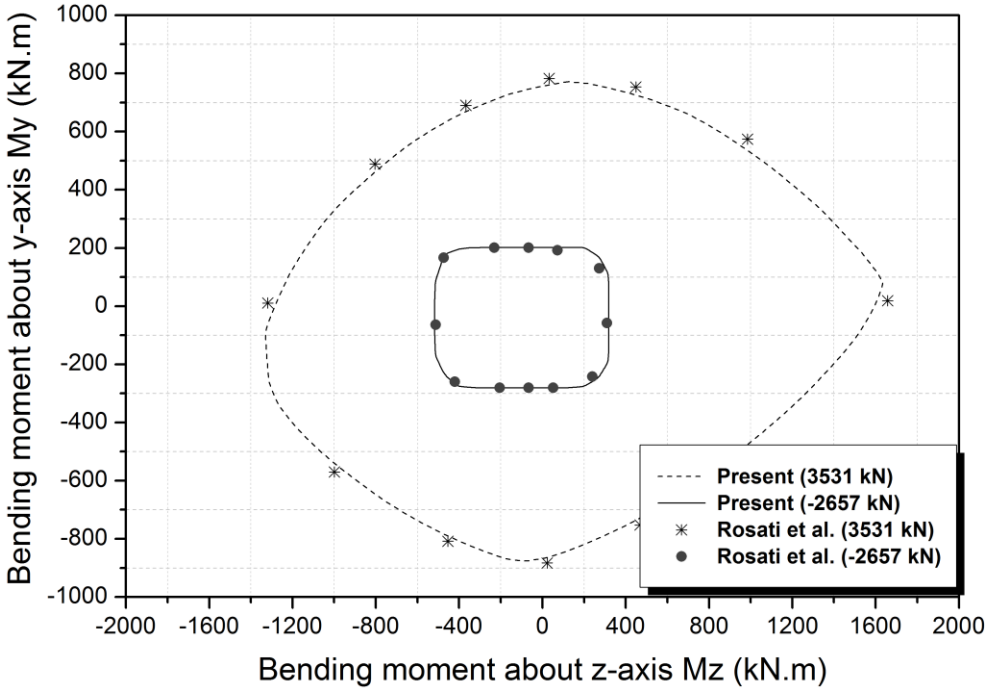

(g) Comparison results – Group 5

Figure 5.22 Comparison results of Rosati's RC Section – G Shaped Section

Concrete: fck=20.75 MPa ;ϒc=1.6 ; Cover is 30 mm

Reinforcement Bars: fyk=375 MPa; ; ϒb=1.15(ϕ20 at corners; ϕ20 on faces)

Stress vs. strain curve of concrete:

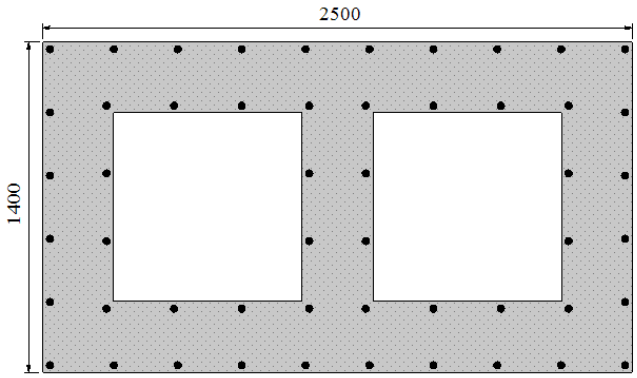

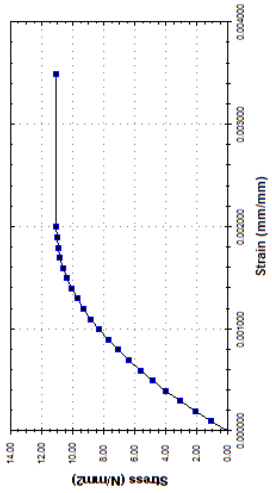

(a) Overview of section

(b) Concrete Properties

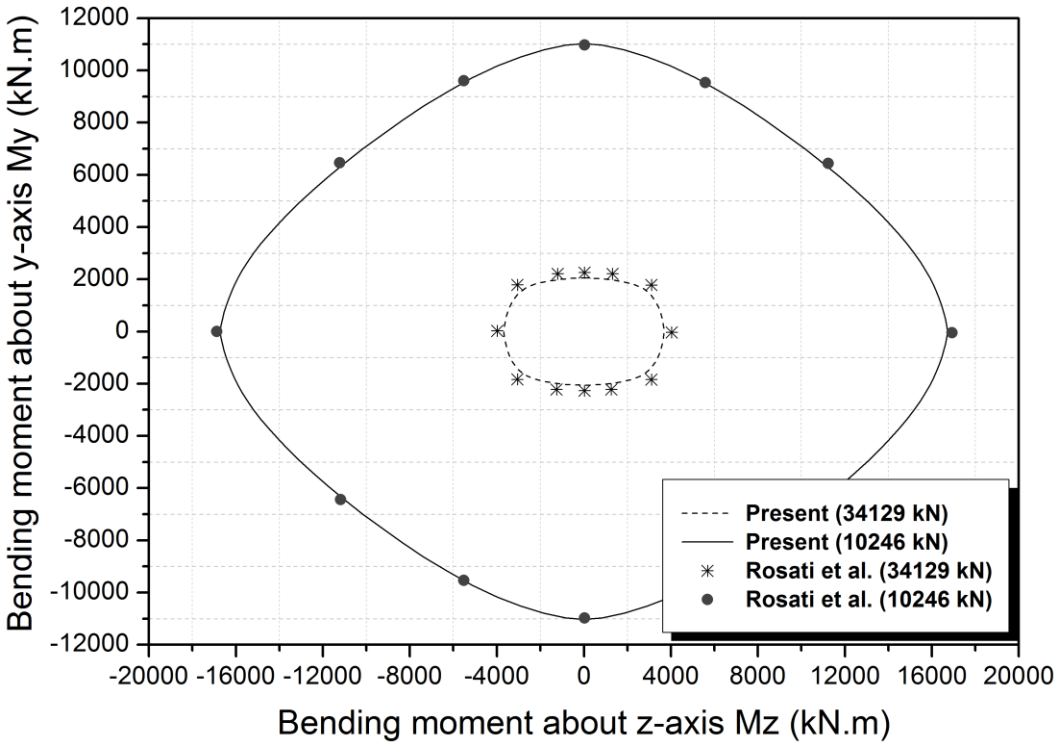

(c) Comparison results – Group 1

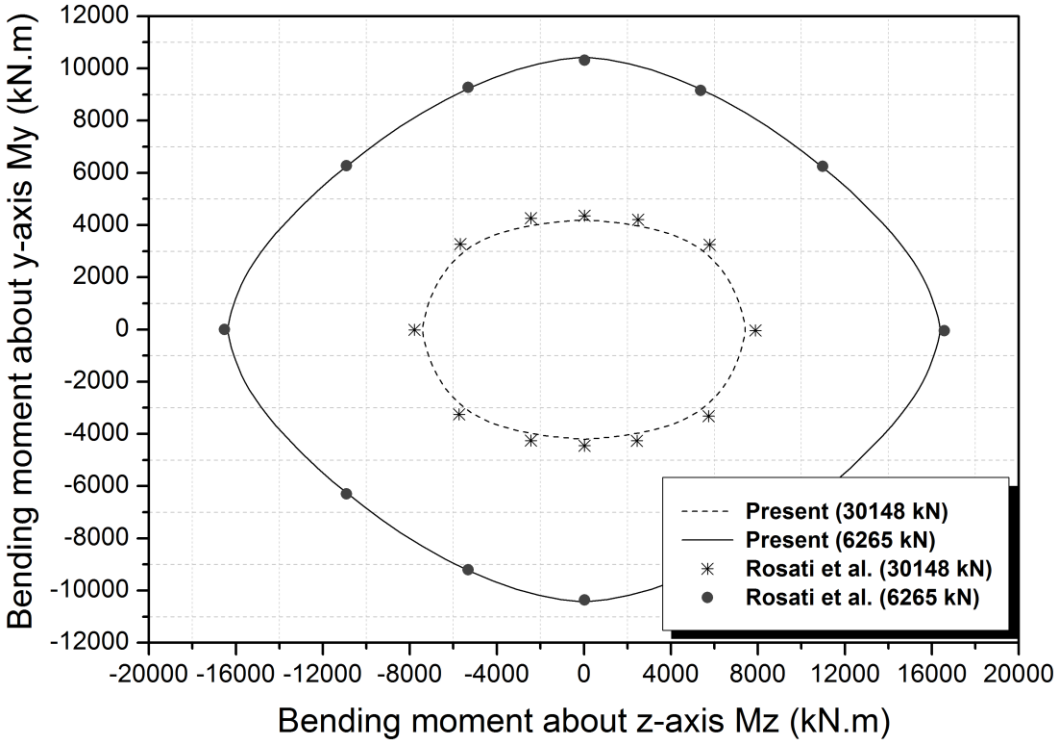

(d) Comparison results – Group 2

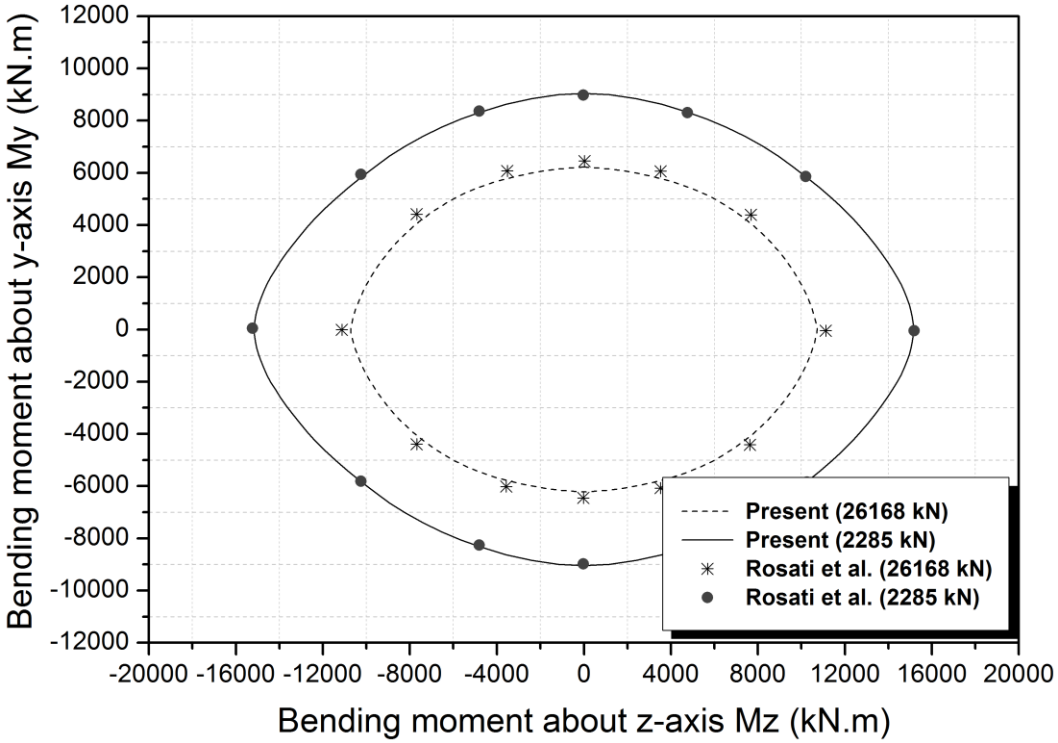

(e) Comparison results – Group 3

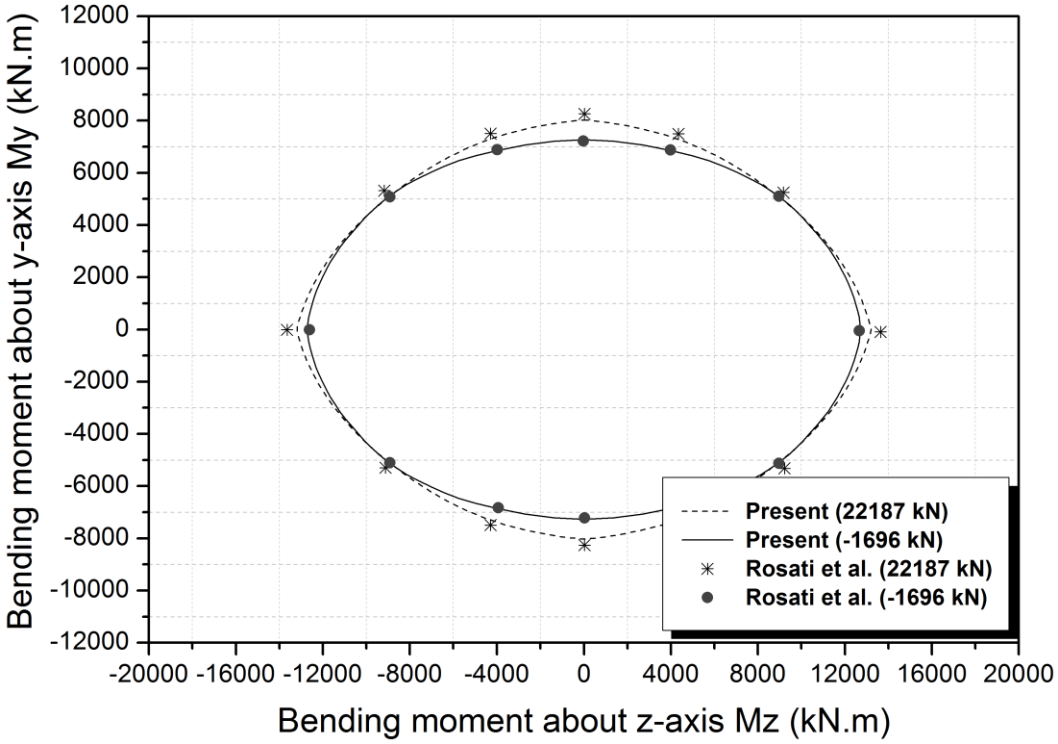

(f) Comparison results – Group 4

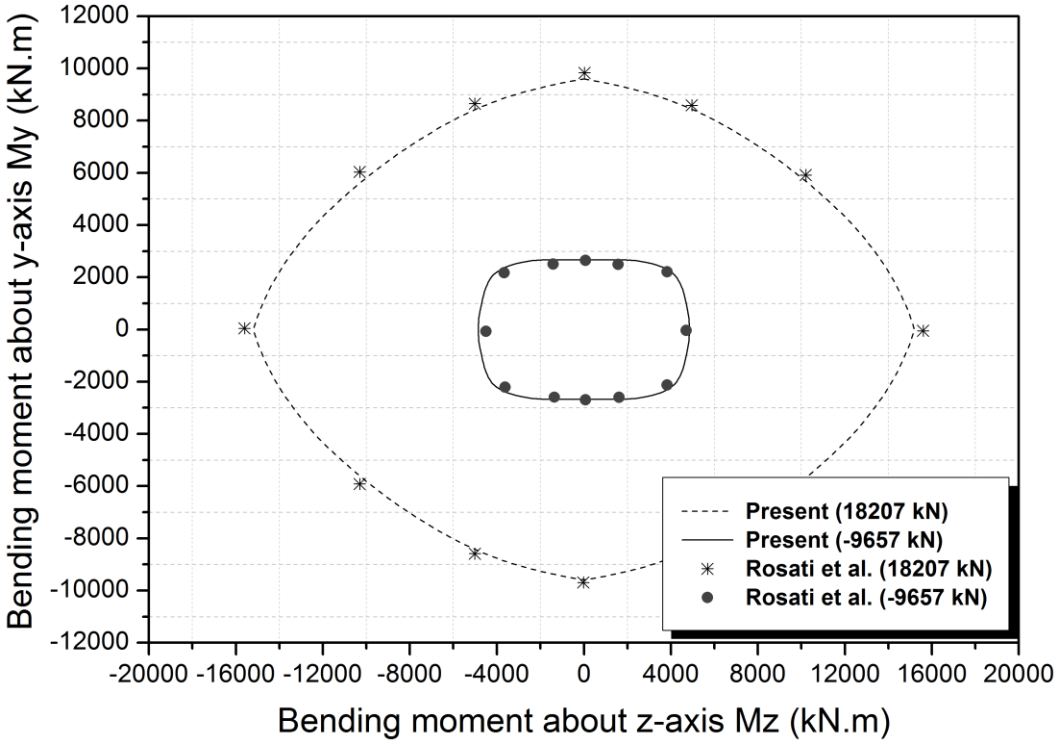

(g) Comparison results – Group 5

Figure 5.23 Comparison results of Rosati's RC Section – Multicell Section

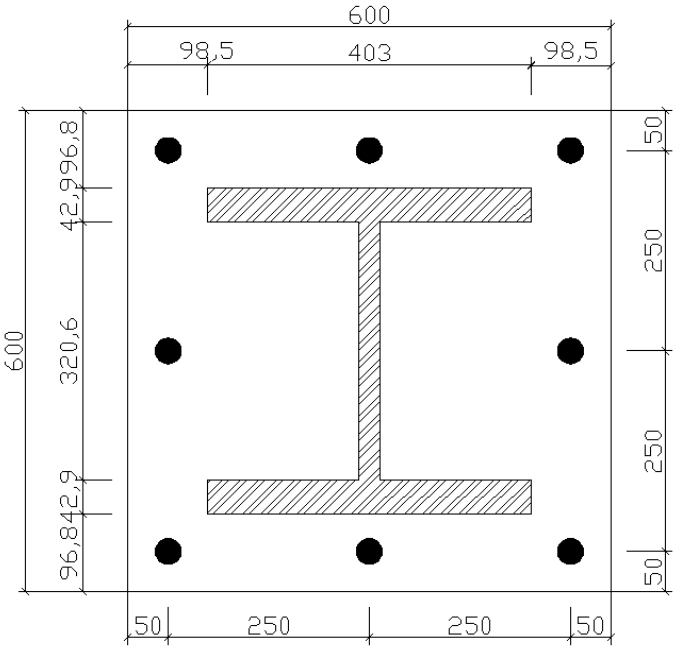

Concrete:

fck=40 MPa ;
Ecm=34 GPa ;
ϒc=1.5

Reinforcement bars:

fy=460 MPa;
Es=205 GPa ;
ϒb=1.15
(ϕ32 at corners; ϕ32 on faces ; Cover is 50 mm)

Structural Steel:

fy=355 MPa ;
Es=200 GPa ;
ϒs=1.05

(a) Overview of section (b) Material Properties

Figure 5.24 Typical encased composite section

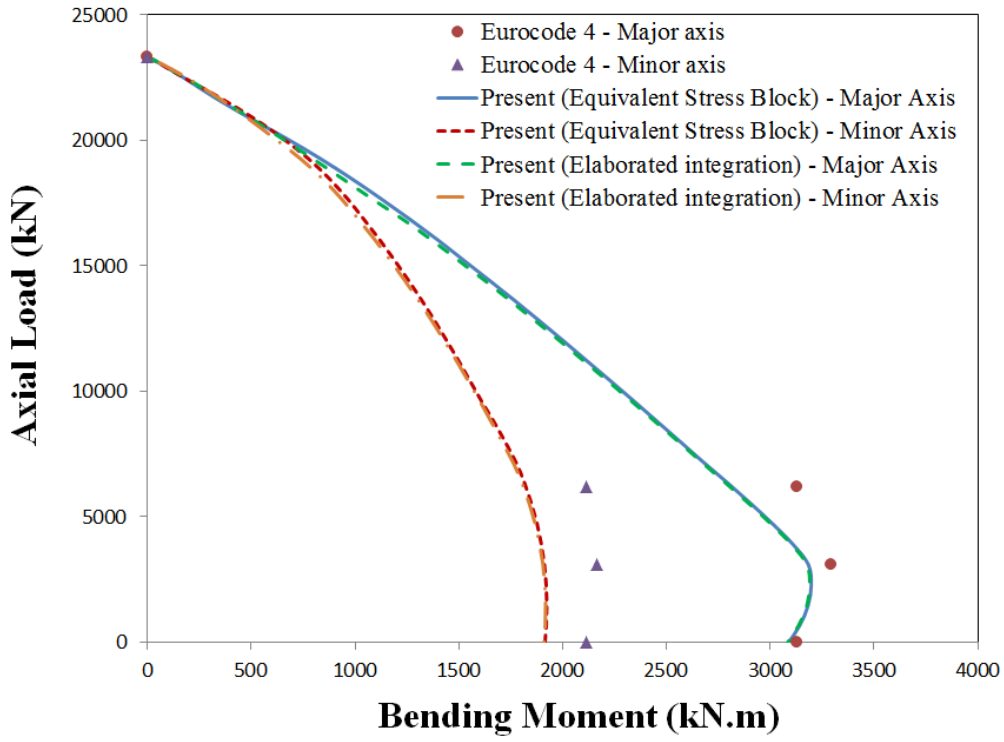

Figure 5.25 Comparison results of typical encased composite section

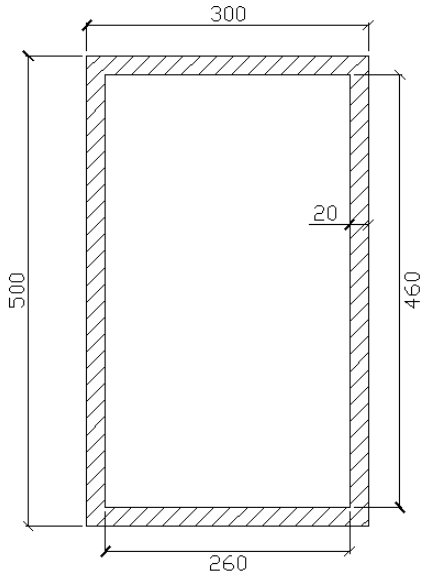

Concrete:

fck=40 MPa ;
Ecm=34 GPa ;
ϒc=1.5

Structural Steel:

fy=355 MPa ;
Es=200 GPa ;
ϒs=1.05

Note: confinement effect is considered.

(a) Overview of section (b) Material Properties

Figure 5.26 Typical concrete filled rectangular hollow section

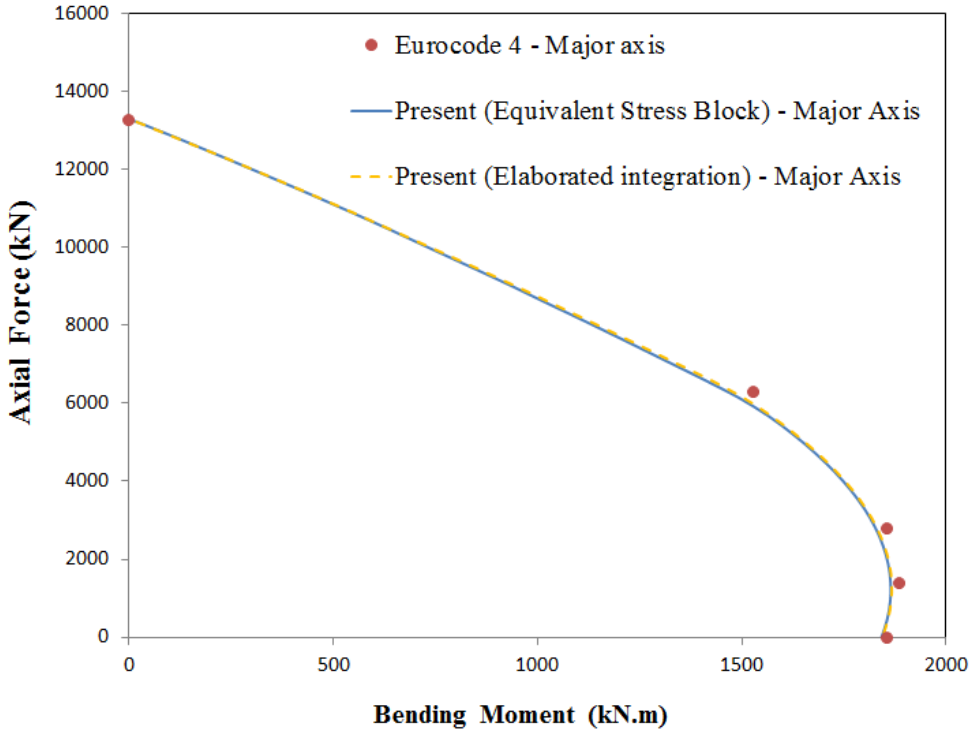

Figure 5.27 Comparison results of concrete filled rectangular hollow section

CHAPTER 6

SECOND-ORDER DESIGN OF HYBRID STEEL AND CONCRETE FRAMES

This chapter proposes a unified design approach for hybrid steel and concrete members and frames. By adopting the curved ALH (Arbitrarily located hinge) element previously discussed in Chapters 3 and 4, the P-Δ-δ effects and initial imperfections can be explicitly reflected in analysis, and then member strength checks can be easily conducted by examining the failure surfaces at critical locations. Thus, a unified design method is materialized and tedious and redundant formulations for considering column buckling based on linear analysis can be avoided. To clarify the design philosophy, this chapter elaborates on the major design principles. Additionally, effective flexural stiffness modeling of members with concrete components is investigated. Finally, a series of individual columns and several simple portal frames are selected, analyzed and designed by the proposed approach with the results compared with those obtained by codified methods based on linear analysis.

6.1 Introduction

Apart from verifying member strength, examining the local and overall stability of framed structures is always a concern in design practice. The conventional approach, which is primarily based on the linear analysis method, requires additional complementary evaluations for the stability of axially compressed members. Given the variations in the corresponding provisions in codes for the second-order analysis of members of different materials, the design process is cumbersome and tedious as illustrated in Figure 6.1.

Generally speaking, the conventional linear analysis approach idealizes a structural model by assuming that members and the entire frame are perfect in geometry and their deformations are small. Therefore, the second-order effects associated with actual nonlinear behaviors cannot be directly reflected in analysis. In design of columns with moderate or high slenderness ratios, two common methods, namely as the effective length approach and moment amplification methods, are used. The former reduces column axial strength, whereas the latter enlarges first-order linear moments. Both methods can be adopted for the design of BS and SCC members in accordance with Eurocodes 3 (2005) and Eurocodes 4 (2004), respectively. The moment amplification method, in which nominal stiffness is adopted, can also be used to carry out the second-order design of RC columns, as indicated in Eurocode 2 (2004).

Despite the simplicities offered by the approximate methods for the second-order design of axially compressive members, these approaches are derived on the

basis of ideally isolated columns. When applied to framed structures that comprise hundreds of members, the assumptions drawn by the methods may be invalid. For example, the effective length method is theoretically accurate in the design of individual columns, but it assumes that all the columns in a frame simultaneously buckle, which seems improper in most actual situations. Moreover, due to the absence of P-Δ and P-δ moments, connection and foundation designs may be unsafe. Another example is a cantilever column under a concentric pure axial load. Although the moment amplification method is used, the design moment at the footing remains zero.

When designing a frame that comprises various types of members, therefore, existing approaches are tedious and involve irrational assumptions, which may present difficulties in generating safe and reliable design results. As an alternative, the current work puts forward a unified second-order nonlinear analysis and design approach for hybrid steel and concrete framed structures. The approach is illustrated in Figure 6.2.

Unlike conventional design approaches, which require different codes associated with cumbersome and tedious formulations for stability design, the proposed method is simple and unified for various types of members. The basic concept behind this method is the accurate simulation of structural behavior, through which local and overall stability problems can be directly reflected in analysis. Thus, the need for the approximated second-order designs based on codes and the unreliable assumptions can be eliminated. Accordingly, the curved ALH element and analytical model

presented in Chapters 3 and 4 are adopted for simulation-based nonlinear analysis, in which initial member imperfections can be explicitly modeled.

Sequentially, the member strength check can be easily conducted by evaluating section capacities at critical locations (Chan & Zhou, 2000). Most codes provide simplified equations for calculating the capacities of simple and regular sections. To develop a generalized method for evaluating the arbitrary sections in a hybrid steel and concrete framed structure, the failure surface generated by the analysis technique discussed in Chapter 5 is introduced. A section capacity factor used with this sectional yield surface is also proposed to facilitate strength evaluation of a cross section.

The second-order analysis method of design is currently extensively used in the design of slender and complex steel framed structures in some places like Hong Kong, and many design codes recommend this method, such codes include AS4100 (1998), AISC (2010), Eurocode 3 (2005), and Hong Kong Steel Code (2011). Moreover, recently published composite codes, e.g., Eurocode 4 (2004), permit the use of the second-order nonlinear analysis method for the design of composite columns. Although the second-order design of slender RC columns is required in concrete codes such as Eurocode 2 (2004), a similar method for the direct second-order analysis of RC members and frames has not been well-documented.

Although codified methods for the second-order design of BS, RC and SCC members may differ, the considerations for P-Δ-δ effects and initial imperfections are theoretically and conceptually the same because these effects objectively exist in

all types of structures. In this thesis, the analytical model based on the curved ALH element is used in nonlinear analysis, and the failure surface generated by the proposed cross-section analysis in Chapter 5 is adopted in the evaluation of member strength. A unified design approach for various members and frames can be accordingly developed.

This chapter mainly focuses on illustrating the major design principles underlying the proposed design method. To appropriately reflect concrete cracking effects, effective flexural stiffness modeling is discussed. Finally, a series of individual columns and several portal frames are designed by the proposed second-order analysis approach, and the results are compared with those obtained by codified methods based on the linear analysis.

6.2 Unified second-order design method

The philosophy of the proposed second-order analysis method is the accurate simulation of crucial factors that affect structural and member stability. These factors include P-δ and P-Δ effects, initial imperfections and so on. In this section, the major design principles of the proposed method are elaborated and the verification of member strength is discussed.

6.2.1 P-Δ and P-δ effects

Both P-Δ and P-δ effects are essential in second-order nonlinear analysis because they represent influence on the geometric changes of a structure and the

deflection of members under applied loads (Figure 6.3). These effects are significant in the analysis of slender members and framed structures, in which large induced moments could affect stability.

The P-Δ effect, also called the frame side-sway effect, is the overall effect caused by the horizontal deflection of a structure. In this study, an additional moment is accordingly induced as the P-Δ moment. This effect is critical to the design of high-rise buildings, which are exposed to heavy vertical forces and strong lateral wind loads. In the present study, the P-Δ effect is considered through a numerical incremental-iterative procedure, in which the geometrical changes of the analytical model are continuously updated in iterations.

The P-δ effects refer to local member effects that are due to the deflection associated with axial loads, wherein an additional moment is induced as the P-δ moment. This moment influences member stiffness and sectional stress at critical locations. If initial member imperfections are not directly simulated in the analytical model, the analysis of these effects is inaccurate. For example, no P-δ moment occurs in a perfectly straight and slender column under purely axial loads, where a situation that does not happen in reality. Furthermore, tedious formulation related complementary check of member buckling is required. In this thesis, the initial curved ALH element is introduced to represent the P-δ effect.

6.2.2 Initial member imperfection

The initial member imperfections unavoidably exist in all kinds of members that stem from fabrication, construction, transportation and other activities like welding; these imperfections significantly affect member strength and stiffness under applied loads. Codes, such as Eurocode 3 (2005), therefore require the consideration of member imperfections in second-order nonlinear analysis. Most conventional analyses assume perfectly straight beam-column members, which may cause improper estimations on the member strength.

Two alternative methods for modeling member imperfections are indicated in Eurocode 3 (2005): the direct modeling approach and equivalent horizontal force method (Figure 6.4). The former explicitly simulates initial curvature by assuming a sine function, whereas the latter introduces an equivalent distributed load that represents the influence of the induced effect due to initial member curvature. Both methods are theoretically valid for analyzing individual members. Nevertheless, using the equivalent distributed load method necessitates the removal of additional forces and moments at boundaries; otherwise, foundation design may be cost-ineffective. This situation prompts the use of the direct modeling method, which may be more suitable and efficient for actual applications.

In direct simulation of initial member curvature, two or more conventional straight elements are usually required. This approach not only dramatically increases computational expense, but also causes difficulties in the identification of critical sections along a member. To address this problem, the curved beam-column element discussed in Chapters 3 and 4 is introduced in the simulation of initial member imperfections, in which one element per member is adequate.

Initial member curvatures vary with respect to member types, making accurate modeling highly challenging. As a solution, codes accordingly provide conservative imperfection values for various member types. For example, Eurocode 3 (2005) provides different types of imperfection values for section types as in Table 6. 1 and Eurocode 4 (2004) presents a table of imperfection values for several types of composite sections as in Table 6. 2. For RC members, a value of L/200 is adopted.

6.2.3 Initial frame imperfection

Initial frame imperfections are caused by out-of-plumpness of a structure, which inevitability occurs during construction. These imperfections can affect the lateral stability of an entire structural system and induce additional P-Δ moments. With the absence of global imperfections, the ultimate loads of a framed structure may be over-estimated. Fong *et al.* (2012) conducted numerical and experimental study on the snap-through buckling behaviors of shallow domes, and reveals that the failure load of a perfect dome is more than 150% larger than the ultimate strength of an imperfect dome. This finding indicates the necessity of considering these global effects for reliable and safe designs for shallow domes and other forms of structures.

Similarly, two types of modeling methods are discussed in Eurocode 3 (2005): the direct modeling approach and equivalent nodal force method as in Figure 6.5. Both methods are simple and efficient. Direct modeling requires the offsetting of beam-column nodes, whereas the equivalent nodal force method requires the calculation and application of additional joint loads. This study employs the former.

Most of the codes require taking into account overall geometric imperfections. A unified sway imperfection for RC, BS and SCC frames is given in Eurocodes 2 (2004), 3 (2005) and 4 (2004), respectively. This imperfection is expressed as

$$\varphi = \varphi_0 \alpha_h \alpha_m \tag{6. 1}$$

in which φ_0 is the basic value of initial frame imperfections (recommended value is 1/200); α_h denotes a reduction factor associated with the overall height h of the frame equal to $\alpha_h = 2/\sqrt{h}$ but $2/3 \leq \alpha_h \leq 1$; and α_m represents another reduction factor for the number of columns in each row in a vertical plane. This reduction factor is written as follows:

$$\alpha_m = \sqrt{0.5\left(1 + \frac{1}{m}\right)} \tag{6. 2}$$

where, m represents the number of columns in a row, which carries the forces in the vertical direction larger than 50%.

6.2.4 Member strength check

The conventional design method based on linear elastic analysis evaluates stability member by member; this method utilizes cumbersome effective length assumptions and related formulations. Different codes are selected in the evaluation of various members; thus, the design procedure for hybrid steel and concrete framed structures is tedious. In the second-order design approach, member strength can be conveniently evaluated by cross-section capacities at critical locations because P-Δ

and P-δ effects, as well as initial member and frame imperfections, are directly reflected in analysis.

Due to the complexities of arbitrary sections, formulating a simple capacity equation for various types of sections is impossible and tedious calculation of ultimate capacities is unavoidable in conventional design. Therefore, the failure surface discussed in Chapter 5 is introduced for a unified verification of arbitrary section strength. Herein, a section capacity factor φ_f is defined as,

$$\varphi_f = \frac{\sqrt{(M_y + N_x\Delta_y + N_x\delta_y)^2 + (M_z + N_x\Delta_z + N_x\delta_z)^2}}{\left|M_p^{\varsigma}\right|} \tag{6. 3}$$

where N_x, M_y and M_z are the currently applied forces at section locations; Δ_y and Δ_z are the global displacements due to applied loads, including the effects of initial frame out-of-plumpness; δ_y and δ_z denote the local member deflections caused by bowing and curvature induced by end forces and initial imperfections; φ_f is the proposed section capacity factor for evaluating a cross-section; and M_p^{ς} represents the plastic moment capacity with the same orientation angle aligned with applied moments under the same axial forces.

In design practice based on the first-plastic hinge method, the ultimate load is determined by the loads that cause the formation of the first plastic hinge, which is detected by calculating the section capacity factor φ_f along a member when it is greater than unity. Therefore, any member that reaches a section capacity factor φ_f larger than 1.0 is considered failed and the corresponding forces are taken as the resistant design loads.

6.2.5 Summary

The major design philosophy inherent to the proposed second-order design method for various members is presented and discussed in this section. Geometric nonlinearity including the P-Δ and P-δ effects is essential to nonlinear analysis. Apart from this factor, initial member and frame imperfections are crucial to second-order design. Two alternative methods are indicated in the design codes, and the direct modeling method is more suitable for this research. Therefore, the curved ALH element proposed in the previous chapters is introduced in the direct simulation of initial member curvature. Moreover, the cross-section analysis technique in Chapter 5 is used to calculate the failure surfaces of arbitrary sections. A section capacity factor is put forward for the easy evaluation of member strength. On this basis, the unified second-order design approach can then be formulated.

6.3 Effective flexural stiffness modeling

Concrete is a brittle material that easily cracks under tensile forces, which influence the force distribution and overall deflection of a framed structure. The accurate simulation of a member composing of concrete components involves many factors; an example includes the load versus deflection behaviors of a cantilever column under eccentric loads as illustrated in Figure 6.6. To accurately simulate this behavior, the advanced analysis approach needs to be adopted and explained in the next chapter. In conventional design practice, only the final deflections and member

forces under ultimate limit states are required, regardless of intermediate load deflection history; and efficiency is always concerned.

To resolve the aforementioned issues, an effective flexural stiffness modelling approach is employed, in which the moment of inertia is reduced and used in designing the approximate reflection of concrete cracking effects. Several design codes and guidelines provide the related reduction factor for RC members. For example, the gross moments of inertia of highly and moderately loaded columns are reduced to 30% and 50% of the gross moment of inertia of non-cracked concrete, respectively, as recommended in FEMA 356 (2000). Moreover, New Zealand codes (1995) provide a detailed table for estimating the effective flexural stiffness of RC members under different loading conditions. In analyzing cracking effects in this work, the following models from Eurocodes 2 (2004) and Eurocodes 4 (2004) are adopted as,

For RC members

$$(EI)_{eff} = k_1 k_2 E_{cd} I_c + E_r I_r \tag{6. 4}$$

For composite members

$$(EI)_{eff} = 0.9(0.5E_{cd} I_c + E_r I_r + E_s I_s) \tag{6. 5}$$

where, E_{cd}, E_r and E_s are the Young's modulus of concrete, reinforcing bars and structural steel respectively; Ic, Ir and Is are the second moments of area for concrete, reinforcing bars and structural steel, respectively; k_1 denotes the factor related to concrete strength; and k_2 is a factor that depends on axial load and slenderness ratio. k_1 and k_2 can be calculated as,

$$k_1 = \sqrt{f_{ck}/20} \tag{6. 6}$$

$$k_2 = n \cdot \lambda/170 \leq 0.20 \quad (6.7)$$

in which f_{ck} is the characteristic concrete strength; n represents the dimensionless factor equal to $P/(A_c f_{cd})$; f_{cd} is the concrete design strength; and λ denotes the slenderness ratio.

The concrete fracture surface proposed in Chapter 5 can also be used for a reasonable estimation of concrete cracking within members. When a member does not crack under all the load combinations, the reduction factors for concrete components can be eliminated. Such a condition yields an economic and accurate design.

6.4 Verification examples

The unified second-order design approach for various members is demonstrated and verified in accordance with design codes. All the members in the examples are modeled by a single element, and the member strength checks are based on the failure surface. A series of individual members and several portal frames are designed by the proposed method, and the results are compared with those derived by codified linear design methods.

6.4.1 Buckling strength of steel columns vs. codified buckling curves

To evaluate the effectiveness of the proposed method against that of a conventional design, a series of steel columns is selected; the design strengths under both approaches are compared on the basis of Eurocode 3 (2005). All the cross-

section sizes are selected from standard section tables, and 20 columns with different non-dimensional slenderness values $\bar{\lambda}(=\sqrt{Psq/Pcr})$ ranging from 0.2 to 3.0 are used for each selected group. All the columns are made of S355 material, with design strength of 355 MPa. The results are compared with the buckling curves in the design codes, derived on the basis of initial imperfections. The buckling curves from "a" to "c" and their corresponding initial curvature values are shown in Table 6. 3.

The proposed method for conventional second-order design is comprehensively investigated, for which six groups of sections are selected as tabulated in Table 6. 4. This study analyses 4320 columns, which cover most of the typical sections in conventional practice as shown in Figure 6.7 to Figure 6.12. The moderate and large slenderness ratios obtained by the proposed method are close to the buckling curves in Eurocode 3 (2005), whereas the small slenderness ratio is slightly conservative. These findings are crucial for applying the current approach to practical second-order design. Using this method automatically reflects the buckling strengths of individual members and eliminates the need for assumptions on effective column length.

6.4.2 Design of an RC portal frame

In this example, a typical RC portal frame is selected for demonstrating and validating the proposed design approach as illustrated in Figure 6.13. The frame is 10 m wide and 6 m high. Two concentrated joint loads as100 and 1200 kN are applied in the vertical and horizontal directions, respectively. All the beam and

columns are rectangular reinforced concrete members that comprise reinforcing bars, and the diameter of the rebar is 32 mm. The characteristic compressive strength f_{ck} and Young's modulus E_{cm} of the concrete are 30 MPa and 33 GPa, respectively. The yield strength of the rebar is 460 MPa and its Young's modulus is 200 GPa. The partial factors for the concrete and rebar are 1.5 and 1.15, respectively. The conventional design method in Eurocode 2 (2004) is introduced for comparison.

Eurocode 2 (2004) provides two methods for carrying out a second-order design of RC columns as the nominal stiffness method and nominal curvature method. The former is suitable for individual members and entire structures, whereas the latter is limited to isolated members. Therefore, the method based on nominal stiffness is used to design the frame and linear analysis is introduced. The design procedure is briefly illustrated in Table 6. 5, which shows that the design process is tedious and inefficient. The effective length for the compressive member needed to be calculated in relation to the K-factors and the slenderness criterion should be checked.

The frame is also designed by the proposed second-order design method, and the comparison results are presented in Table 6. 6. The design results of the two approaches are very close, but the design procedure of the proposed method is simple and efficient. It also does not require assumptions on effective length.

6.4.3 Design of a SCC portal frame

A similar portal frame with geometry and loading pattern identical to those of the previous example is illustrated in Figure 6.14, where the beam and columns are

both SCC sections with embedded structural steel members. The diameter of the reinforcing bars is 20 mm. The yield strength of the structural steel is 355 MPa and its Young's modulus is 205 GPa. The Young's modulus of the concrete is 33 GPa and its characteristic compressive strength is 30 MPa. The yield strength of the reinforcing bar is 460 MPa, with a Young's modulus of 200 GPa. The partial factors for the concrete, rebar and structural steel are 1.5, 1.15 and 1.15, respectively.

The simplified second-order design method from Eurocode 4 (2004) is selected for the design of this SCC portal frame. The moment amplification method based on the effective flexural stiffness method is adopted in analyzing second-order effects. The design procedure is detailed in Table 6. 7. The design method for the composite columns also involves assumptions on effective member length. The overall design approach is similar to the counterpart in steel code as Eurocode 3 (2005).

The results from the proposed method are illustrated in Table 6. 8. And the difference between the results is slight. The direct second-order design approach has been recommended in Eurocode 4 (2004), and the elaborated cross section analysis method for the failure surface has also been allowed. Therefore, the design philosophy of the proposed method is in line with the approaches in Eurocode 4 (2004).

6.5 Concluding remarks

In this chapter, the unified design approach for hybrid steel and concrete members and framed structures is proposed. Using the ALH element enables the

direct reflection of P-Δ-δ effects and initial member curvature, as well as the convenient examination of member strength through the evaluation of section capacities at critical locations. The failure surface generated by the analysis technique proposed in Chapter 5 is introduced to accurately verify the arbitrary sections in a generalized manner. Accordingly, a section capacity factor is proposed for the easy evaluation for the utilization of member strength. The major design principles of the proposed design method are also explained, and the effective flexural stiffness modeling methods for reflecting concrete cracking effects are discussed. Finally, a series of individual columns and several portal frames are designed and compared with codified methods, which is proven to be efficient and reliable effective.

Figures

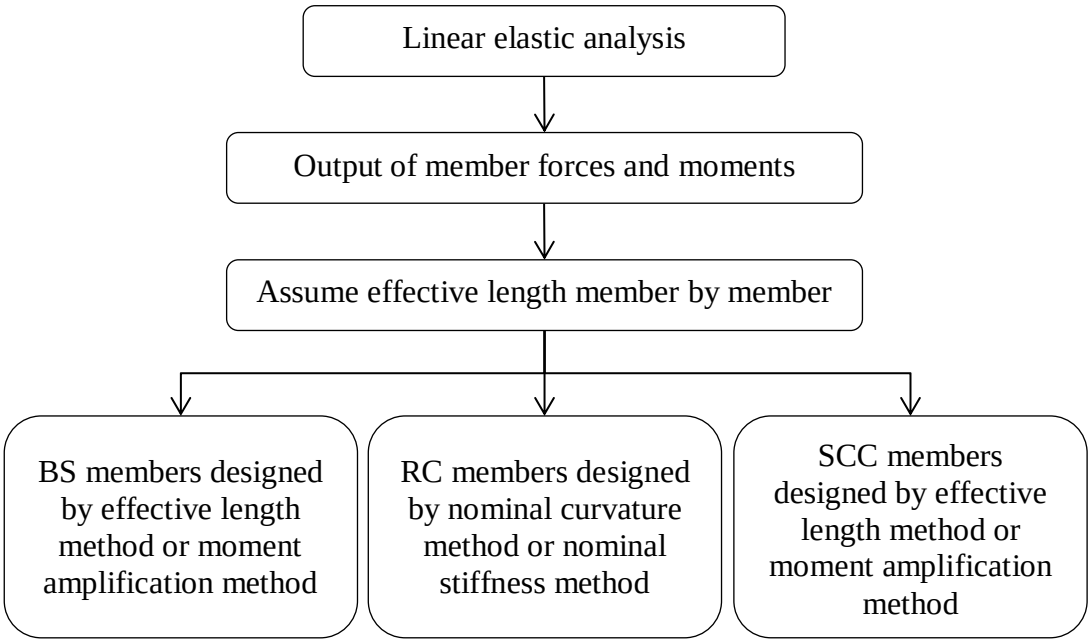

Figure 6.1 The conventional second-order design method

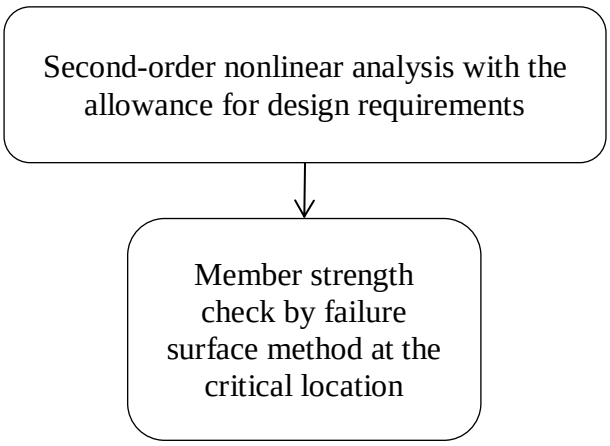

Figure 6.2 The proposed second-order design approach

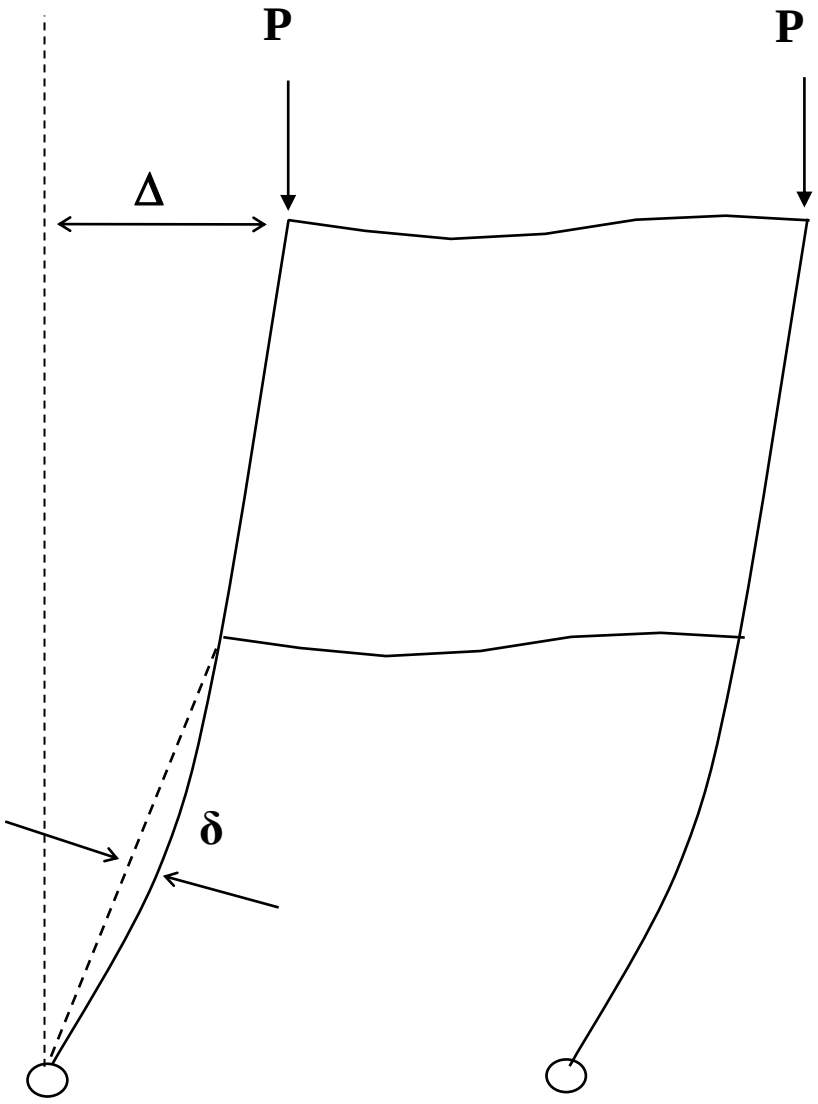

Figure 6.3 The P-Δ and P-δ Effects

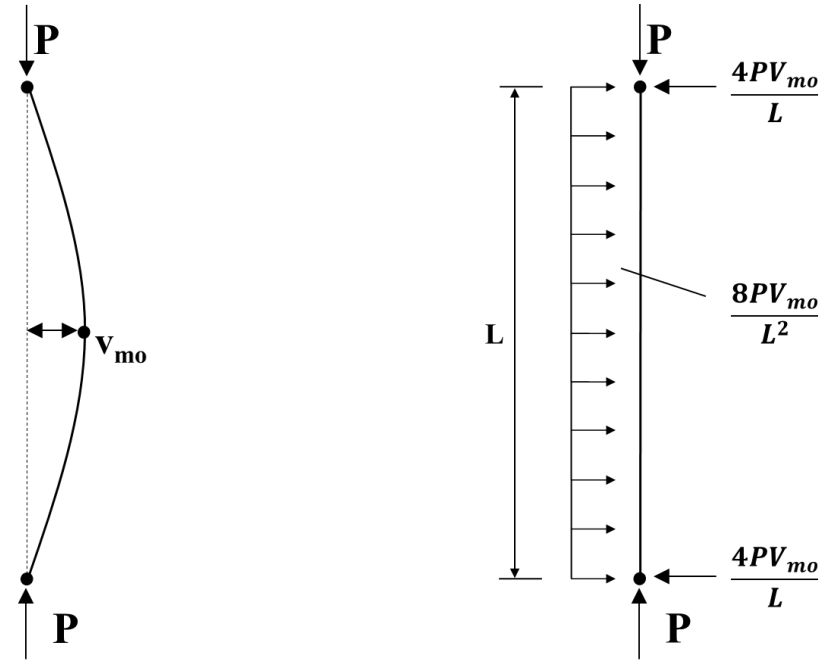

(a) Direct modeling approach (b) Equivalent horizontal forces method

Figure 6.4 Modeling initial member imperfections

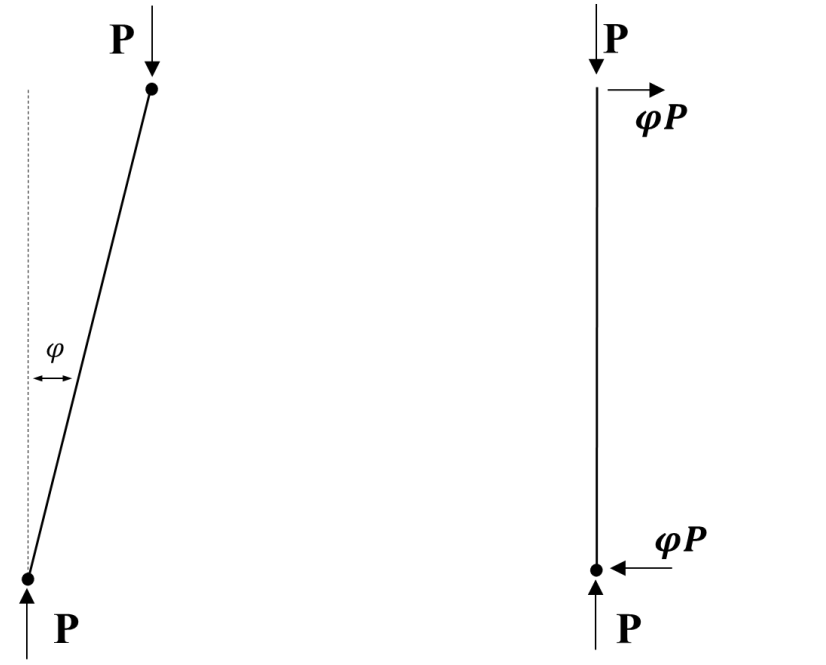

(a) Direct modeling approach (b) Equivalent horizontal forces method

Figure 6.5 Modeling initial frame imperfections

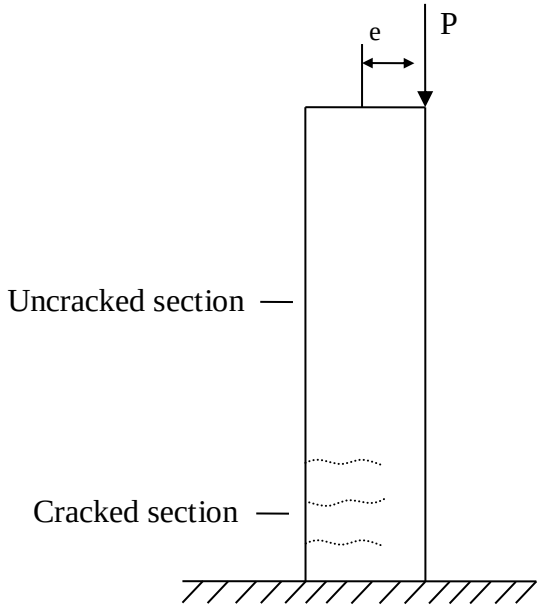

(a) Cantilever column subjected to eccentric axial load

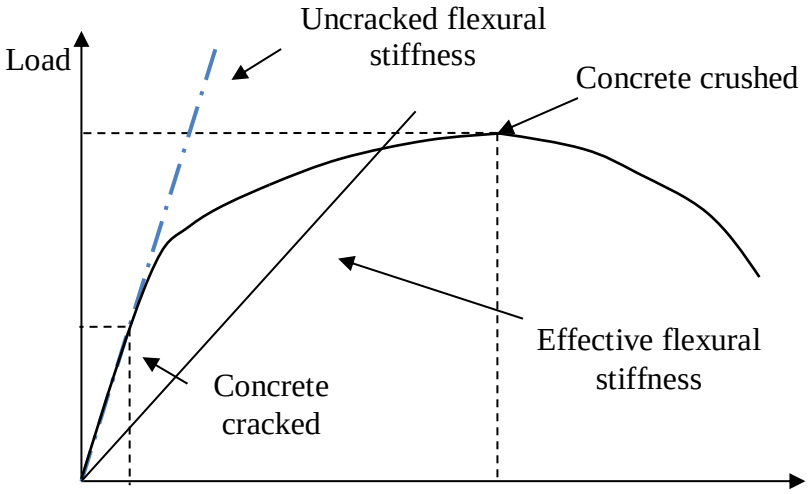

(b) Flexural behaviour at the section level

Figure 6.6 Behaviour of concrete component in flexure

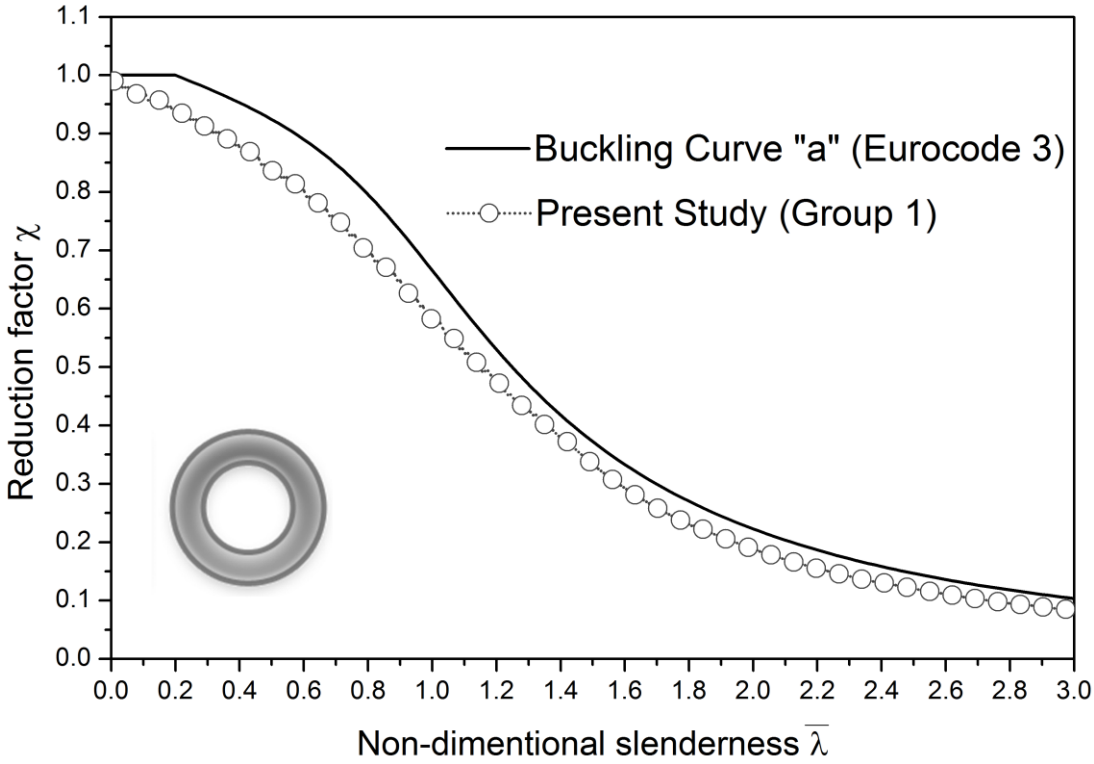

Figure 6.7 Comparison results of buckling curve for Group 1
(Circular hollow section columns with buckling curve a – 340 columns analyzed)

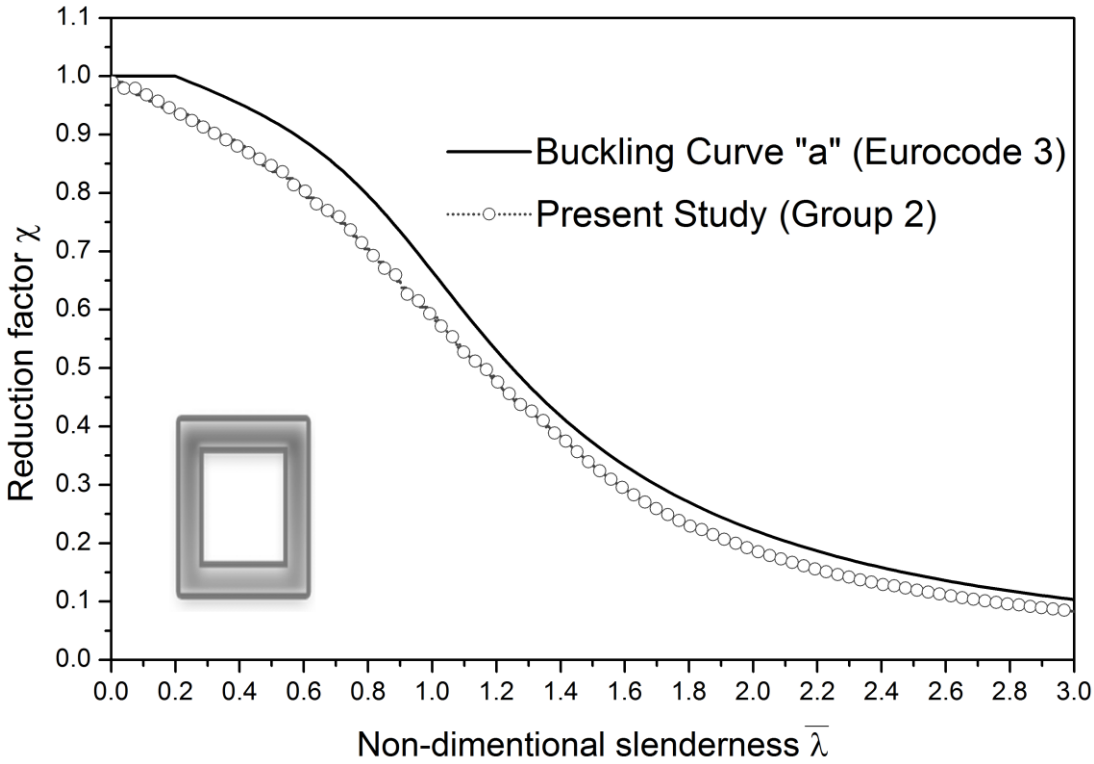

Figure 6.8 Comparison results of buckling curve for Group 2
(Rectangular hollow section columns with buckling curve a – 680 columns analyzed)

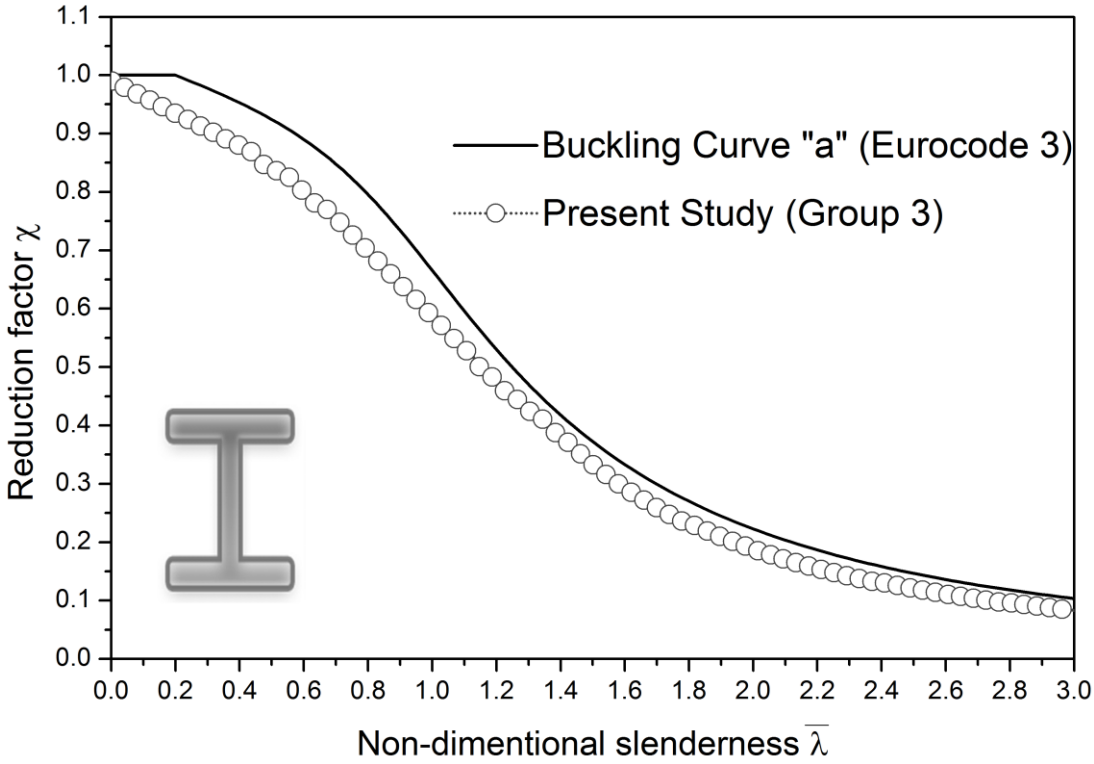

Figure 6.9 Comparison results of buckling curve for Group 3
(Rolled I/H Section columns with buckling curve a – 1520 columns analyzed)

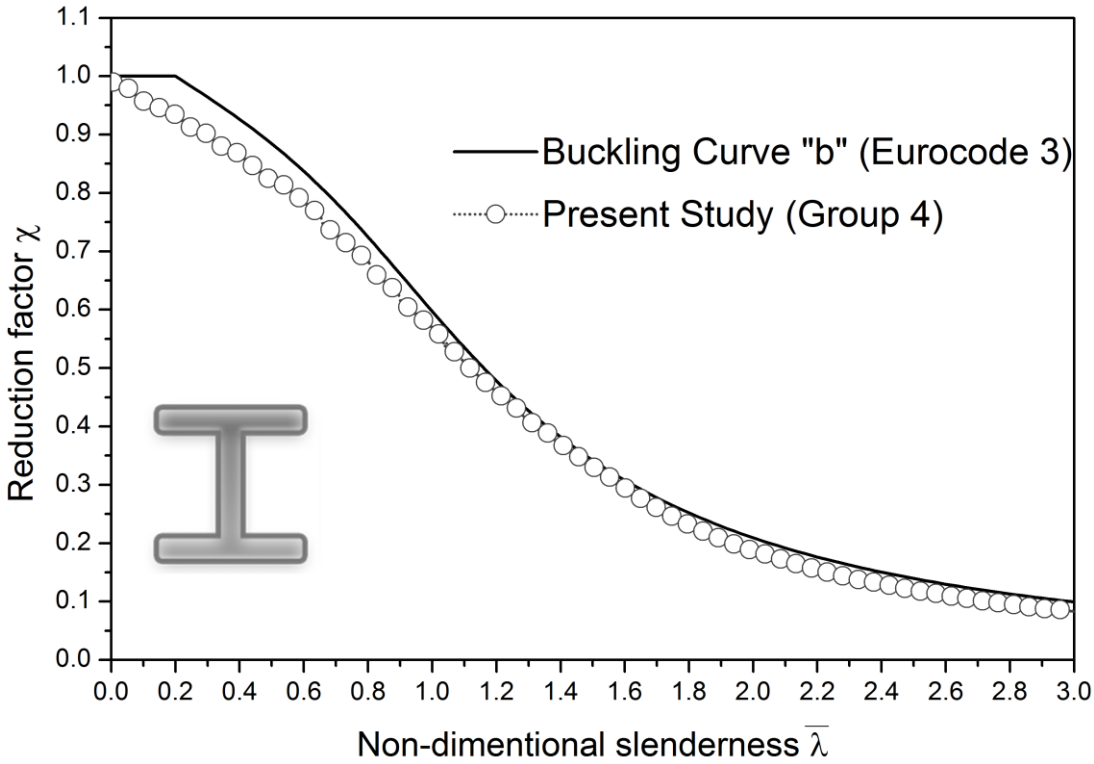

Figure 6.10 Comparison results of buckling curve for Group 4
(Rolled I/H Section columns with buckling curve b – 620 columns analyzed)

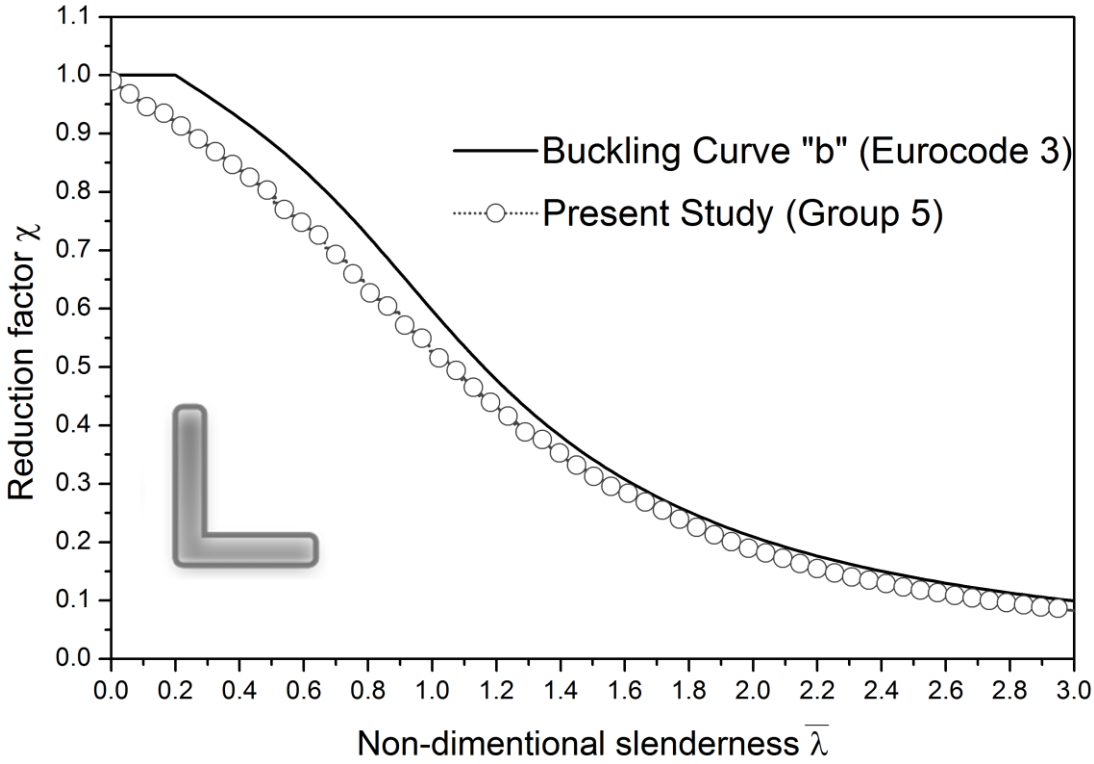

Figure 6.11 Comparison results of buckling curve for Group 5
(Angle section columns with buckling curve b – 840 columns analyzed)

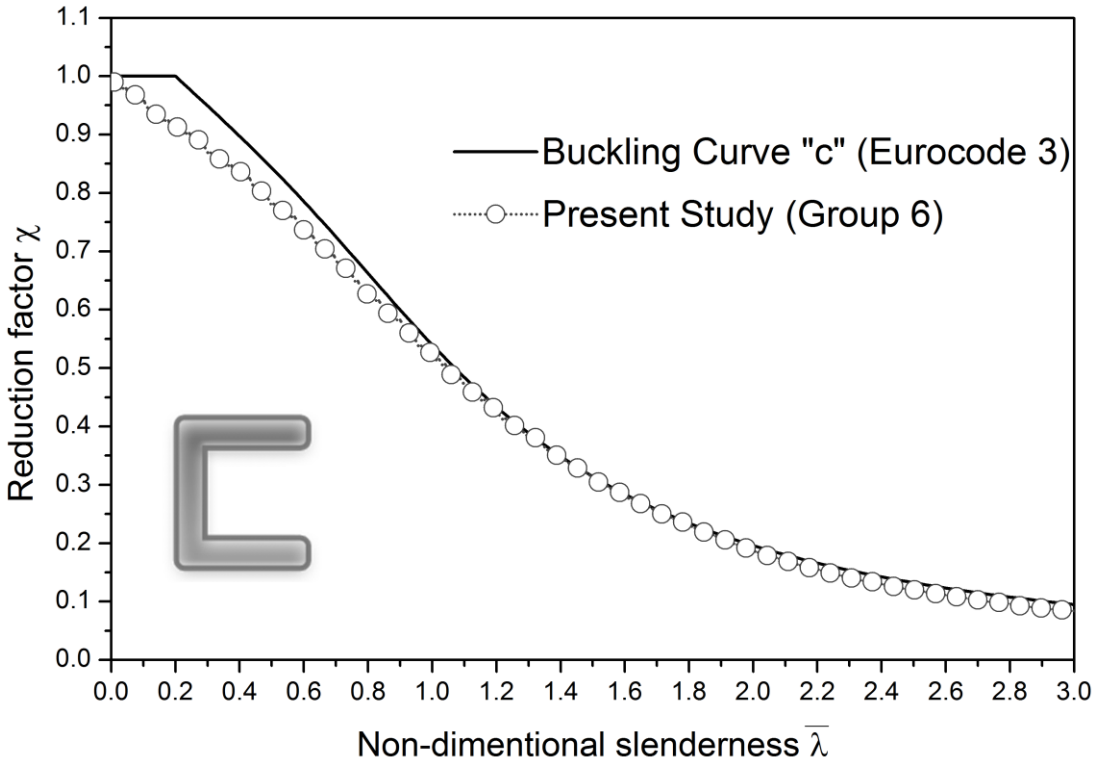

Figure 6.12 Comparison results of buckling curve for Group 6
(Channel section columns with buckling curve c– 320 columns analyzed)

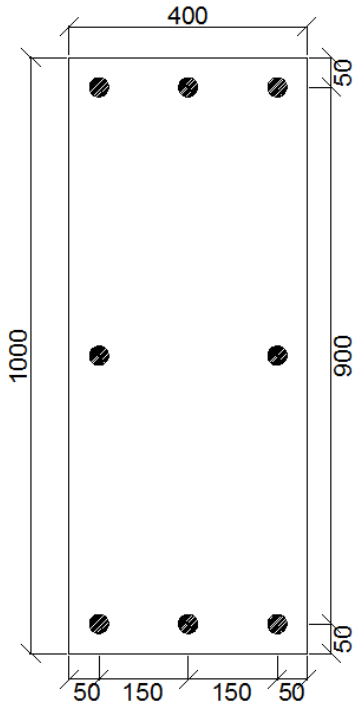

(a) RC Beam Section

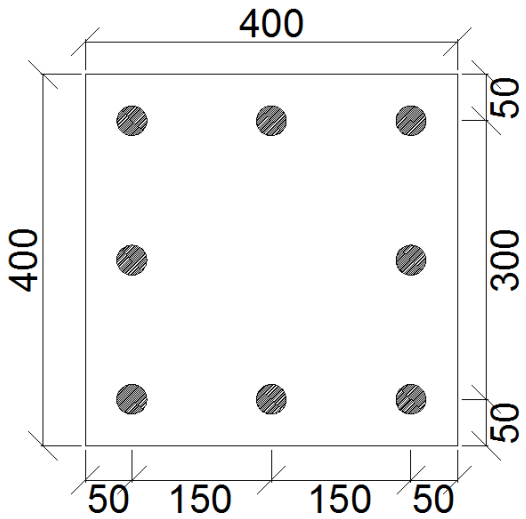

(b) RC Column Section

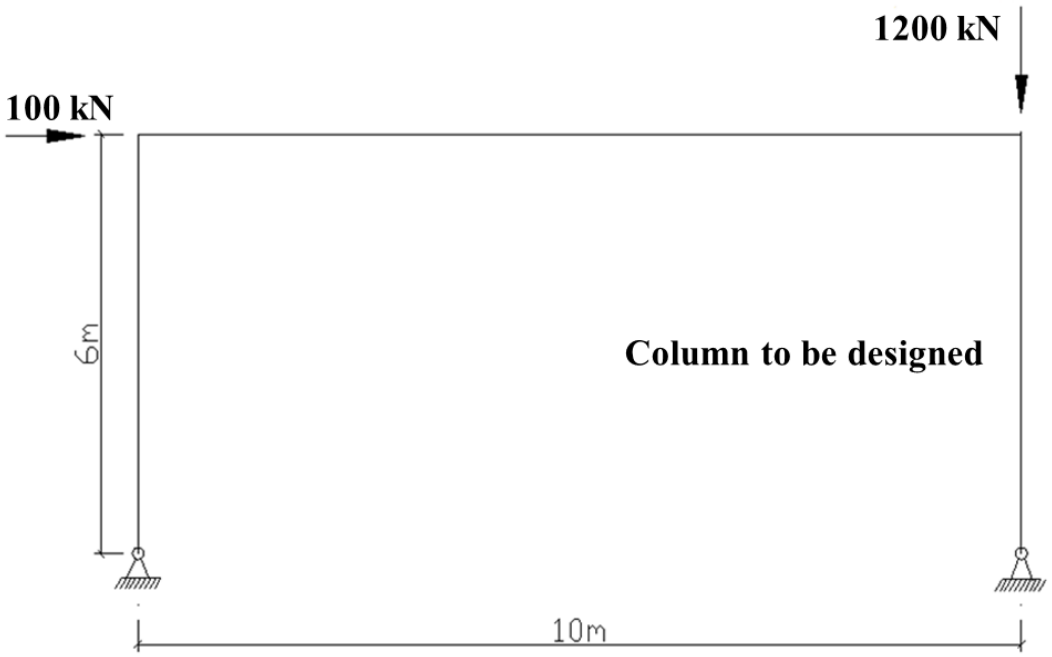

(c) Geometry and loading pattern

Figure 6.13 Properties of the RC portal frame

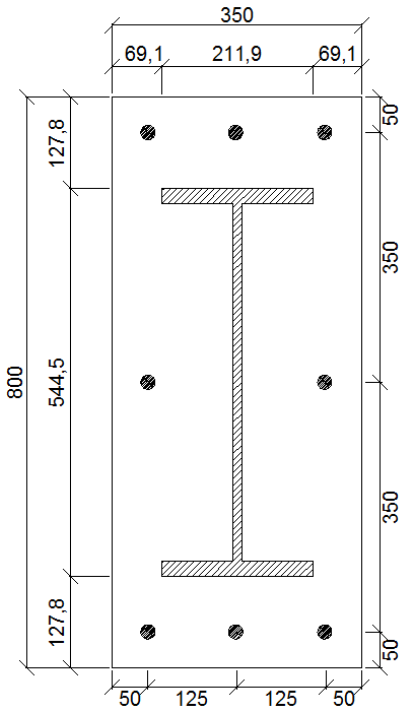

(a) RC Beam Section

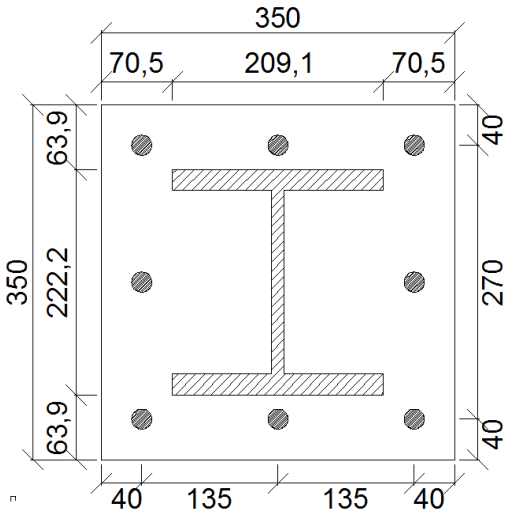

(b) RC Column Section

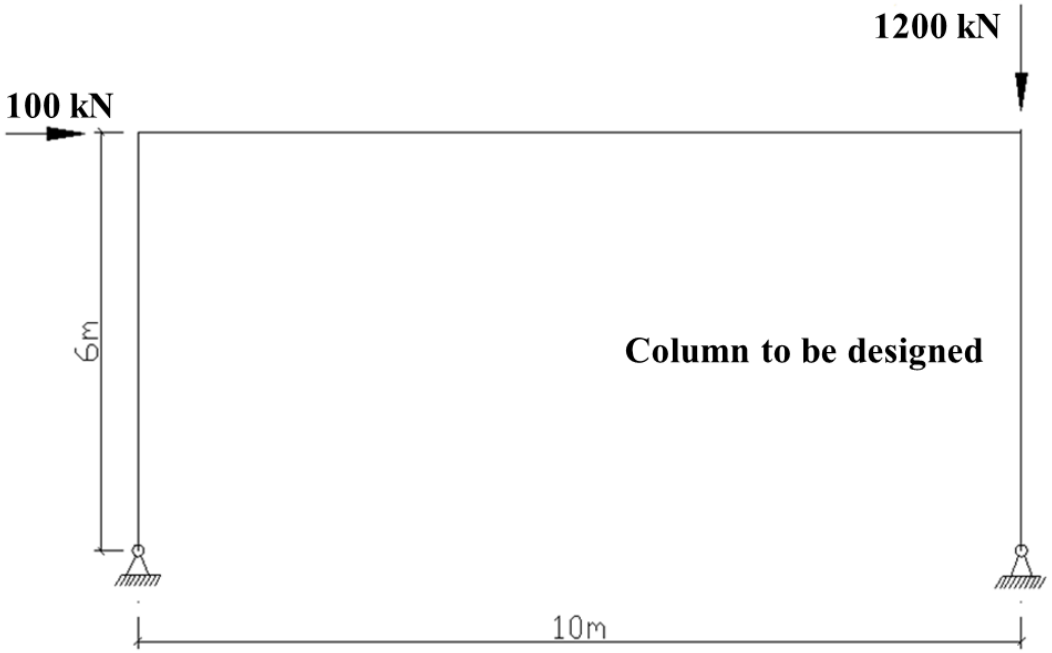

(c) Geometry and loading pattern

Figure 6.14 Properties of the SCC portal frame

Tables

Table 6. 1 Member imperfections for steel members in Eurocode 3 (2005)

Section Types	**Limits**	**Buckling Axis**	**Imperfections**	
			S235 to S420	**S460**
Rolled I-sections	h/b>12	Major	L/300	L/350
	$t_f \leq 40$mm	Minor	L/250	L/350
	h/b>12	Major	L/250	L/300
	$40 < t_f \leq 40$mm	Minor	L/200	L.300
	h/b≤12	Major	L/250	L/300
	$t_f \leq 100$mm	Minor	L/200	L/300
	h/b≤12	Major	L/150	L/200
	$t_f > 100$mm	Minor	L/150	L/200
Welded I-sections	$t_f \leq 40$mm	Major	L/250	L/250
		Minor	L/200	L/200
	$t_f > 40$mm	Major	L/200	L/200
		Minor	L/150	L/150
Hollow Sections	Hot Finished	Any	L/300	L/350
	Cold Formed	Any	L/200	L/200
Welded Box Sections	Generally (except as below)	Any	L/250	L/250
	Thick Welds: $a > 0.5\ t_f$ $b/t_f < 30$, $h/t_w < 30$	Any	L/200	L/200
U-, T- and Solid Sections		Any	L/200	L/200
L-Sections		Any	L/200	L/200

Notes: h is the section height; b is the section width; t_f is the flange thickness; t_w is the web thickness

Table 6. 2 Member imperfections for composite members in Eurocode 4 (2004)

Section Types	**Reinforcing Ratio** ρ_s	**Buckling Axis**	**Imperfection**
Concrete Encased Sections		Major	L/200
		Minor	L/150
Partially Concrete Encased Sections		Major	L/200
		Minor	L/150
Circular and Rectangular Hollow Steel Sections	$\rho_s \leq 3\%$	Any	L/300
	$3\% < \rho_s \leq 6\%$	Any	L/200
Circular Hollow Steel Sections with additional I sections		Major	L/200
		Minor	L/200
Partially Concrete Encased Section with I-sections		Any	L/200

Table 6. 3 Design value of initial imperfection e_0/L for members

Buckling Curve Type	$\boldsymbol{e_0/L}$
a	1/300
b	1/250
c	1/200

Table 6. 4 Selected groups of the columns to be analyzed

ID	Section Type	About Axis	Buckling Curve	Section Sizes		
1	Circular Hollow Section	any	a	CHS508.0x32.0	CHS457.0x25.0	CHS406.4x20.0
				CHS355.6x25.0	CHS323.9x16.0	CHS273.0x20.0
				CHS244.5x25.0	CHS219.1x16.0	CHS193.7x16.0
				CHS168.3x10.0	CHS139.7x8.0	CHS114.3x6.3
				CHS88.9x6.3	CHS76.1x4.0	CHS60.3x4.0
				CHS48.3x5.0	CHS33.7x4.0	
2	Rectangular Hollow Section	major axis	a	SHS400x20.0	SHS350x16.0	SHS300x16.0
				SHS250x16.0	SHS200x16.0	SHS180x12.5
				SHS160x12.5	SHS150x10.0	SHS140x8.0
				SHS120x10.0	SHS100x8.0	SHS90x6.3
				SHS80x8.0	SHS70x8.0	SHS60x6.3
				SHS50x6.3	RHS500x300x20.0	RHS500x200x16.0
				RHS450x250x16.0	RHS400x200x12.5	RHS300x100x10.0
				RHS250x150x12.5	RHS200x150x10.0	RHS200x120x8.0
				RHS200x100x12.5	RHS160x80x10.0	RHS150x100x10.0
				RHS120x80x8.0	RHS100x60x8.0	RHS100x50x10.0
				RHS90x50x6.3	RHS80x40x6.3	RHS70x70x3.0
				RHS60x40x6.3		
3	Rolled I/H Section (D/B>1.2)	major axis	a	UB1016x305x314	UB1016x305x272	UB1016x305x249
				UB1016x305x222	UB914x419x388	UB914x419x343
				UB914x305x289	UB914x305x253	UB914x305x224
				UB914x305x201	UB838x292x226	UB838x292x194
				UB838x292x176	UB762x267x197	UB762x267x173
				UB762x267x147	UB762x267x134	UB686x254x170
				UB686x254x152	UB686x254x140	UB686x254x125
				UB610x305x238	UB610x305x179	UB610x305x149
				UB610x229x140	UB610x229x125	UB610x229x113
				UB610x229x101	UB533x210x122	UB533x210x109
				UB533x210x101	UB533x210x92	UB533x210x82
				UB457x191x98	UB457x191x89	UB457x191x82
				UB457x191x74	UB457x191x67	UB457x152x82
				UB457x152x74	UB457x152x67	UB457x152x60
				UB457x152x52	UB406x178x74	UB406x178x67
				UB406x178x60	UB406x178x54	UB406x140x46
				UB406x140x39	UB356x171x67	UB356x171x57
				UB356x171x51	UB356x171x45	UB356x127x39
				UB356x127x33	UB305x165x54	UB305x165x46
				UB305x165x40	UB305x127x48	UB305x127x42
				UB305x127x37	UB305x102x33	UB305x102x28
				UB305x102x25	UB254x146x43	UB254x146x37
				UB254x146x31	UB254x102x28	UB254x102x25
				UB254x102x22	UB203x133x30	UB203x133x25
				UB203x102x23	UB178x102x19	UB152x89x16
4	Rolled I/H	major	b	UC356x406x634	UC356x406x551	UC356x406x467

	Section (D/B<1.2)	axis		UC356x406x393 UC356x406x235 UC356x368x153 UC305x305x240 UC305x305x137 UC254x254x167 UC254x254x89 UC203x203x71 UC203x203x46 UC152x152x23	UC356x406x340 UC356x368x202 UC356x368x129 UC305x305x198 UC305x305x118 UC254x254x132 UC254x254x73 UC203x203x60 UC152x152x37	UC356x406x287 UC356x368x177 UC305x305x283 UC305x305x158 UC305x305x97 UC254x254x107 UC203x203x86 UC203x203x52 UC152x152x30
5	Angle Section	y-y axis	b	L200x200x24 L200x200x16 L150x150x12 L120x120x12 L100x100x15 L100x100x8 L90x90x8 L80x80x8 L70x70x7 L60x60x8 L50x50x6 L45x45x4.5 L35x35x4 L25x25x4	L200x200x20 L150x150x18 L150x150x10 L120x120x10 L100x100x12 L90x90x12 L90x90x7 L75x75x8 L70x70x6 L60x60x6 L50x50x5 L40x40x5 L30x30x4 L25x25x3	L200x200x18 L150x150x15 L120x120x15 L120x120x8 L100x100x10 L90x90x10 L80x80x10 L75x75x6 L65x65x7 L60x60x5 L50x50x4 L40x40x4 L30x30x3 L20x20x3
6	Channel Section	major axis	c	[430x100x64 [300x90x41 [230x90x32 [200x75x23 [150x90x24 [100x50x10	[380x100x54 [260x90x35 [230x75x26 [180x90x26 [150x75x18	[300x100x46 [260x75x28 [200x90x30 [180x75x20 [125x65x15

Table 6. 5 Linear design of the RC portal frame

The nominal stiffness of the members: Beam : $(EI)_{nom}$ = 4.20x10^5 kNm^2 Column : $(EI)_{nom}$ = 3.61 x10^4 kNm^2	Buckling load based on nominal stiffness $N_B = \pi^2(EI)_{norm}/l_0^2$= 2331.25 kN
Internal forces from linear analysis: N = 1260kN, M_1=300kN.m	The first order design moment: M_{0Ed}=0.6M_{01}+M_{02}=180 kN.m
Effective length l_0 of the column: l_0= 2.06*l = 2.06*6000=12360mm	The total design moment: M_{Ed}= M_{0Ed}/(1-N/N_B)= 391.7 kN.m
Slenderness ratio of the column λ_{col}: i = 115.47 mm , λ_{col}= l_0/i=107.04	Section capacity factor: φ = 0.897
Limiting slenderness ratio λ_{lim}: For unbraced column λ_{lim}=87.51 (<107.04) This is a slender column.	

Table 6. 6 Design results of the RC portal frame

	First-order analysis & design	**Second-order analysis & design**
Design load		
Compressive force	1260kN	1270kN
Design Bending Moment	300kN.m	370.0kN.m
Max. Section capacity factor	0.897	0.847

Table 6. 7 Linear design of the SCC portal frame

The effective flexural stiffness $(EI)_{eff}$: Beam : $(EI)_{eff} = 4.78 \times 10^5$ kNm^2 Column : $(EI)_{eff} = 4.85 \times 10^4$ kNm^2 The effective flexural stiffness $(EI)_{eff,II}$: Beam : $(EI)_{eff,II} = 3.89 \times 10^5$ kNm^2 Column : $(EI)_{eff,II} = 4.03 \times 10^4$ kNm^2 Internal forces from linear analysis: N =1260 kN, M_1=300kN.m Effective length l_0 of the column: $l_0 = 2.10*l = 2.10*6000 = 12600$ mm Plastic compressive resistance: $N_{pl,Rk} = A_r*f_{yr}+0.85f_{cd}*A_c+A_s*f_{ys}$ $= 6253.8$ kN Elastic critical normal force $N_{cr,eff}$: $N_{cr} = \pi^2(EI)_{eff}/l_o^2 = 3.012 \times 10^3$kN $N_{cr,eff} = \pi^2(EI)_{eff,II}/l^2 = 1.104 \times 10^4$kN	The relative slenderness ratio: $\bar{\lambda} = \sqrt{N_{pl,Rk} / N_{cr}} = 1.441$ The reduction factor for moment capacity: $\mu_d = 0.6603$ Moment amplification factor k: $\beta = 0.66$ $k = \beta/(1- N/ N_{cr,eff}) = 0.745$ The total design moment: $M_{tol} = k*M_1 = 223.5$ kN.m Plastic bending resistance: $M_{pl,Rd} = 463.3$ kN.m Section capacity factor: $\alpha_M = 0.9$ for S355 steel $\varphi = M_{tol}/(\mu_d*\alpha_M*M_{pl,Rd}) = 0.812$

Table 6. 8 Design results of the SCC portal frame

	First-order analysis & design	**Second-order analysis & design**
Design load		
Compressive force	1260kN	1274kN
Design Bending Moment	300kN.m	363.0kN.m
Max. Section capacity factor	0.812	0.804

CHAPTER 7

ADVANCED ANALYSIS OF HYBRID STEEL AND CONCRETE FRAMES

This chapter discusses the proposed advanced analysis approach for hybrid steel and concrete members and frames. The curved ALH (Arbitrarily Located Hinge) element, which has one arbitrarily located hinge and two end plastic hinges, is adopted to simulate various effects, such as initial imperfections, as well as geometric and material nonlinearities. Cracking in concrete components significantly influences structural deformation and internal force distribution; thus, it is considered by the effective flexural stiffness approach based on Branson's model, which is also associated with the use of concrete fracture surfaces as proposed in Chapter 5. A refined plastic hinge model, in which sectional yield surfaces are incorporated, is proposed to simulate the inelastic behavior of hybrid steel and concrete members. Moreover, since material properties are a crucial requirement in an accurate analysis, the constitutive models recommended in Eurocodes and available literature are illustrated. The application of high-strength concrete (HSC) in concrete-filled composite columns is not documented in the corresponding codes, and therefore, an experimental investigation is conducted. Finally, several calibrated examples are presented to illustrate the accuracy and validity of the proposed method.

7.1 Introduction

Advanced analysis is regarded as an accurate simulation-based technique for studying the ultimate behaviors of members or framed structures under extreme conditions, such as seismic attacks, super typhoons, and progressive collapse and so on. In order to obtain reliable analysis results, it necessitates the consideration of various significant effects inherent to actual structures, such as initial imperfections, geometric and material nonlinearities, residual stress and concrete cracking.

However, a unified advanced analysis approach for hybrid steel and concrete framed structures cannot be easily obtained due to the mechanical characteristics of various structural members substantially vary. Bare steel (BS) members are usually slender and present an apparently stability problem, especially for columns with high slenderness ratios. In reinforced concrete (RC) members, material nonlinearity is visibly observed. Meanwhile, steel-concrete composite (SCC) members suffer from both stability and nonlinearity issues. Consequentially, advanced analysis should cater for both geometric and material nonlinearities in different types of structural members in framed structures. Other considerations, including initial member and frame imperfections and concrete cracking, should also be covered in analysis. An incomprehensive consideration of these factors may result in inaccurate results.

To these ends, the curved ALH element is introduced in the analysis in this research work, since it is directly derived for the arbitrary members in hybrid steel and concrete frames. The element is initially curved and the P-δ effect due to member imperfection can be reflected. One arbitrarily located hinge and two end

hinges are fabricated in an element, indicating that this element is also suitable for simulations of high material nonlinearity. The updated Lagrangian method associated with the tangent stiffness approach is also introduced in the reflections of large deflections. Furthermore, using only one element per member in the proposed analytical model is sufficient, which is to significantly improve numerical efficiency and minimize the efforts required for data manipulation.

In considering material yielding, the plastic hinge approach is recognized to be more efficient and practical for actual use, as discussed in Chapter 2. The refined plastic hinge method, which has been extensively studied by Chan *et al*. (1997) for the second-order inelastic analysis of BS members, is adopted in this thesis. In the current work, this method is also extended to the inelastic analysis of RC and SCC members to facilitate the advanced analysis method of hybrid steel and concrete framed structures.

Monitoring the yield conditions of a section at plastic hinge locations is generally required during analysis, in which initial yield and failure conditions are needed to be defined. On the basis of these conditions, the plasticization of a section is then modeled through the gradual reduction of pseudo-spring stiffness in line with external load. Most analyses assume over-conservative and simplified linear interpolation equations in calculating the capacities of steel sections under initial yield and ultimate limit states. Due to the nonlinear properties of concrete, the initial yield and failure criteria for typical RC and SCC sections may lead to cost-ineffective or sometimes unsafe designs if the simplified equations are used. As an alternative, the cross-section analysis technique presented in Chapter 5 is introduced

in calculating the initial yield and failure capacities of arbitrary sections, and a generalized refined plastic hinge model that incorporates these sectional yield surfaces is proposed.

Concrete is a brittle material with cracking induced by low tensile fracture stress, which affects the load-deflection response derived in the nonlinear analysis of related members in hybrid steel and concrete frames. Conventionally, the cracking effects of concrete on the stiffness of individual members are considered by assigning reduced moments of inertia. In examining these effects, some researchers have proposed a simplified formula for modifying the effective moment of inertia of concrete components. For example, Branson (1963) proposed an approximated formula for cracked concrete and Ibrahim (2004) suggested a modeling approach for the effective flexural stiffness of concrete. Tikka *et al*. (2005) developed an EI equation for slender reinforced concrete columns. In this thesis, Branson's (1963) formula is introduced in the calculation of the effective moment of inertia of cracked concrete members, so that the effects of gradual cracking can be considered in the analysis. This technique is simple and effective, providing a reliable estimation for conventional engineering purposes.

In this study, constitutive models are necessary since they significantly influence the accuracy in analysis. To appropriately input material properties into the analytical model, the material constitutive models recommended in Eurocodes are discussed. Conventionally, the tensile strength of concrete is usually ignored. In the generation of a concrete fracture surface, which is combined with the use of Branson's model (1963) to reflect concrete cracking effects, the strain softening

model of Bazant (1983) is adopted as the tensile part of the constitutive relationship of concrete.

Concrete-filled tubular (CFT) columns are the most economical and structurally efficient among all composite members in terms of resistance to heavily compressive loads. The steel tubes not only assist in carrying axial load, but also enable confinement to the concrete core, thereby increasing the compressive strength and ductility of the core; these advantages are supported by experimental results and the findings of Knowles and Park (1969). Owing to these advantages, a considerable increment in load bearing capacity is achieved and column size can be reduced. Additionally, the concrete core delays the local buckling of steel tubes and increases column stiffness. Ellobody *et al*. (2006) and Young and Ellobody (2006) concluded that concrete confinement depends on many factors, such as the sectional shape, column diameter, thickness, concrete strength and yield stress of steel tubes. Susantha *et al.* (2001) investigated the Hyogoken-Nanbu earthquake in Japan and found other advantages of CFT columns; that is, they exhibit better ductility performance and larger energy absorption than the conventional reinforced concrete and steel columns. CFT columns are therefore favorable structural components for buildings constructed in high-density urban areas or earthquake-sensitive regions.

HSC ($f_{cu} \geq 60$ MPa) has become an increasingly economic and readily available material, presenting greater stiffness and strength than the normal-strength concrete. However, modern design codes, such as Hong Kong Steel Code (2011) and Eurocode 4 (2004), are applicable only to the design of composite columns made of concrete with normal strength ranging from C25 to C60. Maximizing the benefits of

using HSC to construct CFT columns necessitates figuring out the material properties of confined concrete. This research experimentally explores the material properties of HSC confined in circular and octagonal steel tubes.

In this chapter, the effective flexural stiffness approach based on Branson's model is proposed for simulating concrete cracking effects. A generalized refined plastic hinge model, which incorporates sectional yield surfaces, is put forward to reflect the inelastic behaviors of various material types of members. The material constitutive models are critical in accurate analysis, which prompts the discussion of the constitutive models recommended in Eurocodes and available literature. With HSC in concrete-filled circular and octagonal composite columns, an experimental investigation is established. Finally, several calibrated examples are presented to demonstrate the accuracy and validity of the proposed method.

7.2 Assumptions

For beam-column element and cross-section analyses, the following basic assumptions are adopted:

1) Euler-Bernoulli hypothesis is valid and the second-order effect due to axial loads is considered.
2) Strains are small but the deformations can be large.
3) Plane sections before deformation remain plane after deformation which implies a linear strain distribution exists across the section depth.
4) The bond-slip between the concrete and steel is disregarded and full strain compatibility between the steel and the surrounding concrete is assumed.

5) Material nonlinearity is considered by plastic hinge springs while the element is elastic.

6) The steel reinforcement embedded in concrete does not buckle under compression.

7) The applied loads are nodal and conservative, which are assumed to be independent of the load path and proportional increased.

8) Warping deformation, shear deformation as well as twisting effect are not considered.

9) Tensile strength of concrete is only considered in calculating the sectional strength before cracking, after that, the tensile strength of concrete is neglected.

7.3 Flexural stiffness modeling

As previously stated, concrete easily cracks, thereby affecting the flexural stiffness of members and possibly enlarging the deflections in an entire structure. Mehanny *et al*. (1999) discussed the importance of considering concrete cracking effects; and these affect the internal force distribution, member deformation and dynamic response of a structure. These effects should therefore be appropriately reflected in advanced analysis.

The influence of concrete cracking on the stiffness of individual members is generally evaluated by assigning reduced moments of inertia. Due to numerous uncertainties involved, however, the accurate reflection of concrete cracking is

difficult to quantify. For cracked concrete, Branson (1963) recommended an effective moment of inertia, which is an empirical expression later adopted in various forms by the American Concrete Institute (ACI) (1995), Canadian Standards Association (1994) and Standards Association of Australia (1994) in their building codes. This technique is simple and effective, providing a reasonable estimation of member deflection. The equation proposed by Branson (1963) is revised to model the gradual cracking effects on individual members; specifically, the effective moment of inertia is reduced as follows:

$$I_e = \left(\frac{M_{cr}}{M_a}\right)^3 I_{un} + \left[1 - \left(\frac{M_{cr}}{M_a}\right)^3\right] I_{cr} \qquad \text{for } M_a \geq M_{cr} \tag{7. 1}$$

$$I_e = I_{un} \qquad \text{for } M_a < M_{cr} \tag{7. 2}$$

where, I_{cr} is equal to the initial slope of the bending moment-curvature for zero axial load with no tensile stress in concrete; I_e is the effective moment of inertia as adopted in the analysis; I_{un} is the moment of inertia of the uncracked section in elastic state; and M_{cr} is the moment at the intersecting point by the loading path and concrete fracture surface which is kept unchanged after intersection.

7.4 Plastic hinge formulations

Elastic limit and failure criteria should be defined in the refined plastic hinge analysis approach. Therefore, the initial yield and failure surfaces of the arbitrary sections discussed in Chapter 5 are introduced. The two yield surfaces divide a loading space into three zones: the elastic, elasto-plastic and plastic hardening zones (Figure 7.2). If the loads are within the initial yield surface, a section can be ideally

treated as elastic without in the need to reduce either strength or stiffness. If the load coordinates fall into the elasto-plastic zone, the section is under gradual yielding stage and its strength and stiffness are discussed in the followings. Once the load exceeds the failure surface, the sectional hardening is activated with stiffness reduced to the residual cross sectional capacity.

Section spring stiffness S can be computed by the following equations,

$$S = 10^{+10} \frac{EI_0}{L}, \text{ for } M_i^{\zeta} \le M_{er}^{\zeta} \tag{7. 3}$$

$$S = \frac{EI(\zeta)}{L} \left| \frac{M_{pr}^{\zeta} - M_i^{\zeta}}{M_i^{\zeta} - M_{er}^{\zeta}} \right| \text{ for } M_{er}^{\zeta} < M_i^{\zeta} < M_{pr}^{\zeta} \tag{7. 4}$$

$$S = \frac{EI(\zeta)}{L} \rho, \text{ for } M_i^{\zeta} \le M_{er}^{\zeta} \tag{7. 5}$$

where EI(ζ)/L is the flexural stiffness under current load level, L is the member length and M_{er}^{ζ} and M_{pr}^{ζ} denote the initial yield and failure moments, respectively, reduced due to the presence of current axial force and ρ represents the strain-hardening parameter. Based on this equation, the section stiffness varies from infinity to a small strain-hardening value that represents three sectional stages as the elastic, partially plastic and fully plastic stages with strain-hardening.

7.5 Material constitutive models

Various constitutive models in codes or obtained from laboratory can be adopted in the analysis. When without prescribed statements; the following material constitutive models are adopted.

7.5.1 Constitutive model for structural steel and rebar

For the structural steel and reinforcing bars, the stress vs. strain relationship is assumed to be elastic-perfectly-plastic, as plotted in Figure 7.1(a). Alternatively, it is expressed in mathematical forms as,

$$\sigma_s = f_y \quad \text{for} \quad \varepsilon_{se} \le \varepsilon \le \varepsilon_{su} \tag{7. 6}$$

$$\sigma_s = E_s\varepsilon \quad \text{for} \quad -\varepsilon_{se} \le \varepsilon \le \varepsilon_{se} \tag{7. 7}$$

$$\sigma_s = -f_y \quad \text{for} \quad -\varepsilon_{su} \le \varepsilon \le -\varepsilon_{se} \tag{7. 8}$$

where, f_y is the design stress of steel; ε_{se} and ε_{su} are the elastic-limit and ultimate fracture strain respectively; E_s is the Young's modulus of steel.

7.5.2 Constitutive model for the compression of unconfined concrete

The complete stress–strain relationship of concrete is plotted in Figure 7.1(b), in which the compressive component of the constitutive relationship of concrete is taken from Eurocode 2 (2004) and can be expressed as,

$$\sigma_c = f_c\left[1-\left(1-\frac{\varepsilon_c}{\varepsilon_0}\right)^n\right] \quad \text{for} \quad 0 \le \varepsilon_c \le \varepsilon_0 \tag{7. 9}$$

$$\sigma_c = f_c \quad \text{for} \quad \varepsilon_{c0} \le \varepsilon_c \le \varepsilon_{cu} \tag{7. 10}$$

where f_c is the peak compressive design strength of concrete; ε_0 and ε_{cu} are the strain at reaching the maximum strength and the ultimate respectively; n represents the exponent that can be conventionally taken as 2.0 for normal-strength concrete.

The constitutive model of concrete is highly nonlinear, but an elastic limit strain ε_{ce} should be artificially assumed in the proposed numerical solution, which defines the stress vs. strain relationship prior to this strain as linear. Such idealization and simplification are widely adopted. For example, Izzuddin *et al*. (2000) assumed the elastic limit strain to be the strain at the onset of peak compression strength. In the present study, the elastic limit strain of concrete is

$$\varepsilon_{ce} = f_c / E_c \quad \text{or} \quad \varepsilon_{ce,c} = f_{c,c} / E_{c,c} \tag{7. 11}$$

where ε_{ce} and $\varepsilon_{ce,c}$ are the elastic limit strains of unconfined and confined concrete respectively, f_c and $f_{c,c}$ are the compressive strengths of unconfined and confined concrete respectively; and $E_{c,c}$ is the Young's modulus of confined concrete.

7.5.3 Constitutive model for the tension of concrete

The strain softening model proposed by Bazant (1983) is adopted as the tensile part of the constitutive relationship of concrete. It is described as follows:

$$\sigma_c = -E_c \varepsilon_c \qquad \text{for} \qquad \varepsilon_{t0} \le \varepsilon_c \le 0 \tag{7. 12}$$

$$\sigma_c = -\left[f_t - (\varepsilon_c - \varepsilon_{t0}) E_t \right] \qquad \text{for} \qquad \varepsilon_{tu} \le \varepsilon_c \le \varepsilon_{t0} \tag{7. 13}$$

$$E_t = 70 E_c / (57 + 145 f_t) \tag{7. 14}$$

where σ_c is the stress of concrete at specific strain ε_c; E_c and E_t are the Young's modulus and tangent tensile strain softening modulus, respectively; and ε_{t0} and ε_{tu} denote the strains at peak tensile strength and tensile fracture, respectively.

7.5.4 Constitutive model for the compression of confined concrete

The confinement effect of concrete can be taken into account by modifying the stress–strain relationship indicated in Eurocode 2 (2004) thus:

$$f_{c,c} = f_c(1.000 + 5.0\sigma_2 / f_{ck}) \quad \text{for} \quad \sigma_2 \le 0.05 f_c \tag{7. 15}$$

$$f_{c,c} = f_c(1.125 + 2.50\sigma_2 / f_c) \quad \text{for} \quad \sigma_2 > 0.05 f_c \tag{7. 16}$$

$$\varepsilon_{c0,c} = \varepsilon_{c0}(f_{c,c} / f_c)^2 \tag{7. 17}$$

$$\varepsilon_{cu,c} = \varepsilon_{cu} + 0.2\sigma_2 / f_c \tag{7. 18}$$

in which σ_2 is the effective lateral compression due to confinement; $f_{c,c}$ is the peak compressive strength of confined concrete; and $\varepsilon_{0,c}$ and $\varepsilon_{cu,c}$ represent the confined concrete strains at the maximum and ultimate strengths, respectively. The effective lateral confining stress can be obtained by experimentation or empirical formula, as discussed in the next section.

7.6 Experiment on high-strength concrete (HSC) in steel tubes

7.6.1 Introduction

The use of CFT columns in modern structures is becoming an increasingly popular selection, especially for high-rise buildings. Nevertheless, their applications are commonly limited to typical sectional shapes, such as rectangular and circular sections. Concrete-filled circular tubular sections are extensively used. The concrete core can be effectively confined in a circular steel tube, thereby significantly increasing not only concrete compressive strength, but also concrete ductility. Despite these advantages, difficulties occur in the fabrication of large circular sections with thick steel plates, and therefore, the octagonal shape seems more

practical and feasible for construction. In designing octagonal composite columns, existing codes (e.g. Eurocode 4 (2004)) do not provide a specific design formula or corresponding specifications.

The typical stress vs. strain curves of normal-strength concrete and HSC are shown in Figure 7.3. HSC is an extremely brittle material, with strength that abruptly diminishes once collapse occurs. When the concrete is confined, however, its strength increases and its ductility significantly improves. Therefore, the best application of HSC is to be integrated the use in steel tubes.

In the proposed method, material constitutive relations are the only necessary parameters for design and analysis. With the absence of available material models, an experiment on identifying material properties can be conducted. This section describes the experimental investigation into the material properties of HSC confined in circular and octagonal steel tubes.

The experiment introduces two groups that contain two circular and octagonal specimens with the same reasonable depth-to-thickness (d/t) ratio (38.74). The axial load versus the strain of the concrete, as well as the axial and hoop strains of the steel tubes, are measured. The measurements are used in determining the stress vs. stain relationship of confined concrete. Another group of unconfined specimens, which are of the same size as the concrete core in the confined specimens, is also tested.

7.6.2 Dimensions of specimens

The experimental investigation is intended to study the material characteristics of HSC confined in circular and octagonal steel tubes. To this end, a series of uni-axial and tri-axial compression tests on HSC specimens are designed. The specimens discussed in the preceding section are shown in Figure 7.5. For comparison, a group of unconfined specimens are tested (Figure 7.6). The dimensions of the two groups of confined specimens, namely CHS 194 and OHS 194, are presented in Table 7.1 and Table 7.2, respectively.

7.6.3 Material properties of high strength concrete

To derive the fundamental material characteristics of the HSC, standard cube and cylinder concrete specimens are tested. The dimensions of the cube and cylinder specimens are 100 mm × 100 mm × 100 mm and 150 mm (diameter) × 300 mm (height), respectively. Then, the concrete cubes and cylinders are crushed to fail to determine actual compressive strength, where a compression machine is used operated at loading rates of 2 kN/second and 0.13 mm/min, respectively. The test machine is shown in Figure 7.4 and the results are provided in Table 7.3 and Table 7.4.

7.6.4 Material properties of steel

The material properties of the steel tubes are determined by conducting tension tests on cut coupons, which are machined from the walls of the tubes from the two specimen groups (i.e., CHS 194 and OHS 194). The specimens are prepared according to BS EN 10002 (2001), and four specimens are tested for each group.

Standard experimental procedure is followed with the loading rate as 0.002mm per minute. The results are summarized in Table 7.5.

7.6.5 Experimental design

The experimental program is designed to study the material characteristics of HSC confined in steel tubes. Thus, vertical load is applied only on the concrete core. To facilitate the alignment of vertical load and avoid the direct exertion of stress on the steel tubes, a 32-mm thick loading pad is placed on top of the specimens, which are slightly smaller than the concrete core (Figure 7.7).

Theoretically, the confinement effect does not occur at the early stage of loading owing to the fact that the Poisson ratio of concrete is lower than that of steel at this stage. The core of the specimen is then axially loaded, generating Poisson-type lateral expansion that reacts with the steel tubes to produce confinement. This phenomenon is also called the passive confinement effect. As axial load increases, however, the lateral expansion of concrete gradually exceeds that of steel due to the change in the Poisson ratio of concrete. Therefore, radial pressure develops at the concrete–steel interface. At this stage, the confinement of the concrete core is achieved and the steel is in the hoop tension state. The lateral pressure levels of the circular and octagonal tubes can be calculated by equilibrium relations as follows:

$$f_r = \frac{2t}{D-2t} f_{sr} \tag{7. 19}$$

where, f_r is the confinement stress; t is the thickness of the steel tubes; and D is the overall diameter.

Although vertical load is applied only on the concrete core, the vertical shear force caused by friction is transferred across the steel tubes to the concrete core interface. Besides the hoop stress induced by concrete expansion, the stress state is determined by the Mohr–Coulomb failure criterion:

$$\mathrm{F} = \sqrt{3J_2} = \frac{1}{\sqrt{2}}\sqrt{f_r^2 + f_v^2 + 0.5(f_r - f_r)^2} = \sigma_y \quad (7.20)$$

where, f_v is the vertical stress induced by the friction between the steel and concrete interface; and σ_y is the resultant stress.

Strain gages are attached to the outer surface of the steel tubes to enable the evaluation of actual stresses. The gages are used to measure the hoop and axial strains of the outer surface of the steel tubes at two diametrically opposite points at the mid-height of each specimen. The specimen setup is illustrated in Figure 7.8. The vertical strain on the concrete core is measured by direct deformation measurements using linear variable displacement transducers. The experimental setup is shown in Figure 7.9.

7.6.6 Experimental results

The axial stress–strain relationships of the confined concrete core are illustrated in Figure 7.10. The effects of confinement are highly apparent both as the axial strength and ductility of the specimens increase. As previously mentioned, another comparison groups with the unconfined specimens are also tested. The experimental

results for the CHS 194 group and OHS 194 group specimens are plotted in Figure 7.11 and Figure 7.12, respectively.

7.6.7 Discussions

The results for the two groups are shown in Table 7.6. Some of the experimental findings are discussed as follows. (1) Although HSC is brittle, its ductility in the circular and octagonal tubes significantly increases. (2) The strength enhancement of HSC is also observed in the two comparison groups, in which ultimate compressive strength increases to 69% and 45% in the circular and octagonal groups, respectively. (3) An apparent confinement effect is observed in the core of the octagonal tubes at no less than 85% of the counterpart in circular tubes. Once the material constitutive relations are determined from available codes or through experimental investigation, analysis and design using the proposed method can be conducted.

7.7 Verification examples

The computer program proposed in this research is further developed and combined with the proposed cross-section analysis program (RCD 2013) for the advanced analysis of hybrid steel and concrete members and frames. The sectional yield surfaces are pre-generated and indexed by the proposed cross-section analysis technique. The analytical model based on the curved ALH element is introduced for the simulation of the large deflections and inelastic behaviors of individual members and frames. To verify the accuracy and feasibility of this method, several

experimental examples from published works are selected and analyzed using the proposed approach.

7.7.1 Foure's RC column

In verifying the validity and accuracy of the analysis method for RC members and structures, an eccentrically loaded RC column experimentally tested by Espion (1993) is selected. This column was also recommended by Bratina (2004) as a benchmark. The dimensions and section properties of this column are provided in Figure 7.13.

An eccentric load is applied on top of the column; this load slowly increases until column failure. Three material properties are reported by Espion (1993): the compressive strength of concrete f_c (38.3 MPa), the elastic modulus of concrete E_c (33.6 GPa) and the strength of steel f_y (465 MPa). The other material properties are obtained from Eurocode 2 (2004). The Young's modulus of steel E_s is 200 GPa and the tensile strength of concrete f_t is 2.92 MPa. The initial imperfection of the column is assumed to be L/1000.

The comparison of the results derived by the proposed method and previous experiments is illustrated in Figure 7.14. The ultimate load applied in the proposed analysis method is 461.9 kN, which is close to the failure load measured in the experiment. The analysis results show a satisfactory capacity of the method in tracing the nonlinear behavior of an individual RC column. These findings also indicate that the proposed method can be used to effectively simulate the behavior of

a simple RC column and can therefore be used in the advanced analysis of RC structures under ultimate limit loads.

7.7.2 Concrete-filled steel tubular columns

In this example, eight pin-ended concrete-filled square steel tubes subjected to eccentric loads are analyzed and compared with the results of Bridge (1976). These columns have been studied by many researchers, such as Lakshmi *et al*. (2002), Valipour *et al*. (2009) and Fong *et al*. (2010) to verify their analytical methods. The current study focuses on predicting both failure load and experimental load versus deflection curves. The cross-sectional properties and load conditions are shown in Figure 7.15, and the geometrical dimensions and material properties are listed in Table 7.7 and Table 7.8, respectively.

In these examples, all the columns are assumed to contain initial imperfections equal to L/1000. The minimum residual displacement method (Chan, 1988) is used to trace the equilibrium path in elastic and inelastic ranges. The applied loads and total displacement at the mid-span of the eight columns are shown in Figure 7.16 to Figure 7.23.

The ultimate and observed maximum loads of the eight columns are compared and tabulated in Table 7.9. The comparison shows that the proposed approach accurately predicts the load versus deflection path of individual CFT columns until the loads applied reach failure levels. The numerical results show good agreement with the test results for uni-axial and bi-axial bending cases. The initial yield, failure

loads and deflections derived by the proposed theory agree well with the test results. Note that the cracking effects in these columns should be considered; otherwise, the predicted ultimate loads will be significantly higher than the test results, leading to the creation of a non-conservative design.

7.7.3 Concrete-filled circular hollow steel columns

In this example, 10 steel tubular columns filled with normal-strength concrete tested by Neogi and Sen (1969) are analyzed and compared. The material properties and geometric data of the specimens are listed in Table 7.10. Specimens M1 to M10, which are made of hot-finished seamless mild steel tubes, are pinned at both ends in the bending plane. Neogi and Sen (1969) did not provide the elasticity modulus of concrete; thus, this value is taken from the ACI codes (1995). Given that the initial geometric imperfections of specimens M1 to M7 are not measured, they are assumed sinusoidal with amplitudes equal to L/1000 at mid-height. For specimens M8, M9 and M10, the initial deflections at mid-height are determined as 5.69, 3.73 and 1.016 mm. To ascertain the accuracy of the proposed method, the load versus deflection response of specimen M5 (the only specimen for which Neogi and Sen (1969) provided deflection data) is analyzed and compared (Figure 7.24). The numerical load deflection responses of these columns are shown in Figure 7.25 to Figure 7.27.

The ultimate axial loads of specimens M1 to M10 are presented in Table 7.11 for direct comparison. Figure 7.24 indicates that the load versus deflection curve is identical to the experimental results, with less than 1% difference at ultimate loads. The results shown in Table 7.11 indicate the high prediction accuracy of the

proposed method. The load versus deflection responses of all the specimens are also presented in Figure 7.25 to Figure 7.27, which show the highly nonlinear behavior of slender concrete-filled columns.

7.7.4 Cranston's portal frame

A simply supported RC portal frame, originally tested by Cranston (1965), is selected and tested in this example. The frame is pinned to the ground and two concentrated loads are applied (Figure 7.28). This frame has been studied by several researchers, including Lazaro and Richards (1973), Bazant *et al.* (1987), Sun *et al.* (1994) and Bratina *et al.* (2004).

Cranston (1965) provided only two material properties: the compressive strength of concrete f_c (36.5 MPa) and the tensile strength of steel f_y (293 MPa). The other material properties are taken from Eurocode 2 (2004). The analysis results derived by the proposed method are compared with the experimental results of Cranston (1965). The analysis results of Sun *et al.* (1994) are also introduced for comparison. The comparison results are plotted in Figure 7.29.

The comparison of the present and previously published results shows that the proposed method accurately captures the highly nonlinear behavior of a simple RC portal frame. Adopting the proposed method also enables the accurate prediction of initial yielding load (Figure 7.29), indicating a similarity in trends between the proposed theory and previous experiments. The cracking effects of reinforced concrete members are modeled by the described technique. Furthermore, this gradual

cracking can be accurately simulated via the numerical analysis. The analysis results derived by the proposed approach are slightly higher than previous experimental results, where a discrepancy that might be result from the indirect consideration of concrete cracking.

7.8 Concluding remarks

In this chapter, an advanced analysis approach for hybrid steel and concrete members and frames is proposed. Adopting the ALH element proposed in Chapter 3 and Chapter 4, as well as the cross-section analysis technique as presented in Chapter 5, results in a unified analysis approach, for which only fundamental material constitutive models are required. To analyze concrete cracking effects, the flexural stiffness modeling approach based on Branson's model is introduced. Moreover, a generalized plastic hinge model is put forward for the simulation of gradual yielding in various members. Material constitutive models are crucial to accurate analysis, prompting the discussion of the constitutive models recommended in Eurocodes and literature. An experiment is carried out on HSC confined in concrete-filled composite members. Finally, several calibrated examples are presented to illustrate the accuracy and validity of the proposed method.

Figures

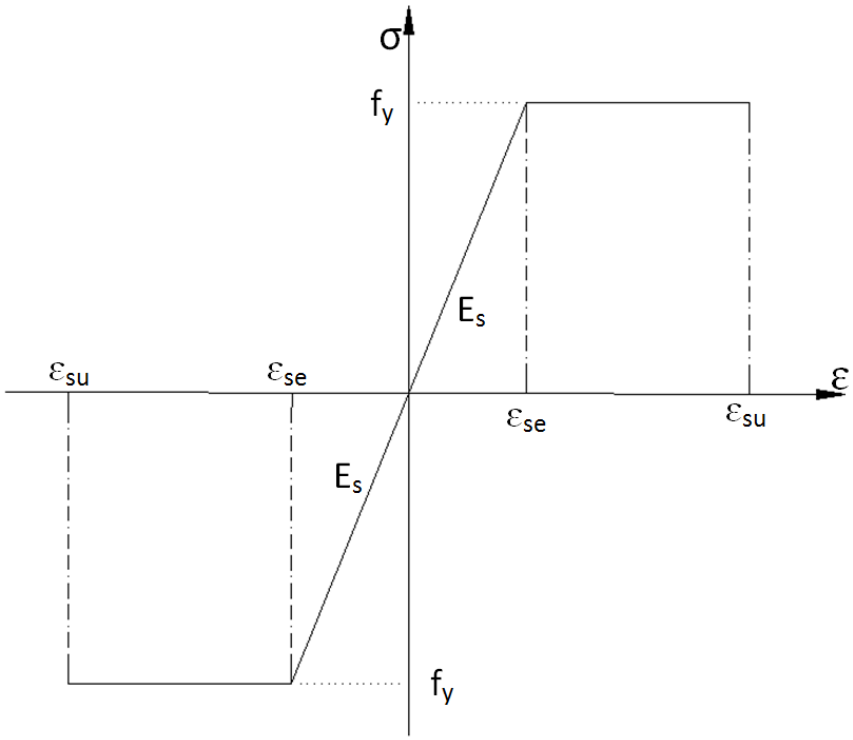

(a) Steel

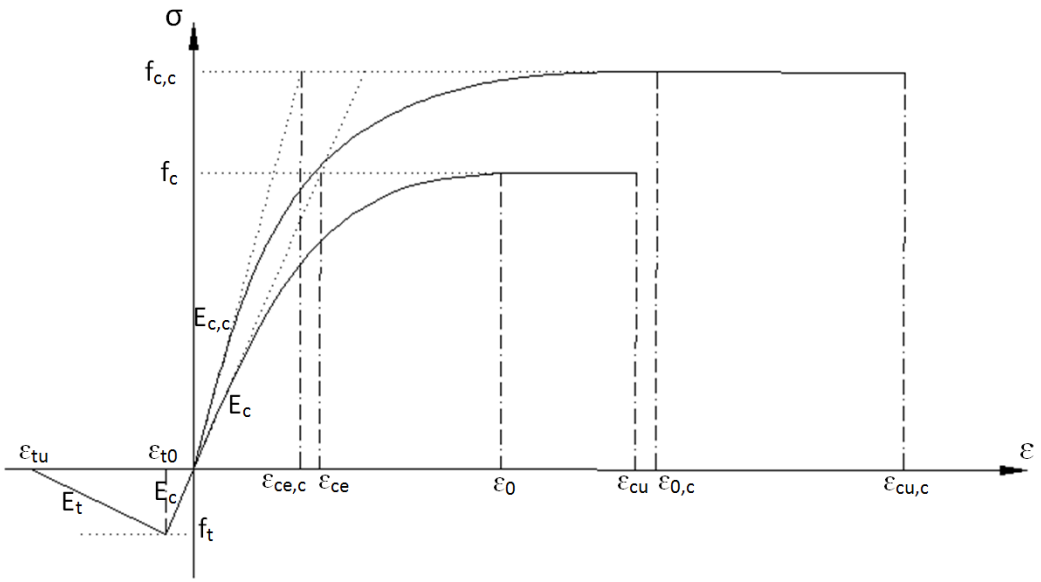

(b) Concrete

Figure 7.1 Constitutive relations of steel and concrete

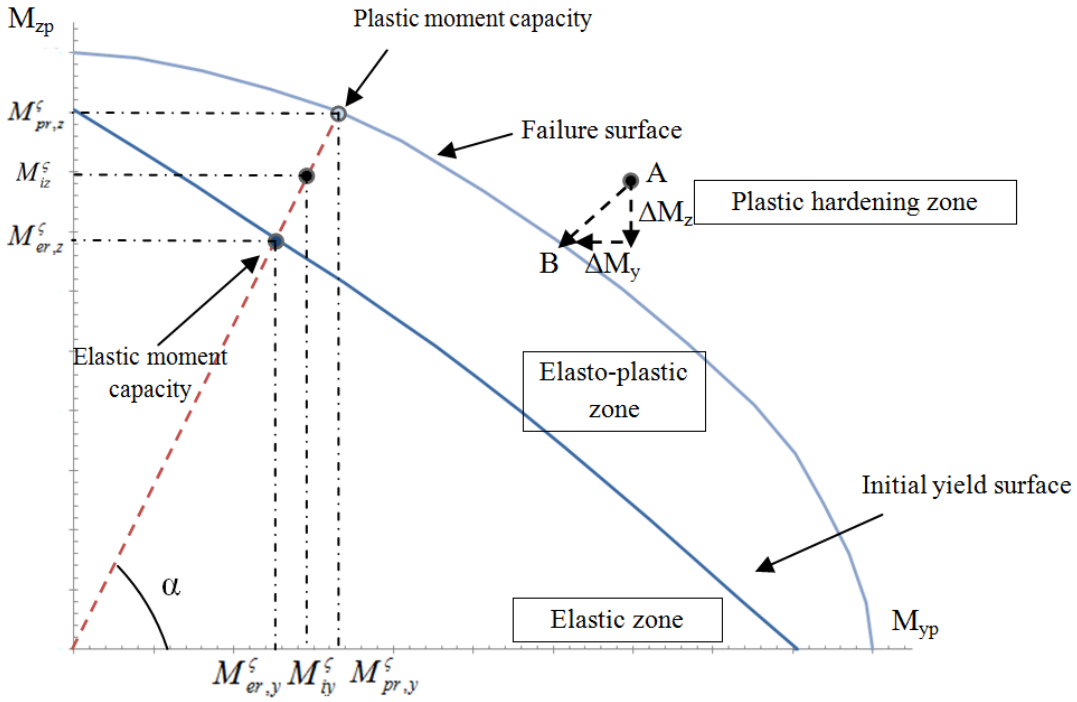

Figure 7.2 Initial and failure yield surfaces under praticular axial force

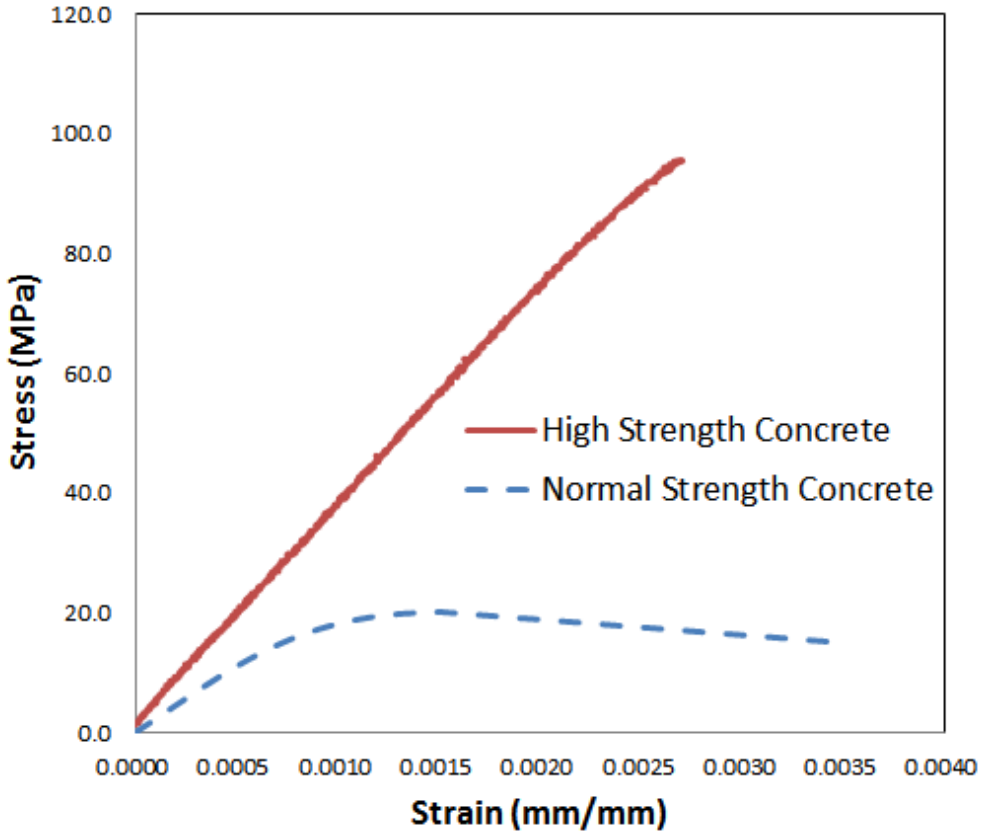

Figure 7.3 Typical stress vs. strain curves for normal and high strength concrete

Figure 7.4 Tests for the cube and cylinder specimens

(a) Circular confined specimen

(b) Octagonal confined specimen

Figure 7.5 Confined specimens with same d/t ratio

(a) Circular unconfined specimen

(b) Octagonal unconfined specimen

Figure 7.6 Unconfined specimens with the same size of concrete core

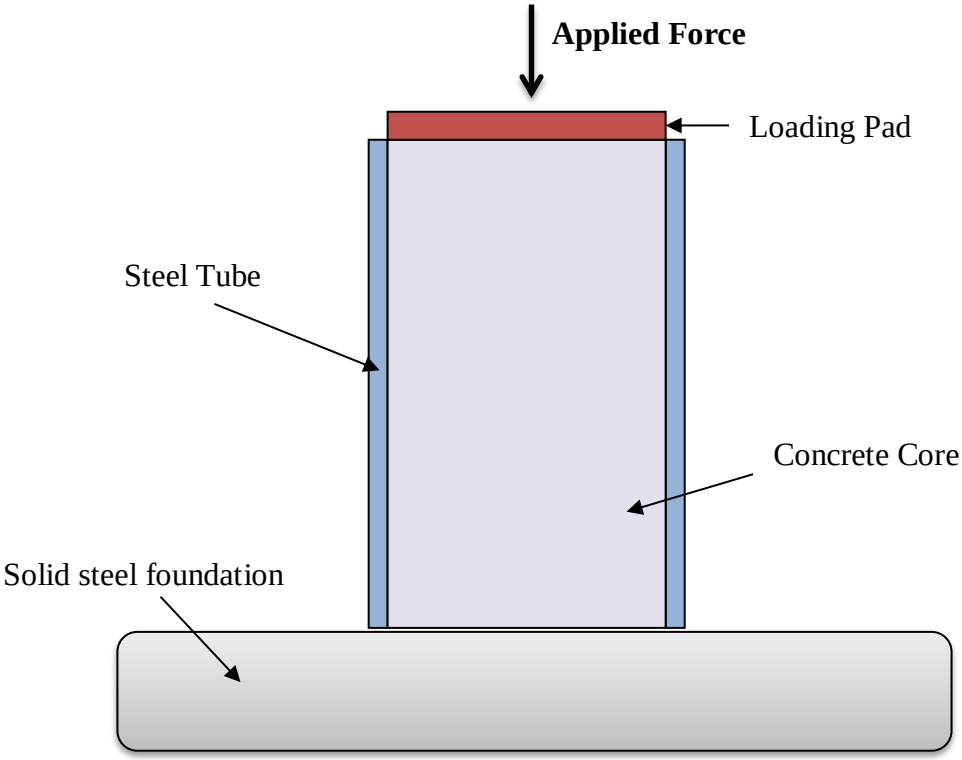

Figure 7.7 Schematic of specimen setup

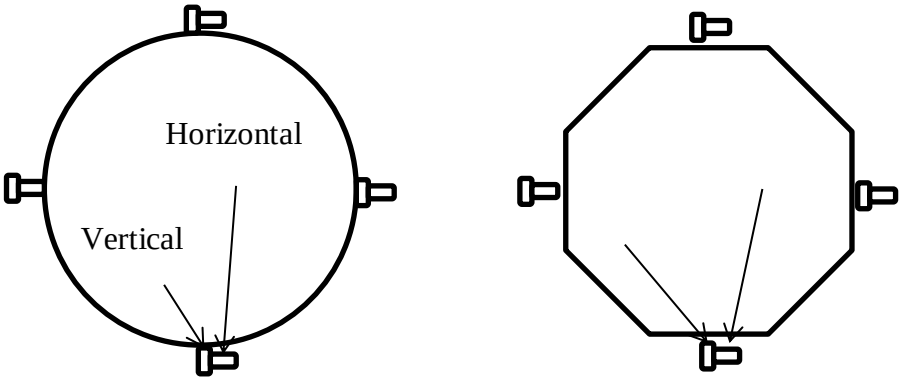

(a) Circular tube (b) Octagonal tube

Figure 7.8 Strain gages setup for confined specimens

(a) Experimental setup for circular confined specimens

(b) Experimental setup for octagonal confined specimens

Figure 7.9 Experimental setup for confined specimens

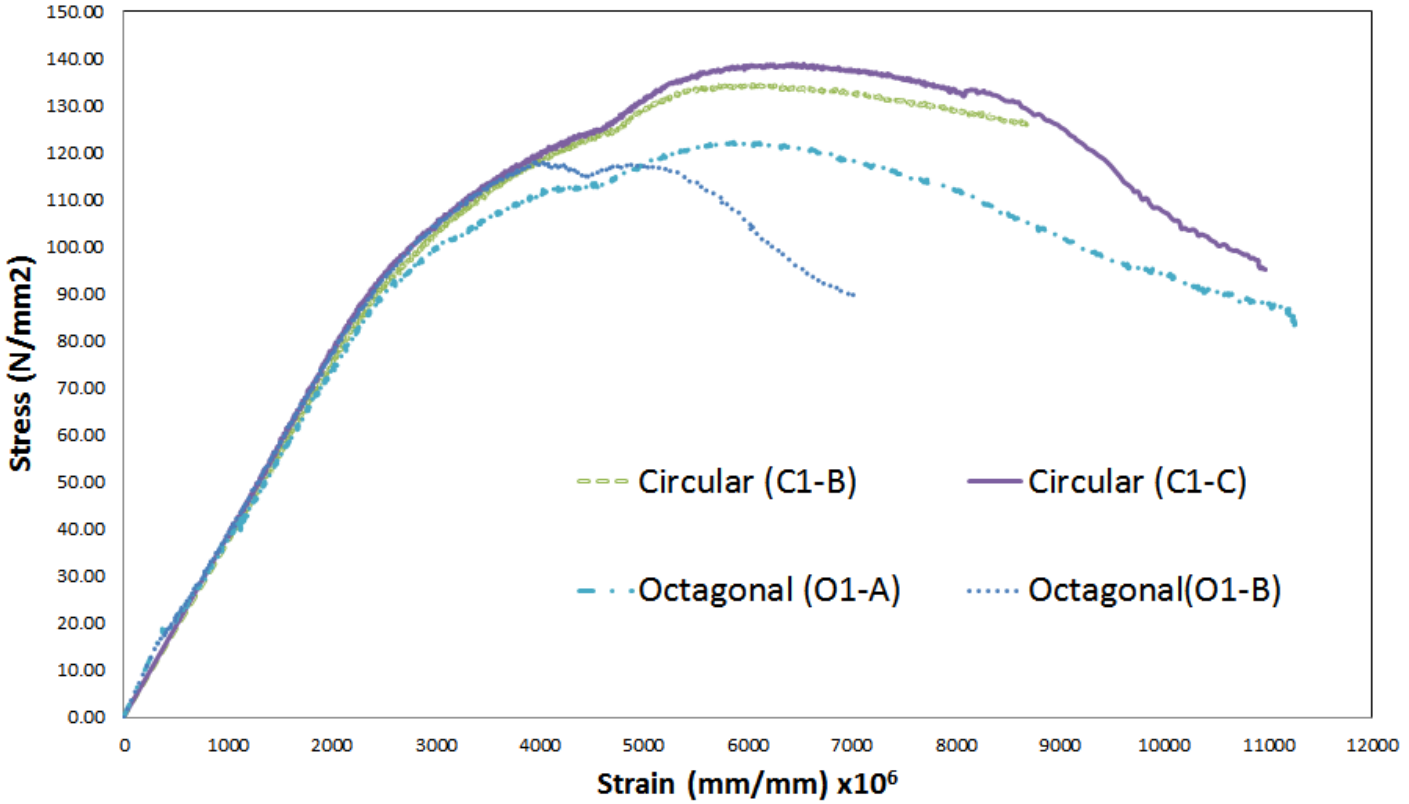

Figure 7.10 Stress vs. strain curves of confined specimens

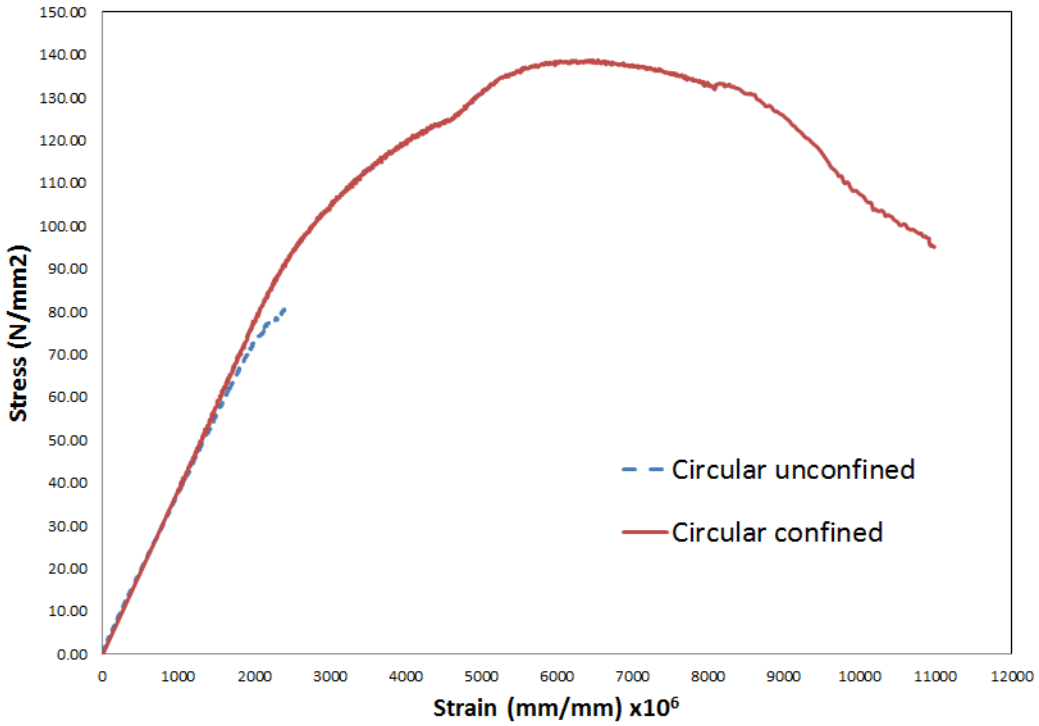

Figure 7.11 Results between the circular confined and unconfined specimens

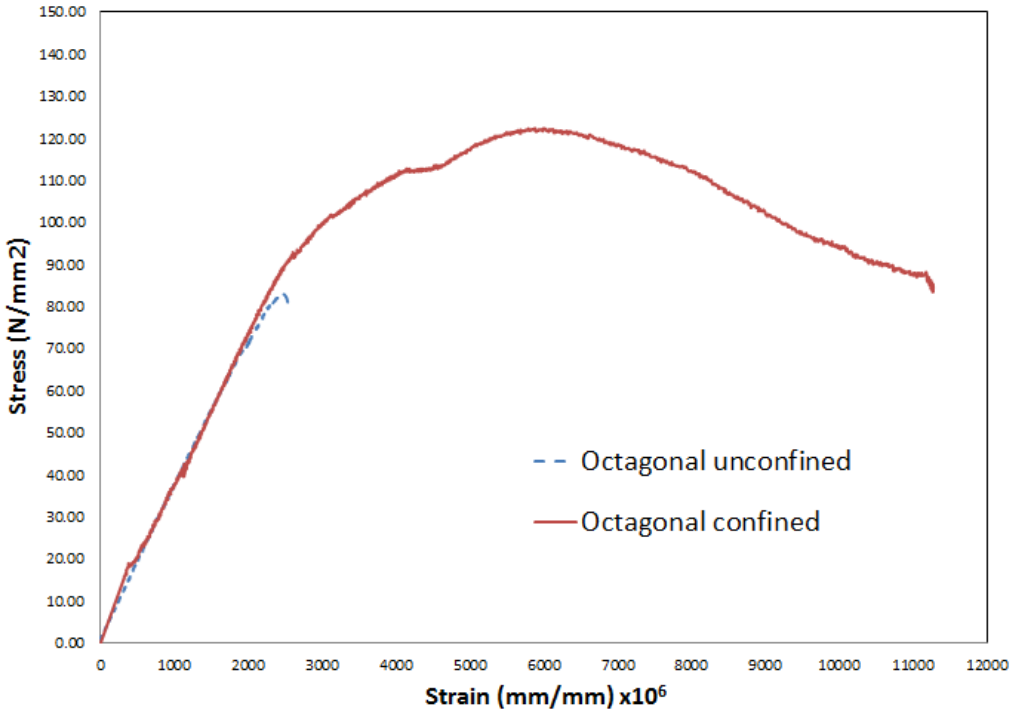

Figure 7.12 Results between the octagonal confined and unconfined specimens

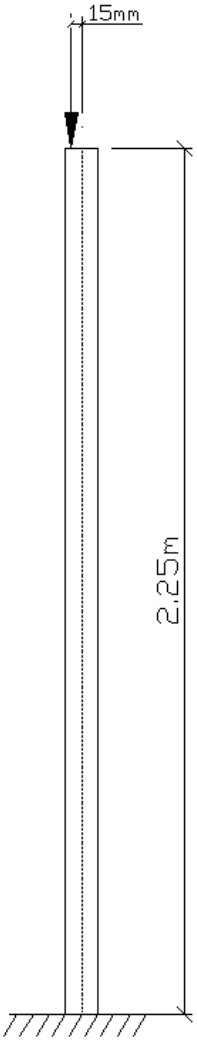

Concrete:

f_c = 38.3 MPa , E_c = 33600 MPa

Reinforcement:

f_y = 465 MPa , E_s = 200000 MPa

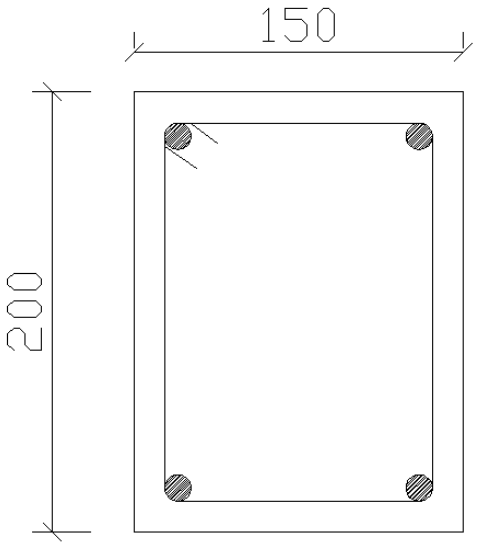

(a) Evaluation (b) Cross section

Figure 7.13 Foure's column

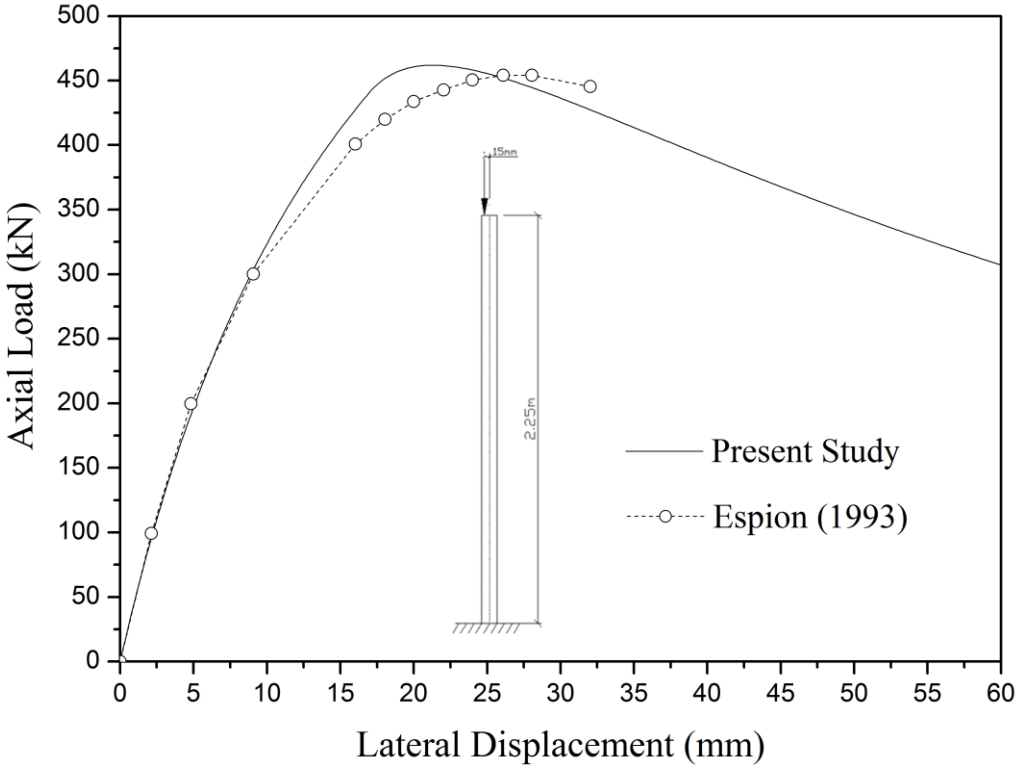

Figure 7.14 Load vs. deflection curve of the Foure's column

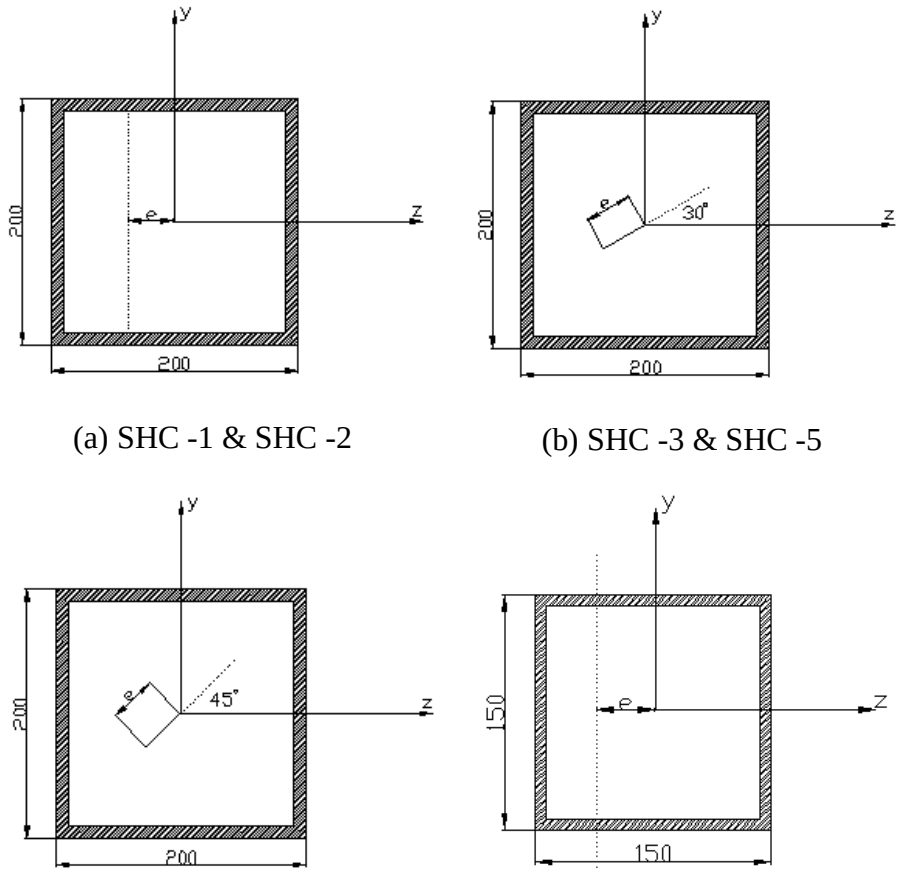

(a) SHC -1 & SHC -2

(b) SHC -3 & SHC -5

(c) SHC -4 & SHC -6

(d) SHC -7 & SHC -8

Figure 7.15 Cross section properties and eccentricity of loading

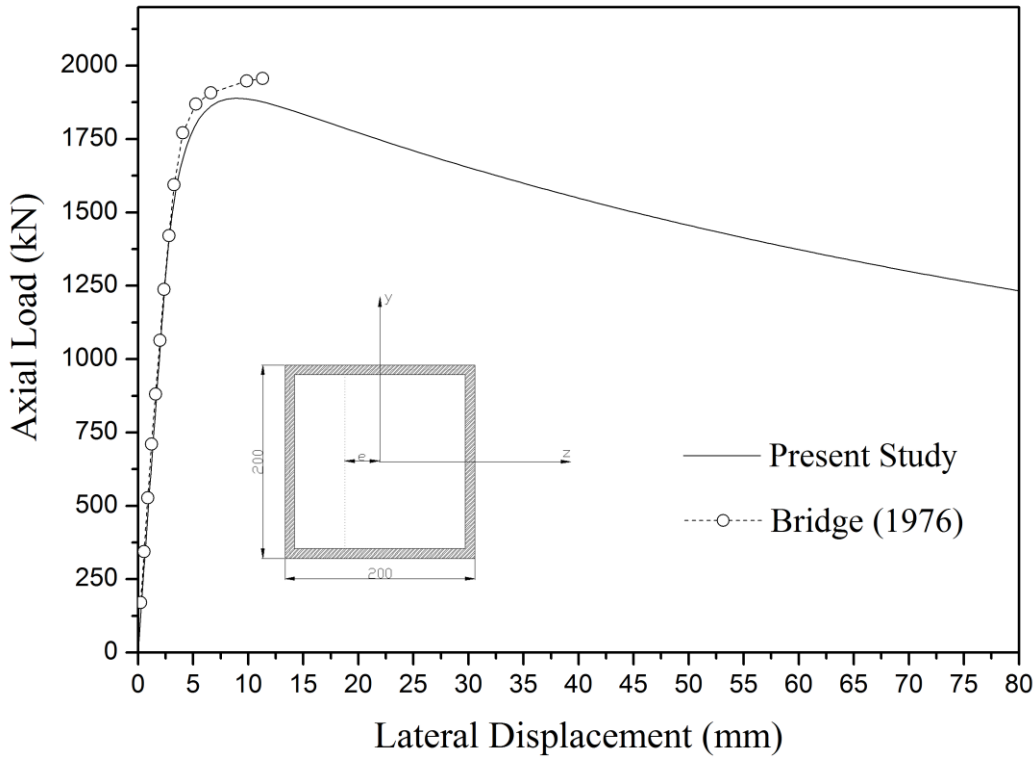

Figure 7.16 Comparison results of SHC -1

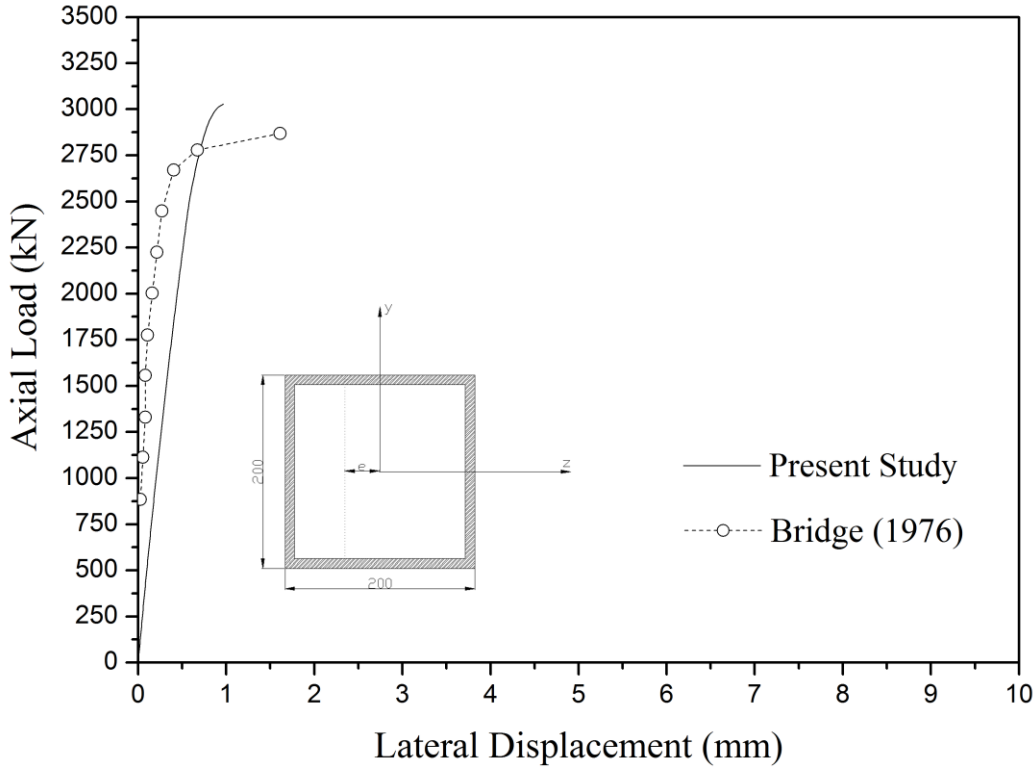

Figure 7.17 Comparison results of SHC -2

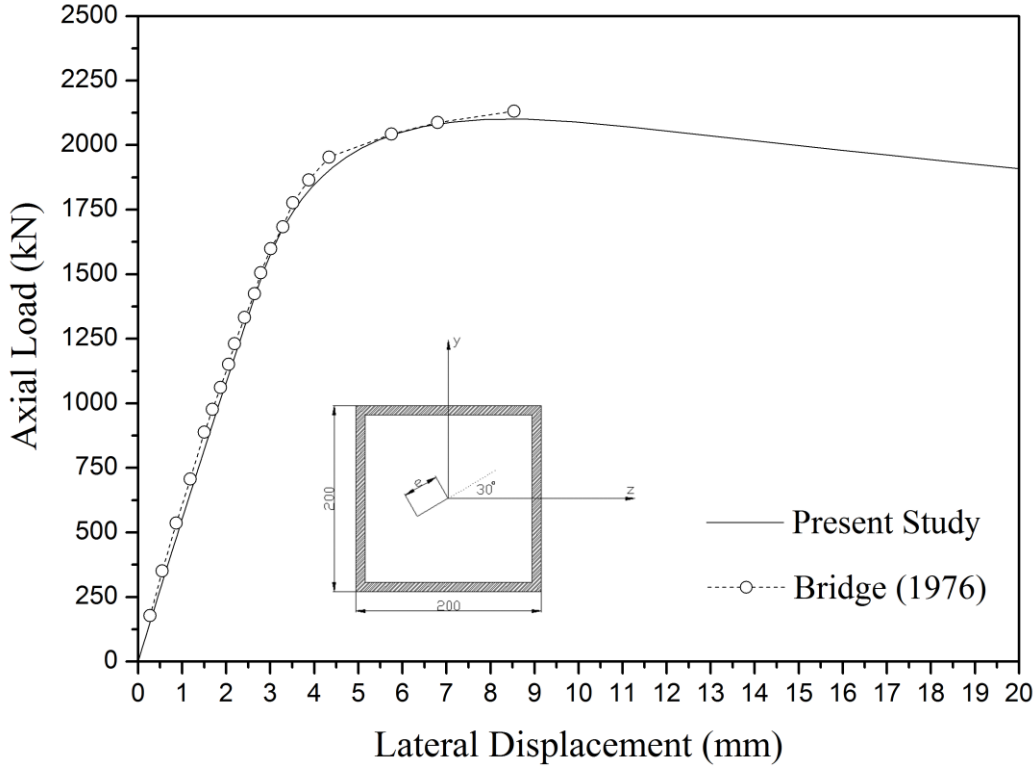

Figure 7.18 Comparison results of SHC -3

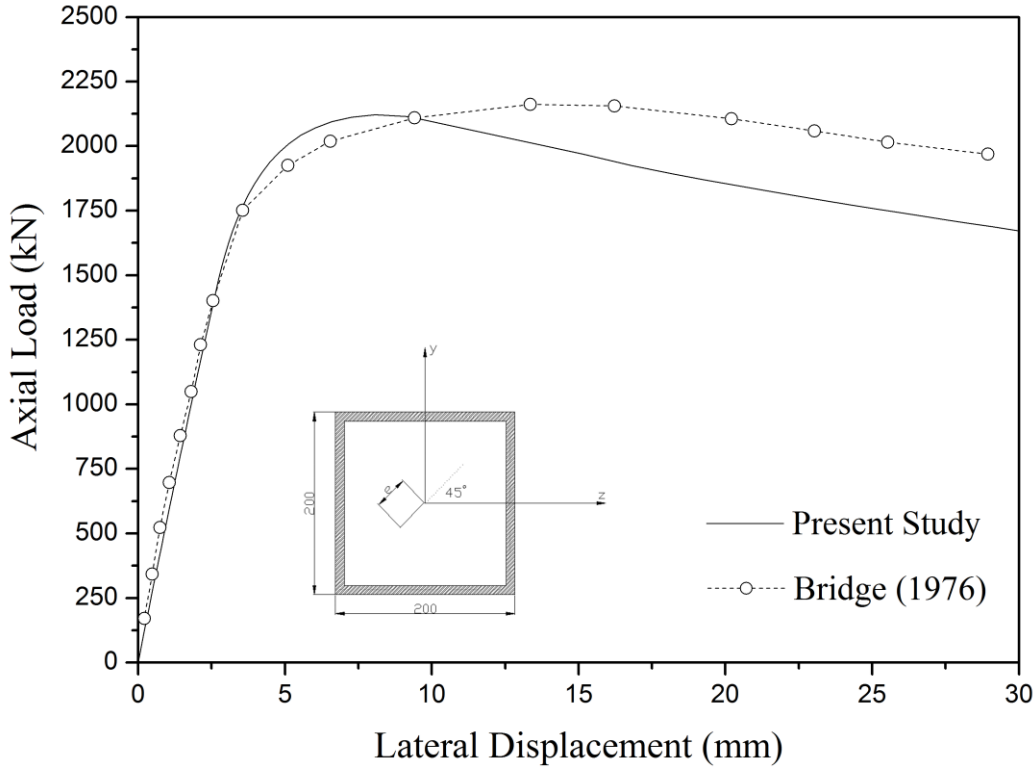

Figure 7.19 Comparison results of SHC -4

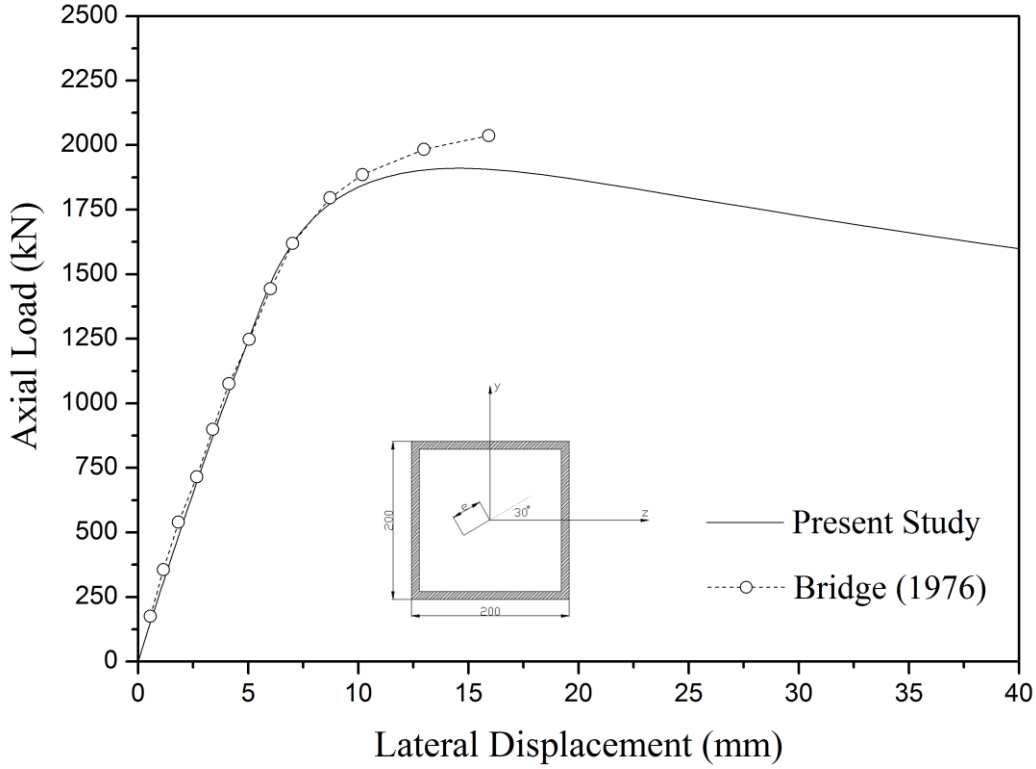

Figure 7.20 Comparison results of SHC -5

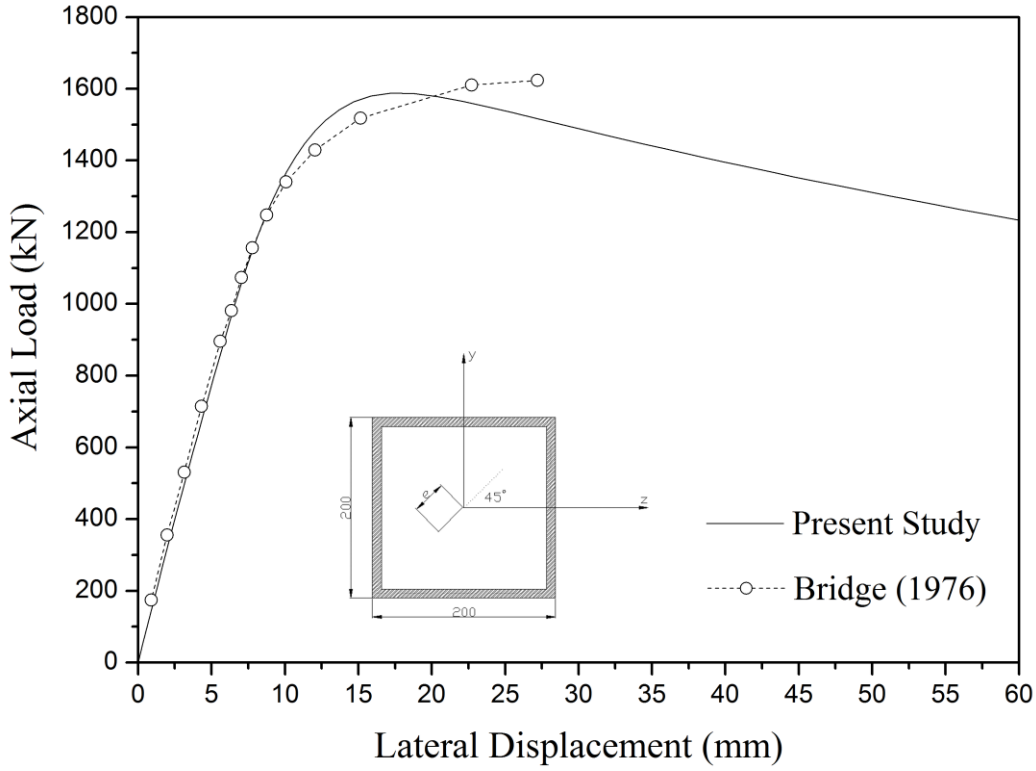

Figure 7.21 Comparison results of SHC -6

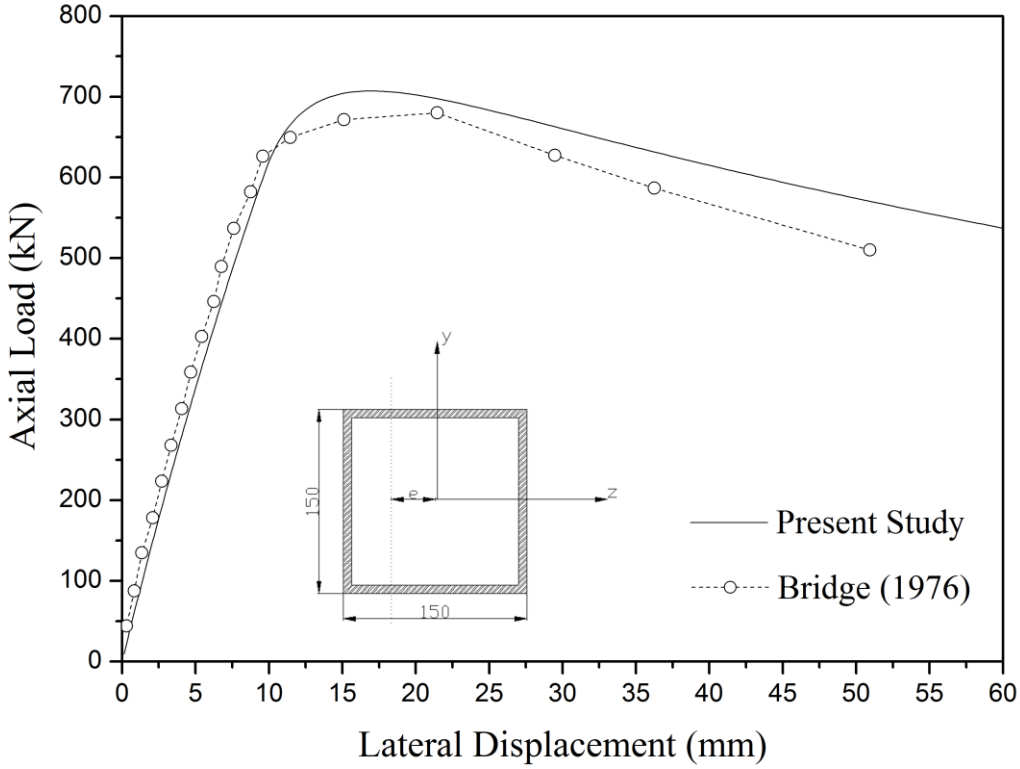

Figure 7.22 Comparison results of SHC -7

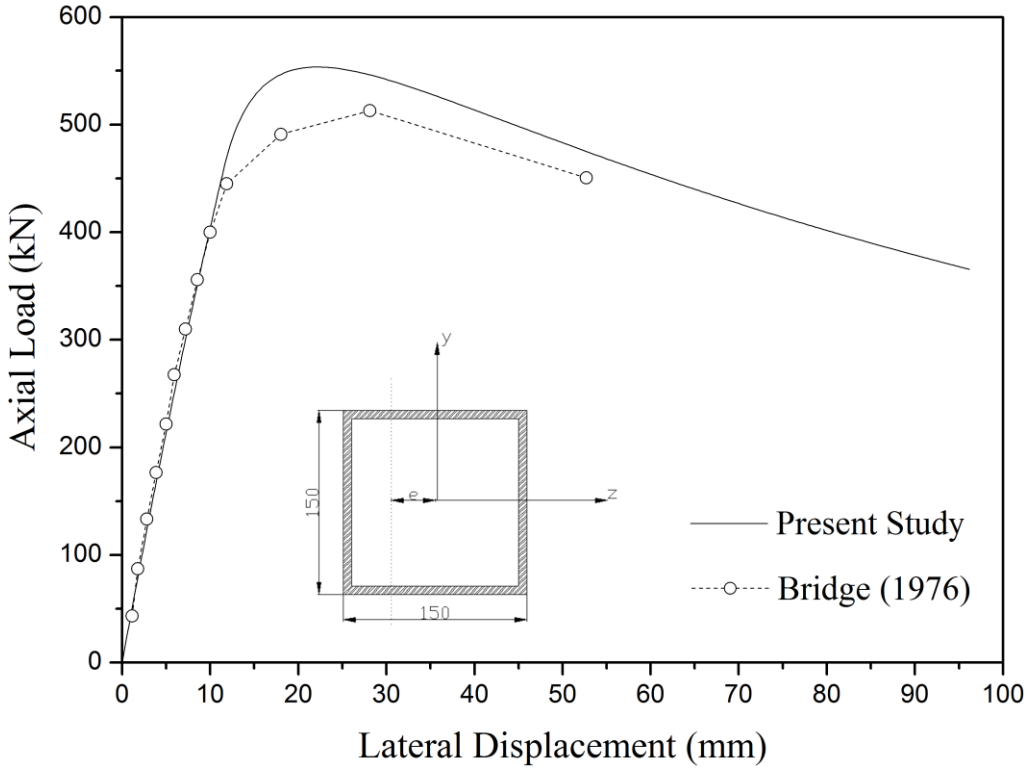

Figure 7.23 Comparison results of SHC -8

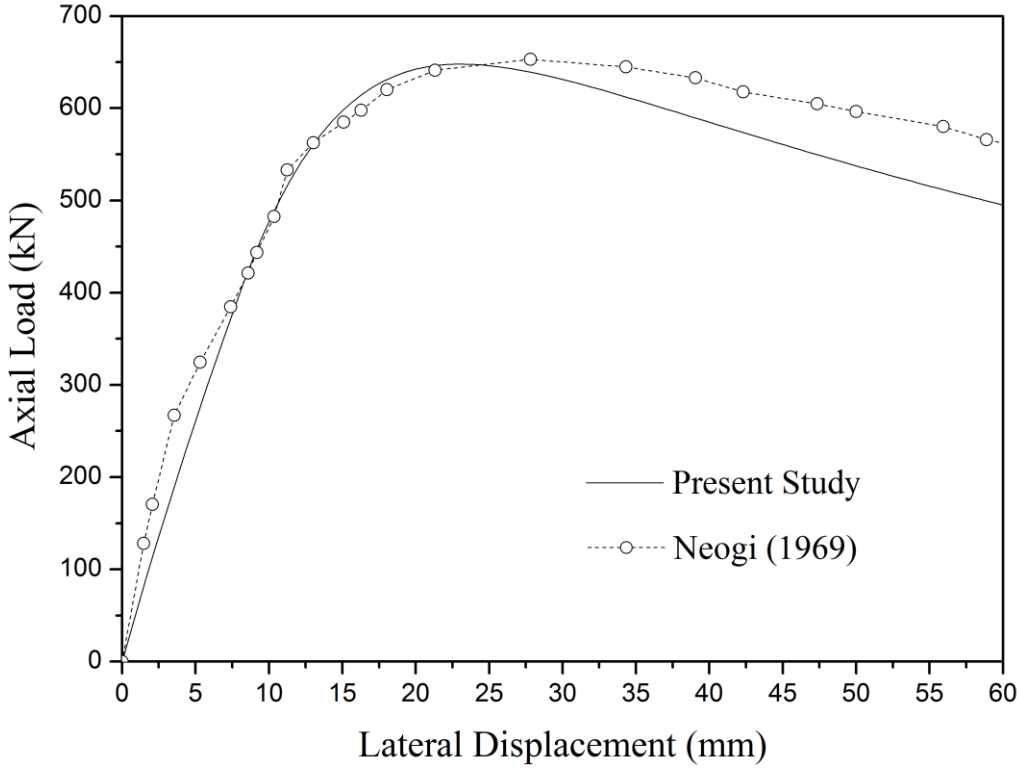

Figure 7.24 Comparison between experiment and present study (M5)

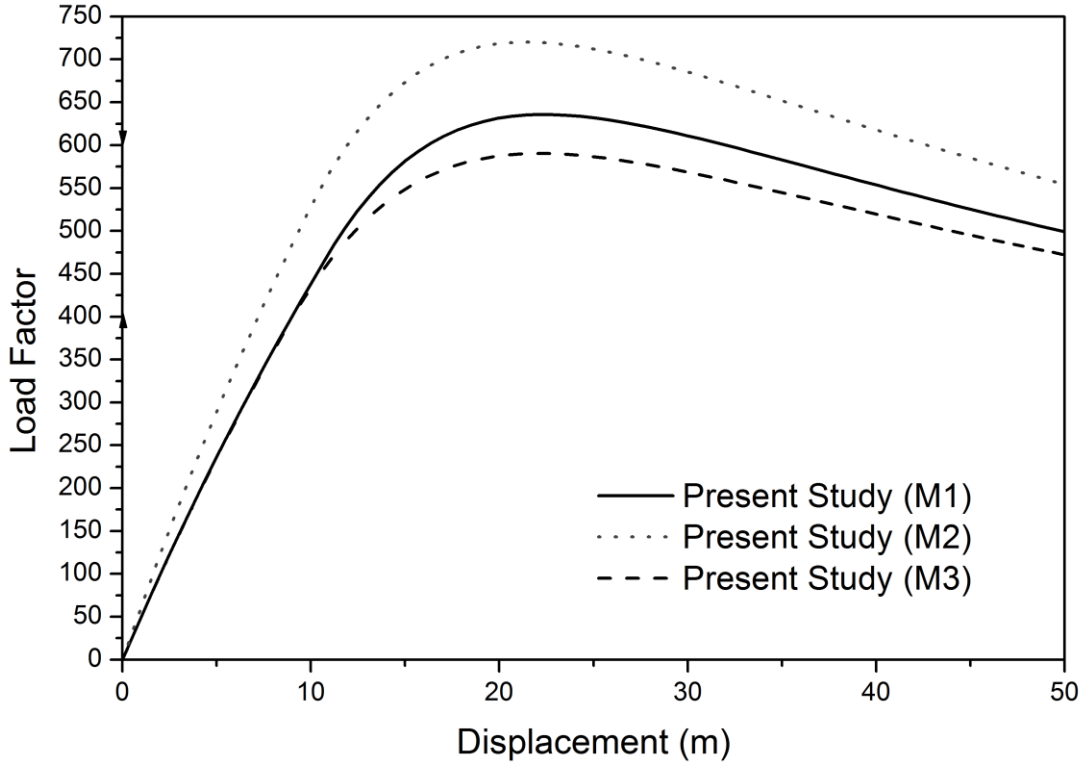

Figure 7.25 Load vs. deflection curves for specimens of M1 to M3

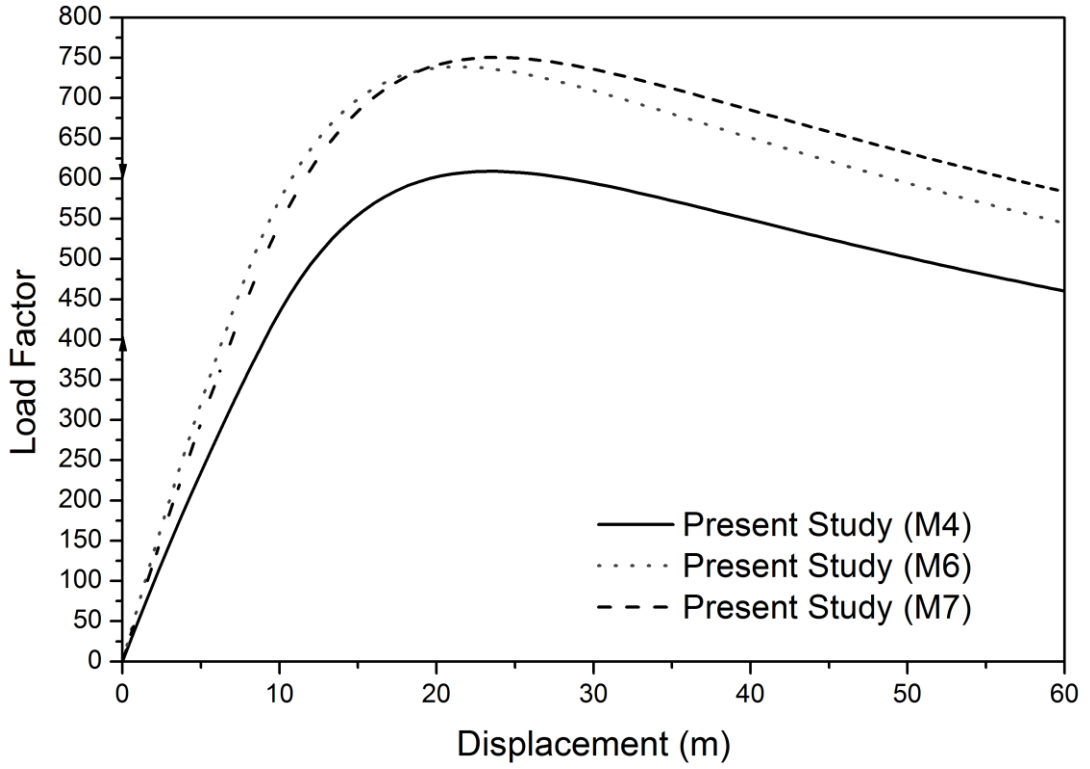

Figure 7.26 Load vs. deflection curves for specimens of M4, M6 and M7

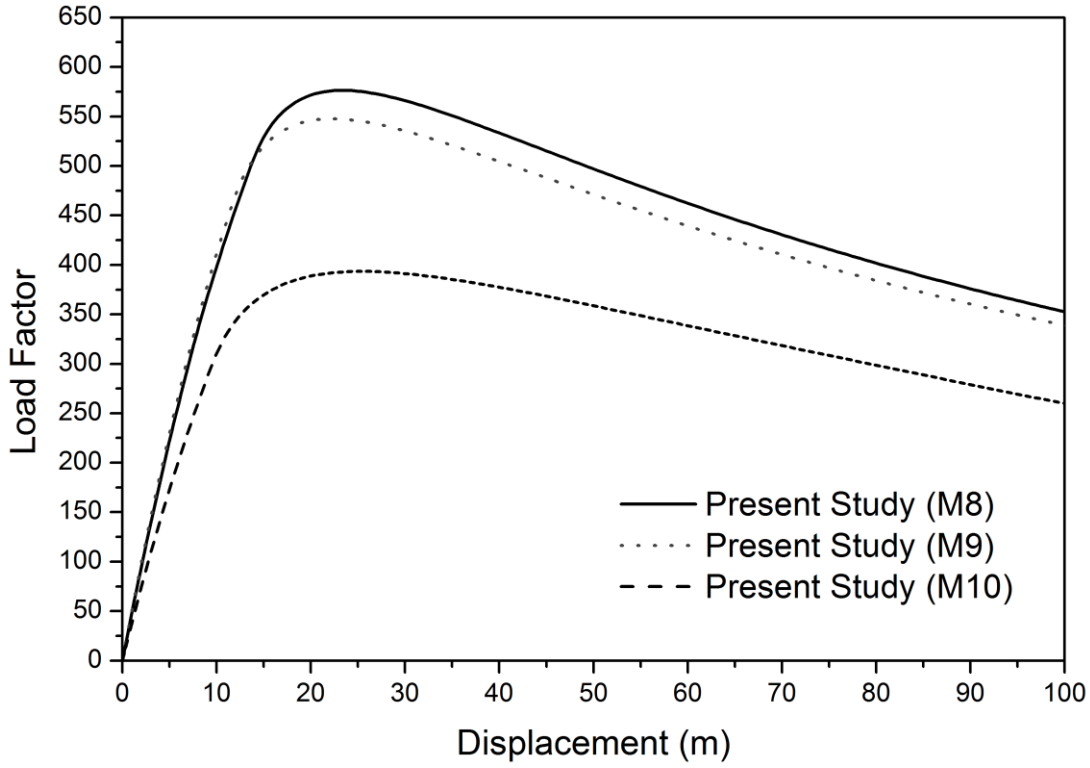

Figure 7.27 Load vs. deflection curves for specimens of M8 to M10

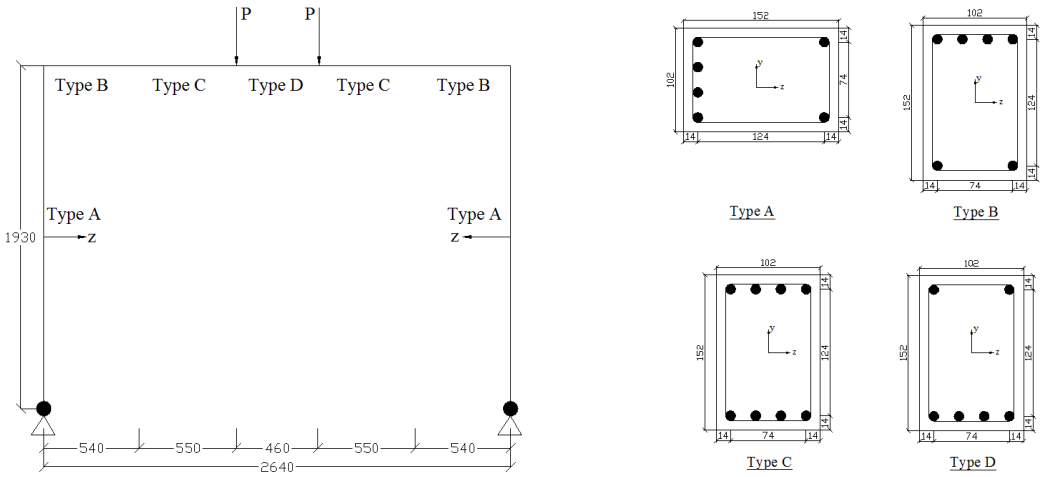

(a) General dimension (b) Section properties

Figure 7.28 Cranston's portal frame

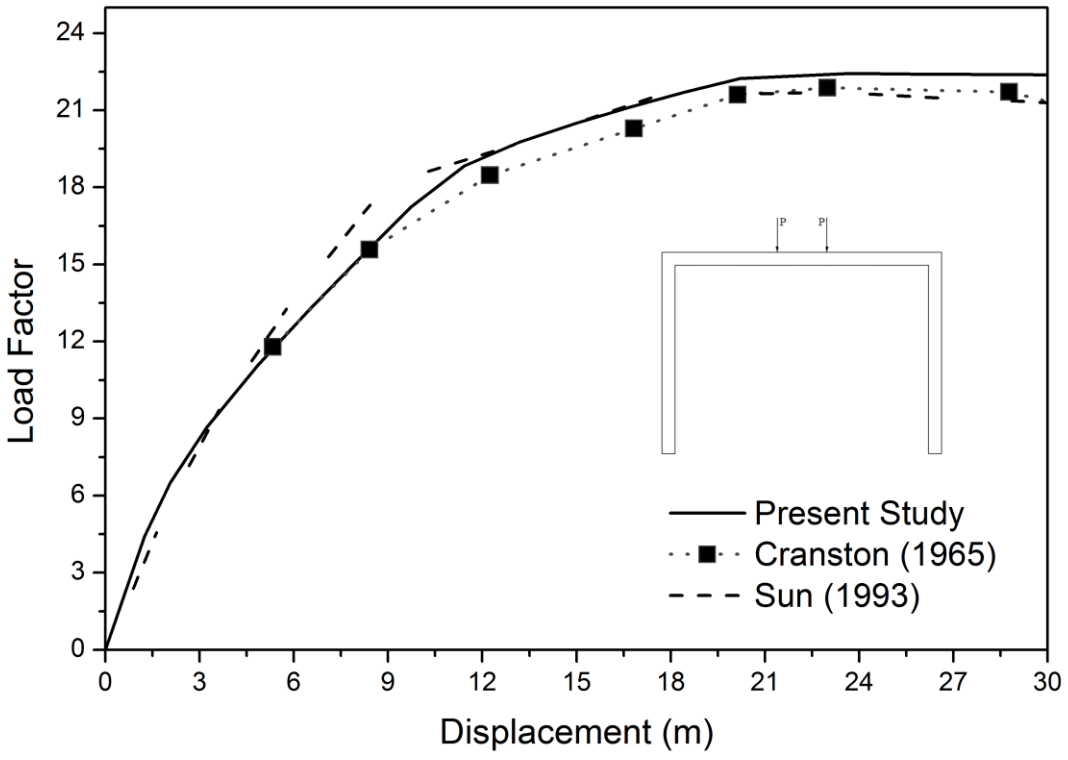

Figure 7.29 Horizontal deflection of Cranston's portal frame

Tables

Table 7.1. Dimensions of confined specimens in CHS 194 group

Specimen	Tube Thickness	External Diameter	Height	Concrete Area	Steel Area
	mm	mm	mm	mm^2	mm^2
C1-B	5.00	193.80	369.04	26532.67	2965.66
C1-C	4.99	193.36	368.48	26411.55	2952.99

Table 7.2. Dimensions of confined specimens in OHS 194 group

Specimen	Tube Thickness	Edge Length	Height	Concrete Area	Steel Area
	mm	mm	mm	mm^2	mm^2
O1-A	5.01	73.73	369.72	23375.95	2871.92
O1-B	5.00	73.81	368.30	23435.31	2869.56

Table 7.3. Compressive strength of concrete obtained from cube and cylinder test

Test day	Cube Strength f_{cu}	Cylinder Strength f_c	f_{cu}/f_c
	N/mm^2	N/mm^2	
28 days	98.40	76.23	0.77
32 days	115.16		
50 days	125.74	95.67	0.76

Table 7.4. Concrete properties obtained from cylinder test

Test day	**f_c**	**Ec**	**ε_0**	**ε_{cu}**
	MPa	GPa	mm/mm	mm/mm
28 days	76.23	38.70	0.002332	0.002332
50 days	95.67	43.60	0.002704	0.002704

Table 7.5. Steel properties obtained from coupon test

Group	**fy**	**fu**	**Es**	**εe**	**Eu**	**Possion's Ratio**
	MPa	MPa	GPa	mm/mm	GPa	
CHS-194	379.25	514.65	206.50	0.0170	1.24	0.3
OCT-194	289.50	455.46	202.46	0.0096	1.21	0.3

Table 7.6. Summarized experimental results

Confined shape	**D/t ratio**	**Yield strength of steel**	**Unconfined concrete strength**	**Confined concrete strength**	**Concrete strength increased**
		MPa	MPa	MPa	
Circular	38.75	379.25	80.85	136.62	69%
Octagonal	38.52	289.50	82.74	120.15	45%

Table 7.7. Geometrical dimension

Column No.	Width	Depth	Thickness	Length	Loading Angle	Ecc
	mm	mm	mm	mm	deg.	mm
SHC - 1	203.7	203.9	9.96	2130	0	38
SHC - 2	204.0	203.3	10.01	3050	0	0
SHC - 3	203.3	202.8	10.03	2130	30	38
SHC - 4	202.8	203.4	9.88	2130	45	38
SHC - 5	202.6	203.2	10.01	3050	30	38
SHC - 6	203.2	202.1	9.78	3050	45	64
SHC - 7	152.5	152.3	6.48	3050	0	38
SHC - 8	152.5	152.3	6.48	3050	0	64

Table 7.8. Material Properties

Column No.	fcu	ftu	Ec	fy	Es
	MPa	MPa	GPa	MPa	MPa
SHC - 1	29.9	3.0	23 300	291	205 000
SHC - 2	31.1	2.9	23 720	290	205 000
SHC - 3	37.2	4.1	26 410	313	205 000
SHC - 4	39.2	4.1	27 850	317	205 000
SHC - 5	44.3	4.4	28 330	319	205 000
SHC - 6	36.1	3.9	27 090	317	205 000
SHC - 7	31.1	3.3	24 060	254	205 000
SHC - 8	31.1	3.3	24 060	254	205 000

Table 7.9. Summary of comparisons

Column No.	**Obs. Max load** kN	**Present Study**	**Exp./Pres.**
SHC - 1	1956	1889	1.04
SHC - 2	2869	3029	0.95
SHC - 3	2180	2101	1.04
SHC - 4	2162	2121	1.02
SHC - 5	2037	1910	1.07
SHC - 6	1623	1587	1.02
SHC - 7	680	707	0.96
SHC - 8	513	554	0.93
Mean			**1.00**
Standard Deviation			**0.050**

Table 7.10. Geometrical layout and material properties

Specimen No.	**Tube Length** mm	**D** mm	**t** mm	**e** mm	**fy** MPa	**Es** GPa	**fcu** MPa
M1	3048	169.4	5.11	47.6	309	207	55.53
M2	3048	169.2	5.26	38.1	309	207	54.00
M3	3048	168.9	5.66	47.6	295	207	42.47
M4	3048	168.4	6.55	47.6	298	207	38.00
M5	3048	169.4	7.19	47.6	312	207	32.00
M6	3048	169.4	7.29	38.1	312	207	33.18
M7	3022.6	168.9	8.81	47.6	323	207	33.06
M8	3048	140.2	9.53	31.8	273	211	41.53
M9	3048	140.2	9.75	31.8	273	211	27.06
M10	3048	121	5.00	31.8	293	207	42.59

Table 7.11. Comparisons between the experiment and proposed approach

Specimen No.	**Experiment**	**Proposed**	**Ratio**
	kN	kN	
M1	622	636	0.98
M2	702	720	0.98
M3	600	590	1.02
M4	625	609	1.03
M5	653	648	1.01
M6	739	739	1.00
M7	758	751	1.01
M8	548	577	0.95
M9	548	548	1.00
M10	417	394	1.06
Mean			**1.00**
Standard Deviation			**0.03**

CHAPTER 8

CONCLUSIONS AND RECOMMENDATIONS

In this chapter, the findings of this thesis are summarized and presented, and the recommendations for the future work are also given.

8.1. Conclusions

A four-year research project is presented in this thesis, detailing the unified second-order design and practical advanced analysis of a hybrid steel and concrete framed structure. A new beam column element with an arbitrarily located plastic hinge is proposed for second-order elastic and advanced plastic analyses, in which derivations are illustrated in detail. The element is extended to three-dimensional spaces, and the incremental secant stiffness method associated with the updated Lagrangian description is adopted for considering large deflections. A robust cross-section analysis technique based on the quasi-Newton numerical scheme is developed for arbitrary sections. Three types of sectional yield surfaces are generated, for which a refined plastic hinge model associated with the use of these surfaces is also proposed. The use of high-strength concrete (HSC) in concrete-filled composite constructions is experimentally investigated. Additionally, extensive examples from available literature and previously published experiments are used to verify the accuracy and feasibility of the proposed analytical methods. Moreover, major design

principles for second-order design are investigated and several design cases are demonstrated.

The research findings and contributions of this work are summarized as follows:

1) An analytical model that uses one element per member for second-order design and advanced analysis is proposed. The model enables the simulations of various effects as initial imperfections, as well as geometric and material nonlinearities. A new beam column element with consideration for an arbitrarily located plastic hinge and initial member curvature is derived. In this element, the initial imperfections of a member are explicitly modeled so that the P-δ effect can be directly reflected in the analysis. Aside from the conventional element that requires two or more elements to capture plastic behavior along member length, an internal plastic hinge can be arbitrarily formed along the member. To improve numerical efficiency and the easy incorporation into existing software, internal degrees of freedom are condensed. Therefore, using one element per member in the proposed analytical model is sufficient and high numerical efficiency can be achieved. This approach consequently brings considerable savings in terms of computing time and data manipulation efforts.

2) An analytical model for the advanced analysis of three-dimensional framed structures is proposed. The model is developed by extending the planar ALH element to three-dimensional spaces. A simplified approach, which assumes a space frame with finite but small rotations, is adopted in deriving

element formulations. The updated Lagrangian description and the incremental secant stiffness method are used for considering large deflections; which are found to be accurate and efficient in iterative convergence rates. Condensing the internal degrees of freedom significantly reduces the size of the global stiffness matrix and improves numerical efficiency. The efficiency and accuracy of the proposed method are verified on the basis of illustrated benchmarking examples.

3) A cross-section analysis technique for arbitrary sections in a hybrid steel and concrete frame is also proposed. A quasi-Newton iterative scheme is adopted in determining the neutral axis of a section and then sectional capacities are computed. Two types of stress-resultant approaches for concrete components are provided as the equivalent stress block and elaborated layer-integration methods. The former is limited to ultimate limit states, whereas the latter is valid for any specified conditions. A structural steel component is automatically meshed into small fibers and each rebar is lumped into a point that occupies a certain area. The openings and voids occupied by other components are removed by the negative area approach.

4) Three types of sectional yield surfaces are put forward as the initial yield, failure, and concrete fracture surfaces. The initial yield and failure surfaces define the elastic and ultimate limit states, whereas the concrete fracture surface is established for combined use with Branson's model in reflecting concrete cracking in the advanced analysis. A refined plastic hinge model

associated with these sectional yield surfaces is also proposed for simulations of the inelastic behavior of various members.

5) This work likewise proposes a unified and practical second-order design approach for hybrid steel and concrete framed structures. Most national codes and design guidelines gradually permit and recommend the use of second-order analysis, and an investigation on the use of Eurocodes for the second-order design of RC, BS, and SCC members and frames is conducted. Furthermore, several simple design examples are presented and the design results obtained by the proposed method are compared with those from the conventional approach.

6) Another contribution is that a practical and efficient advanced analysis for hybrid steel and concrete framed structures has been proposed. This technique enables the simulations of the various effects inherent to actual structures, such as initial imperfections and geometric and material nonlinearities. By adopting the proposed curved ALH element associated with the accurate cross-section analysis, a unified analysis approach can be achieved. Moreover, using only one element per member in the proposed analytical model is sufficient, resulting in considerable savings in terms of computing time and data manipulation efforts. A series of benchmarking examples from literatures and experiments are selected and used as bases in validating the accuracy and feasibility of the proposed method.

7) The use of HSC in circular and octagonal steel tubes is experimentally investigated, on whose basis corresponding constitutive models are obtained and studied. Additionally, the selections of the available constitutive models in Eurocodes are investigated.

8.2. Recommendations for future work

This thesis presents unified analytical models for the second-order design and advanced analysis of hybrid steel and concrete framed structures. The research is limited to static analysis with idealized member connectivity under normal temperature conditions. Recommended research directions are outlined below.

a) In this study, all member connections are assumed pinned or rigid. In certain situations, however, the connections between adjacent members are usually partially restrained; therefore, semi-rigid connection springs can be integrated into the proposed analytical model. A more sophisticated analysis approach with consideration for semi-rigid connection springs can be developed.

b) The proposed element formulations can be extended to allow for the shear deformation. For most practical engineering applications, shear deformation is negligible, but for the stocky members with a slenderness ratio of less than 10, shear deformation should not be disregarded. Therefore, shear strain energy can be incorporated into total potential formulations and the corresponding secant relations and tangent stiffness can be obtained.

c) In this work, the analysis is limited to static conditions. Extending the propose method to dynamic seismic engineering applications (e.g., time–history analysis) necessitates the use of mass and damping matrix as well as hysteric behavior in connections, which are needed to be derived.

d) To extend the proposed numerical approach to fire limit state analysis, the axial spring should be derived in the element formulations and thermal expansion should be reflected. Moreover, the cross-section analysis approach should be revised to enable the consideration of decreases in sectional capacities under high temperatures. A corresponding plastic hinge formulation should accordingly be developed.

REFERENCES

Al-Mashary, F., & Chen, W. F. (1991). Simplified second-order inelastic analysis for steel frames. *J. Inst. Struct. Eng, 69*(23), 395-399.

Alvarez, R. J., & Birnstiel, C. (1969). Inelastic analysis of multistory multibay frames. *Journal of the Structural Division, 95*(ST11), 2477-2503.

American Concrete institute (ACI). (1995). *Building code requirements for reinforced concrete*. Farmington Hills, Mich.

American Concrete Institute (ACI). (2008). *Building code requirements for structural concrete (ACI 318-08) and commentary*: American Concrete Institute, & International Organization for Standardization.

American Institute of Steel Construction. (2010). *Specification for structural steel buildings*: American Institute of Steel Construction.

Argyris, J. (1982). An excursion into large rotations. *Computer Methods in Applied Mechanics and Engineering, 32*(1), 85-155.

Argyris, J. H., Dunne, P. C., & Scharpf, D. W. (1978). On large displacement-small strain analysis of structures with rotational degrees of freedom. *Computer Methods in Applied Mechanics and Engineering, 14*(3), 401-451.

Attalla, M. R., Deierlein, G. G., & Mcguire, W. (1994). Spread of plasticity-quasi-plastic-hinge approach. *Journal of Structural Engineering-Asce, 120*(8), 2451-2473.

Ayrton, W. E., & Perry, J. (1886). On struts. *The engineer, 62*, 464.

Barsan, G. M., & Chiorean, C. G. (1999). Computer program for large deflection elasto-plastic analysis of semi-rigid steel frameworks. *Computers & Structures, 72*(6), 699-711.

Bathe, K.-J., & Bolourchi, S. (1979). Large displacement analysis of three-dimensional beam structures. *International Journal for Numerical Methods in Engineering, 14*(7), 961-986.

Batoz, J. L., & Dhatt, G. (1979). Incremental displacement algorithms for nonlinear problems. *International Journal for Numerical Methods in Engineering, 14*(8), 1262-1267.

Bažant, Z., & Oh, B. (1983). Crack band theory for fracture of concrete. *Materials and Structures, 16*(3), 155-177.

Bazant, Z. P., Pan, J. Y., & Pijaudiercabot, G. (1987). Softening in reinforced-concrete beams and frames. *Journal of Structural Engineering-Asce, 113*(12), 2333-2347.

Bergan, P. G., Horrigmoe, G., Bråkeland, B., & Søreide, T. H. (1978). Solution techniques for non-linear finite element problems. *International Journal for Numerical Methods in Engineering, 12*(11), 1677-1696.

Branson, D. E., & Metz, G. A. (1963). *Instantaneous and time-dependent deflections of simple and continuous reinforced concrete beams*. Auburn, Ala.: Deptment of Civil Engineering and Auburn Research Foundation, Auburn University.

Bratina, S., Saje, M., & Planinc, I. (2004). On materially and geometrically non-linear analysis of reinforced concrete planar frames. *International Journal of Solids and Structures, 41*(24-25), 7181-7207.

Bresler, B. (1960). *Design criteria for reinforced columns under axial load and biaxial bending.* Paper presented at the ACI Journal proceedings.

Bridge, R. Q. (1976). Concrete filled steel tubular columns. *Research Report No. R283*.

Bridge, R. Q., Clarke, M. J., Hancock, G. J., & Trahair, N. S. (1990). *Trends in the analysis and design of steel building frames.* Paper presented at the Second National Structural Engineering Conference: Preprints of Papers.

British Standards Institution. (2001). BS EN 10002-1: 2001. Tensile testing of metallic materials. Method of test at ambient temperature.

Brondum-Nielsen, T. (1985). Ultimate flexural capacity of cracked polygonal concrete sections under biaxial bending. *Journal of the American Concrete Institute, 82*(6), 863-869.

Canadian Standards Association (CSA). (1994). *Design of concrete structures for buildings*. Toronto.

Chajes, A. (1983). *Structural analysis*: Prentice-Hall.

Chan, S. L., & Kitipornchai, S. (1987). Geometric nonlinear analysis of asymmetric thin-walled beam-columns. *Engineering Structures, 9*(4), 243-254.

Chan, S. L. (1988). Geometric and material non-linear analysis of beam-columns and frames using the minimum residual displacement method. *International Journal for Numerical Methods in Engineering, 26*(12), 2657-2669.

Chan, S. L. (1989). Inelastic post-buckling analysis of tubular beam-columns and frames. *Engineering Structures, 11*(1), 23-30.

Chan, S. L. (1992). Large deflection kinematic formulations for three-dimensional framed structures. *Computer Methods in Applied Mechanics and Engineering, 95*(1), 17-36.

Chan, S. L., & Zhou, Z. H. (1994). Pointwise equilibrating polynomial element for nonlinear-analysis of frames. *Journal of Structural Engineering-Asce, 120*(6), 1703-1717.

Chan, S. L., & Zhou, Z. H. (1995). 2nd-order elastic analysis of frames using single imperfect element per member. *Journal of Structural Engineering-Asce, 121*(6), 939-945.

Chan, S. L., & Chui, P. P. T. (1997). A generalized design-based elastoplastic analysis of steel frames by section assemblage concept. *Engineering Structures, 19*(8), 628-636.

Chan, S. L., & Zhou, Z. H. (1998). On the development of a robust element for second-order 'nonlinear integrated design and analysis (NIDA)'. *Journal of Constructional Steel Research, 47*(1-2), 169-190.

Chan, S. L., & Gu, J. X. (2000). Exact tangent stiffness for imperfect beam-column members. *Journal of Structural Engineering-Asce, 126*(9), 1094-1102.

Chan, S. L., & Zhou, Z. H. (2000). Non-linear integrated design and analysis of skeletal structures by 1 element per member. *Engineering structures, 22*(3), 246-257.

Chan, S. L., Huang, H. Y., & Fang, L. X. (2005). Advanced analysis of imperfect portal frames with semirigid base connections. *Journal of Engineering Mechanics, 131*(6), 633-640.

Chan, S. L., & Cho, S. H. (2008). Second-order analysis and design of angle trusses Part I: Elastic analysis and design. *Engineering Structures, 30*(3), 616-625.

Charalampakis, A. E., & Koumousis, V. K. (2008). Ultimate strength analysis of composite sections under biaxial bending and axial load. *Advances in Engineering Software, 39*(11), 923-936.

Chen, S. F., Teng, J. G., & Chan, S. L. (2001). Design of biaxially loaded short composite columns of arbitrary section. *Journal of Structural Engineering, 127*(6), 678-685.

Chen, W. F., & Atsuta, T. (1972). Interaction equations for biaxially loaded sections. *Journal of the Structural Division, 98*(5), 1035-1052.

Chen, W. F., & Lui, E. M. (1987). *Structural stability* (Vol. 198): Elsevier New York.

Chen, W. F., & Chan, S. L. (1995). 2nd-order inelastic analysis of steel frames using element with midspan and end springs. *Journal of Structural Engineering, 121*(3), 530-541.

Chen, W. F., Goto, Y., & Liew, J. Y. R. (1995). *Stability design of semi-rigid frames*: Wiley-Interscience.

Chiorean, C. (2010). Computerised interaction diagrams and moment capacity contours for composite steel–concrete cross-sections. *Engineering Structures, 32*(11), 3734-3757.

Chiorean, C. G., & Barsan, G. M. (2005). Large deflection distributed plasticity analysis of 3D steel frameworks. *Computers & Structures, 83*(19–20), 1555-1571.

Cho, S. H., & Chan, S. L. (2008). Second-order analysis and design of angle trusses, Part II: Plastic analysis and design. *Engineering Structures, 30*(3), 626-631.

Chu, K., & Pabarcius, A. (1964). Elastic and inelastic buckling of portal frames. *Journal of the Engineering Mechanics Division*, 221.

Connor, J. J., Logcher, R. D., & Chan, S. C. (1967). *Nonlinear analysis of elastic framed structures*: Department of Civil Engineering, Massachusetts Institute of Technology.

Cranston, W. B. (1965). *Tests on reinforced concrete frames. Part 1, Pinned portal frames*. London: Cement and Concrete Association.

Crisfield, M. A. (1981). A fast incremental/iterative solution procedure that handles "snap-through". *Computers & Structures, 13*(1), 55-62.

Crisfield, M. A. (1983). An arc-length method including line searches and accelerations. *International Journal for Numerical Methods in Engineering, 19*(9), 1269-1289.

Cuong, N. H., Kim, S. E., & Oh, J. R. (2007). Nonlinear analysis of space steel frames using fiber plastic hinge concept. *Engineering structures, 29*(4), 649-657.

Dafalias, Y. F., & Popov, E. P. (1975). A model of nonlinearly hardening materials for complex loading. *Acta Mechanica, 21*(3), 173-192.

Dafalias, Y. F. (1979). A model of soil behavior under monotonic and cyclic loading conditions. Transactions of Fifth International Conference on Strucutral Mechanics and Reactor Technology. West Berlin, Germany.

De Freitas, J., & Ribeiro, A. (1992). Large displacement elastoplastic analysis of space trusses. *Computers & Structures, 44*(5), 1007-1016.

De Souza, R. M. (2000). *Force-based finite element for large displacement inelastic analysis of frames.* University of California.

De Vivo, L., & Rosati, L. (1998). Ultimate strength analysis of reinforced concrete sections subject to axial force and biaxial bending. *Computer Methods in Applied Mechanics and Engineering, 166*(3), 261-287.

Ekhande, S. G., Selvappalam, M., & Madugula, M. K. (1989). Stability functions for three-dimensional beam-columns. *Journal of Structural Engineering, 115*(2), 467-479.

El-Tawil, S., & Deierlein, G. G. (2001a). Nonlinear analysis of mixed steel-concrete frames. I: Element formulation. *Journal of Structural Engineering-Asce, 127*(6), 647-655.

El-Tawil, S., & Deierlein, G. G. (2001b). Nonlinear analysis of mixed steel-concrete frames. II: Implementation and verification. *Journal of Structural Engineering-Asce, 127*(6), 656-665.

El-Zanaty, M. H., Murray, D. W., & Bjorhovde, R. (1980). *Inelastic behavior of multistory steel frames*: Department of Civil Engineering, University of Alberta.

Ellobody, E., Young, B., & Lam, D. (2006). Behaviour of normal and high strength concrete-filled compact steel tube circular stub columns. *Journal of Constructional Steel Research, 62*(7), 706-715.

Espion, B. (1993). Benchmark examples for creep and shrinkage analysis computer program *Creep and shrinkage of concrete. TC 114 RILEM*.

Euler, L. (1759). Sur la force des colonnes. *Memoires de L'Academie des Sciences et Belles-Lettres, 13*, 252-282.

Eurocode 2. (2004). *Eurocode 2: Design of concrete structures: Part 1-1: General rules and rules for buildings*: European Committee for Standardization (CEN),.

Eurocode 3. (2005). *Eurocode 3: Design of steel structures: Part 1-1: General rules and rules for buildings*: European Committee for Standardization (CEN),.

Eurocode 4. (2004). *Eurocode 4: Design of composite steel and concrete structures. Part 1.1: General rules and rules for buildings*: European Committee for Standardization (CEN),.

Fang, L. X., Chan, S. L., & Wong, Y. L. (1999). Strength analysis of semi-rigid steel-concrete composite frames. *Journal of Constructional Steel Research, 52*(3), 269-291.

Fang, L. X., Chan, S. L., & Wong, Y. L. (2000). Numerical analysis of composite frames with partial shear-stud interaction by one element per member. *Engineering Structures, 22*(10), 1285-1300.

Federal Emergency Management Agency. (2000). *Prestandard and commentary for the seismic rehabilitation of buildings (FEMA356)*. Building Seismic Safety Council, Washington, D.C: FEMA.

Fleming, J. F., & Werner, S. D. (1965). *Design of columns subjected to biaxial bending.* Paper presented at the ACI Journal Proceedings.

Fong, M., Cho, S. H., & Chan, S. L. (2009). Design of angle trusses by codes and second-order analysis with experimental verification. *Journal of Constructional Steel Research, 65*(12), 2140-2147.

Fong, M., Liu, Y. P., & Chan, S. L. (2010). Second-order analysis and design of imperfect composite beam-columns. *Engineering Structures, 32*(6), 1681-1690.

Fong, M., Chan, S. L., & Uy, B. (2011). Advanced design for trusses of steel and concrete-filled tubular sections. *Engineering Structures, 33*(12), 3162-3171.

Fong, M., Liu, Y. P., & Chan, S. L. (2012). Second-order analysis and experiments of semi-rigid and imperfect domes. *Advances in Structural Engineering, 15*(9), 1537-1546.

Furlong, R. W. (1961). Ultimate strength of square columns under axial load and biaxial bending. *ACI Journal, 32*(9), 1129-1140.

Gong, Y. (2006). Adaptive gradual plastic hinge model for nonlinear analysis of steel frameworks. *Canadian Journal of Civil Engineering, 33*(9), 1125-1139.

Goto, Y., & Chen, W. F. (1987). Second-order elastic analysis for frame design. *Journal of Structural Engineering, 113*(7), 1501-1519.

Griffis, L. G. (1986). Some design considerations for composite-frame structures. *Engineering Journal-American Institute of Steel Construction Inc, 23*(2), 59-64.

Guralnick, S., & He, J. (1992). A finite element method for the incremental collapse analysis of elastic-perfectly plastic framed structures. *Computers & Structures, 45*(3), 571-581.

Harrison, H. B. (1965). *The application of the principles of plastic analysis of three dimensional steel structures*: University of Sydney.

Harstead, G., Birnstiel, C., & Leu, K. (1968). Inelastic H-columns under biaxial bending. *Journal of the Structural Division, 94*(ST10), 2371-2398.

Ho, W. M. G., & Chan, S. L. (1991). Semibifurcation and bifurcation analysis of flexibly connected steel frames. *Journal of Structural Engineering, 117*(8), 2299-2319.

Hong Kong Buildings Departement. (2013). *Code of practice of structural use of concrete*: Buildings Department, Hong Kong SAR Government.

Hong Kong Buildings Department. (2011). *Code of practice for the structural use of steel 2011*: Buildings Department, Hong Kong SAR Government.

Hsu, C. T. T. (1987). Channel-shaped reinforced concrete compression members under biaxial bending. *Aci Structural Journal, 84*(3), 201-211.

Hsu, C. T. T. (1988). Analysis and design of square and rectangular columns by equation of failure surface. *Aci Structural Journal, 85*(2), 167-179.

Hsu, C. T. T. (1989). T-shaped reinforced concrete members under biaxial bending and axial compression. *Aci Structural Journal, 86*(4), 460-468.

Ibrahim, A. M. M., & Adebar, P. (2004). Effective flexural stiffness for linear seismic analysis of concrete walls. *Canadian Journal of Civil Engineering, 31*(4), 597-607.

Iu, C. K., & Bradford, M. (2012a). Higher-order non-linear analysis of steel structures, Part I: Elastic second-order formulation. *Advanced Steel Construction, 8*(2), 168-182.

Iu, C. K., & Bradford, M. (2012b). Higher-order non-linear analysis of steel structures, Part II: Refined plastic hinge formulation. *Advanced Steel Construction, 8*(2), 183-198.

Izzuddin, B. A. (1996). Quartic formulation for elastic beam-columns subject to thermal effects. *Journal of Engineering Mechanics, 122*(9), 861-871.

Izzuddin, B. A., & Smith, D. L. (1996). Large-displacement analysis of elastoplastic thin-walled frames. I: Formulation and implementation. *Journal of Structural Engineering, 122*(8), 905-914.

Izzuddin, B. A., & Smith, D. L. (2000). Efficient nonlinear analysis of elasto-plastic 3D R/C frames using adaptive techniques. *Computers & Structures, 78*(4), 549-573.

Jiang, X. M., Chen, H., & Liew, J. Y. R. (2002). Spread-of-plasticity analysis of three-dimensional steel frames. *Journal of Constructional Steel Research, 58*(2), 193-212.

Kam, T. Y., & Lee, F. S. (1986). Nonlinear analysis of steel plane frames with initial imperfections. *Computers & Structures, 23*(4), 553-557.

Kassimali, A. (1983). Large deformation analysis of elasticplastic frames. *Journal of Structural Engineering, 109*(8), 1869-1886.

Kassimali, A., & Abbasnia, R. (1991). Large deformation analysis of elastic space frames. *Journal of Structural Engineering, 117*(7), 2069-2087.

Kim, S. E., & Chen, W. F. (1996). Practical advanced analysis for braced steel frame design. *Journal of Structural Engineering, 122*(11), 1266-1274.

Kim, S. E., & Chen, W. F. (1996). Practical advanced analysis for unbraced steel frame design. *Journal of Structural Engineering, 122*(11), 1259-1265.

Kim, S. E., & Chen, W. F. (1998). A sensitivity study on number of elements in refined plastic-hinge analysis. *Computers & Structures, 66*(5), 665-673.

Kim, S. E., & Choi, S. H. (2001). Practical advanced analysis for semi-rigid space frames. *International journal of solids and structures, 38*(50), 9111-9131.

Kim, S. E., Lee, J., & Park, J. S. (2002). 3-D second-order plastic-hinge analysis accounting for lateral torsional buckling. *International Journal of Solids and Structures, 39*(8), 2109-2128.

Kim, S. E., Lee, J., & Park, J. S. (2003). 3-D second-order plastic-hinge analysis accounting for local buckling. *Engineering Structures, 25*(1), 81-90.

Kim, S. E., Uang, C. M., Choi, S. H., & An, K. Y. (2006). Practical advanced analysis of steel frames considering lateral-torsional buckling. *Thin-walled structures, 44*(7), 709-720.

King, W. S., White, D. W., & Chen, W. F. (1992). Second-order inelastic analysis methods for steel-frame design. *Journal of Structural Engineering, 118*(2), 408-428.

Kishi, N., & Chen, W. F. (1990). Moment-rotation relations of semirigid connections with angles. *Journal of Structural Engineering, 116*(7), 1813-1834.

Knowles, R. B., & Park, R. (1969). Strength of concrete filled steel columns. *Journal of the Structural Division, 95*(12), 2565-2587.

Lakshmi, B., & Shanmugam, N. E. (2002). Nonlinear analysis of in-filled steel-concrete composite columns. *Journal of Structural Engineering, 128*(7), 922-933.

Lau, C. Y., Chan, S. L., & So, A. K. W. (1993). Biaxial bending design of arbitrarily shaped reinforced concrete column. *Aci Structural Journal, 90*(3), 269-278.

Lazaro, A. L., & Richards, R. (1973). Full-range analysis of concrete frames. *Journal of the Structural Division, 99*(8), 1761-1783.

Liew, J. Y. R., White, D. W., & Chen, W. F. (1993a). Second-order refined plastic-hinge analysis for frame design. Part I. *Journal of Structural Engineering, 119*(11), 3196-3216.

Liew, J. Y. R., White, D. W., & Chen, W. F. (1993b). Second-order refined plastic-hinge analysis for frame design. Part II. *Journal of Structural Engineering, 119*(11), 3217-3236.

Liew, J. Y. R., Punniyakotty, N. M., & Shanmugam, N. E. (1997). Advanced analysis and design of spatial structures. *Journal of Constructional Steel Research, 42*(1), 21-48.

Liew, J. Y. R., Chen, H., Shanmugam, N. E., & Chen, W. F. (2000a). Improved nonlinear plastic hinge analysis of space frame structures. *Engineering Structures, 22*(10), 1324-1338.

Liew, J. Y. R., Chen, W. F., & Chen, H. (2000b). Advanced inelastic analysis of frame structures. *Journal of Constructional Steel Research, 55*(1–3), 245-265.

Liu, S. W., Liu, Y. P., & Chan, S. L. (2010). Pushover analysis by one element per member for performance-based seismic design. *International Journal of Structural Stability and Dynamics, 10*(01), 111-126.

Liu, Y. P., & Chan, S. L. (2009). Semi-empirical design of complex metal beams by buckling analysis. *The IES Journal Part A: Civil & Structural Engineering, 2*(1), 85-96.

Livesley, R. K., & Chandler, D. B. (1956). *Stability functions for structural frameworks*: Manchester University Press.

Meek, J. L., & Tan, H. S. (1984). Geometrically nonlinear analysis of space frames by an incremental iterative technique. *Computer Methods in Applied Mechanics and Engineering, 47*(3), 261-282.

Meek, J. L., & Lin, W. J. (1990). Geometric and material nonlinear analysis of thin-walled beam-columns. *Journal of Structural Engineering, 116*(6), 1473-1490.

Mehanny, S. S. F., & Deierlein, G. G. (1999). *Modeling and assessment of seismic performance of composite frames with reinforced concrete columns and steel beams.* Stanford University.

Moreadith, F. L. (1978). *Design of reinforced concrete for combined bending and tension.* Paper presented at the ACI Journal Proceedings.

Neogi, P. K., Sen, H. K., & Chapman, J. C. (1969). Concrete-filled tubular steel columns under eccentric loading. *The structural engineer, 47*, 5.

Neuenhofer, A., & Filippou, F. C. (1998). Geometrically nonlinear flexibility-based frame finite element. *Journal of Structural Engineering, 124*(6), 704-711.

New Zealand Standard. (1995). *Concrete structures standard: Part 2-Commentary on the design of concrete structures*. New Zealand.

Niceno, B. (2002). EasyMesh: A two-dimensional quality mesh generator, version 1.4. *Trieste University, Italy*.

NIDA. (2013). *NIDA User Manual 9.0.*

Nukala, P. K. V. V., & White, D. W. (2004). A mixed finite element for three-dimensional nonlinear analysis of steel frames. *Computer Methods in Applied Mechanics and Engineering, 193*(23–26), 2507-2545.

Oran, C. (1973a). Tangent stiffness in plane frames. *Journal of the Structural Division, 99*(6), 973-985.

Oran, C. (1973b). Tangent stiffness in space frames. *Journal of the Structural Division, 99*(6), 987-1001.

Orbison, J. G., McGuire, W., & Abel, J. F. (1982). Yield surface applications in nonlinear steel frame analysis. *Computer Methods in Applied Mechanics and Engineering, 33*(1–3), 557-573.

Papanikolaou, V. K. (2012). Analysis of arbitrary composite sections in biaxial bending and axial load. *Computers & Structures, 98*, 33-54.

Pi, Y., & Trahair, N. (1994a). Nonlinear inelastic analysis of steel beam-columns. I: Theory. *Journal of Structural Engineering, 120*(7), 2041-2061.

Pi, Y., & Trahair, N. (1994b). Nonlinear inelastic analysis of steel beam-columns. II: Applications. *Journal of Structural Engineering, 120*(7), 2062-2085.

Pi, Y., Bradford, M., & Uy, B. (2006a). Second order nonlinear inelastic analysis of composite steel-concrete members. I: Theory. *Journal of Structural Engineering, 132*(5), 751-761.

Pi, Y., Bradford, M., & Uy, B. (2006b). Second order nonlinear inelastic analysis of composite steel-concrete members. II: Applications. *Journal of Structural Engineering, 132*(5), 762-771.

Ramm, E. (1981). *Strategies for tracing the nonlinear response near limit points*: Springer.

Riks, E. (1979). An incremental approach to the solution of snapping and buckling problems. *International Journal of Solids and Structures, 15*(7), 529-551.

Robertson, A. (1925). The Strength of Struts. *ICE Selected Engineering Papers, 1*(28).

Rodriguez, J., & Aristizabal-Ochoa, J. D. (1999). Biaxial interaction diagrams for short RC columns of any cross section. *Journal of Structural Engineering, 125*(6), 672-683.

Roik, K., & Bergmann, R. (1990). Design method for composite columns with unsymmetrical cross-sections. *Journal of Constructional Steel Research, 15*(1-2), 153-168.

Rotter, J. (1985). Rapid exact inelastic biaxial bending analysis. *Journal of Structural Engineering, 111*(12), 2659-2674.

Santathadaporn, S., & Chen, W. F. (1968). *Interaction curves for sections under combined biaxial bending and axial force*.

Sfakianakis, M. G., & Fardis, M. N. (1991). Bounding surface model for cyclic biaxial bending of RC sections. *Journal of Engineering Mechanics-Asce, 117*(12), 2748-2769.

Sfakianakis, M. G. (1997). Interactive construction of bounding surface of R/C L-shaped columns subjected to biaxial bending with axial load. *Proceedings of the Seventh International Conference on Computing in Civil and Building Engineering, Vols 1-4*, 885-890.

Sfakianakis, M. G. (1998). Bounding surface of reinforced concrete U-shaped column elements subjected to cyclic biaxial bending with axial load. *Advances in Civil and Structural Engineering Computing for Practice*, 197-204.

Sfakianakis, M. G. (2002). Biaxial bending with axial force of reinforced, composite and repaired concrete sections of arbitrary shape by fiber model and computer graphics. *Advances in Engineering Software, 33*(4), 227-242.

So, A. K. W., & Chan, S. L. (1991). Buckling and geometrically nonlinear analysis of frames using one element/member. *Journal of Constructional Steel Research, 20*(4), 271-289.

Sokolnikoff, I. S., Redheffer, R. M., & Avents, J. (1958). Mathematics of physics and modern engineering. *Journal of The Electrochemical Society, 105*(9), 196C-196C.

Spacone, E., Ciampi, V., & Filippou, F. C. (1996). Mixed formulation of nonlinear beam finite element. *Computers & Structures, 58*(1), 71-83.

Srpčič, S., & Saje, M. (1986). Large deformations of thin curved plane beam of constant initial curvature. *International journal of mechanical sciences*, *28*(5), 275-287.

Standard Australia International Ltd. (2004). *Australian standards-bridge design (AS 5100-2004)*.

Standards Association of Australia (SAA). (1994). *Australia concrete structures code*. Sydney, Australia.

Standards Association of Australia Steel Structures. (1998). Australian standard AS 4100-1998. *Standards Association of Australia, Sydney, Australia*.

Sun, C. H., Bradford, M. A., & Gilbert, R. I. (1994). A reliable numerical method for simulating the post-failure behaviour of concrete frame structures. *Computers & Structures*, *53*(3), 579-589.

Susantha, K., Hanbin, G., & Usami, T. (2001). A capacity prediction procedure for concrete-filled steel columns. *Journal of earthquake engineering*, *5*(4), 483-520.

Teh, L. H., & Clarke, M. J. (1999). Plastic-zone analysis of 3D steel frames using beam elements. *Journal of Structural Engineering*, *125*(11), 1328-1337.

Teh, L. H. (2001). Cubic beam elements in practical analysis and design of steel frames. *Engineering Structures*, *23*(10), 1243-1255.

The British Standard Institution. (2005). *BS5400 Steel, concrete and composite bridges, part 5, code of practice for the design of composite bridges*.

Tikka, T. K., & Mirza, S. A. (2005). Nonlinear El equation for slender reinforced concrete columns. *Aci Structural Journal, 102*(6), 839-848.

Timoshenko, S. (1935). Theory of elasticity. *Bull. Amer. Math. Soc., 41*(10), 0002-9904.

Toma, S., & Chen, W. F. (1992). European calibration frames for second-order inelastic analysis. *Engineering Structures, 14*(1), 7-14.

Trahair, N. S., & Chan, S. L. (2003). Out-of-plane advanced analysis of steel structures. *Engineering structures, 25*(13), 1627-1637.

Valipour, H. R., & Foster, S. J. (2009). Nonlinear static and cyclic analysis of concrete-filled steel columns. *Journal of Constructional Steel Research, 66*(6), 793-802.

Vogel, U. (1985). Calibrating frames. *Stahlbau, 10*(Oct), 295-301.

Wen, R. K., & Lange, J. (1981). Curved beam element for arch buckling analysis. *Journal of the Structural Division, 107*(11), 2053-2069.

White, D. W. (1985). *Material and geometric nonlinear analysis of local planar behavior in steel frames using interactive computer graphics*: Cornell University, Aug.

White, D. W. (1993). Plastic-hinge methods for advanced analysis of steel frames. *Journal of Constructional Steel Research, 24*(2), 121-152.

Whitney, C. S. (1965). *Plastic theory of reinforced concrete design*. Emmitsburg, MD: National Emergency Training Center.

Wong, M. B., & Tin-Loi, F. (1990). Analysis of frames involving geometrical and material nonlinearities. *Computers & Structures, 34*(4), 641-646.

Wsu, C. T. T. (1985). Biaxially loaded L-shaped reinforced concrete columns. *Journal of Structural Engineering, 111*(12), 2576-2595.

Yang, T. Y., & Saigal, S. (1984). A simple element for static and dynamic response of beams with material and geometric nonlinearities. *International Journal for Numerical Methods in Engineering, 20*(5), 851-867.

Yang, Y. B., & Chiou, H. T. (1987). Rigid body motion test for nonlinear analysis with beam elements. *Journal of engineering mechanics, 113*(9), 1404-1419.

Yau, C. Y., & Chan, S. L. (1994). Inelastic and stability analysis of flexibly connected steel frames by springs-in-series model. *Journal of Structural Engineering-Asce, 120*(10), 2803-2819.

Yen, J. Y. R. (1991). Quasi-newton method for reinforced-concrete column analysis and design. *Journal of Structural Engineering, 117*(3), 657-666.

Young, B., & Ellobody, E. (2006). Experimental investigation of concrete-filled cold-formed high strength stainless steel tube columns. *Journal of Constructional Steel Research, 62*(5), 484-492.

Zhou, Z. H., & Chan, S. L. (2004). Elastoplastic and large deflection analysis of steel frames by one element per member. I: One hinge along member. *Journal of Structural Engineering, 130*(4), 538-544.

Ziemian, R. D. (1993). Examples of frame studies used to verify advanced methods of inelastic analysis. *Plastic hinge based methods for advanced analysis and design of steel frames*.